OXIDATIVE STRESS AND OGG1:

BEYOND OGG1-INITIATED BER

by

ELLEN HIGGS

A thesis submitted to

The University of Birmingham

for the degree of

DOCTOR OF PHILOSOPHY

School of Biosciences

College of Life and Environmental Sciences

University of Birmingham

September 2020

UNIVERSITY OF
BIRMINGHAM

University of Birmingham Research Archive

e-theses repository

This unpublished thesis/dissertation is copyright of the author and/or third parties. The intellectual property rights of the author or third parties in respect of this work are as defined by The Copyright Designs and Patents Act 1988 or as modified by any successor legislation.

Any use made of information contained in this thesis/dissertation must be in accordance with that legislation and must be properly acknowledged. Further distribution or reproduction in any format is prohibited without the permission of the copyright holder.

Abstract

Oxidative stress and subsequent oxidative DNA damage play an important role in the process of ageing and are also linked to numerous different diseases. A prevalent type of oxidative DNA damage is the oxidation of guanine, generating 8-oxoguanine. It is therefore unsurprising that 8-oxoguanine has been found to be elevated in the genome in a range of pathological conditions, including multiple cancers. However, whether 8-oxoguanine drives the progression of these diseases or is a result of the disease process itself is often unclear.

8-oxoguanine is recognised in genomic DNA by the glycosylase, 8-oxoguanine glycosylase-1 (OGG1), which initiates removal by the base excision repair pathway. To study cellular function, OGG1-null mouse models and *in vitro* cell models have been previously generated. Primarily, this thesis is an investigation into the cellular role of OGG1 and functional changes in cells that lack OGG1-activity. We show that OGG1-null cells exist in a state of oxidative stress, possessing a persistent elevation of intracellular reactive oxygen species. Further increasing the oxidative stress burden by the depletion of the antioxidant, glutathione, induces apoptosis in OGG1-null cells. Surprisingly, however we show that induction of apoptosis is not accompanied by an accumulation of genomic 8-oxoguanine. This finding highlights the importance of backup repair mechanism, which are able to repair 8-oxoguanine in the absence of OGG1. Using gene expression and biochemical studies, we have identified two potential backup mechanisms: components of the nucleotide excision repair pathway (ERCC1, ERCC4 and ERCC5) and the Nei-like DNA glycosylase-3 (NEIL3). Lastly, we have confirmed that OGG1 possesses an additional cellular role, acting as a signalling molecule to activate small GTPases, activating multiple downstream pathways. This stresses the importance of not only considering OGG1 as a glycosylase, with multiple additional functions having already been investigated.

Acknowledgements

I would like to offer my sincere thanks to my entire supervisory team, both at the University of Birmingham and Maastricht University. My experience in Maastricht was unforgettable and I would like to thank my colleagues and friends over there, especially Timme van der Lugt who welcomed me so warmly. Of course, I also want to thank Dr Roger Godschalk and Professor Frederick van Schooten for welcoming me into the department and supporting me during my time there.

A special thanks to Dr Nik Hodges and all of the support he has offered me over the last four years. I consider myself truly lucky to have a supervisor whose door was always open to me (even when I just needed some reassurance and a chat!). I also want to thank Dr Alessio Perotti whose support as a colleague and friend was invaluable, in addition to all of my other colleagues at The University of Birmingham.

Moving to my more sentimental acknowledgements, I want to thank my parents for their continuing support and unwavering belief in me. Lastly, I want to thank my partner Daniel for being there for me every step of the way, despite the ever-changing miles between us. I would like to think I would have still got to this point without you… but there is no doubt it would have been significantly less fun.

Contents

	Page
Abstract	**I**
Acknowledgements	**II**
Contents	**III**
Abbreviations and acronyms	**IX**
List of figures	**XVII**
List of tables	**XX**
Chapter 1 | General introduction: The induction of genomic 8-oxoguanine and its subsequent repair *via* OGG1-initiated base excision repair	
1.1. Oxidative DNA damage	**2**
1.2. Reactive oxygen species	**6**
1.3. Antioxidants	**10**
1.4. Repair of oxidative DNA damage	**13**
1.4.1. Base excision repair pathway	**13**
1.4.2. BER glycosylases	**16**
1.5. 8-oxoguanine glycosylase-1	**17**
1.5.1. An introduction to the structure and function of 8-oxoguanine glycosylase-1	**17**
1.5.2. OGG1 variants	**21**
1.5.3. OGG1 regulation	**23**
1.5.3.1. Post-translational modifications	**23**
1.5.3.2. Protein-protein interactions	**26**
1.5.4. OGG1 and cellular signalling	**28**
1.5.4.1. The OGG1:8-oxoG complex	**28**
1.5.4.2. RAS GTPase and MAPK signalling	**30**
1.5.4.3. RAC1 GTPase and redox regulation	**33**
1.5.4.4. RHO GTPase and cytoskeletal changes	**35**

1.5.5. Other roles of OGG1 ..... **36**

1.5.5.1. OGG1 and inflammation **36**

1.5.5.2. OGG1 and epigenetic modulation **36**

1.6. Mitochondrial oxidative DNA damage **37**

1.7. Other DNA repair pathways **38**

1.7.1. DNA damage response network **38**

1.7.2. Mismatch repair pathway **40**

1.7.3. Homologous recombination & non-homologous end joining ... **40**

1.7.4. Nucleotide excision repair (NER) **41**

1.7.4.1. The NER pathway **41**

1.7.4.2. NER and oxidative DNA damage **44**

1.8. Aims and objectives **48**

Chapter 2 | Induction of apoptosis in *Ogg1*-null mouse embryonic fibroblasts following GSH depletion is independent of DNA damage

2.1. Introduction **50**

2.2. Materials and methods **53**

2.2.1. Cell culture **53**

2.2.2. Treatment of cells **54**

2.2.3. Polymerase chain reaction (PCR) **55**

2.2.4. Western blotting **57**

2.2.5. MTT assay **60**

2.2.6. Crystal violet viability assay **61**

2.2.7. CellTox™ Green cytotoxicity assay **62**

2.2.8. Measurement of apoptotic cells **63**

2.2.9. GSH determination assay **65**

2.2.10. Measurement of intracellular ROS **67**

2.2.11. Quantitative PCR **69**

2.2.12. Adenosine triphosphate measurements **71**

2.2.13. OGG1-modified comet assay **72**

2.2.14. Statistics **75**

2.3. Results **76**

2.3.1. m*Ogg1*$^{-/-}$ MEFs do not express *Ogg1* **76**

2.3.2. m*Ogg1*$^{-/-}$ MEFs show increased sensitivity to GSH depletion ... **78**

2.3.3. GSH depletion induces apoptosis in m*Ogg1*$^{-/-}$ MEFs **81**

2.3.4. BSO treatment results in a decrease in intracellular GSH **83**

2.3.5. Investigating intracellular ROS levels **86**

2.3.6. m*Ogg1*$^{-/-}$ MEFs possess elevated levels of intracellular ROS **88**

2.3.7. Differential antioxidant expression in MEFs **91**

2.3.8. There is no difference in the whole-cell ATP level of WT and m*Ogg1*$^{-/-}$ MEFs **92**

2.3.9. BSO-induced toxicity is unchanged when cellular metabolism is switched in favour of oxidative phosphorylation **93**

2.3.10. BSO treatment increases 8-oxoG sites in m*Ogg1*$^{-/-}$ MEFs **96**

2.3.11. Re-expression of *Ogg1* results in a partial rescue in viability following GSH depletion **98**

2.4. Discussion **101**

2.5. Conclusions and future work **108**

Chapter 3 | *Ogg1*-null mouse embryonic fibroblasts possess back-up mechanisms to prevent the genetic accumulation of 8-oxoguanine

3.1. Introduction **111**

3.2. Materials and methods **115**

3.2.1. Cell culture **115**

3.2.2. Treatment of cells **116**

3.2.3. DNA repair qPCR array **117**

3.2.4. Western blotting **120**

3.2.5. Enzyme modified comet assays **121**

3.2.6. NER-modified comet assay **123**

3.2.7. Thiobarbituric acid reactive substances assay **127**

3.2.8. Statistics **129**

3.3. Results **130**

3.3.1. 8-oxoG does not accumulate in m*Ogg1*$^{-/-}$ MEFs **130**

3.3.2. The qPCR array passed all quality control requirements **131**

3.3.3. Candidate back-up mechanisms to OGG1 were identified in m*Ogg1*$^{-/-}$ MEFs **133**

3.3.4. NER activity is elevated in m*Ogg1*$^{-/-}$ MEFs **136**

3.3.5. NEIL3 as a candidate back-up mechanism to OGG1 ..... **138**

3.3.6. Lipid peroxidation is increased in m*Ogg1*$^{-/-}$ MEFs **141**

3.3.7. A number of the genes that are upregulated in m*Ogg1*$^{-/-}$ MEFs were upregulated in WT MEFs following BSO treatment **142**

3.4. Discussion **144**

3.5. Conclusions and future work **151**

Chapter 4 | Investigating the cellular consequences of 8-oxoguanine treatment in WT and m*Ogg1*$^{-/-}$ MEFs

4.1. Introduction **153**

4.2. Materials and methods **158**

4.2.1. Cell culture **158**

4.2.2. Treatment of cells **159**

4.2.3. MTT assay **160**

4.2.4. RAS activation assay **162**

4.2.5. Crystal violet assay **167**

4.2.6. Measurement of intracellular ROS **169**

4.2.7. Acellular deoxyribose assay **170**

4.2.8. Statistics **171**

4.3. Results **172**

4.3.1. Neither 8-oxoG or 8-oxodG affects the viability of MEFs **173**

4.3.2. Activation of RAS following 8-oxoG treatment is dependent on OGG1 ..... **175**

4.3.3. Phenotype of WT and m*Ogg1*$^{-/-}$ MEFs in cell culture **178**

4.3.4. m*Ogg1*$^{-/-}$ MEFs detach at a faster rate than WT MEFs following incubation with trypsin-EDTA **181**

4.3.5. There are no differences in the rate of attachment between WT and m*Ogg1*$^{-/-}$ MEFs **183**

4.3.6. There are morphological differences between WT and m*Ogg1*$^{-/-}$ MEFs during attachment **185**

4.3.7. Neither 8-oxoG or 8-oxodG had an effect on the rate of detachment of MEFs **187**

4.3.8. 8-oxoG decreases intracellular ROS levels in WT MEFs **190**

4.3.9. 8-oxoG possesses antioxidant activity in an acellular model ... **192**

4.4. Discussion **194**

4.5. Conclusions and future work **199**

Chapter 5 | General discussion and concluding remarks

5.1. General discussion **201**

5.1.1. m*Ogg1*$^{-/-}$ MEFs and oxidative stress **201**

5.1.2. Induction of apoptosis in m*Ogg1*$^{-/-}$ MEFs following GSH depletion **204**

5.1.3. OGG1 backup mechanisms **205**

5.1.4. RAS-GTPase signalling and OGG1:8-oxoG **209**

5.2. Future work **210**

5.3. Concluding remarks **212**

Chapter 6 | References **213**

Chapter 7 | Appendix

7.1. Supplementary materials and methods **245**

7.1.1. Cell culture **245**

7.1.2. Protein determination assays **248**

7.2. Statistical analysis **250**

7.3. qPCR analysis **253**

7.4. qPCR volcano plots **271**

7.5. NEIL3 dot blot **273**

7.6. NEIL3 western blot analysis **274**

7.7. RAS-GTP ELISA optimisation **276**

7.8. Neither 8-oxoG and 8-oxodG had an effect in the rate of detachment of MEFs following a longer treatment duration **277**

7.9. Details of publications **280**

Abbreviations and acronyms

Abbreviations and acronyms are described here. However, those that are used only once within this thesis are not listed, as the full and proper name of these are detailed at the point of use.

Abbreviation	Full name
3'	Three Prime
5'	Five Prime
8-oxoA	8-oxoadenine
8-oxodG	8-oxo-2'-deoxyguanosine
8-oxoG	8-oxoguanine (7,8-dihydro-8-oxoguanine)
A	Adenine
Å	Angstrom
ANOVA	Analysis of Variance
AP	Apurinic/apyrimidinic
ATP	Adenosine Triphosphate
BER	Base Excision Repair
bp	Base Pair
BPDE	Benzo(a)pyrene diol epoxide
BSA	Bovine Serum Albumin
BSO	Buthionine Sulfoximine
C	Cytosine
°C	Degrees Celsius
cDNA	Complementary DNA
Ct	Cycle Threshold
CO_2	Carbon Dioxide
Cu	Copper
DDR	DNA Damage Response
(d)H_2O	(Distilled) Water
DMEM	Dulbecco's Modified Eagle Medium
DMSO	Dimethyl Sulfoxide
DNA	Deoxyribonucleic acid
dNTPs	Deoxyribonucleotide triphosphate

DPI	Diphenyleneiodonium
DSBs	Double-Strand Breaks
ds-	Double Stranded-
e-	Electron
ECACC	European Collection of Authenticated Cell Cultures
E. Coli	*Escherichia Coli*
ECM	Extracellular Matrix
EDTA	Ethylenediaminetetraacetic Acid
ELISA	Enzyme-Linked Immunosorbent Assay
EtBr	Ethidium Bromide
ETC	Electron Transport Chain
EtOH	Ethanol
FAD	Flavin Adenine Dinucleotide
FapyA	4,6-diamino-5-formamidopyrimidine
FapyG	2,6-diamino-4-hydroxy-5-formamidopyrimidine
FBS	Foetal Bovine Serum
FITC	Fluorescein Isothiocyanate
g	Relative Centrifugal Force
G	Guanine
GAP	Guanine Activating Protein
GDC	Genomic DNA Control
GDP	Guanine Diphosphate
GEF	Guanine Exchange Factor
GG-	Global Genome-
Gh	5-guanidinohydantoin
GMP	Guanine Monophosphate
GSH	Glutathione
GSSG	Glutathione Disulfide
GTP	Guanine Triphosphate
h	Hour
H_2O_2	Hydrogen Peroxide
H_2DCF-DA	Dichlorodihydrofluorescein diacetate
HEPES	4-2-hydroxyethyl-1-piperazineethanesulfonic acid

HNPCC	Hereditary Non-Polyposis Colorectal Cancer
HR	Homologous Recombination
HRP	Horseradish peroxide
IC50	Half Maximal Inhibitory Concentration
KD	Equilibrium Dissociation Constant
kDa	Kilodalton
LMA	Low Melting Agarose
MAPK	Mitogen-Activated Protein Kinase
MDA	Malondialdehyde
MEF	Mouse Embryonic Fibroblast
MeoH	Methanol
m*Ogg1*$^{-/-}$	m*Ogg1* null
min	Minute
MMR	Mismatch Repair
Mn	Manganese
mRNA	Messenger Ribonucleic Acid
mtDNA	Mitochondrial DNA
MTT	3-(4, 5-dimethylthiazol -2-yl)-2,5-diphenyltetrazolium Bromide
N	Sample Size
NAD	Nicotinamide Adenine Dinucleotide
NADPH	Nicotinamide adenine dinucleotide phosphate
NER	Nucleotide Excision Repair
NHEJ	Non-Homologous End Joining
NMA	Normal Melting Agarose
ns	Non Significant
NTC	Non-Template Control
O_2	Molecular Oxygen
OGG1:8-oxoG	OGG1:8-oxo-G signalling complex
***O*-GlcNAc**	*O*-GlcNAc Transferase
OGT	*O*-linked β-N-acetyl-glucosamine
OPT	*o*-Phthalaldehyde
p	Statistical *p*-value
p-	Phosphorylated-

PAGE	Polyacrylamide Gel Electrophoresis
PBS	Phosphate Buffered Saline
PCR	Polymerase Chain Reaction
PDT	Population Doubling Time
PFA	Paraformaldehyde
pH	Potential of Hydrogen
PI	Propidium Iodide
PPC	PCR Positive Control
PS	Phosphatidylserine
PTM	Post-Translational Modification
PVDF	Polyvinylidene Difluoride
Q	Ubiquinone
QC	Quality Control
RNA	Ribonucleic Acid
ROS	Reactive Oxygen Species
rpm	Revolutions per Minute
RT	Room Temperature
RTC	Reverse Transcription Control
RTK	Receptor Tyrosine Kinase
S. cerevisiae	*Saccharomyces cerevisiae*
SD	Standard Deviation
SDS	Sodium Dodecyl Sulphate
Sec	Second
SMA	Smooth Muscle Actin
SNP	Single Nucleotide Polymorphism
Sp	Spiroiminodihydantoin
ss-	Single Stranded-
T	Thymine
TBST	Tris-Buffered Saline with Tween
TBA	Thiobarbituric Acid
TBARS	Thiobarbituric Acid Reactive Substances
TCA	Trichloroacetic Acid
TC-	Transcription Coupled-

Tg	Thymine Glycol
TI	Tail Intensity
UV	Ultraviolet
WT	Wild-type
XP	Xeroderma Pigmentosum
Zn	Zinc

The full name of genes and proteins are described below. These are stated within text for key genes/proteins, however any other gene/protein names can be found listed here (note only genes of interest from the qPCR profiler array are included instead of all 84-DNA repair genes).

Abbreviation	Full name
AAG	Alkyladenine DNA glycosylase
ABL	Abelson Tyrosine Kinase
ACTB	Beta (β) Actin
APE1	Apurinic/apyrimidinic endonuclease-1
BRIP1	BRCA1 Interacting Protein C-Terminal Helicase 1
CAT	Catalase
CBP	CREB Binding Protein
CDK4	Cyclin Dependent Kinase-4
CSA/B	Cockayne Syndrome A/B
CUX1/2	Cut-like Homeobox-1/2
Cyt C	Cytochrome C
DUOX	Dual Oxidase
EGF	Epidermal Growth Factor
ERCC1	Excision Repair Cross-Complementing-1
ERCC2	Excision Repair Cross-Complementing-2 (also referred to as XPD)
ERCC3	Excision Repair Cross-Complementing-3 (also referred to as XPB)
ERCC4	Excision Repair Cross-Complementing-4 (also referred to as XPF)
ERCC5	Excision Repair Cross-Complementing-5 (also referred to as XPG)
ERK	Extracellular Regulated Kinase
FEN1	Flap Endonuclease-1
FPG	Formamidopyrimidine-DNA glycosylase
GAPDH	Glyceraldehyde 3-phosphate dehydrogenase
ϒ-GCS	ϒ-Glutamylcysteine Synthetase
GPX	Glutathione Peroxidase
GR	Glutathione Reductase
HRPT1	Hypoxanthine Phosphororiboseyltransferase-1

HSP90AB1	Heat Shock Protein 90 Alpha Family Class B Member-1
LIG1/3	Ligase 1/3
MGMT	O-6 Methylguanine-DNA Methyltransferase
MEK	Mitogen Activated Protein Kinase
MLH1	MutL Homolog-1
MPG	N-methyl Purine DNA Glycosylase
MSH2/5/6	MutS Homolog-2/5/6
MTH1	MutT Homolog
MUTYH/MYH	MutY Homolog
NF-κB	Nuclear Factor Kappa-Light-Chain-Enhancer
NEIL1/2/3	Nei-Like DNA Glycosylase-1/2/3
NTHL1	Nth-Like DNA Glycosylase-1
NOX	NADPH Oxidase
OGG1	8-oxoguanine glycosylase-1
P300	E1A Binding Protein P300
PARP1	Poly [ADP-ribose] Polymerase-1
PCNA	Proliferating Cell Nuclear Antigen
PKC	Protein Kinase C
PMS1/2	Post-Meiotic Segregation-1/2
POL α/δ/ε	DNA Polymerase α/δ/ε
PRKDC	Protein Kinase DNA-Activated Catalytic Subunit
RAC1	Ras-related C3 Botulinum Toxin Substrate-1
RAD23B	RAD23 Homolog B
RAD51D	RAD51 Paralog D
RAF	RAF Proto-Oncogene
RAS	Rat Sarcoma Viral Oncogene Homolog
RFC	Replication Factor C
RHO	Ras Homolog Family Member
RPA	Replication Protein A
SIRT2	Sirtuin-2
SLK	STE20 Like Kinase
SOD	Superoxide Dismutase
TDG	Thymine DNA Glycosylase

TFIIH	Transcription Factor II H
TNF-α	Tumour Necrosis Factor-α
TOP3B	DNA Topoisomerase III Beta
UDG	Uracil DNA Glycosylase
XRCC1/5	X-ray Repair Cross Complementing-1/5
XP(A-G)	Xeroderma Pigmentosum Type (A-G)

List of Figures

Figure	Description	Page
1.1.	The generation of 8-oxoG and FapyG lesions	**3**
1.2.	The structure of common oxidative DNA modifications	**4**
1.3.	Sp and Gh are the major oxidation products of 8-oxoG	**5**
1.4.	Superoxide anion, hydrogen peroxide, and the hydroxyl radical	**6**
1.5.	Endogenous and exogenous sources of ROS	**7**
1.6.	The ETC within the mitochondria consists of four multi-protein complexes	**8**
1.7.	The structure of reduced GSH and oxidised GSH, which is known as GSSG	**11**
1.8.	The BER pathway	**14**
1.9.	OGG1- and MUTYH- initiated repair of 8-oxoG	**18**
1.10.	The crystal structure of OGG1	**20**
1.11.	GTPases shuttle between an inactive (GDP-bound) and an active (GTP- bound) state	**29**
1.12.	The MAPK pathway	**31**
1.13.	Different repair pathways within a cell form the DDR network	**39**
1.14.	The NER pathway	**42**
2.1.	The hOGG1-modified comet assay methodology	**72**
2.2.	m*Ogg1*$^{-/-}$ MEFs do not express *Ogg1*	**77**
2.3.	BSO-induced cytotoxicity is observed in m*Ogg1*$^{-/-}$ MEFs but not in WT MEFs	**79**
2.4.	BSO treatment induces apoptosis in m*Ogg1*$^{-/-}$ MEFs	**82**
2.5.	BSO treatment depletes intracellular GSH levels	**84**
2.6.	Intracellular ROS was investigated using the fluorescent probe H_2DCF-DA	**87**
2.7.	m*Ogg1*$^{-/-}$ MEFs possess elevated levels of intracellular ROS	**89**
2.8.	The expression of antioxidant genes was measured using qPCR	**91**
2.9.	Whole-cell ATP levels were measured in WT and m*Ogg1*$^{-/-}$ MEFs	**92**

2.10. Viability comparison of WT and m*Ogg1*$^{-/-}$ MEFs cultured in the presence of glucose or galactose **94**

2.11 The levels of 8-oxoG were measured using a hOGG1-modified comet assay **97**

2.12. The viability of m*Ogg1*$^{-/-}$ MEFs following GSH depletion is increased through *Ogg1* re-expression **99**

2.13. Proposed model explaining the induction of apoptosis in m*Ogg1*$^{-/-}$ MEFs..... **102**

2.14. The elevation of ROS in m*Ogg1*$^{-/-}$ MEFs explained by an increased production of mitochondrial superoxide combined with changes in antioxidant expression **106**

3.1. G, 8-oxoG, Gh and Sp **113**

3.2. The methodology for the NER-modified comet assay is displayed **124**

3.3. There is no difference in the basal level of 8-oxoG in WT and m*Ogg1*$^{-/-}$ MEFs **130**

3.4. Quality control qPCR **132**

3.5. NER is upregulated in m*Ogg1*$^{-/-}$ MEFs **137**

3.6. NEIL3 is upregulated in m*Ogg1*$^{-/-}$ MEFs **139**

3.7. Lipid peroxidation is increased in m*Ogg1*$^{-/-}$ MEFs..... **141**

3.8. The genes upregulated in WT MEFs following BSO treatment are displayed alongside the corresponding changes measured in untreated m*Ogg1*$^{-/-}$ MEFs **143**

3.9. Substrate excision in NER is primarily performed by ERCC1, ERCC4 and ERCC5 .... **146**

3.10. Proposed model for the NEIL3-mediated repair of 8-oxoG oxidation products **150**

4.1. The RAS GTPase superfamily is divided into five subfamilies..... **154**

4.2. The structure of 8-oxoG and 8-oxodG **157**

4.3. The principle of the RAS-GTP ELISA is displayed **166**

4.4. 8-oxoG and 8-oxodG treatment does not affect the viability of MEFs **173**

4.5. Active RAS was measured using a RAS-GTP specific ELISA **176**

4.6. Cell morphology and growth kinetics of WT and m*Ogg1*$^{-/-}$ MEFs **179**

4.7. m*Ogg1*$^{-/-}$ MEFs detach at a faster rate than WT MEFs **182**

4.8. The attachment of WT and m*Ogg1*$^{-/-}$ MEFs occurs at the same rate..... **184**

4.9. Morphological differences exist between WT and m*Ogg1*$^{-/-}$ MEFs in the initial period following the seeding of cells **185**

4.10. Neither 8-oxoG or 8-oxodG had an effect on the rate of detachment of cells **188**

4.11. Intracellular ROS was measured using the redox sensitive probe H_2DCF-DA **191**

4.12. Acellular deoxyribose experiments indicate that 8-oxoG possesses antioxidative capabilities but that 8-oxodG does not **193**

4.13. The OGG1:8-oxoG signalling molecule **194**

7.1. Example BSA standard curve of a Bradford assay **248**

7.2. Volcano plots produced for qPCR gene expression analysis **271**

7.3. NEIL3 dot blot using different dilutions of hNEIL3 ..... **273**

7.4. The bands generated in the NEIL3 western blot were analysed using ImageJ **275**

7.5. Determination of optimal protein concentration for RAS-GTP experiments **276**

7.6. Neither treatment with 8-oxoG or 8-oxodG had an effect on the rate of detachment following incubation with trypsin EDTA (extended treatment) **278**

List of Tables

Table	Description	Page
1.1.	OGG1 post-translational modifications affect OGG1 activity	**23**
1.2.	Protein-protein interactions are capable of affecting OGG1 activity	**26**
2.1.	*Ogg1* PCR conditions	**56**
2.2.	Antibodies used	**59**
2.3.	Annexin V-FITC and PI detection of apoptotic cells	**64**
2.4.	Taqman qPCR probes	**70**
2.5.	qPCR conditions	**70**
3.1.	The DNA repair genes included in the qPCR profiler array	**118**
3.2.	qPCR conditions for RT^2 profiler array	**119**
3.3.	Antibodies used	**120**
3.4.	Gene expression fold-changes in m*Ogg1*$^{-/-}$ MEFs compared to WT MEFs	**134**
3.5.	Gene expression fold-changes in WT MEFs following BSO treatment	**135**
4.1	Preparation of RAS-GTP ELISA reagents	**162**
7.1.	Mycoplasma PCR conditions	**247**
7.2.	Details of statistical analysis	**250**
7.3.	ΔCt values of WT control samples	**253**
7.4.	Fold-change values of m*Ogg1*$^{-/-}$ MEFs compared to WT MEFs	**256**
7.5.	Fold-change values of WT MEFs following BSO treatment	**261**
7.6.	Fold-change values of m*Ogg1*$^{-/-}$ MEFs following BSO treatment	**266**

1

General introduction | The induction of genomic 8-oxoguanine and its subsequent repair *via* OGG1-initiated base excision repair

Maintaining the integrity of the genome is imperative within the cells of the human body, with DNA constantly at risk of damage from both exogenous and endogenous sources. It is estimated that each cell will encounter thousands of DNA-damaging reactions every day, with DNA modifications capable of generating mutations and contributing to genomic instability. Therefore, in order to respond to DNA damage, a complex and thorough DNA repair system exists within cells.

1.1. Oxidative DNA damage

DNA can be damaged through a number of different mechanisms, and different sources of damage will result in the formation of different types of DNA damage (Hansen and Kelley, 2000; Lindahl and Barnes, 2000). One major type of DNA damage is oxidative modification, with a number of different oxidative DNA modifications having been discovered. The most extensively studied of these modifications is a guanine lesion named 7,8-dihydro-8-oxoguanine (8-oxoG). This modification is understood to be one of the most prevalent forms of oxidative DNA damage, with the presence of 8-oxoG within the genome being considered a hallmark of oxidative stress. Therefore 8-oxoG can be utilised as a marker of oxidative stress and oxidative stress-linked diseases (Shigenaga, Gimeno and Ames, 1989; Bjelland and Seeberg, 2003; Evans, Dizdaroglu and Cooke, 2004; Wu *et al.*, 2004; Poulsen *et al.*, 2014).

As with guanine, 8-oxoG is able to form a stable Watson-Crick base pair with cytosine. However, this oxidation also allows the base to alternatively form a stable Hoogsteen base pair with adenine (Gannett and Sura, 1993; Wang, Kreutzer and Essigmann, 1998). This mispairing of 8-oxoG with adenine can therefore lead to GC -> TA transversions, leading to mutations that are commonly found in a host of different diseases. This finding led to a plethora of studies involving 8-oxoG, which have since linked oxidative stress and 8-oxoG to neurodegenerative diseases, cardiovascular disease, and multiple cancers (Bjelland and Seeberg, 2003; Cooke *et al.*, 2003; Evans, Dizdaroglu and Cooke, 2004; Benz and Yau, 2008; Kryston *et al.*, 2011; Cardozo-Pelaez, Sanchez-Contreras and Nevin, 2012; Helleday, Eshtad and Nik-

Zainal, 2014; Jeggo, Pearl and Carr, 2016). One explanation for the high prevalence of 8-oxoG is that guanine has the lowest redox potential of the four DNA bases. Therefore, guanine is easily oxidised (Margolin *et al.*, 2006; Paleček and Bartošík, 2012; Fleming and Burrows, 2017). This oxidation of guanine produces a hydroxyl radical intermediate, which can generate either 8-oxoG or 2,6-diamino-4-hydroxy-5-formamidopyrimidine (FapyG), depending on reaction conditions. Oxidation results in the production of 8-oxoG, whereas reduction results in the production of FapyG (Figure **1.1**.). Similarly to 8-oxoG, FapyG is capable of forming a base pair with adenine, subsequently causing GC -> TA transversions (Wiederholt and Greenberg, 2002; Kalam *et al.*, 2006; Klungland and Bjelland, 2007; Delaney *et al.*, 2012).

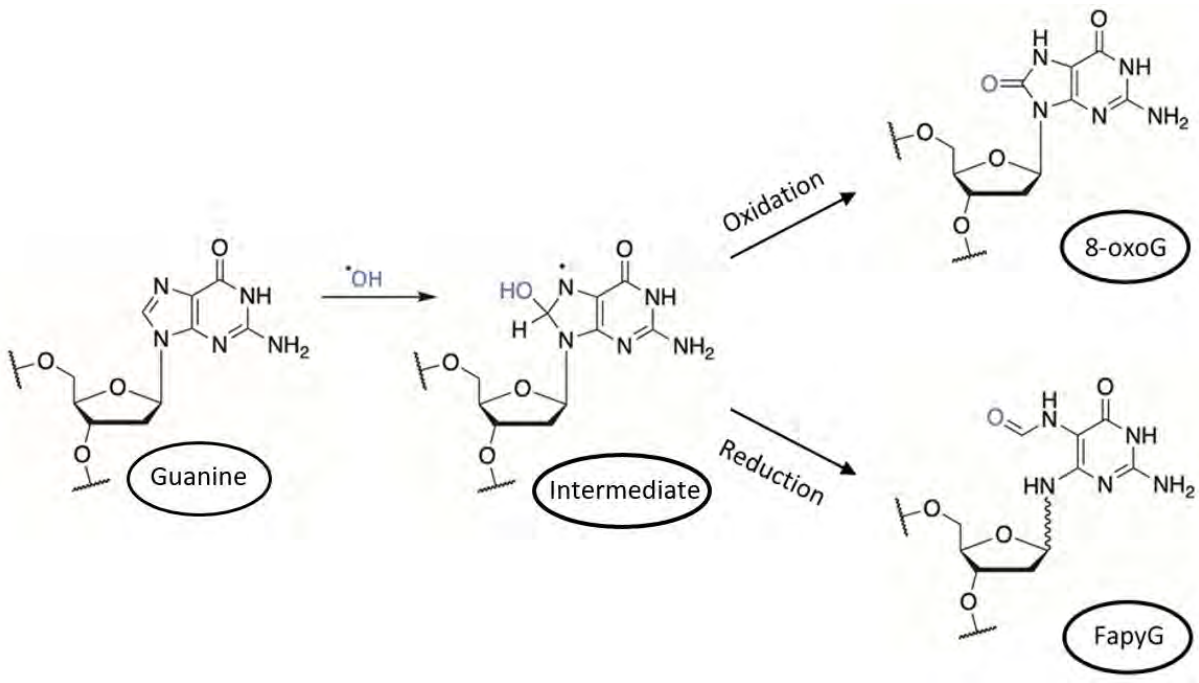


Figure 1.1. The generation of 7, 8-dihydro-8-oxoguanine (8-oxoG) and 2, 6-diamino-4-hydroxy-5-formamidopyrimidine (FapyG) lesions. A hydroxyl radical adduct is produced following the oxidation of guanine, which then allows for the generation of either 8-oxoG or FapyG. Under oxidative conditions, 8-oxoG is produced; whereas under reductive conditions, FapyG is produced (Delaney *et al.*, 2012)

The structure of 8-oxoG and FapyG are shown in Figure **1.2**. alongside other common oxidative modifications (Wang, Kreutzer and Essigmann, 1998; Bjelland and Seeberg, 2003; Cooke *et al.*, 2003; Slupphaug, Kavli and Krokan, 2003; Evans, Dizdaroglu and Cooke, 2004; Cadet and Wagner, 2013). Interestingly, the distribution of oxidative DNA modifications does not appear random. Instead, genome-wide profiling revealed a high frequency of 8-oxoG in regions of the genome that are devoid of protein-coding genes. 8-oxoG was found to be especially abundant in guanine-rich regions within promotors, enhancers, and telomeres; including at CpG islands (Yoshihara *et al.*, 2014; Sampath and Lloyd, 2019). Guanine residues towards the 5' end of a sequence of guanines are preferentially oxidised, with this partly due to the migration of a radical cation to the guanine that has the lowest ionisation potential. Here, the radical cation becomes trapped, resulting in the formation of the final oxidation product (Hall, Holmlin and Barton, 1996; Margolin *et al.*, 2006; Ba, Aguilera-Aguirre, *et al.*, 2014).

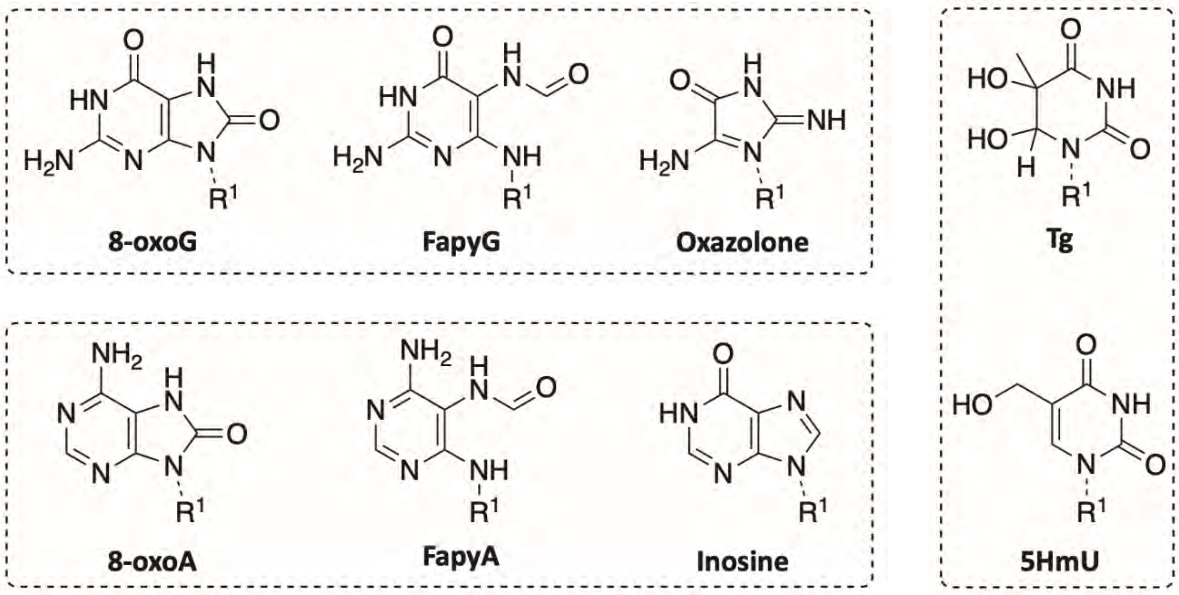
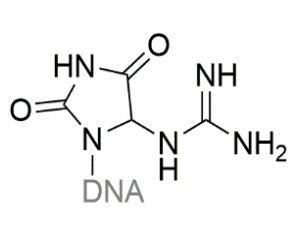
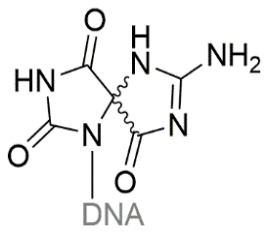


Figure 1.2. The structure of common oxidative DNA modifications. These include 8-oxoguanine (8-oxoG), 2,6-diamino-4-hydroxy-5-formamidopyrimidine (FapyG), oxazolone, thymine glycol (Tg), 8-oxoadenine (8-oxoA), 4,6-diamino-5-formamidopyrimidine (FapyA), inosine, and 5-hydroxymethyluracil (5HmU).

As mentioned, guanine has a low redox potential. Often the products of guanine-oxidation possess even lower redox potentials, deeming these products vulnerable to further oxidation. This is true for 8-oxoG, which possesses a significantly lower redox potential than guanine, which allows 8-oxoG to be further oxidised with relative ease (Henderson *et al.*, 2002; Fleming and Burrows, 2017). The primary products of this oxidation of 8-oxoG are two complex DNA structures; spiroiminodihydantoin (Sp) and 5-guanidinohydantoin (Gh), which are both displayed in Figure **1.3**. These lesions are highly mutagenic and studies have also shown that they have the ability to stall transcription (Henderson *et al.*, 2002; Suzuki and Ohshima, 2002; Kornyushyna and Burrows, 2003; Niles, Wishnok and Tannenbaum, 2004; Yu *et al.*, 2005; Cui *et al.*, 2013; Norabuena *et al.*, 2016; Martin *et al.*, 2017)



Spiroiminodihydantoin



5-guanidinohydantoin

Figure 1.3. Spiroiminodihydantoin (Sp) and 5-guanidinohydantoin (Gh) are the major oxidation products of 8-oxoG. Both lesions have been shown to be highly mutagenic (Kornyushyna and Burrows, 2003).

1.2. Reactive oxygen species

The main source of oxidative DNA damage is reactive oxygen species (ROS), a term which describes an oxygen-derived and pro-oxidant molecule (Kohen and Nyska, 2002). Three of the most abundant of these species present within a cell are displayed in Figure **1.4.** These species can be radical or non-radical, however the unpaired electrons of a radical species will result in a more reactive and unstable species. These radical species are therefore more likely to directly react with cellular macromolecules (Halliwell and Aruoma, 1991; Kohen and Nyska, 2002; Cadet *et al.*, 2012). Despite the potential risk of reaction between ROS and biological molecules, low levels of ROS are actually considered beneficial as they are necessary for certain cellular functions, including immune function, cellular signalling and redox regulation (Thannickal and Fanburg, 2000; Forman and Torres, 2001; Lambeth, 2004; Fisher, 2009; Bhattacharya, 2015).

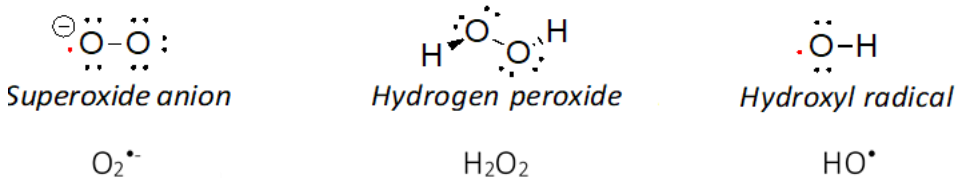


Figure 1.4. Superoxide anion ($O_2^{\bullet-}$), hydrogen peroxide (H_2O_2) and the hydroxyl radical ($HO^{\bullet}$). The structure of these common reactive oxygen species (ROS) are displayed and unpaired electrons are highlighted in red. These species represent just a small range of the different reactive species that can exist within a cell (Cadet *et al.*, 2012; Bhattacharya, 2015).

Intracellular ROS can arise from endogenous and exogenous sources, with some of these summarised in Figure **1.5.** A primary endogenous source of ROS is mitochondria, however, alternative sources include peroxisomes and phagocytic cells. Alternatively, ROS can arise from exogenous sources, including pollution, alcohol intake and tobacco smoke (Kohen and Nyska, 2002; Lambeth, 2004; Bertram *et al.*, 2006; Indo *et al.*, 2007; Murphy, 2009; Bhattacharya, 2015; Phaniendra, Jestadi and Periyasamy, 2015).

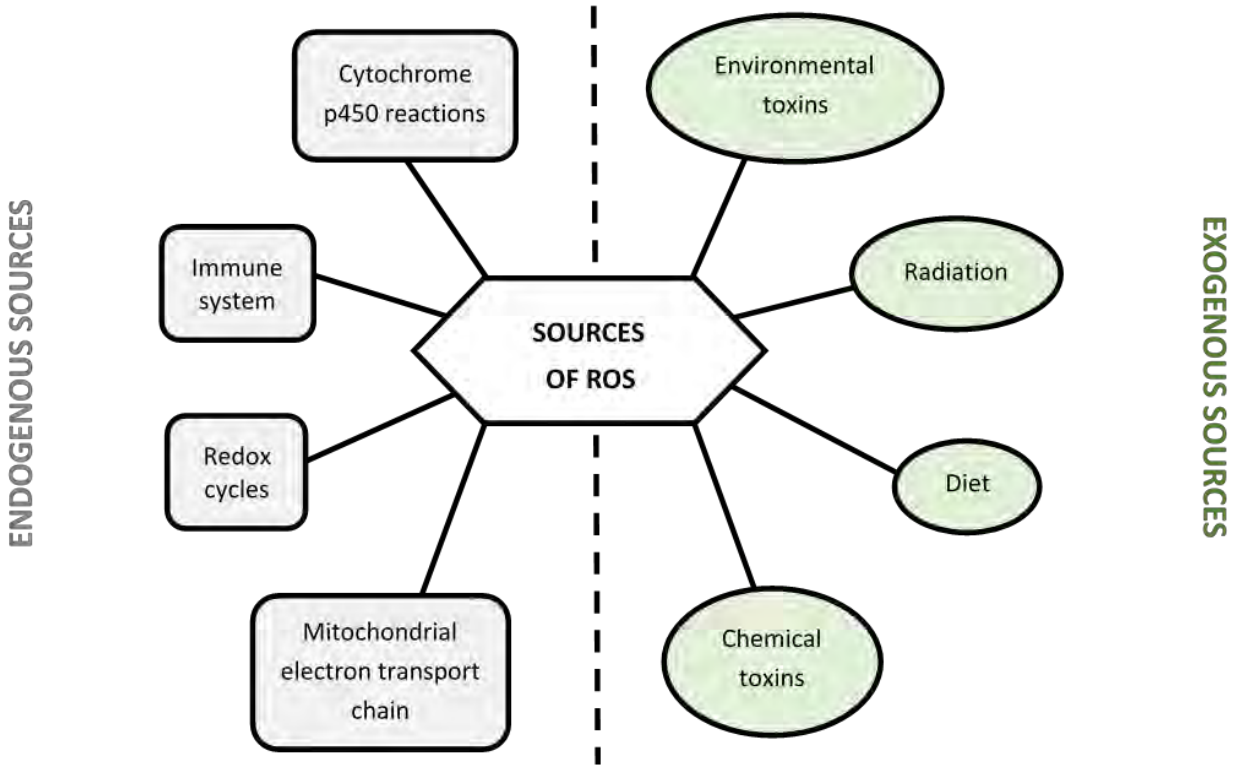


Figure 1.5. Endogenous and exogenous sources of ROS. Endogenous sources usually consist of cellular pathways that produce ROS as a by-product, *e.g.* mitochondrial energy production (and the electron transport chain), immune functions such as inflammation, redox cycles, and cytochrome p450 reactions. Exogenous sources include diet, chemical toxins (*e.g.* products generated from smoking), environmental toxins (*e.g.* exposure to heavy metals), and radiation (*e.g.* ultraviolet radiation).

A major source of intracellular ROS is the mitochondria, which releases ROS during energy production *via* the electron transport chain (ETC) (Figure **1.6.**), with superoxide (O_2•-) arising from both complex I and complex III (Bertram *et al.*, 2006; Indo *et al.*, 2007; Murphy, 2009). The superoxide species has a relatively low reactivity towards biomolecules. However, the antioxidant superoxide dismutase (SOD) catalyses the dismutation of superoxide into hydrogen peroxide (H_2O_2), which is capable of crossing cellular-membranes in order to travel to other compartments of the cell (Antunes and Cadenas, 2000; Makino *et al.*, 2004; Bienert, Schjoerring and Jahn, 2006; Fisher, 2009; Abreu and Cabelli, 2010; Hempel, Carrico

and Melendez, 2011; Cadet *et al.*, 2012). Although H_2O_2 does not directly react with DNA, it does produce hydroxyl radicals *via* a Haber-Weiss reaction, with hydroxyl radicals highly reactive towards biomolecules (Winterbourn, 1981; Sato *et al.*, 1992; Hislop and Bolton, 1999; Maier and Chan, 2002; Bienert, Schjoerring and Jahn, 2006; Cadet *et al.*, 2012). This example demonstrates how the presence of different reactive species, including non-radical species, will result in subsequent modifications of biomolecules.

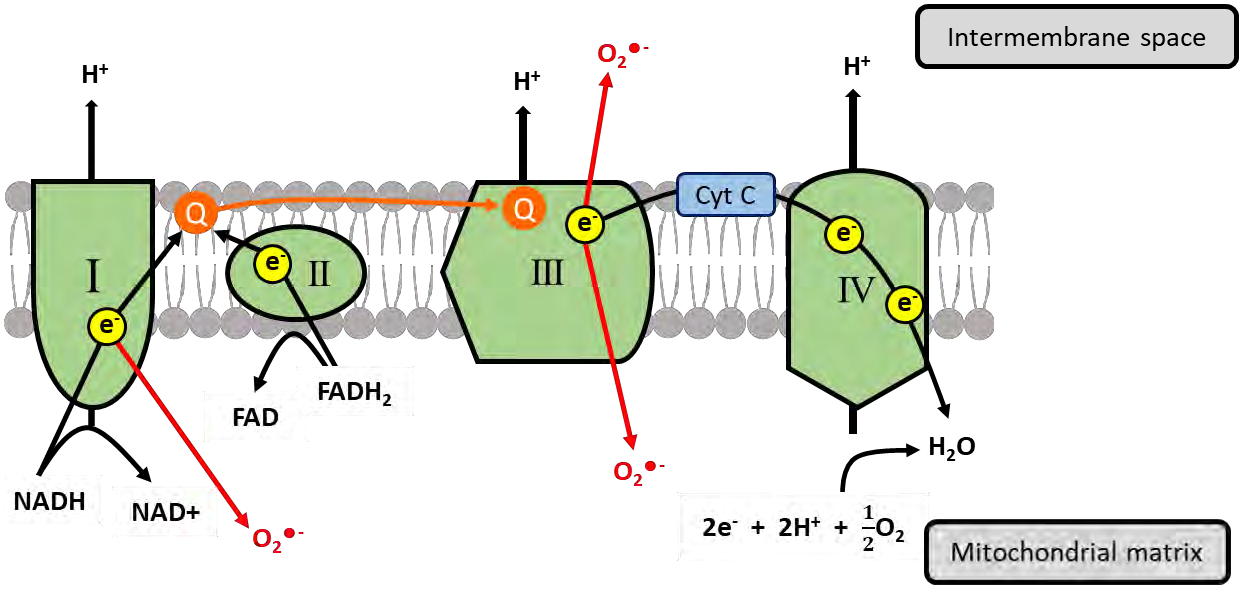


Figure 1.6. The electron transport chain (ETC) within the mitochondria consists of four multi-protein complexes (I – IV). The oxidation of nicotinamide adenine dinucleotide (NADH -> NAD) and flavin adenine dinucleotide ($FADH_2$ -> FAD) result in the release of electrons (e^-), which are subsequently shuttled through the chain from high to low energy. NADH releases an electron to complex I, whereas $FADH_2$ is a poorer electron donator that instead releases an electron to complex II. Both complexes proceed to shuttle these electrons to a small electron carrier called ubiquinone (Q), which delivers the electrons to complex III. The electrons are then shuttled through complex III and delivered to another electron carrier, cytochrome C (Cyt C), which carries the electrons to complex IV. Here, the electrons are transferred to molecular oxygen, generating energy to pump protons from the mitochondrial matrix into the intermembrane space, thereby establishing an electrochemical gradient.

Numerous biomolecules within the cell are vulnerable to modification by ROS. These biomolecules include DNA, free nucleotides, lipids and proteins; with oxidative DNA modifications capable of causing mutations and genomic instability (Cooke *et al.*, 2003; Evans, Dizdaroglu and Cooke, 2004). Furthermore free nucleotides can be oxidised within the nucleotide pool and subsequently incorporated into DNA, which presents yet another route in which mutations can arise in the genome as a result of ROS (Fujikawa *et al.*, 1999; Fotouhi *et al.*, 2011). The repair of these oxidative DNA modifications will be fully discussed further on (*refer to* the later chapter, **1.4.**).

The oxidation of proteins rather than DNA results in a different range of consequences, with such protein modifications having been linked to ageing and disease (Levine and Stadtman, 2001; Shringarpure and Davies, 2002; Korolainen *et al.*, 2006; Chakravarti and Chakravarti, 2007). The majority of oxidatively modified proteins are successfully removed during protein turnover, during which these modified proteins will be degraded by the proteasome (Davies, 2001; Shringarpure and Davies, 2002; Shringarpure *et al.*, 2003). However, studies show that severe oxidative stress can cause more extensive protein modifications, which may not be recognised by the proteasome, and additionally it has been shown that proteasome action is significantly reduced in ageing cells (Davies, 2001; Shringarpure and Davies, 2002). Therefore, some of these modified proteins will go unrecognised by the proteasome and the cellular accumulation of such proteins is thought to contribute to cellular ageing and senescence (Levine and Stadtman, 2001; Shringarpure and Davies, 2002; Chakravarti and Chakravarti, 2007).

1.3. Antioxidants

Although a steady-state production of ROS is important within a cell, it is critical that there is not an excessive level of intracellular ROS present. To prevent this, cells possess a number of antioxidants that detoxify these species. Therefore, the term oxidative stress does not refer to the simple presence of intracellular ROS (as these species are necessary) but instead refers to a level of intracellular ROS that exceeds the antioxidant activity of the cell. This imbalance allows these species to subsequently react with biomolecules within the cell (Sies, 1991; Rizzo *et al.*, 2010; Sies, 2015). The antioxidant activity of cells can be increased by increasing an individual's dietary intake of antioxidants, including an increased intake of vitamins, caffeine, and flavonoids (Husain, Cillard and Cillard, 1987; O'Byrne *et al.*, 2002; Vivekananthan *et al.*, 2003; Egert and Rimbach, 2011; Kozłowska and Szostak-Wegierek, 2014). Furthermore, the efficiency of using dietary antioxidants as treatments for certain diseases has been investigated in multiple studies; although evidence to show the effectiveness of such treatment is very lacking, and many challenges have been identified (Moosmann and Behl, 2002; Vivekananthan *et al.*, 2003; Devasagayam *et al.*, 2004; Singh, Sharad and Kapur, 2004; Raghavamenon *et al.*, 2009).

The antioxidant defence of a cell consists of a diverse group of proteins. With respect to this thesis; antioxidants of particular interest include superoxide dismutase (SOD), glutathione peroxidase (GPX), and catalase (CAT) (Michiels *et al.*, 1994; Devasagayam *et al.*, 2004). SOD enzymes convert superoxide into H_2O_2 and oxygen, performing this through sequential reduction and oxidation reactions. To date, there are three isoforms of SOD identified in humans (SOD 1-3), which differ in cellular localisation and metal ion (Maier and Chan, 2002; Zelko, Mariani and Folz, 2002; Abreu and Cabelli, 2010). A subsequent reaction, catalysed by CAT, then converts H_2O_2 into water and oxygen (Percy, 1984; Michiels *et al.*, 1994). Another important player in the detoxification of ROS is glutathione (GSH), a tripeptide consisting of cysteine, glutamate and glycine. GSH is able to donate an electron to reactive species through its sulfhydryl group, thereby neutralising the species and deeming them unable to react with cellular

macromolecules. This reaction can be spontaneous but can also be catalysed by GPX, with the oxidation of two molecules of GSH producing one molecule of glutathione disulfide (GSSG) (Figure **1.7.**) (Michiels *et al.*, 1994; Dickinson and Forman, 2002; Forman, Zhang and Rinna, 2009; Zitka *et al.*, 2012).

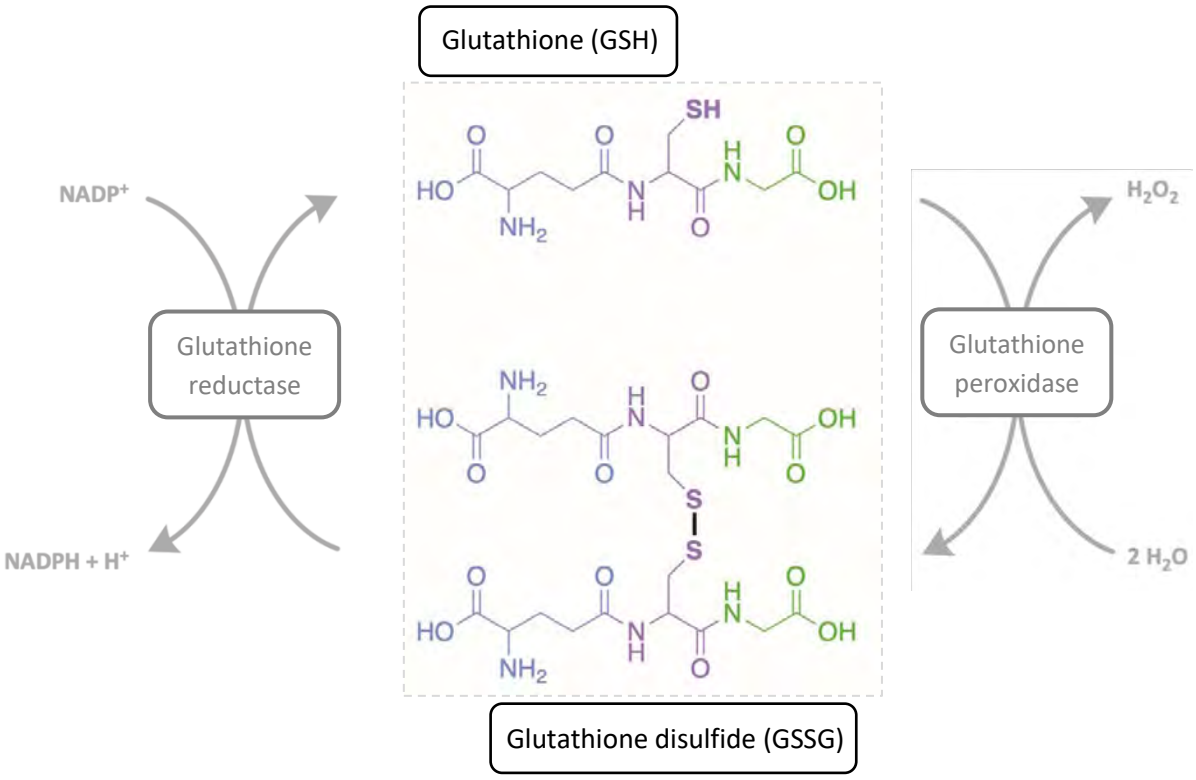


Figure 1.7. The structure of reduced glutathione (GSH) and oxidised glutathione, which is known as glutathione disulfide (GSSG). GSH is a tripeptide consisting of the amino acids; glutamate, cysteine, and glycine. A molecule of GSH is capable of donating one electron to a reactive molecule. Following this, a disulfide bond can form between two oxidised molecules of GSH to generate one molecule of GSSG. The reaction is catalysed by glutathione peroxidase (GPX) whereas the reduction of GSSG to GSH is catalysed by glutathione reductase (GR).

Therefore, the GSH:GSSG ratio of a cell can be used as a measure of oxidative stress, with this ratio decreasing as available GSH molecules are oxidised, generating GSSH. It is estimated that under normal conditions, the GSH:GSSG ratio within the cytoplasm of cells is likely to exceed 100:1. This ratio is known to significantly decrease in conditions of oxidative stress, reaching ratios of less than 10:1 across different models (Dalle-Donne *et al.*, 2008; Zitka *et al.*, 2012; Giustarini *et al.*, 2017). It has therefore been suggested that this ratio, within the blood of patients, could be utilised as a biomarker for oxidative stress (Rossi *et al.*, 2006; Zitka *et al.*, 2012).

Healthy cells maintain a high level of cellular GSH through an enzymatic synthetic pathway, with significant subcellular GSH pools having been identified in the cytoplasm, mitochondria and nucleus (Edgren and Révész, 1987; Green *et al.*, 2006). It is possible to experimentally deplete GSH in cells through the inhibition of this pathway, with one example of this being the treatment of cells with buthionine sulfoximine (BSO). The mechanism of BSO is the inhibition of ϒ-glutamylcysteine synthetase (ϒ-GCS), which is the enzyme involved in the rate-limiting step of GSH synthesis. This therefore prevents cells from replenishing GSH stores once they have been depleted, allowing further investigation of the cellular effects induced by oxidative stress (Griffith, 1982; Drew and Miners, 1984; Edgren and Révész, 1987; Dickinson and Forman, 2002; Forman, Zhang and Rinna, 2009; Lu, 2014).

1.4. Repair of oxidative DNA damage

1.4.1. Base excision repair pathway

Despite antioxidant activity, reactions between ROS and cellular macromolecules are inevitable. This will result in a level of oxidative DNA modifications across the genome, which must be recognised and repaired prior to replication. The base excision repair (BER) pathway is considered the primary mechanism for the repair of these modifications (David, O'Shea and Kundu, 2007).

The BER pathway has a broad range of substrates, including many oxidative modifications. Generally speaking, the BER pathway is responsible for the repair of non-helix distorting modifications, usually spanning a short length of 1-13 nucleotides (Kim and Wilson, 2012; Krokan and Bjørås, 2013). The pathway consists of the recognition and subsequent removal of the modification *via* specific DNA glycosylases. This results in the production of an apurinic/apyrimidinic (AP) site, which is subsequently removed once the DNA backbone has been cleaved. Here in the pathway, depending on the size of the DNA modification, the DNA will be repaired either by short- or long- patch repair (Dodson, Michaels and Lloyd, 1994; Krokan, Standal and Slupphaug, 1997; Fortini *et al.*, 1999; Sattler *et al.*, 2003; David, O'Shea and Kundu, 2007; Robertson *et al.*, 2009; Kim and Wilson, 2012; Krokan and Bjørås, 2013). This process has been summarised in Figure **1.8**.

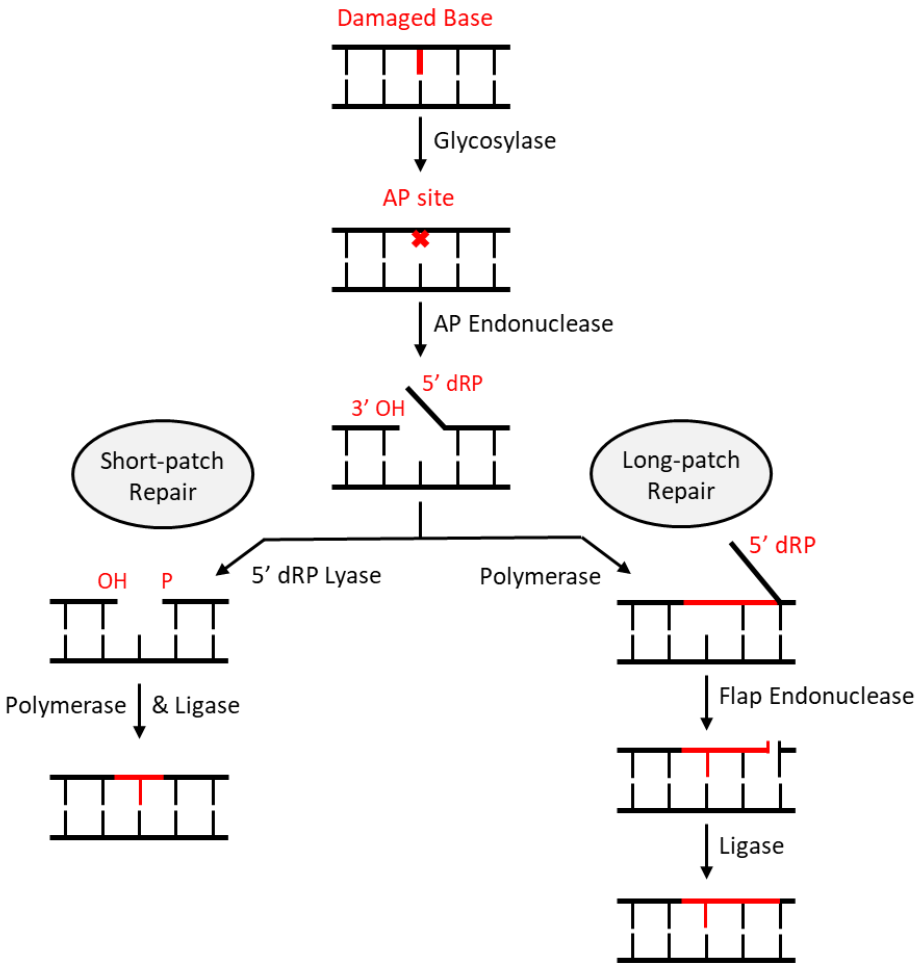


Figure 1.8. The base excision repair (BER) pathway. BER is a primary repair mechanism in mammalian cells, responsible for the repair of non-bulky and non-helix distorting DNA modifications. BER depends on a family of enzymes called glycosylases, with specific glycosylases capable of recognising specific types of DNA modification. The recognition of the modification by the specific glycosylase is the first step of the pathway, followed by the subsequent removal of the modified base. This leaves an apurinic/apyrimidinic (AP) site, which is subsequently removed following cleavage of the phosphodiester backbone. This results in 3'hydroxyl (OH) and 5'deoxyribose phosphate (dRP); with 5'dRP then converted to 5'phosphate *via* dRPase activity. The correct nucleotide(s) is then incorporated by DNA polymerase. This step is performed by POLβ in short-patch repair and POLδ/ε in long-patch repair. An additional step in long-patch repair is the removal of the 5-flap structure by flap endonuclease (FEN1). *Figure legend continues on next page*

Finally, the phosphodiester backbone is sealed by a member of the DNA ligase family; this step is performed by the XRCC1-LIG3 complex in short-patch repair and LIG1 (with assistance from PCNA) is long-patch repair. The exact mechanistic stages of BER can vary depending on the glycosylase that initiates the pathway (Krokan, Standal and Slupphaug, 1997; Fortini *et al.*, 1999; Robertson *et al.*, 2009; Kim and Wilson, 2012).

Another role of BER is preventing the incorporation of oxidatively modified nucleotides into DNA, avoiding the need for repair once subsequently incorporated (Fujikawa *et al.*, 1999; David, O'Shea and Kundu, 2007; Klungland and Bjelland, 2007; Krokan and Bjørås, 2013). The *de novo* synthesis of guanine nucleotides begins with the formation of guanine monophosphate (GMP), which is then converted to guanine diphosphate (GDP) by the enzyme, guanylate kinase. Guanylate kinase possesses poor activity towards oxidised-GMP, therefore preventing the conversion to oxidised-GDP and the incorporation of the oxidised guanine into RNA and DNA. However, GDP is also vulnerable to oxidation, and the direct oxidation of GDP will produce oxidised-GDP which can then be converted into oxidised-guanine triphosphate (GTP) and used in RNA synthesis (Nakabeppu, 2001; Sekiguchi *et al.*, 2013; Hashiguchi *et al.*, 2018). The prevention of this requires the human MutT homologue 1 (hMTH1) protein, which is a GTPase that hydrolyses the oxidized nucleotide. The nucleotide is then excreted to the extracellular matrix before it can be misincorporated into DNA (Grollman and Moriya, 1993; Igarashi *et al.*, 1997; Fujikawa *et al.*, 1999; Nakabeppu, 2001; Tsuzuki *et al.*, 2001; Sakumi *et al.*, 2003; Fotouhi *et al.*, 2011; Sekiguchi *et al.*, 2013; Hashiguchi *et al.*, 2018).

1.4.2. BER glycosylases

As mentioned, a group of specific DNA glycosylases catalyse the first step of the BER pathway. A DNA glycosylase will bind to the site of the damage following recognition and catalyse the cleavage of the N-glycosidic bond between the base and deoxyribose, resulting in the release of the free base and producing an AP site (Dodson, Michaels and Lloyd, 1994; Krokan, Standal and Slupphaug, 1997; Kim and Wilson, 2012).

These glycosylases are specific to different DNA modifications and can be described as either monofunctional- or bifunctional- glycosylases. A monofunctional glycosylase will perform the excision of the base, performing a nucleophilic attack on the N-glycosidic bond *via* the addition of a water molecule. The AP site will then remain until an AP endonuclease, primarily AP endonuclease-1 (APE1), is recruited to the site, which will subsequently produce a nick 5' to the AP site. Bifunctional glycosylases will perform a similar excision of the base, but will instead form a Schiff-base intermediate, and these glycosylases possess lyase activity. This activity allows a bifunctional glycosylase to cleave the phosphodiester backbone 3' to the AP site (Krokan, Standal and Slupphaug, 1997; Fortini *et al.*, 1999; Robertson *et al.*, 2009). All glycosylases share a conserved helix-hairpin-helix (HhH) motif, which is a recognised DNA-binding motif. This is characteristically followed by a glycine/proline- rich loop, followed by a conserved aspartic acid residue (Krokan, Standal and Slupphaug, 1997; Bruner, Norman and Verdine, 2000).

1.5. 8-oxoguanine glycosylase-1

1.5.1. An introduction to the structure and function of 8-oxoguanine glycosylase-1

The glycosylase that recognises 8-oxoG is 8-oxoguanine glycosylase-1 (OGG1). OGG1 has been reported to function as both a monofunctional and bifunctional glycosylase, but is believed to primarily act as a monofunctional glycosylase *in vivo* (Krokan, Standal and Slupphaug, 1997; Dalhus *et al.*, 2011; Faucher, Doublié and Jia, 2012; Kim and Wilson, 2012).

OGG1 was first discovered in *Saccharomyces cerevisiae (S. cerevisiae)* (Nash *et al.*, 1996; van der Kemp *et al.*, 1996) when it was identified as a functional homologue of the bacterial formamidopyrimidine-DNA glycosylase (FPG) protein, which had been shown to excise 8-oxoG in *Escherichia coli (E. coli)* (Boiteux *et al.*, 1990; Michaels *et al.*, 1991; Castaing *et al.*, 1993). This allowed for the identification and characterisation of the human *OGG1* gene (h*OGG1*), which was localised to chromosome 3p26 using in-situ hybridisation (Arai *et al.*, 1997; Kuo and Sklar, 1997; Ishida *et al.*, 1999). The purification of the OGG1 protein determined that hOGG1 possesses both N-glycosylase and β-lyase activity, indicating that OGG1 has the capability to act as a bifunctional glycosylase (Aburatani *et al.*, 1997; Bjørås *et al.*, 1997; Lu, Nash and Verdine, 1997; Boiteux and Radicella, 2000), although as mentioned it primarily acts through a monofunctional mechanism *in vivo* (Faucher, Doublié and Jia, 2012; Kim and Wilson, 2012).

OGG1 is highly specific with respect to substrate recognition. The known substrates of OGG1 are 8-oxoG, 8-oxoA, FapyG and FapyA (*refer to* Figure **1.2.** to see structures). Furthermore, the glycosylase is only able to recognise and excise these oxidised-purine modifications if they are present as a base pair opposite a cytosine residue (Boiteux and Radicella, 2000; Bjørås *et al.*, 2002; Jensen *et al.*, 2003; Hu, de Souza-Pinto, *et al.*, 2005; Klungland and Bjelland, 2007). Therefore, OGG1 is not capable of the excision of an 8-oxoG residue that has formed a Hoogsteen mispair with adenine. These 8-oxoG:A mismatches instead require an additional repair step prior to OGG1-initiated BER, which consists of the removal of the adenine

residue followed by the insertion of a cytosine. This reaction is initiated by a different glycosylase called mutY homolog (MUTYH), which is often also referred to as MYH. This repair of 8-oxoG by OGG1- or MUTYH- initiated repair is summarised in Figure **1.9.** (Hayashi *et al.*, 2002; Slupphaug, Kavli and Krokan, 2003; Russo, M *et al.*, 2004; David, O'Shea and Kundu, 2007; Banda *et al.*, 2017).

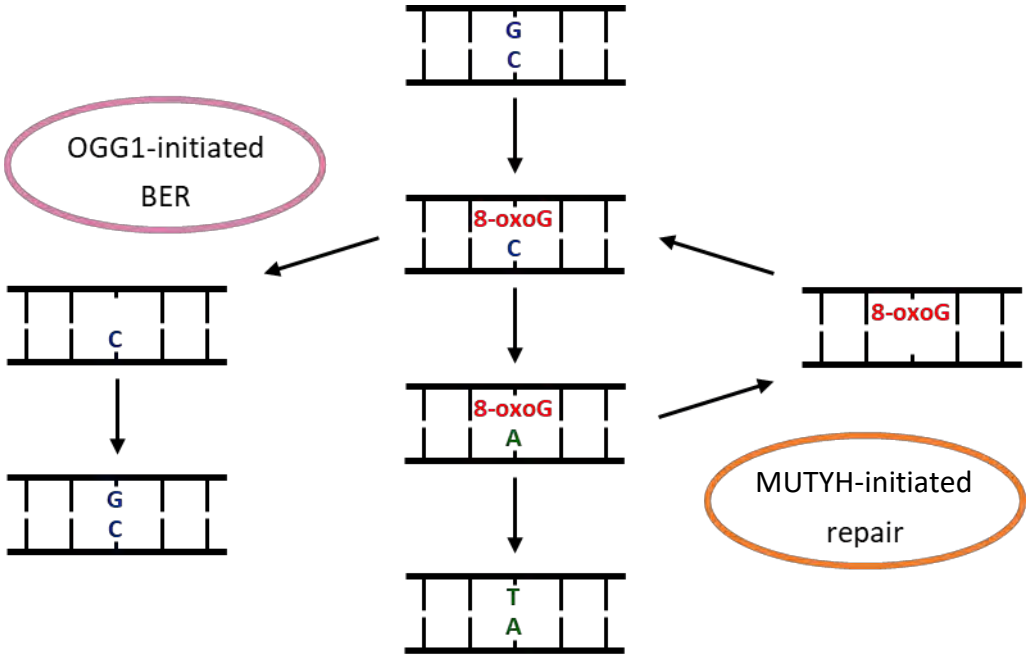


Figure 1.9. OGG1- and MUTYH- initiated repair of 8-oxoG. OGG1-initiated BER is the mechanism responsible for the removal of 8-oxoG when it is present opposite a cytosine (C). However, if 8-oxoG is instead present opposite an adenine (A), it will instead be repaired by MUTYH-initiated repair (Hayashi *et al.*, 2002; David, O'Shea and Kundu, 2007). Failure to successfully repair 8-oxoG will lead to GC -> TA transversions during DNA replication. This will ultimately result in a thymine (T) residue present at the position originally occupied by guanine (G) residue, as shown.

The mechanism of substrate recognition by OGG1 was investigated by Bjørås *et al.* (2002) using the crystal structures of OGG1 in both its native- and DNA bound- form. The two structures were superimposed, which allowed the authors to identify key differences in the backbone and side chains of OGG1 in the two states. Based on this study, the authors concluded that OGG1 uses an induced fit model of binding. There were residues identified within the specificity pocket of OGG1 (Gly42, Gln43, Phe45, Cys253, Gln315, and Phe319), which were all shown to interact with the DNA substrate. Furthermore, conformational changes across these residues ultimately 'closed off' the specificity pocket when OGG1 was present in a native form. On substrate recognition, conformational changes then allow the substrate to be 'flipped' into the specificity pocket, followed by the cleavage of the N-glycosidic bond, and the subsequent release of the free base (Bjørås *et al.*, 2002). This model is described in Figure **1.10.** using the crystal structures solved by Bjørås *et al.* (2002), highlighting some of the key functional residues of hOGG1. This mechanism differs significantly to the mechanism of other DNA glycosylases, with the crystal structures of many glycosylases showing that the specificity pocket remains present and accessible in both their native- and DNA bound- form. This is true for multiple BER glycosylase (*e.g.* MUTYH, UDG and AAG) (Mol *et al.*, 1995; Yamagata *et al.*, 1996; Barrett *et al.*, 1998).

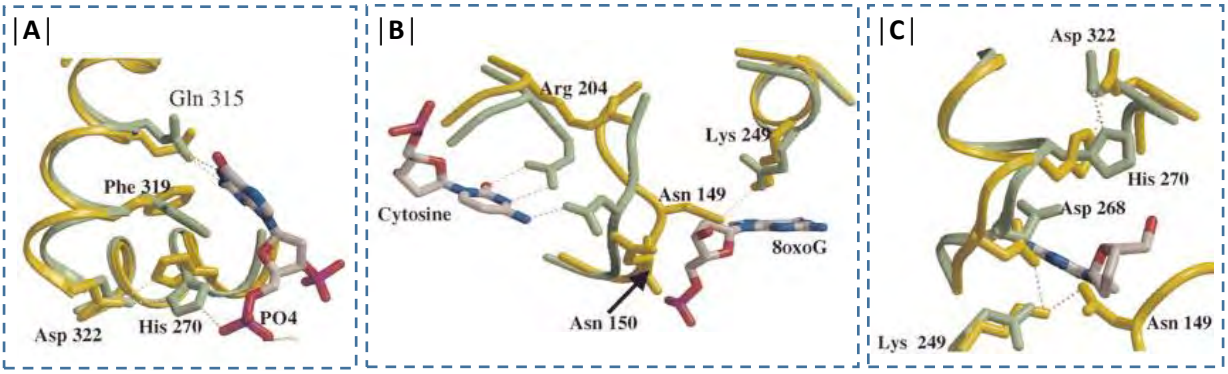


Figure 1.10. The crystal structure of OGG1. The crystal structure of native hOGG1 (yellow) and DNA bound hOGG1 (green) were solved by Bjørås *et al.* (2002) and superimposed to identify conformational changes |**A**| His270 changes conformation, interacting with other key residues (Gln315, Phe319, and Asp322) to form a 'trigger' mechanism, which switches the binding pocket between a closed and an open position. |**B**| Other changes occur in the substrate recognition site, including conformational changes in the Arg204 and Asn149 residues, which both form hydrogen bonds with Lys249 when OGG1 is in the native state. On DNA binding, Asn149 is flipped (≈9Å) to instead interact with the cytosine of the substrate base pair. |**C**| The loss of these hydrogen bonds in the DNA-bound hOGG1 leaves the catalytic lysine residue with a neutral amino group.

1.5.2. OGG1 variants

Since its discovery, numerous polymorphisms of OGG1 have been identified, with these having already been the subject of comprehensive reviews (Goode, Ulrich and Potter, 2002; Weiss *et al.*, 2005). Many of these identified polymorphisms of OGG1 consist of a single nucleotide change, and many of these are non-synonymous, resulting in an alteration in the amino acid sequence of the encoded protein. A variant that is present in ≥ 1% of the population is classed as a polymorphism (Spencer, Zhang and Pfeifer, 2015).

Two single nucleotide polymorphisms (SNPs) that have been shown to have no effect on OGG1 function are G308E (Gly → Glu) and A85S (Ala → Ser). Although these non-synonymous SNPs were both previously identified in individuals with cancer (head and neck, and lung), there was no significant difference between the glycosylase activity of these polymorphic variants when compared to the wild-type (WT) OGG1 protein (Blons *et al.*, 1999; Audebert *et al.*, 2000). Alternatively, there is evidence that supports the hypothesis that a different OGG1 polymorphism, S326C (Ser → Cys), possesses compromised BER activity (Kohno *et al.*, 1998; Sugimura *et al.*, 1999; Xing *et al.*, 2001; Goode, Ulrich and Potter, 2002; Yamane *et al.*, 2004; Weiss *et al.*, 2005; Lee, Hodges and Chipman, 2005; Luna *et al.*, 2005; Hill and Evans, 2006; Smart, Chipman and Hodges, 2006; Bravard *et al.*, 2009; Sidorenko *et al.*, 2009; Zielinska *et al.*, 2011; Kershaw and Hodges, 2012; Kaur *et al.*, 2014).

This polymorphism is caused by a substitution of a cytosine residue for a guanine residue within exon 7 of *OGG1*, which results in a change from a serine to a cysteine at position 326 (Kohno *et al.*, 1998; Sugimura *et al.*, 1999; Xing *et al.*, 2001; Weiss *et al.*, 2005). The allele frequency of this Cys-326 varies significantly between different populations, ranging from 0.13-0.27 in Caucasian populations and 0.33-0.5 in Asian populations (Xing *et al.*, 2001; Goode, Ulrich and Potter, 2002; Weiss *et al.*, 2005; Sidorenko *et al.*, 2009). There is evidence to suggest that individuals that are homozygous for the Cys326-OGG1 polymorphism have an increased susceptibility to oxidative pathologies, however other evidence

suggests that this is not the case (*refer to* epidemiologic review papers; Goode, Ulrich and Potter, 2002; Weiss *et al.*, 2005).

The Hodges group have previously utilised the FPG-modified comet assay to assess the capability of the Cys326-OGG1 variant with respect to OGG1-initiated BER, with this methodology measuring DNA damage within cells. Following the induction of oxidative stress, there was a significant accumulation of FPG-dependent strand breaks measured in cells harbouring the Cys326-OGG1 variant, with these FPG sites primarily representing sites of oxidative DNA damage. These results indicated that the repair capabilities of Cys326-OGG1 were impaired, when compared to cells harbouring either WT (Ser326-) OGG1 or an artificially generated (Gly326-) OGG1 variant (Smart, Chipman and Hodges, 2006). A similar accumulation of FPG-dependent damage was also measured in Cys326-OGG1 in two other studies (Lee, Hodges and Chipman, 2005; Kaur *et al.*, 2014). The Cys326-OGG1 variant was further investigated with the generation of m*Ogg1*-null MEFs that stably expressed either, Ser326- or Cys326- OGG1 (Kershaw and Hodges, 2012). The activity of both cell lines did increase following oxidative stress, however, there was a significant difference between the repair kinetics of the two variants. This reflected the results of an earlier publication, which had measured that the repair rate of the Cys326-OGG1 variant was significantly slower (3 - 4 fold) when compared to WT OGG1 (Zielinska *et al.*, 2011). This impaired repair ability in Cys326-OGG1 has been shown in multiple papers, with it measured that activity is decreased between 1.5 - 6 fold compared to WT (Ser326-) OGG1 (Hill and Evans, 2006; Bravard *et al.*, 2009; Sidorenko *et al.*, 2009). It has been hypothesised that this change in repair activity could be due to the absence of phosphorylation of the serine residue, an increase in oxidation at the cysteine residue, or changes in structure and/or localisation (Luna *et al.*, 2005; Hill and Evans, 2006; Smart, Chipman and Hodges, 2006; Bravard *et al.*, 2009). The findings of these key papers together confirm that OGG1-initiated BER is impaired cells harbouring the Cys326-OGG1 variant.

1.5.3. OGG1 regulation

Multiple protein modifications and protein-protein interactions have been described for OGG1. These different regulatory mechanisms can result in different effects on the glycosylase activity of OGG1.

1.5.3.1. Post-translational modifications

Post-translational modification (PTMs) are a key regulatory mechanism within a cell, describing the modification of proteins following biosynthesis. These PTM's usually involve the addition of a moiety (*e.g.* PO_3^-/ CH_3CO/ O), with examples of such PTMs towards OGG1 summarised in Table **1.1.**

Table 1.1. OGG1 post-translational modifications affect OGG1 activity

Modification	Protein involved	Consequence to OGG1	References
Acetylation	CBP/p300	Increased activity	(Bhakat *et al.*, 2006; Kang *et al.*, 2015)
Phosphorylation	CDK4	Increased incision activity	(Hu, Imam, *et al.*, 2005)
Phosphorylation	c-ABL PKC	No observed consequence	(Dantzer *et al.*, 2002; Hu, Imam, *et al.*, 2005; Luna *et al.*, 2005)
Oxidation	ROS	Decreased activity	(Morreall *et al.*, 2015)
O-GlcNAcylation	OGT	Decreased activity	(Cividini *et al.*, 2016)
Ubiquitination	E3 Ligase	Decreased activity	(Fantini *et al.*, 2013; Hughes and Parsons 2020)

The regulation of DNA repair proteins by acetylation is well documented. This includes the acetylation of the BER proteins, APE1 and OGG1 (Bhakat *et al.*, 2006; Kang *et al.*, 2015; Roychoudhury *et al.*, 2017). The acetylation of OGG1 has been shown *in vivo* by Bhakat *et al.* (2006), with this modification performed by the histone acetyltransferase complex, CBP/p300. This acetylation occurs at two lysine residues within

close proximity to one another (Lys338 and Lys341) and results in an increase in OGG1 activity. The authors hypothesise that the purpose of this acetylation could be to weaken the interaction between OGG1 and APE1, thereby increasing the turnover of OGG1. Furthermore, acetylation of OGG1 is increased (2.5 -fold) following induction of oxidative stress but decreases again once redox homoeostasis is restored. The authors suggest that this rapid return to the cellular basal level of acetylated-OGG1 indicates that deacetylation must occur. It has been proposed that this is likely through interaction with class I histone deacetylates (HDACs) (Bhakat *et al.*, 2006) and/or the deacetylase Sirtuin-2 (SIRT2) (Kang *et al.*, 2015). This relationship between the redox state of the cell and the acetylation status of OGG1 could be due to the redox regulation of p300, and furthermore it suggests that OGG1 activity could become compromised in conditions of sustained oxidative stress.

The idea that the repair activity of OGG1 could become compromised in conditions of oxidative stress seems almost paradoxical, as this oxidative stress will produce oxidative DNA damage that is dependent on OGG1 for repair. However, a decrease in OGG1 activity in conditions of oxidative stress has also been shown following cadmium exposure, with this heavy metal known to cause intracellular oxidative stress (Bravard *et al.*, 2006; Bravard et al., 2010). Additionally, Morreall *et al.* (2015) showed that tumour necrosis factor-α (TNF-α) inhibited the activity of the common Cys26-OGG1 variant that was described previously (*refer to* **1.5.2.**), with this variant shown to be oxidised at the polymorphic cysteine residue. The oxidation of this cysteine is often acknowledged as an explanation for the impaired repair activity of the Cys326-OGG1 variant, with this cysteine residue located in a highly positively charged environment, allowing the cysteine residue to be easily oxidised (Smart, Chipman and Hodges, 2006; Bravard *et al.*, 2009; Morreall *et al.*, 2015).

Phosphorylation is a major post-translational modification, which involves the addition of a phosphoryl group (PO_3^-). Phosphorylation can occur at serine, threonine and tyrosine residues, depending on the kinase that catalases the transfer of the phosphate group. *O*-GlcNAcylation is another PTM that targets

serine and threonine residues, with crosstalk between *O*-GlcNAcylation and phosphorylation commonly occurring (Wang, Gucek and Hart, 2008; Hart *et al.*, 2011). *O*-GlcNAcylation describes the addition of an N-acetyl-glucosamine (GlcNAc) moiety by an *O*-GlcNAc transferase (OGT). Hu *et al.* (2005) reported the phosphorylation of OGG1 by the serine-threonine kinase, CDK4. This study showed this phosphorylation to cause an increase (2.5 -fold) in the incision activity of OGG1 (Hu, Imam, *et al.*, 2005). Alternatively, Dantzer *et al.* (2002) reported the phosphorylation of OGG1 by two different kinases. These phosphorylation events, by either a tyrosine kinase (c-ABL) or a serine-threonine kinase (PKC), do not result in any significant changes to OGG1 activity (Dantzer *et al.*, 2002; Hu, Imam, *et al.*, 2005). Together these studies show how the consequence of OGG1 phosphorylation appears dependent on the kinase involved and/or the exact phosphorylation reaction. In terms of *O*-GlcNAcylation, Cividini *et al.* (2016) measured a significantly higher level of *O*-GlcNAcylated OGG1 in the genome of diabetic mice compared to healthy controls, with this *O*-GlcNAcylation resulting in an inhibition of OGG1 activity. Furthermore, *O*-GlcNAcylation was inhibited with an inactive OGT variant, which subsequently restored OGG1 activity and reduced 8-oxoG levels (Cividini *et al.*, 2016).

The ubiquitination of proteins is crucial for the degradation of proteins through the ubiquitin-proteasome pathway. This proteasomal degradation was already mentioned in **1.2.** with respect to the degradation of oxidatively-modified proteins, however ubiquitination of proteins has also been linked to the regulation of DNA repair pathways (Brinkmann *et al.*, 2015). This ubiquitination has been shown for multiple BER proteins, including APE1, POLB and XRCC1 (Parsons *et al.*, 2008; Parsons *et al.*, 2009; Meisenberg *et al.*, 2012). It is now also understood that OGG1 can be ubiquitinated through an E3 ligase-mediated process, as shown by Fantini *et al.* (2013); with this E3 ligase recently having been identified as NEDD4L (Hughes and Parsons 2020).

1.5.3.2. Protein-protein interactions

Another key regulatory mechanism is through protein-protein interactions, examples of which are summarised in Table **1.2.**

Table 1.2. Protein-protein interactions are capable of affecting OGG1 activity

Protein	Consequence to OGG1	References
APE1	Increased activity	(Hill *et al.*, 2001; Saitoh *et al.*, 2001)
XRCC1	Increased activity	(Marsin *et al.*, 2003; Campalans *et al.*, 2015)
PARP1	Decreased activity	(Hooten et al., 2011)
XPC	Increased activity (to be discussed; *refer to* **1.7.4.2.**)	(Klungland, Höss, *et al.*, 1999; D'errico *et al.*, 2006; Dušinská *et al.*, 2006)
CUX1/2	Increased activity	(Pal *et al.*, 2015; Ramdzan *et al.*, 2017)
Ribosomal protein S3	Increased activity	(Hegde, Wang and Deutsch, 2004)

As mentioned previously (*refer to* **1.5.1.**), OGG1 possesses the capabilities to function as a bifunctional glycosylase. This means that OGG1 can both excise the substrate base and subsequently cleave the phosphodiester bond. The resulting AP site is removed by APE1, however the ability of OGG1 to cleave this phosphodiester bond was shown to be significantly increased (~ 5 -fold) by the presence of APE1 *in vitro* (Hill *et al.*, 2001; Saitoh *et al.*, 2001). Alternative studies have suggested that OGG1 may act as a monofunctional *in vivo*, with APE1 instead inducing the cleavage of the phosphodiester backbone by releasing OGG1 from the AP site (Dalhus *et al.*, 2011). Either mechanism details a mechanism in which

the induction of the BER pathway downstream of substrate recognition is dependent on this OGG1-APE1 interaction (Hill *et al.*, 2001; Saitoh *et al.*, 2001; Dalhus *et al.*, 2011; Allgayer *et al.*, 2016).

There is also evidence that OGG1 interacts with other DNA repair proteins. This includes interaction with XRCC1, a scaffold protein that forms a complex with DNA ligase III (LIG3) to be involved at the terminal step of BER (*refer to* Figure **1.8.)** (Marsin *et al.*, 2003; Campalans *et al.*, 2015). Marsin *et al.* (2003) showed that this interaction between OGG1 and XRCC1 resulted in an increase (3 -fold) in OGG1 activity. Campalans *et al.* (2015) showed that cells harbouring an XRCC1 polymorphism, which this polymorphism not capable of interacting with OGG1, possessed deficiencies with respect to BER. Furthermore, OGG1 has also been shown to interact with proteins from other repair pathways, including PARP1 and XPC (Klungland, Höss, *et al.*, 1999; Marsin *et al.*, 2003; D'errico *et al.*, 2006; Dušinská *et al.*, 2006; Hooten *et al.*, 2011; Campalans *et al.*, 2015).

Two other proteins shown to interact with OGG1 are the transcription factors, CUX1 and CUX2, both of which interact with OGG1 through a conserved DNA-binding domain (CUT domain). These CUX proteins are involved in the transcriptional activation of important DNA repair genes, and these CUX1/2-OGG1 interactions appear to increase OGG1 activity, whilst not affecting the transcription activity of the CUX proteins. It is proposed that other transcription factors that possess this DNA-binding CUT-domain may also be able to act as accessory proteins, increasing OGG1 activity, in a similar manner as CUX 1/2 (Pal *et al.*, 2015; Ramdzan *et al.*, 2017).

In conclusion, although there is already literature surrounding the regulation of OGG1, with it unlikely that all of these OGG1-regulatory mechanisms have yet been discovered. This shows the complex network of modifications and protein interactions that can affect the activity of OGG1, and the subsequent cellular consequences that these modifications cause.

1.5.4. OGG1 and cellular signalling

1.5.4.1. The OGG1:8-oxoG complex

OGG1 has been extensively studied since its discovery, and therefore its mechanism as a DNA glycosylase within the BER pathway is now well established. More recently, studies have implicated OGG1 in a host of different cellular roles that reach beyond its traditional glycosylase role. Specifically, research by the Boldogh research group (The University of Texas) has described how OGG1 and 8-oxoG can form a complex with one another, with this complex then subsequently linked to cellular signalling. They have reported that following the excision of 8-oxoG during OGG1-initiated BER, OGG1 can subsequently bind to 8-oxoG with high affinity (Boldogh *et al.*, 2012). The group has since published multiple studies (German *et al.*, 2013; Hajas *et al.*, 2013; Luo *et al.*, 2014) implicating this subsequent signalling molecule (OGG1:8-oxoG) with the downstream activation of the Ras superfamily of GTPases.

Over 150 GTPases within the Ras superfamily have been identified, with these small proteins playing an important role in the signalling network of a cell (Wennerberg, Rossman and Der, 2005). GTPases acting as binary, molecular switches; with GTPases constantly shuttling between an inactive/GDP-bound state and an active/GTP-bound state. A number of mechanisms regulate this GTPase shuttling, including guanine exchange factors (GEFs) and GTPase-activating proteins (GAPs). GEFs substitute GDP for GTP, activating the GTPase and promoting downstream signalling. GAPs however induce GTP hydrolysis, resulting in GDP-bound GTPases and therefore usually causing the termination of a signalling pathway (Figure **1.11.**) (Sahai and Marshall, 2002; Wennerberg, Rossman and Der, 2005; Bos, Rehmann and Wittinghofer, 2007; Van Buul, Geerts and Huveneers, 2014).

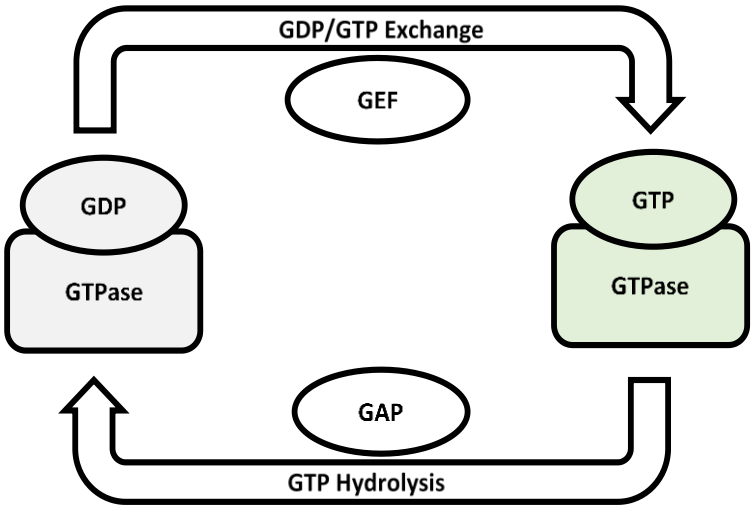


Figure 1.11. GTPases shuttle between an inactive (GDP-bound) and an active (GTP- bound) state. Guanine exchange factors (GEFs) catalyse the substitution of GDP to GTP. GTPase-activating proteins (GAPs) catalyse the substitution of GTP to GDP (Bos, Rehmann and Wittinghofer, 2007).

The key papers published by the Boldogh group will be briefly summarised within this section. In conclusion these papers implicate OGG1: 8-oxoG molecule in the activation of GTPase signalling, suggesting that OGG1:8-oxoG acts as a GEF (Boldogh *et al.*, 2012; German *et al.*, 2013; Hajas *et al.*, 2013; Luo *et al.*, 2014; Ba *et al.*, 2015). The studies show that an increase in the OGG1: 8-oxoG signalling molecule can result in an increase in the activity of multiple small GTPases; including RAS (Boldogh *et al.*, 2012; German *et al.*, 2013), RAC1 (Hajas *et al.*, 2013) and RHO (Luo *et al.*, 2014).

The downstream effects of the activation of these GTPases are varied and extensive, including proliferation, cytoskeletal changes, and differentiation. Furthermore, the downstream cellular effects of these pathways are often linked to carcinogenesis, with Ras GTPases often possessing both tumour-promoting and tumour-suppressing activities (Sahai and Marshall, 2002; Romanowska *et al.*, 2007; Fleming *et al.*, 2009; McCain, 2013). This interaction between OGG1:8-oxoG and Ras GTPases therefore show the importance of OGG1 within a cell, and importantly show how the role of OGG1 is much broader than DNA repair.

1.5.4.2. RAS GTPase and MAPK signalling

This relationship between Ras GTPases and OGG1 was first published with respect to RAS (Boldogh *et al.*, 2012). The study showed that the addition of 8-oxoG to OGG1 proficient MRC5-cells resulted in an increase in RAS-GTP levels in a time- and concentration- dependent manner. However, the addition of 8-oxoG to OGG1-depleted cells did not result in an increase in RAS-GTP levels. The authors conclude that OGG1 binds 8-oxoG with high affinity and proposed that the experimental addition of 8-oxoG in their experiments mimicked the generation of 8-oxoG that occurs following OGG1-initiated BER. The resulting OGG1: 8-oxoG complex was shown to interact with H-RAS, an interaction that does not occur in the absence of 8-oxoG. This proves that an interaction does not occur between OGG1 and H-RAS alone, and that this interaction requires 8-oxoG. This suggests that the OGG1 conformational changes induced by 8-oxoG (as described in **1.5.1.**) allows this H-RAS interaction to occur. These results were replicated with the other two human isoforms of RAS, with OGG1 shown to successfully interact with both K- and N-RAS. The addition of an alternative OGG1 substrate (FapyG) did not result in an increase in OGG1 activity or a subsequent increase in Ras-GTP levels. Furthermore, no such interactions were observed between RAS and the alternative BER glycosylases, Nei-like DNA glycosylases 1/2 (NEIL1/2).

The conclusion of the study was that following the OGG1-initiated excision of 8-oxoG, the nucleotide interacts with OGG1 to form the OGG1: 8-oxoG complex. Boldogh *et al.* (2012) hypothesise that this OGG1: 8-oxoG complex is then able to interact with RAS, increasing the exchange of GDP for GTP, and subsequently resulting in an increase in active (GTP-bound) RAS. The authors propose that OGG1: 8-oxoG therefore acts as a GEF towards RAS, implying that the complex exerts this effect through a similar mechanism to other GEFs (Mosteller, Han and Broek, 1994; Boldogh *et al.*, 2012). Active RAS is then capable of binding to the RAS-binding domain of a downstream serine/threonine kinase, thereby initiating the mitogen-activated protein kinase (MAPK) pathway **(**Figure **1.12)**.

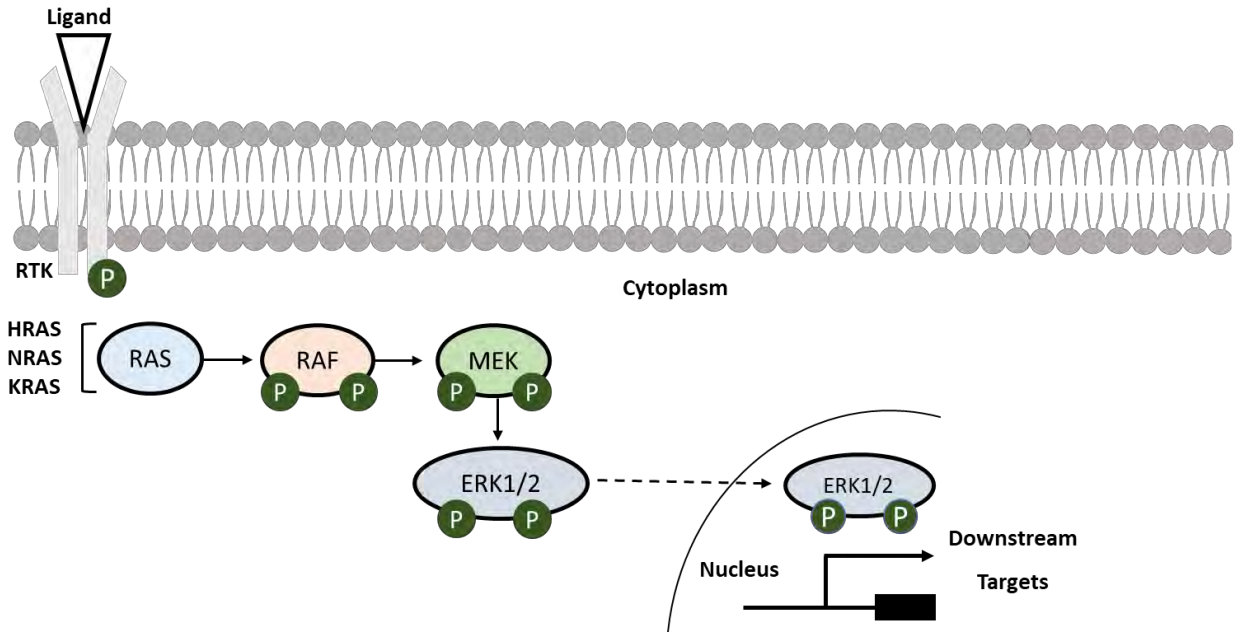


Figure 1.12. The MAPK pathway. The pathway consists of a chain of kinases, which once activated are capable of activating their downstream target. This therefore results in a signalling cascade, based on phosphorylation events, which conclude with the activation of transcription factors within the nucleus (McCain, 2013). The pathway is initiated when a ligand binds to a receptor tyrosine kinase (RTK). On ligand binding, two RTK subunits then form a dimer. This results in the phosphorylation of the RTKs within their cytoplasmic domains and subsequent activation. This active form of RTK is capable of recruiting adaptor proteins, which will subsequently recruit guanine nucleotide exchange factors (GEFs) to the plasma membrane. These GEFs activate the small GTPase RAS by stimulating the substitution of GDP to GTP. Active (GTP-bound) RAS is then capable of activating a downstream serine/threonine kinase, RAF. The activated RAF protein subsequently activates its downstream target MEK through phosphorylation of a threonine residue (primarily Thr292) with active MEK subsequently activating its downstream target ERK. This activation requires phosphorylation at both a tyrosine residue and a threonine residue, which MEK is capable of performing. This dual-phosphorylation allows ERK to translocate to the nucleus, where it functions as an enzyme to phosphorylate and activate transcription factors.

The addition of 8-oxoG was subsequently proven to result in the phosphorylation of MEK1/2 and ERK1/2, which are both MAPK proteins located downstream of RAS (*refer to* Figure **1.12**.). This ultimately confirms that the addition of 8-oxoG results in an increase in MAPK/ERK signalling. This MEK1/2 and ERK1/2 phosphorylation was not observed in RAS-depleted or OGG1-null cells, allowing the authors to conclude that this phosphorylation was dependent on both OGG1 and RAS activity (Boldogh *et al.*, 2012).

This initial study was soon followed up, with the aim to provide a clear connection between BER and cellular signalling, rather than the simple induction of RAS-GTP through the exogenous addition of 8-oxoG as previously shown (Boldogh *et al.*, 2012). German *et al.* (2013) utilised KG-1 cells that expressed a thermolabile OGG1 variant that lacked OGG1 activity at 37 °C; OGG1 activity was then restored by decreasing the temperature to 25°C. An increase in the levels of GTP-bound RAS was measured in these KG-1 cells at 25 °C, followed by a subsequent increase in the phosphorylation of downstream MAPK kinases (p-MEK1/2 and p-ERK1/2). No such increase in RAS-GTP levels was measured in the KG-1 cells at 37 °C. The authors conclude that this directly links the increase in RAS-GTP levels seen in their earlier paper (Boldogh *et al.*, 2012) with OGG1-initiated BER (German *et al.*, 2013).

These results indicate that an increase in oxidative stress, oxidative DNA damage, and subsequent OGG1-initiated repair results in an increase in the activation of RAS. This increases the downstream effects of the MAPK pathway including survival, proliferation and transcriptional activation of downstream genes. Although the reasons for this are unclear, German *et al* (2013) propose that this downstream signalling could be essential for re-establishing cellular conditions following oxidative insult, and therefore maintaining a homeostasis. Furthermore, they hypothesise that it could be through this GTPase activation through which OGG1 is linked to cellular pathologies and ageing processes.

1.5.4.3. RAC1 GTPase and redox regulation

Next, Hajas *et al.* (2013) focused on the interaction between OGG1:8-oxoG and the small Ras GTPase RAC1. The authors hypothesised that OGG1:8-oxoG could act as a GEF through a similar mechanism in which it acted as a GEF towards RAS (Boldogh *et al.*, 2012; German *et al.*, 2013). The authors found that OGG1 bound poorly with RAC1, however this interaction was improved in the presence of 8-oxoG. This indicated once again that this interaction was dependent on 8-oxoG, with the OGG1:8-oxoG complex preferentially interacting with GDP-bound RAC1 (compared to GTP-bound RAC1 and unbound RAC1).

The addition of 8-oxoG was shown to increase active (GTP-bound) RAC1 levels in OGG1-proficient A549 and MRC5 cells, and furthermore was shown to increase active RAC1 levels in an OGG1-proficent animal model. However, this increase in active RAC1, following 8-oxoG addition, was not measured in OGG1-depleted cells. As with the original paper (Boldogh *et al.*, 2012), the addition of FapyG or guanine did not increase levels of GTP-bound RAC1. Fluorescently labelled GDP and GTP were then utilised to show that the addition of OGG1:8-oxoG resulted in an increase in the rate of exchange between RAC1-GDP and RAC1-GTP, a result not reflected with the addition of OGG1 alone. These results are similar to the data collected for RAS, with the authors proposing that the OGG1:8-oxoG complex is capable of acting as a GEF towards RAC1 and RAS (Boldogh *et al.*, 2012; German *et al.*, 2013; Hajas *et al.*, 2013).

The GTPase RAC1 has been implicated in the regulation of nicotinamide adenine dinucleotide phosphate (NADPH) oxidases, a family of membrane-bound multi-subunit enzymes. These enzymes are an important component of redox regulation and represent a major source of ROS. NADPH oxidases have been linked to the regulation of multiple functions including cellular signalling and gene expression. Hajas *et al.* (2013) propose that interactions between the OGG1:8-oxoG complex and RAC1 could be the mechanism through which 8-oxoG addition increases intracellular ROS levels, as also observed in a previous study (Hajas *et al.*, 2012). This transient increase in ROS following 8-oxoG treatment was not however observed

in OGG1 depleted cells. This increase in ROS was significantly lower when cells were pre-treated with the antioxidant N-acetylcysteine or the NAPDH oxidase inhibitor diphenyleneiodonium (DPI) prior to 8-oxoG addition (Hajas *et al.*, 2013). Alternatively, separate studies showed that the induction of oxidative stress in cells resulted in an increase in active (GTP-bound) RAC1 levels, with this shown following both H_2O_2 treatment and the inhibition of the antioxidant GSH (Kuiper *et al.*, 2011; Nagase *et al.*, 2012; Hobbs *et al.*, 2014). Hajas *et al.* (2013) propose that this localised ROS generation is specific to OGG1:8-oxoG, with this effect not measured following the addition of FapyG, 8-oxoA, or uric acid.

As discussed previously, the oxidation of cysteine residues within OGG1 can regulate OGG1 activity (*refer to* **1.5.3.**). Therefore, it has been suggested that this transient increase in ROS following OGG1-initiated repair of 8-oxoG could me a mechanism to modulate OGG1 activity. Again, possibly implicating the OGG1:8-oxoG molecule in maintaining cellular conditions following oxidative insult (Boldogh *et al.*, 2012; Hajas *et al.*, 2013).

1.5.4.4. RHO GTPase and cytoskeletal changes

Luo *et al*. (2014) hypothesised that cytoskeletal changes observed in cells following DNA damage could be linked to an interaction between the OGG1:8-oxoG complex and Ras GTPases. In particular, it is well established that the RHO group of small GTPases are involved in the regulation of actin dynamics (Hobbs *et al.*, 2014; Van Buul, Geerts and Huveneers, 2014). This study showed that OGG1-initiated BER resulted in an increase in active (GTP-bound) RHO, with this resulting in an increase in α-smooth muscle actin (α-SMA) polymerisation. Cells were challenged with either glucose oxidase (GOx) or 8-oxoG, with both conditions resulting in an increase in active RHO. However, this increase in active RHO was not observed in OGG1-depleted cells. As observed in the previous papers (Boldogh *et al.*, 2012; Hajas *et al.*, 2013), neither FapyG or 8-oxo-2'-deoxyguanosine (8-oxodG) addition had an effect on the levels of the active GTPase (RHO-GTP). The authors suggest that this shows this role to be specific to the OGG1:8-oxoG system.

Interestingly, OGG1 was shown to interact with RHOA both in the absence and presence of 8-oxoG, which differs from what was observed by Boldogh *et al.* (2012) with respect to the interaction between OGG1:8-oxoG and RAS. The authors conclude that the study demonstrates another example in which OGG1:8-oxoG functions as a GEF towards a GTPase, albeit through a slightly different mechanism (Luo *et al.*, 2014). Therefore, this paper indicates an unexpected relationship between BER and the regulation of the cytoskeleton. This paper is of particular interest to this thesis, with it having previously been observed that WT and OGG1-null cells have cytoskeletal differences from one another. This difference could arise from differences in RHO signalling, and could be linked to the cytoskeletal differences observed in cells following DNA damage (Luo et al., 2014; Soza et al., 2009; Gourlay and Ayscough, 2005 (a); Gourlay and Ayscough, 2005 (b)).

1.5.5. Other roles of OGG1

1.5.5.1. OGG1 and inflammation

Surprisingly OGG1-null cells appear to possess a level of protection against inflammation. This resistance to inflammation in OGG1-null/OGG1-depleted mouse models has been demonstrated using multiple inflammatory models; all of which demonstrate a decrease in multiple hallmarks of inflammation in the absence of OGG1, including decreased levels of important cytokines (macrophage inflammatory proteins and interleukins) and chemokines (Mabley *et al.*, 2004; Li *et al.*, 2012; Bacsi *et al.*, 2013). These models implicate OGG1 in inflammatory and immune responses within the cell, with studies linking the induction of inflammation by OGG1 to the RAS-NFκB pathway *via* the OGG1: 8-oxoG complex (*refer to* **1.5.4.**) (Aguilera-Aguirre *et al.*, 2014; Ba, Aguilera-Aguirre, *et al.*, 2014; Ba, Bacsi, *et al.*, 2014; Ba *et al.*, 2015).

1.5.5.2. OGG1 and epigenetic modulation

Alternatively, this inflammation-resistant phenotype of OGG1-null cells has been linked to epigenetic regulation *via* 8-oxoG and OGG1 (see Seifermann and Epe, 2017 or Sampath and Lloyd, 2019 for review). Pan *et al.* (2016) show that treatment with the pro-inflammatory cytokine TNF-α results in an increased level of 8-oxoG in the promotor regions of pro-inflammatory genes, which is mirrored by an increase in OGG1 recruitment to these sites. This OGG1:8-oxoG interaction upstream of NFκB-binding sites increases NFκB-binding and subsequently increases the expression of NFκB-driven genes. Furthermore, OGG1 depletion resulted in a decrease in NFκB-binding at these sites, whereas the DNA glycosylases NEIL1/2 had little effect (Pan *et al.*, 2016). This was reflected by a study by Allgayer *et al.* (2016) which showed the presence of 8-oxoG in the non-transcribed strand of a reporter gene resulted in a decrease in the transcription of that gene, with this negative correlation associated with the excision of 8-oxoG by the OGG1-APE1 system of the BER pathway (Allgayer *et al.*, 2016). These papers propose that 8-oxoG in the genome acts as an epigenetic target, recruiting OGG1 to sites where it can bind and modulate gene expression in conditions of oxidative stress (Allgayer *et al.*, 2016; Pan *et al.*, 2016; Hao *et al.*, 2020).

1.6. Mitochondrial oxidative DNA damage

Although studies have described the interaction that exists between different DNA pathways and their substrates, this is usually with respect to nuclear DNA, and the repair of mitochondrial DNA (mtDNA) is less understood. It was first believed that the mitochondria possessed no DNA repair activity. However, this is no longer the case and studies have shown the cells do possess repair activity towards mtDNA, albeit in a limited capacity compared to nuclear DNA repair (Clayton, Doda and Friedberg, 1974; Kang and Hamasaki, 2002; Takao *et al.*, 2002; Liu and Demple, 2010; Gredilla, 2011; Alexeyev *et al.*, 2013). This includes a fully active BER system within the mitochondria, including the discovery of a mitochondrial specific isoform of OGG1, referred to as β-OGG1 (de Souza-Pinto *et al.*, 2001; Jensen *et al.*, 2003; Gredilla, 2011; Furihata, 2015).

An accumulation of mtDNA has been linked to mitochondrial dysfunction, ageing, and disease in multiple studies (Wallace, 2001; Liu and Demple, 2010; Yuzefovych *et al.*, 2013; Cividini *et al.*, 2016; Leon *et al.*, 2016). As discussed earlier, the mitochondria are a major source of ROS and therefore mtDNA is highly susceptible to oxidative DNA damage in particular (Yakes and Van Houten, 1997; Murphy, 2009). It is yet to be determined if there is a back-up repair system capable of repairing oxidative mtDNA damage in the absence of OGG1, and therefore the true consequences of lack of OGG1 activity in the mitochondria are not fully understood.

1.7. Other DNA repair pathways

1.7.1. DNA damage response network

There are a variety of different DNA repair pathways and mechanisms, which together form the DNA damage response (DDR). Presently over 130 human DNA repair genes have been identified, with the main DNA repair pathways shown in Figure **1.13.** (Hansen and Kelley, 2000; Lindahl and Barnes, 2000; Wood *et al.*, 2001; Friedberg, 2008; Jackson and Bartek, 2009; Dexheimer, 2013; Jeggo, Pearl and Carr, 2016; Tubbs and Nussenzweig, 2017). These different pathways are primarily responsible for repairing particular types of DNA damage, for example the role of BER in the repair of oxidative DNA modifications (discussed in **1.4.**). However, the real complexity of the network is generated *via* extensive crosstalk between the multiple pathways and this crosstalk is yet to be fully understood. Through the DDR, cells should be able successfully recognise DNA damage, alert the cell to the presence of the damage and finally mediate its repair through the correct pathway. Thereby, the DDR prevents genomic instability, with the incidence of DNA damage across a genome largely driven by the repair efficiency of the cell rather than damage formation (Lindahl and Barnes, 2000; Freitas and De Magalhães, 2011; Hu *et al.*, 2016; Jeggo, Pearl and Carr, 2016; Tubbs and Nussenzweig, 2017).

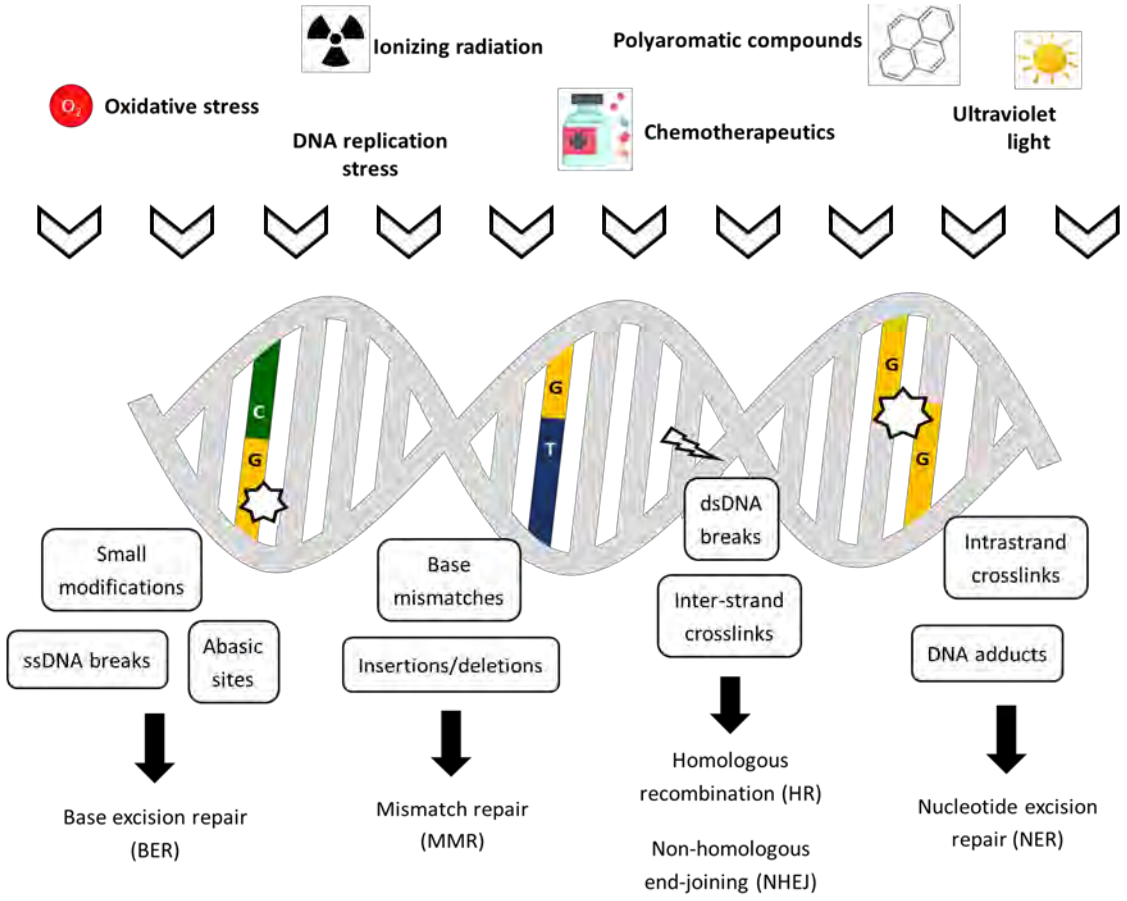


Figure 1.13. Different repair pathways within a cell form the DNA damage response (DDR) network. These different repair pathways within a cell are responsible for repairing different types of DNA damage (Boland *et al.*, 2005; Dexheimer, 2013). Different types of DNA damage are induced in response to DNA-damaging events (*e.g.* oxidative stress, radiation, DNA replication stress, polyaromatic compounds, chemotherapeutic agents, and ultraviolet light). The base excision repair (BER) pathway is responsible for repairing smaller and non-helix distorting lesions, including oxidative DNA modifications and single strand- (ss-) DNA breaks. Alternatively, the nucleotide excision repair (NER) pathway is responsible for repairing larger and helix distorting lesions, including DNA adducts and intra-strand crosslinks. Mismatch repair (MMR) is responsible for the repair of base mismatches, insertions, and deletions. Finally, double strand- (ds-) DNA breaks and intra-strand crosslinks are repaired by one of two mechanisms; homologous recombination (HR) or non-homologous end-joining (NHEJ).

1.7.2. Mismatch repair pathway

One of the most highly conserved pathways is the mismatch repair (MMR) pathway. The MMR pathway is responsible for repairing base mismatches and insertions/deletions, with these often generated during replication and recombination. Inactivation of MMR is associated with genomic instability and numerous cancers, including hereditary non-polyposis colorectal cancer (HNPCC). This relationship between defective MMR and HNPCC is well established, with the mutation status of four MMR genes (*MLH1, MSH2, PMS2* and *MSH6*) routinely tested in suspected HNPCC cases. This example highlights the importance of the pathway in maintaining genomic stability (Fishel *et al.*, 1993; Fishel and Wilson, 1997; Hansen and Kelley, 2000; Jiricny and Marra, 2003; van der Klift *et al.*, 2005; Li, 2008).

1.7.3. Homologous recombination and non-homologous end joining

Another frequent type of DNA damage found in the genome is double strand breaks (DSBs). A cell may cause a DSB intentionally during meiotic recombination or immunoglobulin rearrangement; however, the majority of DSBs are caused by exogenous sources. These breaks can be lethal for a cell and can lead to apoptosis, entry into senescence, and chromosomal aberrations (Jackson and Bartek, 2009; Lieber, 2010; Thompson, 2012). Therefore, the repair of these breaks is crucial. The repair of DSBs can be carried out by two distinct pathways, homologous recombination (HR) and non-homologous end joining (NHEJ). HR is dependent on an intact sister chromatid being present, which is used as a template, and therefore HR is considered the 'error-free' mechanism to repair DSBs (Jackson and Bartek, 2009; Thompson, 2012). NHEJ instead directly ligates the broken DNA in order to eliminate the break, making NHEJ capable of repairing a broader range of DSBs. This mechanism is however much more error-prone and can result in insertions, deletions, and translocations (Lieber, 2010; Lieber and Wilson, 2010; Thompson, 2012). The lethality of DSBs are routinely manipulated in order to treat cancer, with both radiation and numerous chemotherapeutic drugs resulting in these breaks (Jackson and Bartek, 2009; Woods and Turchi, 2013).

1.7.4. Nucleotide excision repair

1.7.4.1. The nucleotide excision repair pathway

The last DNA repair pathway to be discussed is the nucleotide excision repair (NER) pathway (Figure **1.14.**), which is responsible for the repair of helix-distorting lesions such as bulky adducts or intra-strand DNA crosslinks. Examples of exogenous sources of such lesions include ultraviolet (UV) light and the polycyclic aromatic hydrocarbons contained within cigarette smoke (Cleaver, 1968; Sinha and Häder, 2002). The start of the NER pathway can follow two different sub-pathways, either following global genome- (GG-) or transcription coupled- (TC-) NER (Wood, 1997; Schärer, 2013) .

The NER pathway excises the damaged DNA as an oligonucleotide fragment unlike the excision of free bases in the BER pathway. There are a number of proteins involved, which assemble at the site of the damage to form a complex to subsequently excise the damaged region. Multiple crucial NER proteins are included within a multi-protein complex, a transcription factor known as TFIIH, which includes the important helicase proteins ERCC2 (also referred to as XPD) and ERCC3 (also referred to as XPB). The resulting excised oligonucleotide is 24 – 32 nucleotides in length, leaving a gap that is repaired using the remaining intact DNA strand as a template (Wood, 1997; de Laat, Jaspers and Hoeijmakers, 1999; Lindahl and Barnes, 2000; Friedberg, 2001; Kim and Wilson, 2012; Schärer, 2013; Rimel and Taatjes, 2018). Disorders within the NER pathway will prevent the repair of this DNA damage and can lead to serious diseases such as xeroderma pigmentosum (XP), Cockayne syndrome (CS) and trichothiodystrophy (TTD) (Cleaver, 1968; Cleaver, 2005; Cleaver, Lam and Revet, 2009; Bowden *et al.*, 2015).

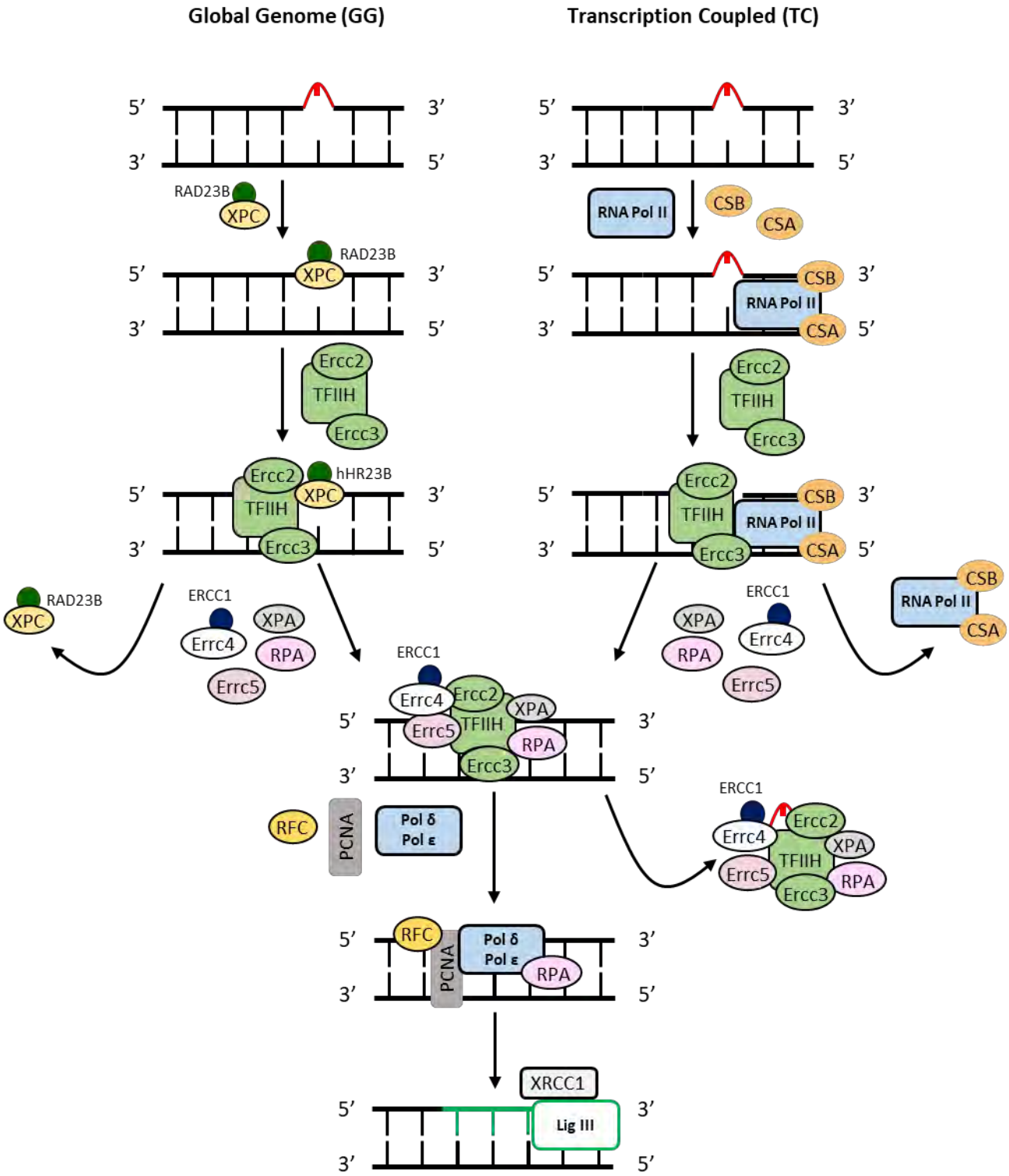


Figure legend continues on next page

Figure 1.14. The nucleotide excision repair (NER) pathway. NER can be separated into two sub-pathways, the global genome- (GG) and the transcription coupled- (TC-) pathway (Schärer, 2013). GG-NER can occur across the genome, and is initiated when the XPC-RAD23B complex recognises DNA damage. Alternatively, TC-NER only repairs lesions within the transcribed stand of active genes, and is initiated when RNA polymerase II becomes blocked on encountering a bulky DNA damage substrate. The stalled RNA polymerase results in the recruitment of the CSA and the CSB complexes. At this point in both pathways, the 10-subunit TFIIH complex is recruited, with two subunits of TFIIH unwinding the DNA to create a 20 - 30 nucleotide bubble encompassing the DNA damage. The remaining NER proteins are then recruited; before XPC-RAD23B (GG-NER) or RNA polymerase II (TC-NER) become displaced. The ERCC1-ERCC4 is then responsible for the 5' incision, and ERCC5 is responsible for the 3' end incision. Following excision, the resulting oligonucleotide (containing the DNA lesion) is released from the DNA with TFIIH. DNA polymerase (Pol δ/ε) is then responsible for repair synthesis, alongside PCNA, RFC, and RPA. Finally, the subsequent nick is ligated by DNA ligase III (LIG3) and XRCC1.

1.7.4.2. NER and oxidative DNA damage

An increasing number of studies have described crosstalk between DNA repair pathways, with such an overlap helping to maintain genomic stability (Slupphaug, Kavli and Krokan, 2003; Kovtun and McMurray, 2007). Classically BER and NER were considered separate and distinct pathways, both responsible for the repair of distinct types of DNA damage as outlined previously. Studies have however implicated NER in the recognition of DNA modifications usually repaired *via* BER, possibly proposing an overlap between these pathways.

Although the majority of oxidative modifications are recognised by specific glycosylases and subsequently repaired by the BER pathway, a number of oxidative modifications are instead recognised and repaired *via* the NER pathway. An example are 5', 8-purine cyclodeoxynucleosides, which are bulkier and helix-distorting lesions when compared to other oxidative DNA modifications (*e.g.* 8-oxoG). These lesions have now been identified as substrates of the NER pathway (Brooks *et al.*, 2000; Kuraoka *et al.*, 2000). Multiple studies have suggested that other smaller oxidative modifications could also act as substrates for the NER pathway, or alternatively that proteins within the NER pathway can aid in the repair of such modifications by acting as co-factors to BER (Reardon *et al.*, 1997; Klungland, Höss, *et al.*, 1999; Miao *et al.*, 2000; Shimizu *et al.*, 2003; Hollander *et al.*, 2005; D'errico *et al.*, 2006; Dušinská *et al.*, 2006).

An early study to implicate NER in the repair of oxidative modifications was Reardon *et al.* (1997), which was based on patients suffering from the NER-linked disease XP. There are multiple types of XP depending on the NER protein that is defective, however all XP patients share a phenotype of impaired NER activity (Cleaver, Lam and Revet, 2009). XP patients are unable to remove pyrimidine dimers due to a defective NER pathway, and therefore have a highly increased risk of developing cancers in response to sun exposure. Interestingly another notable observation in XP patients is an increased risk of neurodegeneration due to neuronal death. Reardon *et al.* (1997) noted that neuronal tissue is protected from sun damage, and therefore they hypothesised that this neurodegeneration was instead due to a

defect in the BER of oxidative modifications, showing that *in vitro* the human NER system was capable of removing both 8-oxoG and Tg (Reardon *et al.*, 1997).

A study almost a decade later by D'errico *et al.* (2006) agreed that the NER system was implicated in the removal of 8-oxoG, demonstrating that XPC possesses repair activity towards 8-oxoG by acting as a cofactor to OGG1 in the recognition and binding of this modification. The paper used keratinocytes and fibroblasts from XP patients to demonstrate that XPC-deficient cells had a higher sensitivity towards oxidative agents compared to WT controls. This was because although XPC-deficient cells were capable of repairing 8-oxoG, due to fully functioning OGG1 activity, this repair occurred at a slower rate due to difficulties with the cleavage of 8-oxoG. This result suggests that XPC plays a role in the cleavage of 8-oxoG, but that XPC is not fundamental to this repair. Furthermore, they utilised purified XPC-RAD23B, which is a crucial component in GG-NER, to show that the complex increased the activity of OGG1. However, XPC-RAD23B alone demonstrated no activity towards 8-oxoG. This ability of XPC to increase the activity of OGG1 towards 8-oxoG was suggested to be due to a direct interaction between the two proteins however the study did struggle to show this interaction, only able to identify a weak interaction through Far-Western analysis (D'errico *et al.*, 2006).

D'errico *et al.* (2006) is not the only study to link XPC to the repair of oxidative DNA damage. Additionally Miao *et al.* (2000) showed that RAD23B interacts with the BER glycosylase, N-methylpurine DNA glycosylase (MPG), to function as an accessory protein. This MPG-RAD23B complex resulted in an increase in the rate of excision of an MPG substrate from DNA. The authors propose that this is evidence that RAD23B is a universal accessory protein, which is not only involved in NER through the XPC-RAD23B complex (Miao *et al.*, 2000). The XPC-RAD23B complex was again implicated in BER by Shimizu *et al.* (2003) with it shown to interact with another BER glycosylase, TDG. This interaction stimulated TDG activity by inducing the release of TDG from abasic sites, and this was found to be particularly significant in the presence of APE1 (Shimizu *et al.*, 2003). Finally, with respect to XPC, Hollander *et al.* (2005)

suggested that the increase in GC->TA transversions that was observed in $XPC^{-/-}$ mice, and the resulting increase in spontaneous lung tumours, was caused by a decrease in the repair of oxidative modifications. Together, these studies provide further evidence that NER and BER are not independent pathways, and propose that they are linked through XPC-RAD23B.

Other NER proteins have also been suggested as candidate NER proteins that are capable of increasing the BER of oxidative modifications. These include the endonuclease ERCC5 (which is often referred to as XPG in earlier papers) (Klungland, Höss, *et al.*, 1999) and XPA (Dušinská *et al.*, 2006). Klungland *et al.* (Klungland, Höss, *et al.*, 1999) proposed that ERCC5 functions as a co-factor to the endonuclease NTHL1, promoting the binding of NTHL1 to DNA substrates. Importantly, this increase in NTHL1 binding activity is also observed in cells harbouring a mutant ERCC5 protein that is inactive with respect to its NER function. This highlights another relationship between NER and BER, showing proteins from the two pathways interacting to increase the repair of oxidative DNA damage. The authors propose that this implicates an inefficiency in the repair of oxidised modifications to the development of disease in ERCC5-linked diseases (Klungland, Rosewell, *et al.*, 1999). Dušinská *et al.* (2006) performed a study with patients harbouring a polymorphic variant of XPA and showed that this polymorphism affected the repair of DNA damage with an accumulation of damage (including 8-oxoG) measured. Furthermore, they showed that OGG1 activity varied between individuals harbouring the XPA polymorphism when compared to individuals with WT XPC. The authors suggest that XPA may therefore play a part in the repair of oxidised DNA (Dušinská *et al.*, 2006).

If the NER pathway does possess a function in the repair of oxidative DNA modifications, it would be expected that NER activity would be affected in conditions of oxidative stress. Langie *et al.* (2007) induced oxidative stress in A549 cells *via* H_2O_2 treatment, with this treatment significantly inducing the expression of multiple NER genes (*Xpa, Xpc, Ercc1, Ercc4* and *Ercc5*). The most significant of these changes was with respect to *Ercc1*, and this result was reflected in a subsequent decrease in the NER capacity of the cell

(Langie *et al.*, 2007). These results show that NER activity is modulated by oxidative stress, indicating the involvement of NER in the cellular response to oxidative stress. Langie *et al.* (2010) extended this research into an animal model, inducing oxidative stress in newborn piglets. They showed that NER capacity became significantly reduced at day seven, when compared to day one. Furthermore, they showed this decrease in NER capacity was reduced in piglets that had undergone antioxidant supplementation (Langie *et al.*, 2010). A separate study by Gopalakrishnan *et al.* (2010) utilised lymphoblastic cells from patients with different NER-deficiencies to show that loss of ERCC2 or ERCC3 function resulted in enhanced sensitivity following H_2O_2 treatment. Interestingly, the loss of functional XPA did not result in changes; but both ERCC3- (XPB-) and XPA-deficient cells did show altered regulation of ERCC2 expression following H_2O_2 treatment. This again highlights the importance of NER in the cellular response to oxidative stress (Gopalakrishnan *et al.*, 2010).

Although these publications do suggest possible details of how the NER and BER interplay with respect to the repair of oxidative modifications, a full and clear mechanism is yet to be elucidated. Authors propose different hypotheses with differing levels of explanation and evidence, without a full understanding of the conditions needed for NER to contribute to the repair of oxidative modifications or the extent to which NER components do contribute.

1.8. Aims and objectives

The aim of this thesis was to investigate the role of OGG1, specifically beyond its role in OGG1-initiated BER, which is often the solitary role that is described for OGG1. This involved investigating the cellular consequences that arise when OGG1 activity is absent, with OGG1-null cells having already been established and shown to be viable. These OGG1-null MEFs were cultured alongside appropriate WT controls, and the differences between the cells investigated.

We hypothesise that an OGG1-independent repair mechanism exists in cells, which is capable of repairing 8-oxoG in the absence of OGG1. This would prevent the accumulation of 8-oxoG in the genome of OGG1-null cells, and could indicate that any differences between WT and of OGG1-null cells are not exclusively linked to OGG1's role in DNA repair.

This work has been separated into four primary objectives:

1. To establish whether the oxidative DNA modification, 8-oxoG, accumulates within the genome of *Ogg1* null MEFs (m*Ogg1*$^{-/-}$ MEFs).
2. To investigate the mechanism of cell death observed in m*Ogg1*$^{-/-}$ MEFs in response to GSH depletion.
3. To identify potential back-up repair mechanisms, which may be capable of repairing 8-oxoG in the absence of OGG1 function.
4. To investigate the consequence of 8-oxoG and 8-oxodG treatment in both WT and m*Ogg1*$^{-/-}$ MEFs.

2

Induction of apoptosis in *Ogg1* null mouse embryonic fibroblasts by GSH depletion is independent of DNA damage

Adapted from publication

Higgs E. B., *Godschalk R., Coltman N., Stewart G. S., van Schooten F. J., Hodges N. J. (2020) Induction of apoptosis in Ogg1-null mouse embryonic fibroblasts by GSH depletion is independent of DNA damage. Toxicology Letters.*

2.1. Introduction

DNA is constantly at risk of encountering DNA damaging events, with it estimated that cells will encounter approximately 70,000 such events each day (Lindahl and Barnes, 2000; Tubbs and Nussenzweig, 2017). This includes the production of oxidative DNA damage, primarily produced on reaction with ROS. Despite the potential risk of oxidative stress and subsequent oxidative DNA damage, low levels of intracellular ROS are physiologically important for redox signalling (Thannickal and Fanburg, 2000; Forman and Torres, 2001; Lambeth, 2004; Fisher, 2009; Murphy, 2009; Ray, Huang and Tsuji, 2012). Therefore, the cell possesses a host of defences that protect against oxidative DNA damage; including cellular antioxidants, DNA repair pathways and apoptosis if necessary (Norbury and Zhivotovsky, 2004; David, O'Shea and Kundu, 2007; Robertson *et al.*, 2009; Rizzo *et al.*, 2010; Roos and Kaina, 2013).

The first line of defence against oxidative DNA damage is the antioxidant response of a cell, with this antioxidant activity composed of a variety of different proteins, as described in Chapter **1** (*refer to* **1.3.**). Crucial to this antioxidant activity are the SOD family of enzymes, which are responsible for the dismutation of superoxide radicals ($O_2^{\bullet-}$) into H_2O_2 and molecular oxygen (O_2) (Michiels *et al.*, 1994; Abreu and Cabelli, 2010). There are different isoforms of SOD, which are expressed in different intracellular locations. Specifically, SOD1 (Cu,Zn SOD) is expressed within the cytoplasm of cells; whereas SOD2 (Mn SOD) is expressed in the mitochondrial matrix, responsible for protecting cells from superoxide generated from the ETC during oxidative phosphorylation (Maier and Chan, 2002; Zelko, Mariani and Folz, 2002; Abreu and Cabelli, 2010). Other important components of the cellular antioxidant defence system include the GSH/GPX system and the enzyme CAT, both antioxidant mechanisms involved in the detoxification of H_2O_2 ($H_2O_2 \rightarrow H_2O$) (Percy, 1984; Michiels *et al.*, 1994; Dickinson and Forman, 2002; Forman, Zhang and Rinna, 2009).

It is important to recognise that despite its non-radical nature, and therefore absence of unpaired electrons, H_2O_2 still poses a risk to the cell. As an electrically neutral species, H_2O_2 is permeable to many cell membranes, meaning it is capable of travelling throughout the cell and exerting its effects in different cellular compartments (Antunes and Cadenas, 2000; Makino *et al.*, 2004; Bienert, Schjoerring and Jahn, 2006; Fisher, 2009). Furthermore, hydroxyl radicals ($HO^{\bullet}$) can be generated from H_2O_2. Hydroxyl radicals are able to abstract hydrogen atoms from cellular macromolecules, and therefore hydroxyl radicals are capable of reacting with genomic DNA to produce both strand breaks and DNA-base oxidation (Winterbourn, 1981; Sato *et al.*, 1992).

If ROS escape the cellular antioxidant defence, they will likely go on to react with nuclear DNA and produce oxidative DNA damage (Cooke *et al.*, 2003). DNA repair is considered the next defence mechanism, with the BER pathway considered the primary repair mechanism for oxidative DNA damage, and the prevalent oxidative DNA modification 8-oxoG being repaired *via* OGG1-mediated BER (David, O'Shea and Kundu, 2007; Klungland and Bjelland, 2007). Although the primary role of OGG1 is considered to be the repair of oxidative DNA damage, studies have also implicated OGG1 in a range of different cellular roles including chromatin remodelling, DNA-methylation, transcriptional activation and cellular signalling (Dantzer *et al.*, 2002; Mabley *et al.*, 2004; Boldogh *et al.*, 2012; German *et al.*, 2013; Hajas *et al.*, 2013; Ba, Aguilera-Aguirre, *et al.*, 2014; Ba, Bacsi, *et al.*, 2014; Luo *et al.*, 2014; Allgayer *et al.*, 2016; Pan *et al.*, 2016; Seifermann and Epe, 2017; Ba and Boldogh, 2018; Sampath and Lloyd, 2019). Despite the research concerning alternative roles of OGG1, it remains common that OGG1 is described solely in terms of its glycosylase role. However, the loss of OGG1 function would likely instead result in a number of downstream effects that are believed to be entirely independent of this glycosylase activity.

The BER pathway is just one of the numerous DNA repair mechanisms that exist within mammalian cells, as discussed in Chapter **1**. (*refer to* **1.7.**). This network of DNA repair pathways have evolved to effectively reduce the occurrence of mutations and maintain genomic stability (Hansen and Kelley, 2000; Jackson

and Bartek, 2009). However, if damage is not effectively repaired then apoptosis can be induced. The induction of apoptosis prevents the replication of damaged DNA and is considered the last defence mechanism against DNA damage (Norbury and Zhivotovsky, 2004; Roos and Kaina, 2006; Foster *et al.*, 2012). Programmed cell death *via* apoptosis is an important mechanism in maintaining genome stability, and defects in these apoptotic pathways have been linked to both carcinogenesis and the development of resistance towards chemotherapeutic drugs (Pommier *et al.*, 2004; Roos and Kaina, 2013). Apoptosis has been linked to DNA damage using knockout models that lack different DNA repair genes, with the majority of such models displaying an increased susceptibility to apoptosis. Furthermore, both ROS and redox signalling have been implicated in the induction of apoptosis, and many antioxidants (*e.g*. N-acetylcysteine) have been shown to inhibit apoptosis (Kannan and Jain, 2000; Kaina, 2003; Norbury and Zhivotovsky, 2004; Ray, Huang and Tsuji, 2012; Roos and Kaina, 2013). Therefore, the evidence suggests that oxidative stress could be a potential mediator of apoptosis but the extent to which oxidative DNA damage contributes is unclear.

In this chapter, the induction of apoptosis in m*Ogg1*$^{-/-}$ MEFs in response to the depletion of GSH is studied. We hypothesised that the *Ogg1*-null MEFs would possess an increased sensitivity to this induction of oxidative stress due to an accumulation of genomic 8-oxoG, which would remain unrepaired in the genome due to lack of OGG1 activity, potentially resulting in apoptosis. We show that, unexpectedly, this induction of apoptosis appears to be independent of oxidative DNA damage. We instead propose that apoptosis is induced in response to a significant increase in mitochondrial superoxide, which causes an increase in oxidative stress across the cell due to the differential expression of key antioxidants. We bring attention to the issue of assuming the only key role of OGG1 is as a DNA glycosylase, proposing that this induction of apoptosis is independent of this glycosylase activity.

2.2. Materials and methods

2.2.1. Cell culture

WT and m*Ogg1*$^{-/-}$ MEFs were a generous gift from T. Lindahl (Klungland, Rosewell, *et al.*, 1999) (Cancer Research UK, Clare Hall Laboratories). Also utilised, were m*Ogg1*$^{-/-}$ MEFs that had previously been stably transfected with two variants of OGG1 in our laboratory (Kershaw and Hodges, 2012). Briefly described, pcDNA3 plasmids that contained either Ser326- (WT) or Cy326- h*OGG1* cDNA (J. Yokota, National Cancer Centre, Tokyo, Japan) (Yamane *et al.*, 2004) were subcloned into mammalian expression vectors (Smart, Chipman and Hodges, 2006), and transfected into m*Ogg1*$^{-/-}$ MEFs. Selection of clones was performed using hygromycin B and the sequence of h*OGG1* confirmed. Gene expression, genomic DNA incorporation and protein expression were also measured (Kershaw and Hodges, 2012).

All cells were maintained in Dulbecco's Modified Eagles Medium (DMEM) (Gibco: catalogue no. 41965047, with phenol-red, L-glutamine and 4.5 g/L D-glucose). DMEM was supplemented before use with foetal bovine serum (FBS) (10% v/v), L-glutamine (2 mM), penicillin (100 units/mL) and streptomycin (100 μg/mL). To switch the energy source within media from glucose to galactose, glucose-free DMEM (Gibco: catalogue no. 11966025, with phenol-red and L-glutamine) was supplemented with 10 mM galactose on top of the standard supplementation regime described (FBS/L-glutamine/penicillin/streptomycin) (Marroquin *et al.*, 2007). All media and supplements were purchased from either Gibco (ThermoFisher) or Sigma-Aldrich (Merck). Once prepared, complete media was stored at 4°C for a maximum of one month. All cell culture work was carried out under suitable sterile conditions in a Class 2 tissue culture hood (Aura B4, Bio Air, Italy) and cells were incubated at 37°C and 5% CO_2 (Sanyo MCO-19AIC Incubator). Cells were frequently assessed to monitor growth and check for contamination and cells were routinely passaged on reaching 80 - 90% confluence. Full details of cell culture methodology, including mycoplasma testing, is described in the appendix (**7.1.1.**).

2.2.2. Treatment of cells

BSO Treatment

DL-buthionine-(*S,R*)-sulfoximine (BSO) (Sigma-Aldrich, Merck: catalogue no. B2640) was prepared as a stock solution (50 mM) in supplemented DMEM. Diluted aliquots (5 mM) were prepared and subsequently stored at -20°C. Aliquots were thawed a maximum of two times before disposal. Immediately prior to use, BSO was further diluted with supplemented DMEM to the required concentration.

H_2O_2 Treatment

H_2O_2 (30% v/v) (VWR International) was freshly prepared immediately prior to an experiment. A stock solution (0.5 M) was prepared in supplemented DMEM on the day of the experiment, and this was further diluted with supplemented DMEM to the required concentration.

Etoposide Treatment

Etoposide (Sigma-Aldrich, Merck: catalogue no. E1383) was prepared as a stock solution (3.4 mM) in dimethyl sulfoxide (DMSO), with this stock solution subsequently stored at room temperature (RT). Immediately prior to use, etoposide was further diluted with supplemented DMEM.

Antimycin-A Treatment

Antimycin-A (Sigma-Aldrich, Merck: catalogue no. A8674) was prepared as a stock solution (5 mM) in ethanol (EtOH) (95% v/v) and stored at -20°C. Immediately prior to use, antimycin-A was further diluted with supplemented DMEM.

Rotenone treatment

Rotenone (Sigma-Aldrich, Merck: catalogue no. R8875) was prepared as a stock solution (10 mM) in DMSO (VWR International) and stored at -20°C. Immediately prior to use, rotenone was further diluted with supplemented DMEM to the required concentration, ensuring a final DMSO concentration ≤ 0.5%.

2.2.3. Polymerase chain reaction (PCR)

Total RNA extraction

Total RNA extraction was carried out using the RNeasy Mini Kit as per the manufacturer's instructions (Qiagen: catalogue no. 74104). Cells (< 2 x 10^5) were first trypsinised, centrifuged (1500 rpm, 5 minutes (min)) and the supernatant removed. The RNA extraction method consisted of resuspending the pelleted cells in lysis buffer (350 μL), followed by a brief vortex, and the addition of EtOH (350 μL, 70% v/v). Samples were transferred to a spin column and centrifuged (8000 g, 15 seconds (sec)). The flow-through was discarded and the column was washed with RW1 buffer (350 μL) and was again centrifuged (8000 g, 15 sec). The flow-through was again discarded and DNase I incubation mix (80 μL) was added directly to the column and incubated RT (15 min), with this step necessary to prevent genomic DNA contamination. RW1 buffer (350 μL) was again added and the column centrifuged (8000 g, 15 sec). The flow-through was discarded and the column washed twice more with RPE buffer. Total RNA was then eluted from the column with RNase-free water (40 μL) and quantified by UV spectroscopy (NanoDrop ™ spectrophotometer, Thermo Scientific). RNA was then stored at -80°C until needed.

Complementary DNA synthesis

Complementary DNA (cDNA) was synthesised using the Tetro cDNA synthesis kit as per the manufacturer's instruction (Bioline: catalogue no. BIO-65042). RNA (5 μg) was added to a sterile Eppendorf containing the following: oligo (dT) primers (1 μL), dNTP mix (1 μL, 10 mM), buffer (4 μL), RNase inhibitor (1 μL, 10 unit/μL), Tetro reverse transcriptase (1 μL, 200 unit/μL) and RNase free water. Samples were incubated at 45°C (30 min) to allow the reverse transcription to occur, and the reaction terminated by incubating at 85°C (5 min). cDNA was stored at -20°C until needed.

PCR and gel electrophoresis

cDNA was used in a PCR reaction in order to amplify a specific sequence of m*Ogg1* mRNA using specific primers (synthesised by AltaBioscience).

Forward Primer: **5'** ACT – CAC – CTG – AGG – AAG – TTG – GG **3'**

Reverse Primer: **5'** CCC – TTA – GCC – TGG – GAT – GTC – TT **3'**

Reaction mixes were prepared with cDNA (250 ng), forward primer (20 pmol), reverse primer (20 pmol), MyTaq™ DNA polymerase (1 μL) and MyTaq™ reaction buffer (10 μL) (Bioline: catalogue no. BIO-21105). PCR was performed (*refer to* Table **2.1.** for conditions) and the resulting PCR product (20 μL) added to loading dye (5 μL) (New England BioLabs: catalogue no. B7025S). The products were separated on a 2% agarose gel containing ethidium bromide (EtBr) (0.5 μg/mL), alongside a suitable marker ladder (100 bp DNA ladder, New England BioLabs: catalogue no. N3231L). The gel imaged under UV light to identify the PCR product of 290 bp (Geneflash, Syngene Bio imaging).

Table 2.1. *Ogg1* PCR conditions

Number of cycles	Temperature (°C)	Duration
1	95	2 min
35	95	30 sec
	55	30 sec
	72	2 min
1	72	10 min

2.2.4. Western blotting

Nuclear protein extraction

The proteins of interest were DNA repair proteins primarily located in the nucleus. Therefore, nuclear-enriched extractions were prepared using NE-PER™ Nuclear and Cytoplasmic Extraction Reagents (Thermo Scientific: catalogue no. 78833).

Cells were seeded in a T_{75} flask and grown until confluent. The cells were then trypsinised and cells (approximately 1 x 10^6) collected and centrifuged (500 g, 5 min). Cells were briefly washed with phosphate buffered saline (PBS) and centrifuged again (500 g, 5 min). The supernatant was removed from the pellet, and ice-cold CER I reagent (200 μL) added. The sample was vortexed (15 sec) and then incubated on ice for 10 min. Ice-cold CER II reagent (11 μL) was added to the sample, which was then vortexed (5 sec) and briefly incubated on ice (60 sec). The sample was vortexed once again (5 sec) before centrifugation (16000 g, 5 min) at 4°C. The resulting supernatant, comprising the cytoplasmic extract, was discarded. The remaining nuclear pellet was resuspended in ice-cold NER reagent (100 μL) and vortexed (15 sec). The sample was placed on ice for 40 min and was briefly vortexed (15 sec) at 10 min intervals, prior to another centrifugation step (16000 g, 10 min) at 4°C. The resulting supernatant (nuclear extract) was transferred to an Eppendorf and stored at -80°C.

Buffers and solutions

Tris-buffered saline with Tween (TBST) | Tris base (0.1 M), NaCl (0.15 M), tween-20 (0.05% v/v)

Sodium dodecyl sulfate (SDS) - polyacrylamide gel electrophoresis (PAGE) running buffer | Tris base (25 mM), glycine (192 mM), SDS (0.1% w/v).

Transfer buffer | Tris base (20 mM), glycine (150 mM), methanol (MeOH) (20% v/v)

Blocking buffer | Non-fat milk powder (5% w/v) in TBST

Resolving gel | Protogel (12.5% v/v) (National Diagnostics: catalogue no. EC-890), SDS (0.1% w/v), tris-HCl (375 mM) (pH 8.8).

Stacking gel | Protogel (4% v/v) (National Diagnostics: catalogue no. EC-890), SDS (0.1% w/v), and tris-HCl (125 mM) (pH 6.8).

Note: Tetramethylethylenediamine (*0.15% v/v) and ammonium persulfate* (*0.15% w/v) were added to resolving and stacking gel immediately prior to use.*

SDS-PAGE and transfer method

Protein concentration was determined with the Bradford assay (Bradford, 1976) (appendix **7.1.2.**) and extracts diluted to a constant concentration. Equal volumes of protein extracts were added to equal volumes of Laemmli buffer (Sigma-Aldrich, Merck), and heated at 95°C (5 min). Samples (30 μL/well, 20 μg protein) were loaded alongside a protein marker ladder (Colour Prestained Protein Standard, Broad Range, 11-245 kDa) (New England BioLabs: catalogue no. P7712). All empty wells loaded with Laemmli buffer (30 μL). The gel was resolved in the presence of running buffer (120 V) and the separated proteins subsequently transferred to polyvinylidene fluoride (PVDF) (GE healthcare Amersham™) in the presence of transfer buffer whilst maintained on ice (100 V, 2 hours (h)). Prior to this transfer reaction, the PVDF membrane was activated by soaking in MeOH (30 sec).

Antibody binding and blot development

Following the protein transfer, membranes were rocked in blocking buffer at RT (1 h). Primary antibodies were then added at appropriate dilutions (Table **2.2.**) and rocked overnight at 4°C. The following day, the membrane was washed three times in TBST (15 min/wash) and membranes subsequently incubated with a secondary antibody at RT (1 h). The membrane underwent another three TBST washes prior to protein detection, which was achieved using chemiluminescence reagents (SuperSignal™ West Femto, Thermo Scientific: catalogue no. 34094). The membrane was placed in saran wrap and, in appropriate darkroom

conditions, x-ray film (HyperFilm™ ECL, GE healthcare Amersham: catalogue no. 28-9068-37) was incubated on the membrane for varying exposure times. The film was then developed (Curix 60 film processor, AGFA).

Table 2.2. Antibodies used

Target	Dilution	Supplier	Catalogue number	Secondary antibody
OGG1	1:500	ProteinTech	15125-1-AP	Goat anti-rabbit IgG H+L (HRP) 1:500 dilution (Invitrogen, ThermoFisher Scientific)
β-ACTIN	1:10000	Sigma-Aldrich, Merck	A2228	Goat anti-mouse IgG H+L (HRP) 1:10000 dilution (Abcam)

2.2.5. MTT assay

3-[4,5-Dimethylthiazol-2-yl]-2,5-diphenyl tetrazolium bromide (MTT) is a water-soluble dye that can easily cross cell membranes. Once within the cell, the dye is reduced, predominantly by the mitochondrial enzyme succinate dehydrogenase. This reduction produces formazan crystals, which are soluble in DMSO, resulting in a purple solution that can be detected at the absorbance of 570 nm. The principle of the assay is that cells with functional mitochondria are able to successfully reduce the dye and produce formazan crystals, whereas non-viable cells are not capable of this. Therefore the absorbance measured at 570 nm can be considered proportional to the number of viable cells within a population (Hussain, Nouri and Oliver, 1993).

MEFs were seeded in 96-well plates (7 x 10^3 cells/well) and treated appropriately the following day. Once the treatment was compete, the existing media in each well was removed and replaced with media (100 μL) containing MTT solution (0.5 mg/mL). Cells were then incubated at 37°C for 3 h, allowing formazan crystals to form. Following incubation the media was carefully removed and replaced with DMSO (VWR International) (200 μL). The plates were gently rocked in the dark at RT (30 min) to allow the formazan crystals to dissolve. The absorbance of each well was measured at 570 nm (Infinite® 200 Pro, Tecan) and the absorbance of DMSO blank wells subtracted. Absorbance was then converted to percentage viability using non-treated cells.

2.2.6. Crystal violet viability assay

Crystal violet is a purple dye that binds to proteins and DNA; and can therefore be used to measure the number of adherent cells present. Healthy adherent cells will strongly adhere to the surface of plastic vessels, whereas cells that undergo cell death will lose this adherence. During the assay, cells are washed with PBS and non-attached cells will be removed from the well during these washing steps. Viable cells will remain attached and will be stained with crystal violet. The assay works on the principle that healthy cells will remain attached, whereas non-viable cells will not. Therefore the total number of cells attached is a measure of viability (Saotome, Morita and Umeda, 1989).

MEFs were seeded in 96-well plates (7×10^3 cells/well) and treated appropriately the following day. Once the treatment was complete, media was removed from cells, and cells were then washed with PBS three times. Paraformaldehyde (PFA) (100 μL, 4% v/v) was added to each well and incubated at RT (15 min). The PFA was removed from cells and replaced with crystal violet (100 μL, 0.5% v/v). The cells were incubated in the crystal violet at RT (20 min). The crystal violet was removed from wells, and cells thoroughly washed with distilled H_2O (dH_2O). The plates were allowed to air-dry for a minimum of 30 min, before acetic acid (100 μL, 10% v/v) was added to each well. The plate was gently rocked at RT (20 min) and the absorbance of each well was measured at 595 nm (Infinite® 200 Pro, Tecan). The absorbance of acetic acid blanks were subtracted from each measurement, and absorbance was then converted to percentage viability using non-treated cells.

2.2.7. CellTox™ Green cytotoxicity assay

The CellTox™ Green cytotoxicity assay (Promega) utilises a cyanine dye which binds to DNA, but is only able to cross the membranes of dead cells. Therefore, fluorescence is produced in response to dead cells, allowing it to be used as a measure of cytotoxicity. The dye can be added to cells at the dosing stage and fluorescence measured over time, allowing for the kinetic measurement of cytotoxicity in response treatment.

MEFs were seeded in 96-well plates (6 x 10^3 cells/well) and allowed to adhere overnight. Appropriate treatments and CellTox™ dye was simultaneously added to wells. The plate was gently rocked (10 min) and fluorescence measured ($\lambda_{excitation}$ 485 nm; $\lambda_{emission}$ 535 nm) (Infinite® 200 Pro, Tecan). The plate was then returned to incubation (37°C, 5% CO_2) and fluorescence was measured at intervals over the treatment period. A positive lysis control (Promega) was used to treat a group of positive control cells; and cells that did not have the CellTox™ reagent added were used as a blank. The fluorescence of the blank cells were subtracted, and the positive control cells were used to calculate the cytotoxicity (%) of treated cells, as described in Equation **1**.

Equation 1 | $$\%\ \boldsymbol{cytotoxicity} = \left(\frac{absorbance - blank}{absorbance\ of\ positive\ control} \right) x\ 100$$

2.2.8. Measurement of apoptotic cells

Apoptosis (annexin V and propidium iodide) assay

Apoptosis is a type of cell death that is characterised by a set of distinct biochemical and physical changes within the cell. One of these changes is the translocation of phosphatidylserine (PS) from the inner layer of the plasma membrane, where PS is maintained in healthy cells, to the outer leaflet of the plasma membrane. This externalisation of PS ultimately leads to the phagocytosis of apoptotic cells (Fadok *et al.*, 2000).This externalisation of PS was measured as an indication of apoptotic cells using a fluorescent conjugate of annexin V. Annexin V is able to recognise PS on the surface of cells and bind to it with high affinity, with the conjugation of fluorescein isothiocyanate (FITC) allowing the quantification of annexin V-bound PS ($\lambda_{excitation}$ 494 nm; $\lambda_{emission}$ 518 nm). Propidium iodide (PI) can be utilised as a counterstain, with PI intercalating with DNA. However, PI is actively excluded from viable cells, and therefore PI will only bind to the DNA of non-viable cells. The fluorescence of PI is greatly enhanced when bound to DNA, and this fluorescence can be measured alongside the fluorescence of annexin V-FITC ($\lambda_{excitation}$ 535 nm and $\lambda_{emission}$ 617 nm). Therefore, by using annexin V-FITC and PI in conjunction, it is possible to distinguish early apoptotic-, late apoptotic- and non-viable- cells (Aubry *et al.*, 1999).

MEFs were seeded in 6-well plates (1.2 x 10^5 cells/well) and treated appropriately the following day. Cells treated with etoposide (60 μM; 16 h) were included as a positive control for apoptosis (Karpinich *et al.*, 2002). Once the treatment was complete, media was gently removed from each well and transferred into a corresponding falcon tube. Cells were briefly washed with PBS (500 μL). The PBS was then gently removed from wells and transferred into those same corresponding falcon tubes. Trypsin-ethylenediaminetetraacetic acid (EDTA) (250 μL, 0.25% w/v) was added to cells, ensuring that all cells had detached from the surface, and complete media was then added to deactivate the trypsin. The cell suspension was removed and again transferred to the corresponding falcon tube. It was important that all cells for each sample (including detached, non-viable cells) were combined into one falcon tube and

analysed. The complete samples were then centrifuged (1500 rpm, 10 min), resuspended in DMEM, and again centrifuged (1500 rpm, 10 min). The supernatant was discarded and each pellet resuspended in the binding buffer included within the kit (500 μL). Annexin V-FITC (7.5 μg) and PI (12.5 μg) were added to each sample (Annexin V-FITC apoptosis kit, RayBiotech: catalogue no. 68FT-AnnV-S25), and all samples were subsequently incubated at RT in the dark (5 min). The samples were analysed by flow cytometry (BD FACS Calibur™, BD Biosciences) using the FL1 (530/30 nm) channel for annexin V-FITC measurement and the FL2 (585/42) channel for PI measurement. Each sample was briefly vortexed immediately prior to analysis, and 10,000 events were measured per sample.

Analysis of apoptotic cells

Flowing software (http://flowingsoftware.btk.fi/) was used for the analysis of data. Initially, all cellular debris and doublet cells were excluded from measurement through the production of gates. The data was then presented as a dot plot, with PI fluorescence plotted against annexin V-FITC fluorescence. The negative and positive samples were used to set appropriate quadrants, with each quadrant representing cells in a different apoptotic state, as shown in Table **2.3.** Cells that were annexin (–) and PI (-) represented healthy cells; cells that were annexin (+) and PI (–) represented early-apoptotic cells; and cells that were annexin (+) and PI (+) represented non-viable cells. Literature suggests that annexin (–) and PI (+) cells represent necrotic cells (Vermes *et al.*, 1995; Crowley *et al.*, 2016), however few cells of this status were detected in these experiments. The percentage of cells in each quadrant was calculated, and annexin (+): PI (–) cells and annexin (+): PI (+) cells were combined to represent total apoptotic cells (%).

Table 2.3. Annexin V-FITC and PI detection of apoptotic cells

	Healthy	Early apoptosis	Late apoptosis	Necrosis
Annexin V-FITC	–	+	+	–
PI	–	–	+	+

2.2.9. GSH determination assay

Buffers and solutions

Phosphate-EDTA buffer | Na_2EDTA (5 mM), and NaH_2PO_4 (100 mM). Adjusted to pH 8

Cell lysis buffer | Triton X-100 (0.1% v/v) in phosphate-EDTA buffer

Protein precipitation buffer | Trichloroacetic acid (TCA) (50% w/v) in phosphate-EDTA buffer

***o*-Phthalaldehyde (OPT) solution** | OPT (1 mg/mL) (MP Biomedical: catalogue no. SKU 0210264901) in MeOH

Whole cell GSH

OPT (*o*-phthalaldehyde) is a non-fluorescent aldehyde, which will fluoresce when it reacts with GSH, and the resulting fluorescence can be used to measure GSH levels, as first described by Hissin and Hilf (1976). MEFs were seeded in 6-well plates (1×10^5 cells/wells) and treated appropriately the following day. Once treatment was complete, cells were briefly washed with PBS and ice-cold lysis buffer (450 μL) added to each well. From this stage, the assay was carried out on ice and all solutions kept ice-cold. The cells were thoroughly scraped into the lysis buffer, ensuring that all cells had detached from the surface. At this stage, 20 μL of each sample was stored at -80°C until needed for protein quantification using the Bradford assay (Bradford, 1976). The remainder of each sample was transferred to a sterile Eppendorf and protein precipitation buffer (50 μL) added. Samples were centrifuged (13,000 rpm, 5 min) at 4°C, and the resulting supernatant stored at -80°C until use.

Mitochondrial GSH

GSH content of mitochondrial extracts was also carried out. This used the same method as described above, however ice-cold lysis buffer (50 μL) was added directly to mitochondrial extracts, which were thoroughly vortexed at regular intervals over 30 min, whilst incubated on ice. Mitochondrial extracts were prepared using a mitochondrial isolation kit for cultured cells following the Dounce homogenisation

method, as per the manufacturer's instruction (Thermo Scientific: catalogue no. 89874). Cells were trypsinised and centrifuged (850 g, 2 min). The supernatant was removed and reagent A (plus protease inhibitor) (800 μL) added to the pellet. The sample was vortexed at medium speed (5 sec) and then incubated on ice (2 min). The sample was transferred to a chilled Dounce tissue homogeniser, and cells homogenised on ice (> 60 strokes). The lysed cells were added reagent C (plus protease inhibitor) (800 μL), and the Eppendorf inverted several times. Samples were centrifuged (700 g, 15 min) and the supernatant (containing the cytosolic fraction) discarded, prior to the addition of Reagent C (500 μL) to the pellet and centrifugation (12,000 g, 5 min). The supernatant was again discarded and the pellet (which contained the mitochondrial extract) was stored at -80°C until needed.

GSH assay

The assay was done using a 96-well plate that contained both the samples and a GSH standard curve. The GSH standard curve (0 - 1 μg) was produced by adding varying volumes of GSH to wells containing phosphate-EDTA buffer (180 μL) and TCA (100 μL, 5% w/v). The test samples were prepared by adding each sample (100 μL) to wells containing phosphate-EDTA (180 μL). OPT (100 μL, 1 mg/mL) was then added to both standard curve and test samples. The plate was gently rocked in the dark at RT (20 min) prior to fluorescence being measured ($\lambda_{excitation}$ 355 nm and $\lambda_{emission}$ 420 nm) (Infinite® 200 Pro, Tecan). The resulting fluorescence of each test sample was then converted to GSH (μg) using the standard curve, which was used to calculate the amount of GSH (μg/μL) within each sample. Finally, these values were normalised using the Bradford assay (Bradford, 1976) (appendix **7.1.2**.), and converted to nmol GSH/mg total protein.

2.2.10. Measurement of intracellular ROS

H_2DCF-DA assay

The compound 2',7'-dichlorodihydrofluorescin-diacetate (H_2DCF-DA) (Invitrogen, ThermoFisher Scientific) was used to detect intracellular ROS. Cells were incubated with media containing H_2DCF-DA, allowing the compound to be taken up by cells and rapidly hydrolysed by intracellular esterases. This reaction results in the production of the non-fluorescent compound 2, 7-dichlorodihydrofluorescin (H_2DCF), which is oxidised to the fluorophore, dichlorofluorescein (DCF). This reaction occurs in the presence of intracellular ROS, which results in the production of DCF. The fluorescence produced by DCF is measured using flow cytometry, and this can therefore be used as a measure of intracellular ROS (Carini *et al.*, 2000; Gomes, Fernandes and Lima, 2005; Bartosz, 2006; Eruslanov and Kusmartsev, 2010).

MEFs were seeded in 6-well or 12-well plates and treated appropriately the following day. Once treatment was complete, cells were incubated (1 h) with media containing 10 μM H_2DCF-DA. It was important that blank samples were always included in the assay, with these samples having not been incubated with H_2DCF-DA.

Following incubation with H_2DCF-DA, the media was removed and cells were briefly washed with PBS. Trypsin-EDTA was added to cells and once all cells had detached from the surface (~ 7 min), complete media was added (deactivating the trypsin-EDTA) and cells thoroughly resuspended to encourage a single cell suspension. Each sample was transferred to an Eppendorf and centrifuged (4000 rpm, 4 min). The cells were resuspended in PBS, vortexed just prior to analysis, and then 10,000 events analysed per sample (BD FACS Calibur™, BD Biosciences) using the FL1 (530/30 nm) channel.

Mitochondrial superoxide detection

The fluorescent probe MitoSOX™ Red (Invitrogen, ThermoFisher Scientific: catalogue no. M36008), which is a derivative of dihydroethidium, was used to detect mitochondrial superoxide (Mukhopadhyay *et al.*, 2007). Cells were incubated with media containing MitoSOX™ Red, allowing the probe to permeate live cells and be rapidly taken up by actively respiring mitochondria, where it can be oxidised to form a fluorescent product. This fluorescence is measured using flow cytometry, thereby detecting superoxide species within mitochondria.

MEFs were seeded in 6-well or 12-well plates and treated appropriately the following day. Following treatment, cells were incubated for 15 min with media containing MitoSOX™ Red (5 μM). Once again, it was important that blank samples, which were not incubated with the probe, were included in the assay. The media was then removed and cells were briefly washed with PBS. Trypsin-EDTA was added to cells until all cells had detached from the surface (~ 7 min). Complete media was then added and cells were thoroughly resuspended to encourage a single cell suspension, prior to centrifugation (4000 rpm, 4 min). The cells were resuspended in PBS, vortexed just prior to analysis, and then 10,000 events analysed per sample (BD FACS Calibur™, BD Biosciences) using the FL2 (585/42) channel.

Analysis of flow cytometry data

Flowing software (http://flowingsoftware.btk.fi/) was used for the analysis and presentation of all flow cytometry data. All non-viable cells and doublet cells were excluded from measurement through the production of gates. The fluorescent-negative populations of cells were then used to determine a fluorescence threshold for each probe, which would act as a blank reading. Once gates had been applied and the fluorescence threshold determined, a histogram was created per sample. Data was then presented as median fluorescence, after subtracting the median fluorescence of the blank samples.

2.2.11. Quantitative PCR

For quantitative PCR (qPCR), total RNA was extracted from WT and MEFs with the RNeasy mini kit (Qiagen: catalogue no. 74104), as described in **2.2.3.**

cDNA synthesis

The total RNA extracted was used to synthesise cDNA using the high capacity cDNA reverse transcription kit as per the manufacturer's instructions (Applied Biosystems, ThermoFisher Scientific: catalogue no. 4368814). A reverse transcription mix was prepared which contained the following: buffer (2 μL, 10x conc.), dNTP mix (0.8 μL, 25x conc.), random hexamers (2 μL, 10x conc.), RNase inhibitor (1 μL), Multiscribe™ reverse transcriptase (1 μL), and RNase free water (3.2 μL). cDNA (10 μL, 1 μg) was subsequently added to this reverse transcription mix (10 μL), which was then mixed well and briefly centrifuged. The samples were loaded into a thermocycler (Eppendorf) and incubated at 25°C (10 min), followed by incubation at 37°C (2 h). The reaction was subsequently terminated by incubating samples at 85°C (5 min), and cDNA was stored at -20°C until needed.

qPCR

Taqman gene expression assays (Applied Biosystems, ThermoFisher Scientific) were obtained for catalase (*Cat*), superoxide dismutase 1 (*Sod1*), superoxide dismutase 2 (*Sod2*), glutathione peroxidase (*Gpx*), glyceraldehyde 3-phosphate dehydrogenase (*Gapdh*) and heat shock protein 90 alpha family class B member 1 (*Hsp90ab1*) (*refer to* Table **2.4.** for details). A mastermix was prepared for each reaction (50 μL) containing the following: Taqman gene expression mastermix (25 μL, 2x conc.), Taqman gene expression assay (2.5 μL), and cDNA (22.5 μL, 50 ng diluted in H_2O). The mastermix was maintained on ice and was briefly centrifuged before use. Each reaction (50 μL) was then transferred to a qPCR compatible 96-well plate, which was subsequently sealed. The plate was centrifuged (600 g, 1 min) prior to PCR (*refer to* Table **2.5.** for PCR conditions).

Table 2.4. Taqman qPCR probes

Gene	Catalogue number *	Gene	Catalogue number *
Ogg1	Mm00501781_m1	*Gpx*	Mm00656767_g1
Cat	Mm00437992_m1	*Gapdh*	Mm99999915_g1
Sod1	Mm01344233_g1	*Hsp90ab1*	Mm00833431_g1
Sod2	Mm01313000_m1		

** all primers obtained from Applied Biosystems, ThermoFisher Scientific*

Table 2.5. qPCR conditions

Number of cycles	Temperature (°C)	Duration
1	50	2 min
1	95	10 min
40	95	15 sec
	60	1 min

Analysis

The probes for *Gapdh* and *Hsp90ab1* were included as endogenous controls and used to calculate ΔCt values for each reaction. Comparisons between samples were calculated as ΔΔCt values, which were then converted to fold-change. These calculations are described in Equation **2.**

Equation 2 | I. $\Delta \boldsymbol{Ct} = Ct_{Gene} - Ct_{Endogenous\ Control\ Gene}$

II $\Delta\Delta \boldsymbol{Ct} = \Delta Ct_{Treated} - \Delta Ct_{Control}$

III. $\boldsymbol{Fold\ Change} = 2^{-\Delta\Delta Ct}$

2.2.12. Adenosine triphosphate measurements

The production of adenosine triphosphate (ATP) was measured using a commercially available kit, the CellTiter-Glo® luminescent cell viability assay (Promega: catalogue no. G7570). This assay uses ATP quantitation as a measure of cell viability but can also be used to directly measure ATP. The reagent was added to cultured cells, simultaneously lysing cells and producing a luminescent signal in response to ATP. The reagent contains luciferin and Ultra-Glo™ Luciferase, which will together form the luminescent product oxyluciferin in the presence of ATP. Therefore, the resulting luminescent signal is proportional to the amount of ATP present in the sample.

MEFs were seeded at varying densities (1 - 8 x 10^3 cells/well) in two identical plate set-ups, using one opaque 96-well plate and one clear 96-well plate. The following day, the supplied reagent was added to the opaque 96-well plate and the plate mixed on an orbital shaker (2 min). The plate was briefly incubated at RT (10 min) and luminescence measured (Infinite® 200 Pro, Tecan). The clear 96-well plate was used for a Bradford assay (Bradford, 1976) (appendix **7.1.2.**), which was then used to normalise the luminescence data considering cell number.

2.2.13. OGG1-modified comet assay

The standard alkaline comet assay quantitates single strand- (ss-) breaks in DNA, with the method having been extensively used since its development in the 1980s (Singh *et al.*, 1988). Utilising an additional step of incubation with OGG1, additional single strand breaks can be measured and these represent sites of oxidative DNA damage (Cadet *et al.*, 2000; Smith, O'Donovan and Martin, 2006; Collins, 2014). Each sample in the assay was used to produce two paired slides. One slide was incubated with hOGG1 (Trevigen: catalogue no. 4130-100-FK) and one slide was incubated with enzyme buffer, which represented the vehicle control. The difference in the single strand breaks between the two slides represents the oxidative DNA damage (measured in terms of % tail intensity) (Figure **2.1.**).

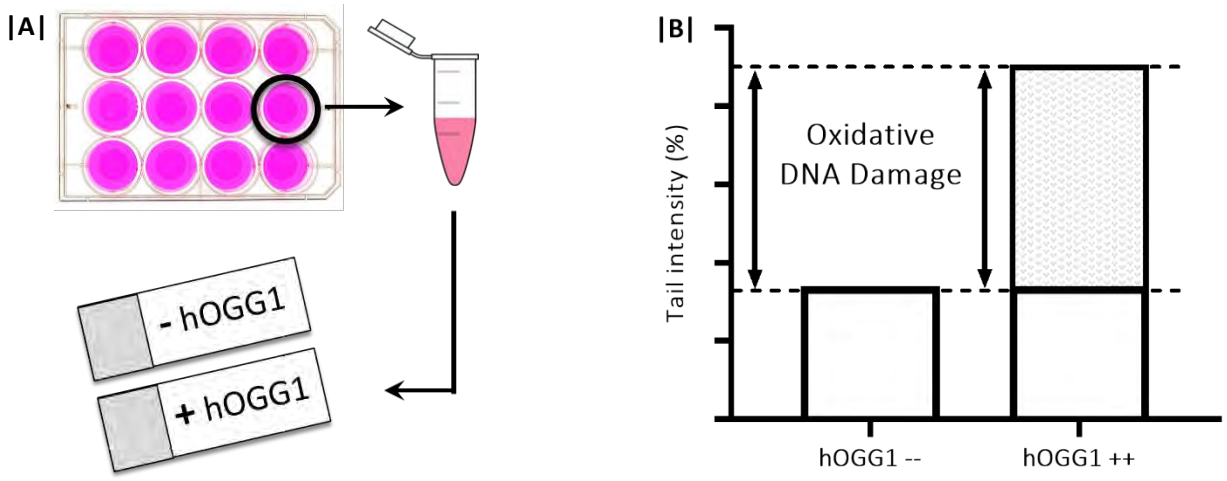


Figure 2.1. The hOGG1-modified comet assay methodology. **|A|** One sample is used to produce two identical slides, one of which will be incubated with hOGG1 enzyme, and one of which will be incubated with a vehicle control. **|B|** The difference in tail intensity (%) between the hOGG1-negative slide and hOGG1-positive slide is representative of the genomic 8-oxoG lesions present in the sample.

Buffers and solutions

Normal melting agarose (NMA) | Agarose (1% w/v) in PBS.

Low melting agarose (LMA) | Agarose (0.7% w/v) in PBS.

Lysis solution | NaCl (2.5 M), Na_2EDTA (0.1 M), tris-HCl (8 mM), NaOH (200 mM), DMSO (10% v/v), and triton-X (1% v/v). Adjusted to pH 10.

Enzyme buffer | 4-(2-hydroxyethyl)-1-piperazineethanesulfonic acid (HEPES) (40 mM), KCl (0.1 M), EDTA (0.5 mM), bovine serum albumin (BSA) (0.2 mg/mL). Adjusted to pH 8.

Electrophoretic buffer | NaOH (300 mM) and Na_2EDTA (1 mM).

Neutralisation solution | Tris-HCl (0.4 M) adjusted to pH 7.5.

Slide preparation and lysis

Cells were seeded in 12-well plates (4 x 10^4 cells/well) and treated appropriately the following day. Following treatment, cells were trypsinised and the cell suspension was diluted to give a density of 1 - 5 x 10^4 cells/ml. The cells were briefly centrifuged (3500 rpm, 1 min) and the pellet resuspended in PBS. Samples were again briefly centrifuged (3500 rpm, 1 min) and the supernatant removed. Cells were resuspended in LMA (180 μL) and this was loaded onto two paired slides (90 μL/slide), which had been pre-coated with NMA. The slides were incubated at 4°C (20 min) before another 90 μL LMA was added to each slide. The slides were again incubated at 4°C (20 min) and then placed in lysis solution for 1 h.

Enzyme incubation, electrophoresis and fixation

Following lysis, the cells were either incubated with hOGG1 (1 unit/slide) or enzyme buffer at 37°C (30 min). The slides were immediately placed in an electrophoretic chamber containing electrophoretic buffer at 4°C to allow the unwinding of DNA, and remained in the buffer for 30 min. Electrophoresis was then carried out (300 mA and 0.78 V/cm) for 30 min. Neutralisation solution was added to each slide (2 mL, 5 min) and slides then fixed with ice-cold EtOH (2 mL).

Comet scoring

Once dry, the slides were stained with SYBR gold staining solution overnight (90 μL, 1:1000 dilution in dH_2O) (Invitrogen, ThermoFisher Scientific: catalogue no. S11494). The cells were evaluated under a fluorescent microscope (Zeiss Axiovert 10 (*20x* objective); $\lambda_{excitation}$ 515-560 nm; 540 nm barrier filter). Cells (50 cells/slide) were scored using Comet Assay IV software, with DNA damage being measured in terms of tail intensity (%) (Duez *et al.*, 2003).

2.2.14. Statistics

All results are presented as the mean values ± standard deviation (SD) (N = number of biological experiments), unless otherwise stated. When two different samples were being compared, a two-tailed unpaired *t*-test was used. Larger datasets were analysed by two-way ANOVA and then corrected for multi-comparison testing using appropriate post-hoc testing. For parametric data, a Dunnett's test (comparison of each group with a control group) or Tukey's test (multi-comparison testing between all groups) was performed; and for non-parametric data, the Bonferroni correction was performed. A detailed report of the statistics performed for each experiment is detailed in the appendix (**7.2.**). Graphs were prepared and statistical analysis performed using GraphPad Prism (version 8.0.1); and $p < 0.05$ was considered statistically significant (*); $p < 0.01$ (**); $p < 0.001$ (***).

2.3. Results

2.3.1. m*Ogg1*$^{-/-}$ MEFS do not express *Ogg1*

The *Ogg1*-null status of m*Ogg1*$^{-/-}$ MEFs was confirmed by PCR and western blotting (Figure **2.2.**) PCR was carried out using primers specific to m*Ogg1* and the PCR products separated using gel electrophoresis. The band visualised (290 bp) represents the PCR product, which can only be seen in the WT cDNA sample and is not present in m*Ogg1*$^{-/-}$ cDNA. Additionally, qPCR analysis using specific m*Ogg1* primers consistently resulted in Ct values above 35 (Ct = 37.5 ± 1.6) in m*Ogg1*$^{-/-}$ MEFs. These values are representative of no template and are consistent with the Ct values produced by no template control (NTC) samples (Ct = 34.3 ± 0.6). This was compared to the Ct value of WT MEFs (Ct = 22.2 ± 0.3), which was significantly lower than the Ct values produced by both m*Ogg1*$^{-/-}$ MEFs and NTCs ($p < 0.001$). This result confirmed that *Ogg1* is absent in m*Ogg1*$^{-/-}$ MEFs, and this was further confirmed at protein level through western blotting. A band observed in the western blot at 39 kDa represents OGG1 and is clearly observed in WT MEFs, however this band is not present in extracts prepared from m*Ogg1*$^{-/-}$ MEFs.

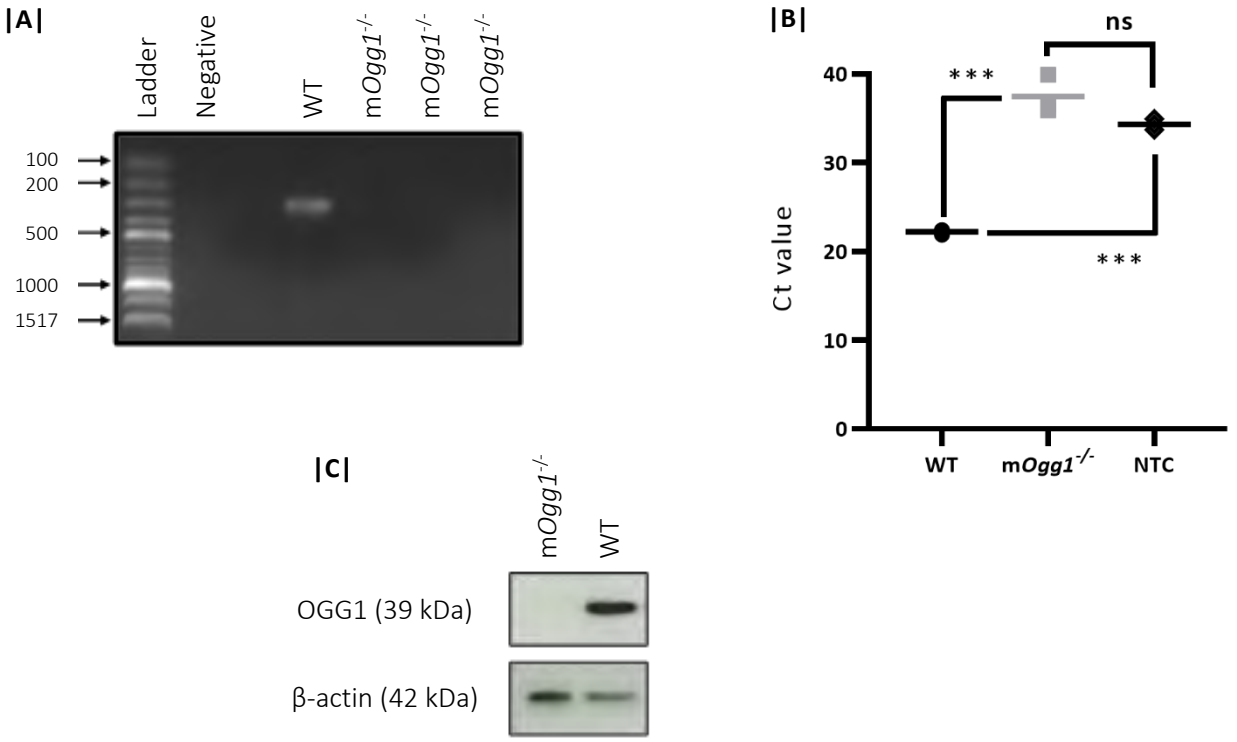


Figure 2.2. m*Ogg1*$^{-/-}$ MEFs do not express *Ogg1*. **|A|** PCR products were separated on a 2% agarose gel, with a band visualised at 290 bp in the WT sample, representing the PCR product of interest. This band was not present in the negative sample or m*Ogg1*$^{-/-}$ samples. **|B|** qPCR reactions were performed with primers specific to *Ogg1*. The mean Ct value measured in each biological replicate is shown (N=3) alongside the overall mean value. The Ct values of m*Ogg1*$^{-/-}$ MEFs (■) (37.5 ± 1.6) indicated a lack of *Ogg1* expression, with these Ct values not significantly differing from the Ct values of non-template control (NTC) samples (◆) (34.3 ± 0.6) ($p > 0.05$). The Ct values of WT MEFs (●) (22.2 ± 0.3) were significantly lower than those of m*Ogg1*$^{-/-}$ MEFs and NTCs ($p < 0.001$). Significance was determined using a two-tailed unpaired *t*-test. **|C|** Western blotting was performed with specific primary antibodies (OGG1 or β-actin). A band correlating to OGG1 was visualised at 39 kDa in the WT sample only whereas the endogenous control gene (β-actin) (42 kDa) can be observed in both samples.

2.3.2. m*Ogg1*$^{-/-}$ MEFs show an increased sensitivity to GSH depletion

The response of WT and m*Ogg1*$^{-/-}$ MEFs following BSO treatment (24 h) was measured in terms of viability and cytotoxicity, using multiple different endpoint measurements. BSO treatment did not significantly affect the viability of WT MEFs and did not result in a cytotoxic response (Figure **2.3.**). However, BSO treatment (≥ 20 μM; 24 h) did significantly decrease the viability of m*Ogg1*$^{-/-}$ MEFs as measured using an MTT assay ($p < 0.001$) and a crystal violet assay ($p < 0.001$). Cytotoxicity was subsequently assessed using a commercial assay, with BSO treatment (24 h) causing a significant increase in cytotoxicity at concentrations of 10 μM (29 ± 5.5%) ($p < 0.01$) and higher ($p < 0.001$). This BSO cytotoxicity was measured in of m*Ogg1*$^{-/-}$ MEFs following BSO treatment (20 μM) over 24 h, with a significant increase in cytotoxicity occurred from 10 h onwards ($p \leq 0.05$).

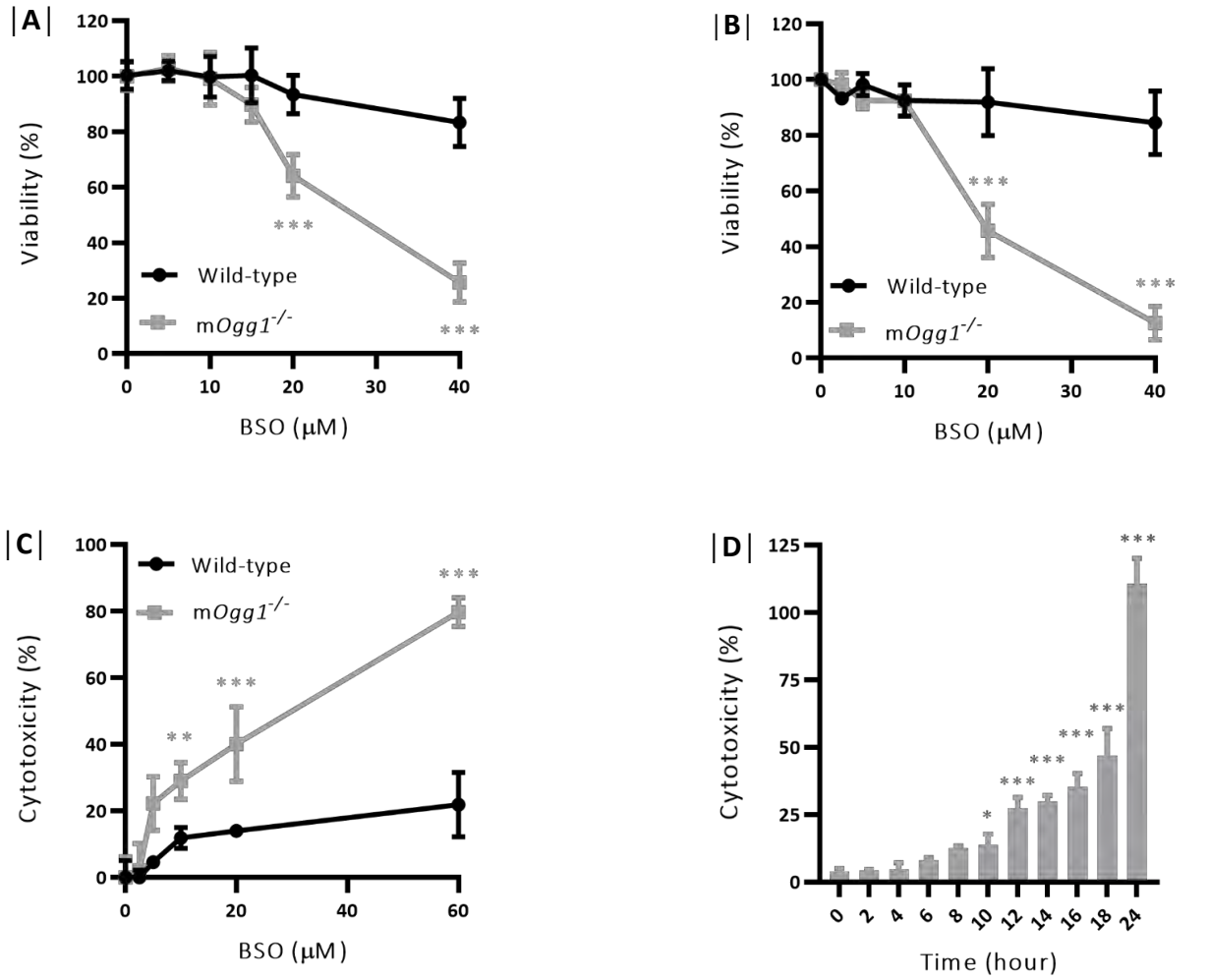


Figure 2.3. BSO-induced cytotoxicity (24 h) is observed in m*Ogg1*$^{-/-}$ MEFs but not in WT MEFs. There was no significant effect on the viability of WT MEFs in any of the three assays, at any of the BSO concentrations tested ($p > 0.05$). Significance was determined using a two-way ANOVA and a subsequent Dunnett's test. **|A|** MTT assay showed a significant decrease in the viability of m*Ogg1*$^{-/-}$ MEFs at 20 μM- (64.1 ± 6.5%) and 40 μM- BSO (25.6 ± 7.1%) ($p < 0.001$). Absorbance was converted to viability (%) when compared to untreated controls. Mean values presented ± SD (N=4). **|B|** Crystal violet assay showed a significant decrease in the viability of m*Ogg1*$^{-/-}$ MEFs following treatment with 20 μM- (45.7 ± 9.6%) and 40 μM- BSO (12.5 ± 6.0%) ($p < 0.001$). Absorbance was converted to viability (%) when compared to untreated controls. Mean values presented ± SD (N=3). *Figure legend continues on next page*

|C| Cytotoxicity was measured using the CellTox™ assay, with a significant increase in cytotoxicity measured in m*Ogg1*$^{-/-}$ MEFs following BSO treatment at a concentration of 10 μM (29 ± 5.5%) ($p < 0.01$) and above (20-40 μM) ($p < 0.001$). Fluorescence was converted to cytotoxicity (%) when compared to a positive lysis control. Mean values presented ± SD (N=4). **|D|** Cytotoxicity was measured over 24 h following BSO treatment (20 μM). BSO treatment induced significant cytotoxicity following treatment for 10 h (13.8 ± 5.4%) ($p < 0.05$). Fluorescence was converted to cytotoxicity (%) when compared to a positive lysis control. Mean values presented ± SD (N=4).

2.3.3. GSH depletion induces apoptosis in m*Ogg1*$^{-/-}$ MEFs

The mechanism of cell death in m*Ogg1*$^{-/-}$ MEFs, following BSO treatment, was shown to be apoptosis (Figure **2.4.**). Apoptosis was detected in cells using two fluorescent probes; annexin V-FITC and PI. Annexin V-FITC fluorescence represents cells that are undergoing apoptosis, whereas Annexin V-FITC and PI dual-fluorescence represents apoptotic cells with a compromised membrane. Etoposide treatment (60 μM; 16 h) was used as a positive control for apoptosis (Karpinich *et al.*, 2002). Single cells were analysed using flow cytometry and suitable quadrants defined, allowing the proportion of early- and late- apoptotic cells to be determined. The percentage of total apoptotic m*Ogg1*$^{-/-}$ MEFs (early- and late- apoptotic events combined) significantly increased following 40 μM BSO treatment (16 h) (22.3 ± 1.7%) ($p < 0.001$). This induction of apoptosis following BSO treatment (40 μM) was subsequently monitored over the 16 h treatment period. A significant increase in apoptotic cells was measured following 12 h of BSO treatment (9.8 ± 2.1%) ($p < 0.001$), with this continuing to increase over the remainder of the time-course and reaching 22.8 ± 2.8% at 16 h ($p < 0.001$).

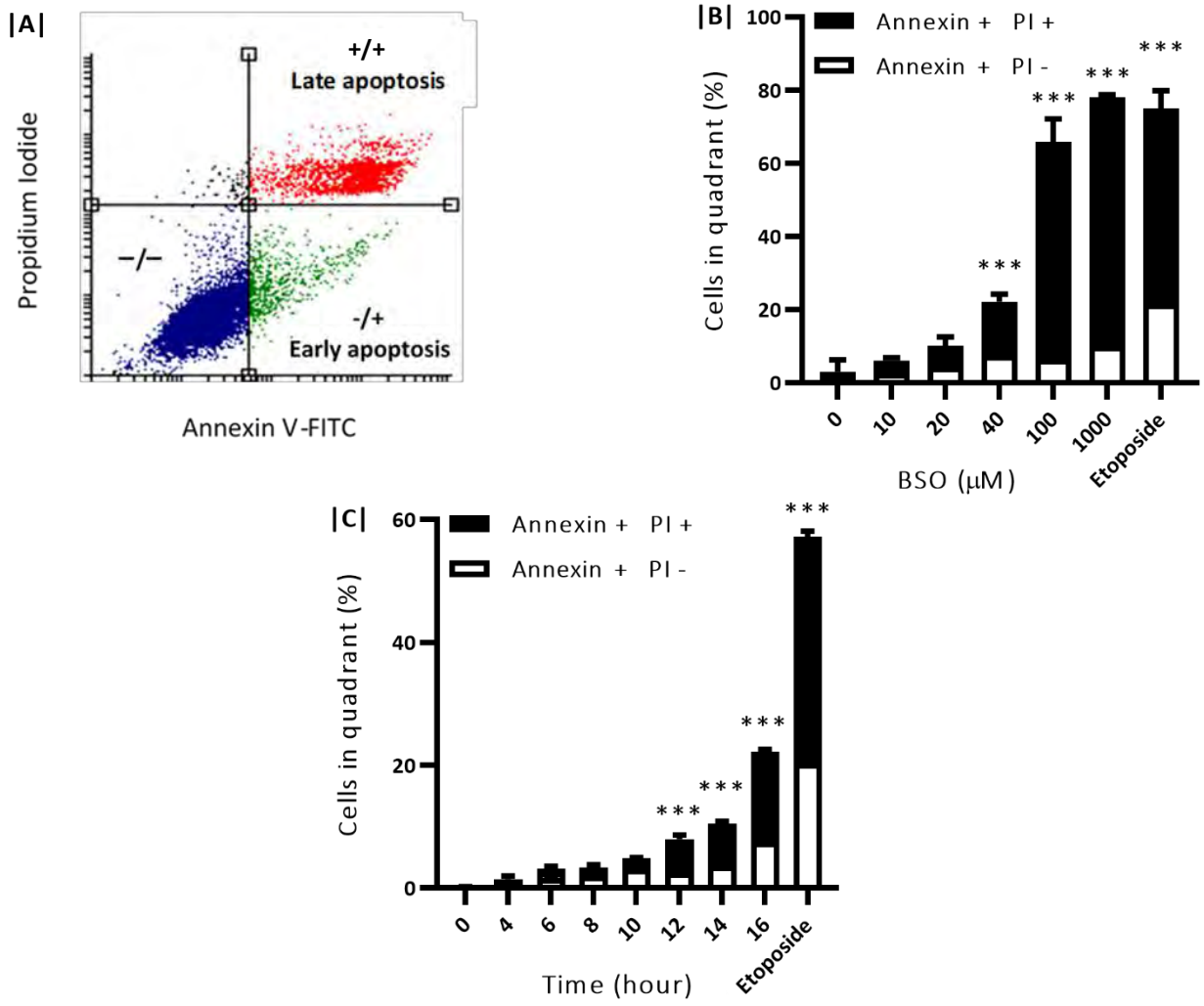


Figure 2.4. BSO treatment induces apoptosis in m*Ogg1*$^{-/-}$ MEFs. Apoptotic cells were detected using annexin V-FITC and PI. Etoposide treatment (60 μM; 16 h) was included as a positive apoptotic control. Mean values presented ± SD (N=3), with significance determined with a two-way ANOVA and a subsequent Dunnett's test. **|A|** Quadrants were constructed to identify early apoptotic cells (annexin V-FITC +) (PI –) and late apoptotic cells (annexin V-FITC +) (PI +), as displayed for m*Ogg1*$^{-/-}$ MEFs following BSO treatment (40 μM; 16 h). **|B|** Early- [□] and late- [■] apoptotic events were combined to calculate the total number of apoptotic cells. A significant increase in total apoptotic m*Ogg1*$^{-/-}$ MEFs was measured following BSO treatment (16 h) at a concentration of 40 μM and above ($p < 0.001$). **|C|** Early- [□] and late- [■] apoptotic cells were combined to calculate the total number of apoptotic cells. BSO treatment (40 μM) resulted in a significant increase in total apoptotic m*Ogg1*$^{-/-}$ MEFs following 12 h ($p < 0.001$).

2.3.4. BSO treatment results in a decrease in intracellular GSH

BSO treatment was shown to decrease intracellular GSH levels in WT and m*Ogg1*$^{-/-}$ MEFs (Figure **2.5.)**. There was no significant difference between the basal level of intracellular GSH in WT (19.1 ± 2.3 nmol GSH/mg protein) and m*Ogg1*$^{-/-}$ MEFs (19.7 ± 2.5 nmol GSH/mg protein) ($p > 0.05$). Treatment with BSO (24 h) resulted in a significant decrease in intracellular GSH levels in both cell types at a concentration of 5 μM and higher ($p < 0.01$). Following 10 μM BSO treatment, a GSH decrease of 51 ± 5.2% was observed in WT MEFs and 58.6 ± 3.1% in m*Ogg1*$^{-/-}$ MEFs ($p < 0.001$). GSH depletion (%) was lower with regards to mitochondrial GSH but remained significant ($p < 0.01$) with BSO treatment (10 μM) resulting in a GSH decrease in WT (25.7 ± 4.9%) and m*Ogg1*$^{-/-}$ (29.3 ± 3.0%) MEFs. No significance differences existed between the cell types in whole-cell or mitochondrial GSH at any of the concentrations tested ($p > 0.05$). A time-dependent decrease in whole-cell GSH levels was measured in both cell types following 12 h of BSO treatment (10 μM), but this decrease was not significant until 16 h ($p < 0.01$).

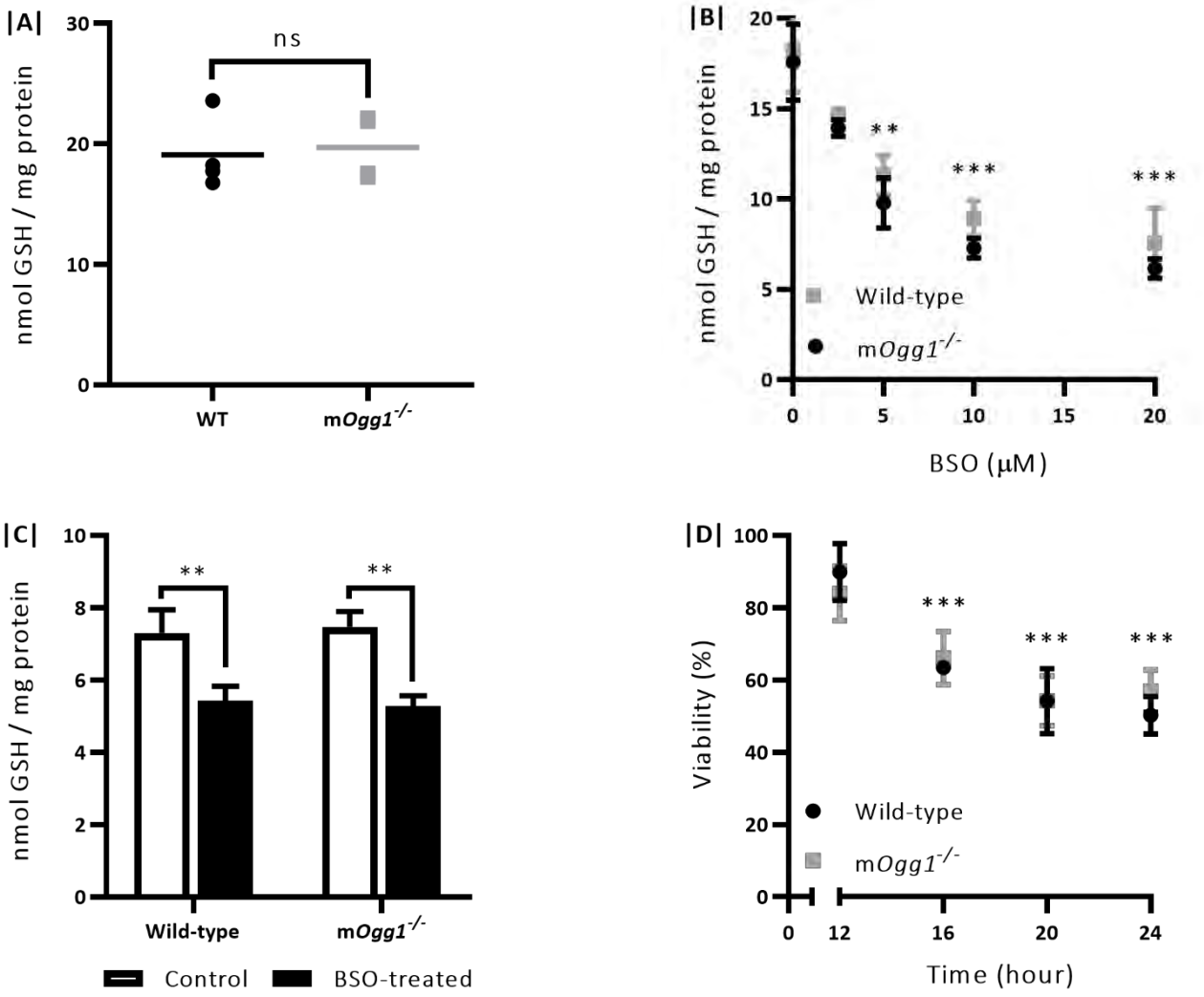


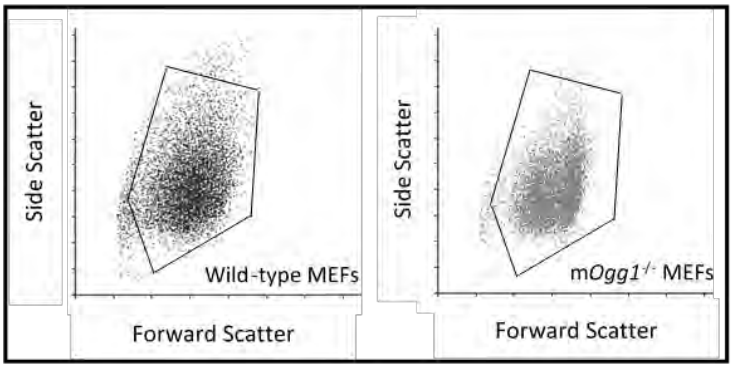
Figure 2.5. BSO treatment depletes intracellular GSH levels. **|A|** Whole cell GSH levels were measured in WT (19.1 ± 2.3 nmol GSH/mg protein) and m*Ogg1*$^{-/-}$ (19.7 ± 2.5 nmol GSH/mg protein) MEFs. There was no statistical difference detected between the cell types ($p > 0.05$) as determined using a two-tailed unpaired *t*-test. Individual replicates are shown alongside mean values (—) (N=3). **|B|** Whole-cell GSH levels significantly decreased in both WT and m*Ogg1*$^{-/-}$ MEFs at BSO concentrations of ≥ 5 μM (24 h) ($p < 0.01$). Mean values presented ± SD (N=3), and significance was determined with a two-way ANOVA and a subsequent Dunnett's test. *Figure legend continues on next page*

|C| Mitochondrial GSH levels were measured in mitochondrial extracts prepared from untreated and BSO-treated (10 μM, 24h) MEFs. GSH is significantly depleted in both cell-types following BSO treatment ($p < 0.01$). There was no significant difference between WT and m*Ogg1*$^{-/-}$ MEFs at either condition ($p > 0.05$). Mean values presented ± SD (N=3), and significance was determined with a two-way ANOVA and a subsequent Tukey's test. **|D|** Whole-cell GSH level were measured over 24 h following BSO treatment (10 μM) and a significance decrease was measured at 16 h in both WT (36.5 ± 1.3 %) and m*Ogg1*$^{-/-}$ (33.9 ± 7.9 %) MEFs ($p < 0.001$). Mean values presented ± SD (N=4), and significance was determined with a two-way ANOVA and a subsequent Dunnett's test.

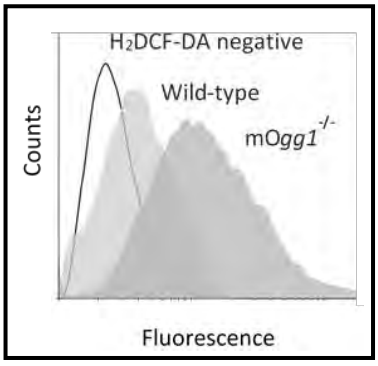
2.3.5. Investigating intracellular ROS levels

Total intracellular ROS levels in untreated control cells were measured using the redox sensitive probe, H_2DCF-DA (Figure **2.6.**). The fluorescence of 10, 000 cells were measured by flow cytometry. The fluorescence peak of m*Ogg1*$^{-/-}$ MEFs was clearly shifted to the right, when compared to the peak of WT MEFs. The fluorescence data was collected in three forms: mean, median, and positive events (%). A significant increase in the fluorescence of m*Ogg1*$^{-/-}$ MEFs was observed ($p < 0.01$) using all three parameters, when compared to WT MEFs. As the data was normally distributed (as determined with a Shapiro-Wilks test; $p > 0.05$), both mean and median fluorescence were deemed suitable parameters; however the median was chosen in case subsequent treatment regimens resulted in a skewed distribution.

|A|



|B|



|C|

	WT MEFs	m*Ogg1*$^{-/-}$ MEFs	Difference	Significance
Mean (RFU)	**5.25**	**26.25**	**21.00**	***
Median (RFU)	**5.51**	**24.90**	**19.39**	***
Positive events (%)	**4.57**	**37.94**	**33.37**	**

Figure 2.6. Intracellular ROS was investigated using the fluorescent probe, H_2DCF-DA. **|A|** An example dot-plot was obtained from both WT and m*Ogg1*$^{-/-}$ MEFs, with the gating of viable cells shown. **|B|** These example fluorescent peaks that were collected from WT and m*Ogg1*$^{-/-}$ MEFs are displayed alongside H_2DCF-DA-negative cells. The peak of m*Ogg1*$^{-/-}$ MEFs is clearly shifted to the right when compared to the peak of WT MEFs. **|C|** The fluorescence of m*Ogg1*$^{-/-}$ MEFs are significantly higher than the fluorescence of WT MEFs, as measured by mean ($p < 0.001$), median ($p < 0.001$) and positive events (%) ($p < 0.01$). Positive events (%) were determined by creating a florescence threshold using H_2DCF-DA-negative cells, and the number of cells (%) that exhibited fluorescence exceeding this threshold was calculated (N=5). Significance was determined for each parameter using a paired *t*-test.

2.3.6. m*Ogg1*$^{-/-}$ MEFs possess elevated levels of intracellular ROS

BSO treatment (24 h) significantly increased the ROS levels of both WT MEFs (20 μM)($p < 0.001$) and m*Ogg1*$^{-/-}$ MEFs (10 μM) ($p < 0.05$). A significant difference ($p < 0.01$) remained between the cell-types at each BSO concentration tested. Next, cells were incubated with a probe that is specific to superoxide within the mitochondria (MitoSOX™ Red), with mitochondrial ROS shown to significantly increase in both WT (1.6 ± 0.3 -fold increase) and m*Ogg1*$^{-/-}$ (1.3 ± 0.1 -fold increase) MEFs following GSH depletion (*via* 15 μM BSO treatment) ($p < 0.001$). A significant difference in mitochondrial ROS existed between WT and m*Ogg1*$^{-/-}$ MEFs ($p < 0.001$), proving that ROS production is elevated in the mitochondria of untreated m*Ogg1*$^{-/-}$ MEFs ($p < 0.001$). Cells were treated with the NOX/DUOX inhibitor DPI (0.1 - 5 mM) (1 - 3 h), which did not significantly decrease the intracellular ROS level of *mOgg1*$^{-/-}$ MEFs ($p > 0.05$), as measured using the H_2DCF-DA assay (Figure **2.7.**).

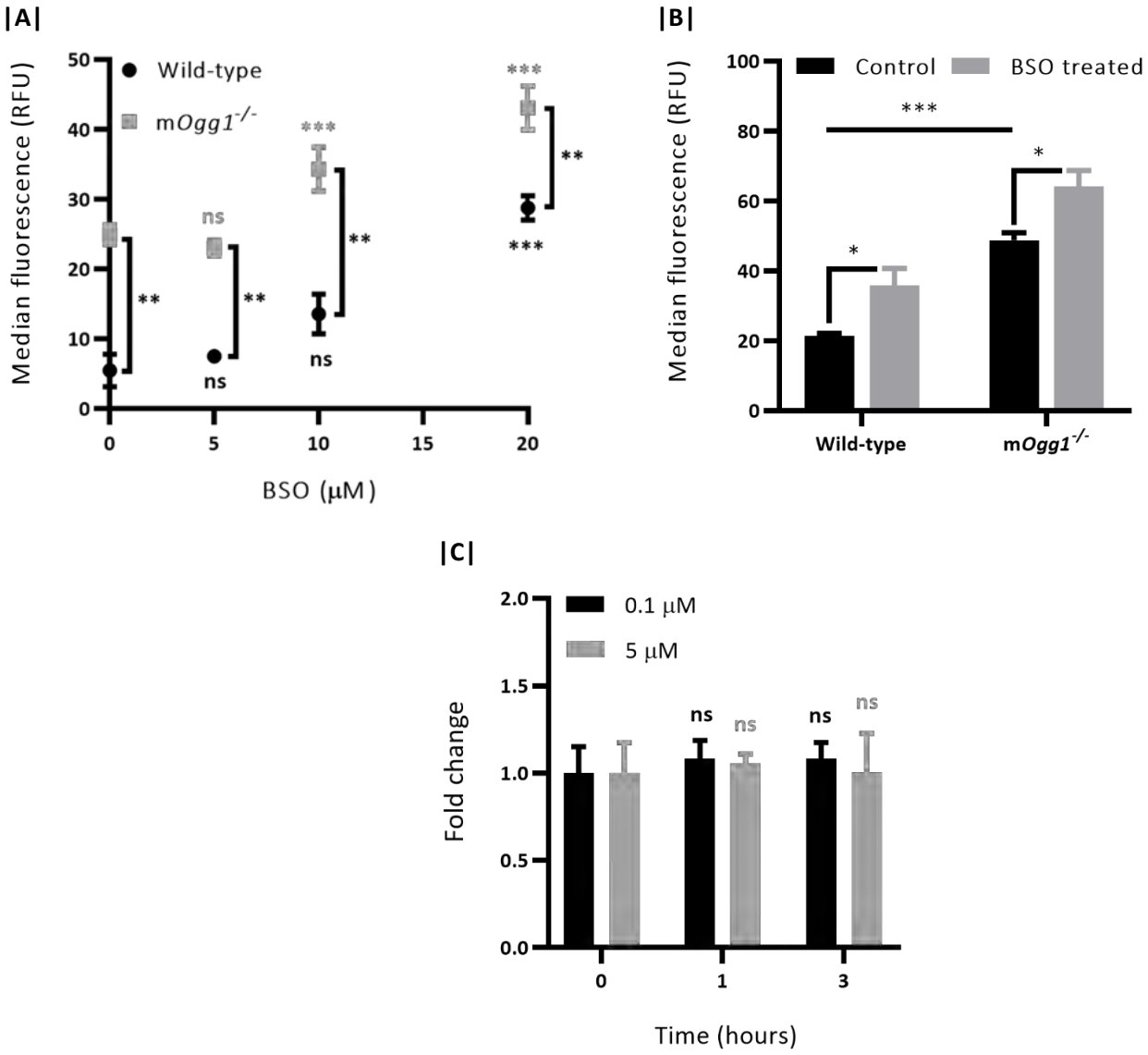


Figure 2.7. m*Ogg1*$^{-/-}$ MEFs possess elevated levels of intracellular ROS. Statistical significance was determined with a two-way ANOVA and a subsequent Tukey's test, for all experiments. **|A|** Following incubation with the redox-sensitive probe H_2DCF-DA (10 μM; 1 h), fluorescence significantly increased in m*Ogg1*$^{-/-}$ MEFs following 10 μM BSO treatment (24 h), and in both cell types following 20 μM BSO treatment (24 h) ($p < 0.001$). A significant difference remained between the cell types at all doses tested ($p < 0.01$). Mean values presented ± SD (N=4). *Figure legend continues on next page*

|B| Following incubation with MitoSOX™ Red (5 μM; 15 min), fluorescence significantly increased in WT and m*Ogg1*$^{-/-}$ MEFs following BSO treatment (15 μM; 24 h) ($p < 0.05$). A significant difference exists between the cell types at both conditions ($p < 0.001$). Mean values presented ± SD (N=3). **|C|** Treatment with the NOX/DUOX inhibitor DPI (0.1-5 mM; 1-3 h) did not significantly decrease the intracellular ROS level of *mOgg1*$^{-/-}$ MEFs ($p > 0.05$), as measured using the H_2DCF-DA assay. Mean values presented ± SD (N=3).

2.3.7. Differential antioxidant expression in MEFs

The expression of four antioxidants (*Cat, Sod1, Sod2* and *Gpx*) in WT and m*Ogg1*$^{-/-}$ MEFs was measured using qPCR (Figure **2.8.**). *Cat, Sod1* and *Gpx* were expressed at a significantly lower level in m*Ogg1*$^{-/-}$ MEFs compared to WT MEFs ($p < 0.001$), whereas *Sod2* expression was significantly higher (1.48 ± 0.05 -fold) in m*Ogg1*$^{-/-}$ MEFs ($p < 0.001$). In response to BSO treatment (15 μM; 24 h), and therefore a subsequent decrease in GSH, *Gpx* was significantly down regulated in WT MEFs ($p < 0.01$); however there were no other significant changes across the remaining antioxidants ($p > 0.05$). On the contrary, BSO treatment in mOgg1$^{-/-}$ MEFs resulted in a significant decrease in the expression of both *Gpx* and *Sod2* ($p < 0.001$).

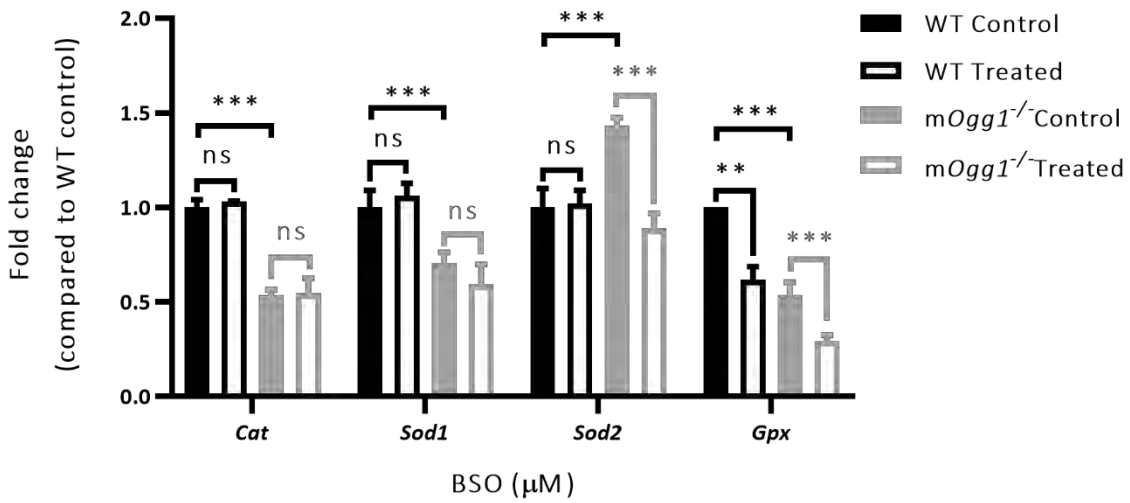


Figure 2.8. The expression of antioxidant genes was measured using qPCR. Fold-change is presented when compared to untreated WT control (■). *Cat*, *Sod1*, and *Gpx* are all expressed at a significantly lower level in m*Ogg1*$^{-/-}$ MEFs (■) ($p < 0.001$), whereas *Sod2* is expressed at a significantly higher level in m*Ogg1*$^{-/-}$ MEFs ($p < 0.001$). Following BSO treatment (15 μM, 24 h), there is a significant decrease in *Gpx* expression is measured in WT MEFs (□) ($p < 0.01$), however no other changes are detected ($p > 0.05$). Following BSO treatment (15 μM, 24 h), there is a significant decrease in both *Sod2* and *Gpx* expression ($p < 0.001$) in m*Ogg1*$^{-/-}$ MEFs (□). Mean values presented ± SD (N=3), and significance determined with a two-way ANOVA and a subsequent Tukey's test.

2.3.8. There is no difference in the whole-cell ATP level of WT and m*Ogg1*$^{-/-}$ MEFs

In aerobic conditions *in vivo* the majority of ATP is produced *via* oxidative phosphorylation in the mitochondria. Therefore, ATP measurements would indirectly measure capacity of mitochondria to produce ATP, and this approach was utilised as an initial test of mitochondrial functionality. WT and m*Ogg1*$^{-/-}$ MEFs are identical with respect to cellular ATP levels, with no significant differences measured between the cell-types ($p > 0.05$) (Figure **2.9.**).

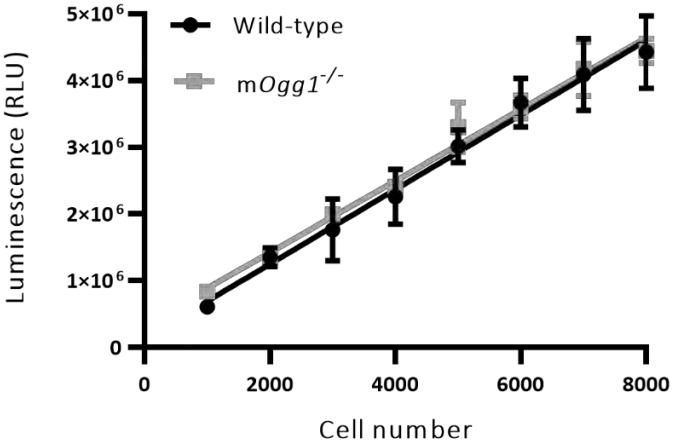


Figure 2.9. Whole-cell ATP levels were measured in WT and *mOgg1*$^{-/-}$ MEFs. Cells were seeded at different densities and subsequently incubated for 18 h. A Bradford assay was performed in parallel and used to normalise luminescence to the number of cells present. No significant difference was detected between the ATP levels of the two cell-types ($p > 0.05$). Linear regression was performed for WT and m*Ogg1*$^{-/-}$ MEFs and the regression lines found to be statistically similar ($p > 0.05$).

2.3.9. BSO-induced toxicity is unchanged when cellular metabolism is switched in favour of oxidative phosphorylation

To further investigate mitochondrial function, cultured cells were grown in DMEM containing galactose (10 mM) instead of glucose (25 mM) (Figure **2.10.**). This switch to galactose reverses the Crabtree effect, and switches energy production within cells from glycolysis to oxidative phosphorylation. BSO toxicity (5 - 20 μM; 24 h) was not enhanced in either WT or m*Ogg1*$^{-/-}$ MEFs following the switch to oxidative phosphorylation. In fact, a significant decrease in viability was observed in WT MEFs cultured in glucose following 80 μM BSO treatment (82.8 ± 9.2%) ($p < 0.01$), but this was not observed in WT MEFS cultured in galactose (95.7 ± 8.4%) ($p > 0.05$). There was no significant difference detected in for the viability of m*Ogg1*$^{-/-}$ MEFs between the two growth-conditions at any of the BSO concentrations tested ($p > 0.05$). Antimycin-A (0.0001 - 10 μM; 24 h) was used as a positive control, and is a compound that inhibits the ETC. In response to antimycin-A treatment, the viability of both cell-types significantly decreased in galactose-cultured cells when compared to glucose-cultured cells. A significant difference in the viability of WT and m*Ogg1*$^{-/-}$ MEFs was measured between the two conditions in response to 0.1 μM antimycin-A ($p < 0.001$). Additionally, N. Coltman (PhD student, University of Birmingham) carried out experiments with rotenone, which is another inhibitor of the ETC. There was no statistical difference between the IC50 values of WT and m*Ogg1*$^{-/-}$ MEFs (cultured in galactose-containing media) in response to antimycin-A or rotenone treatment.

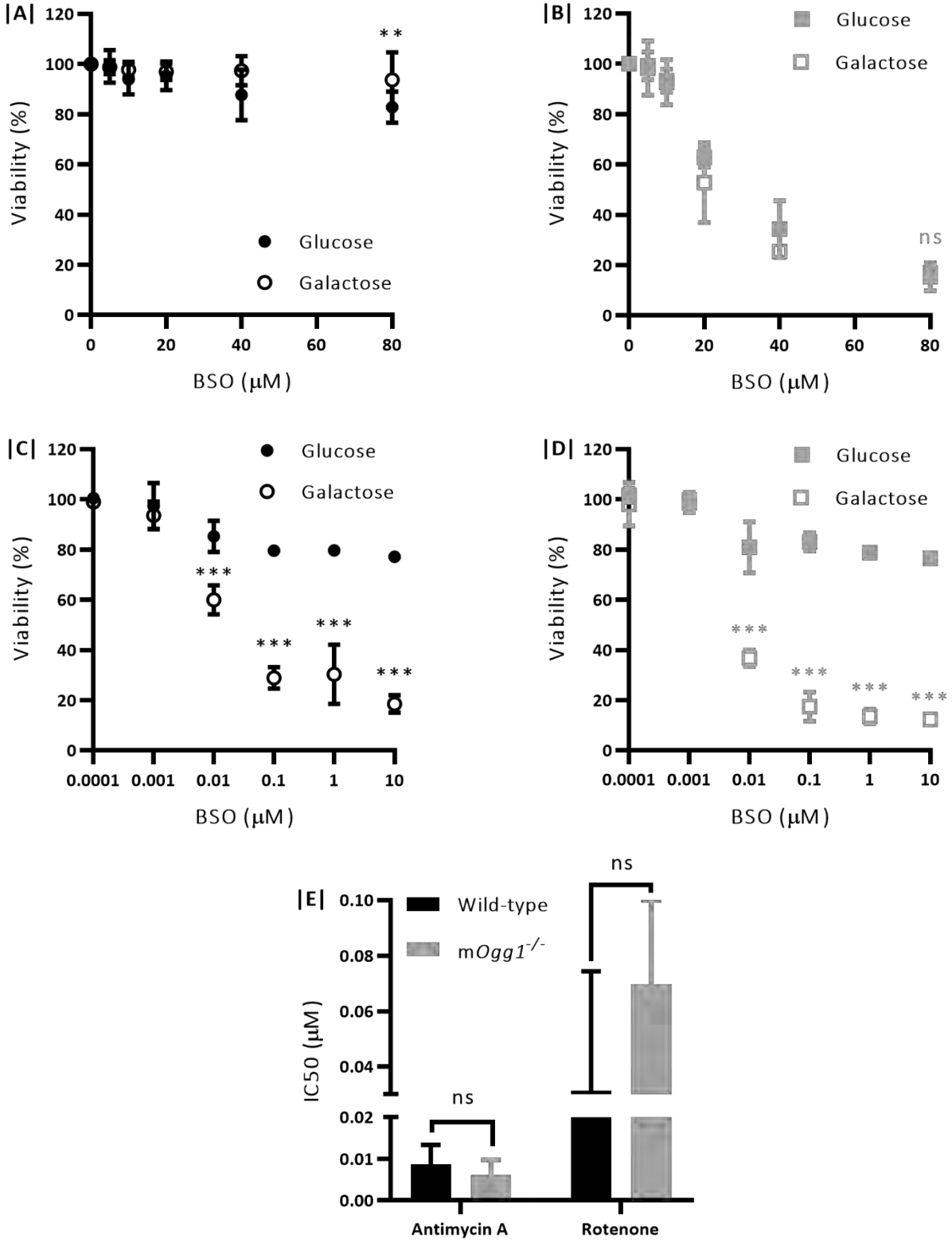


Figure legend continues on next page

Figure 2.10. Viability comparison of WT and m*Ogg1*$^{-/-}$ MEFs cultured in the presence of glucose or galactose. Mean values are presented ± SD (N=4) and significance determined using a two-way ANOVA and a subsequent Dunnett's test, unless otherwise stated. **|A|** BSO treatment (24 h) at a concentration ≤ 40 μM does not result in a significant decrease in the viability of WT MEFs cultured in either glucose or galactose ($p > 0.05$). However, following 80 μM BSO treatment (24 h), a significant decrease in the viability of WT MEFs cultured in glucose is measured (82.8 ± 9.2%) ($p < 0.01$). This is not observed in galactose-cultured WT MEFs ($p > 0.05$). **|B|** There is no significant difference in the viability of m*Ogg1*$^{-/-}$ MEFs cultured in glucose compared to m*Ogg1*$^{-/-}$ MEFs cultured in galactose, at any of the BSO concentrations tested (5 - 80 μM; 24 h) ($p > 0.05$). **|C|** There is a significant decrease in the viability of WT MEFs grown in galactose (60.0 ± 5.0%) compared to WT MEFs grown in glucose (85.4 ± 4.1%), following 0.01 μM antimycin-A treatment (24 h) ($p < 0.001$). **|D|** There is a significant decrease in the viability of m*Ogg1*$^{-/-}$ MEFs grown in galactose (36.8 ± 5.1%) compared to m*Ogg1*$^{-/-}$ MEFs grown in glucose (80.9 ± 16.8%), following 0.01 μM antimycin-A treatment (24 h) ($p < 0.001$). **|E|** The IC50 of antimycin-A (24 h) and rotenone (24 h) was calculated for both WT and m*Ogg1*$^{-/-}$ MEFs, which were grown in the presence of galactose. There is no statistically significant difference between the antimycin-A IC50 values of WT (8.6×10^{-3} μM) and m*Ogg1*$^{-/-}$ MEFs (6.2×10^{-3} μM) ($p > 0.05$) (N=3). Similarly, the IC50 of rotenone does not significantly differ between WT (3.1×10^{-2} μM) and m*Ogg1*$^{-/-}$ MEFs (6.9×10^{-2} μM) ($p > 0.05$) (N=5). Significance was instead determined using two-tailed unpaired *t*-tests (per compound) in this experiment.

2.3.10. BSO treatment increases 8-oxoG sites in m*Ogg1*$^{-/-}$ MEFs

Tail intensity (% TI) was measured for both hOGG1 negative and hOGG1 positive slides and the difference in tail intensity was used as a measure of the number of 8-oxoG sites (Figure **2.11.**). There was no statistical difference in the tail intensity (representative of 8-oxoG sites) measured in WT (0.52 ± 1.2%) and m*Ogg1*$^{-/-}$ MEFs (1.1 ± 1%) ($p > 0.05$). Additionally, there was no significant increase in tail intensity in WT MEFs following BSO treatment (15 μM; 24 h) (0.61 ± 0.63%) ($p > 0.05$), however there was a significant increase in tail intensity in m*Ogg1*$^{-/-}$ MEFs following BSO treatment (7.1 ± 0.8%) ($p < 0.001$). The number of 8-oxoG sites in BSO-treated m*Ogg1*$^{-/-}$ MEFs is significantly lower than that of H_2O_2-treated (50 μM; 1 h) m*Ogg1*$^{-/-}$ MEFs (25.4 ± 5.2%) ($p < 0.001$). This dose of H_2O_2 was shown to be non-cytotoxic over 24-h, and therefore this data suggests that the BSO-induced generation of 8-oxoG lesions is not expected to cause cytotoxicity.

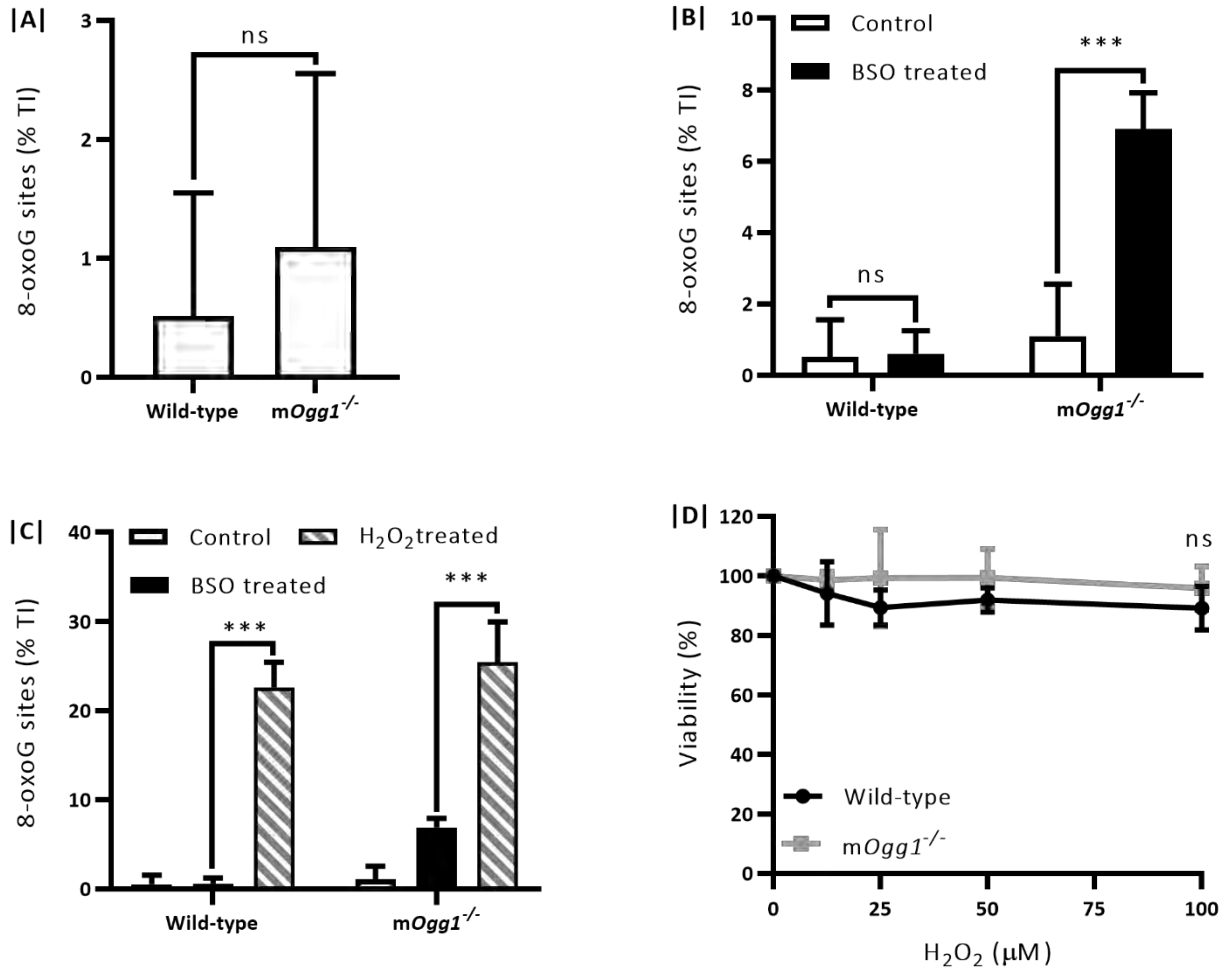
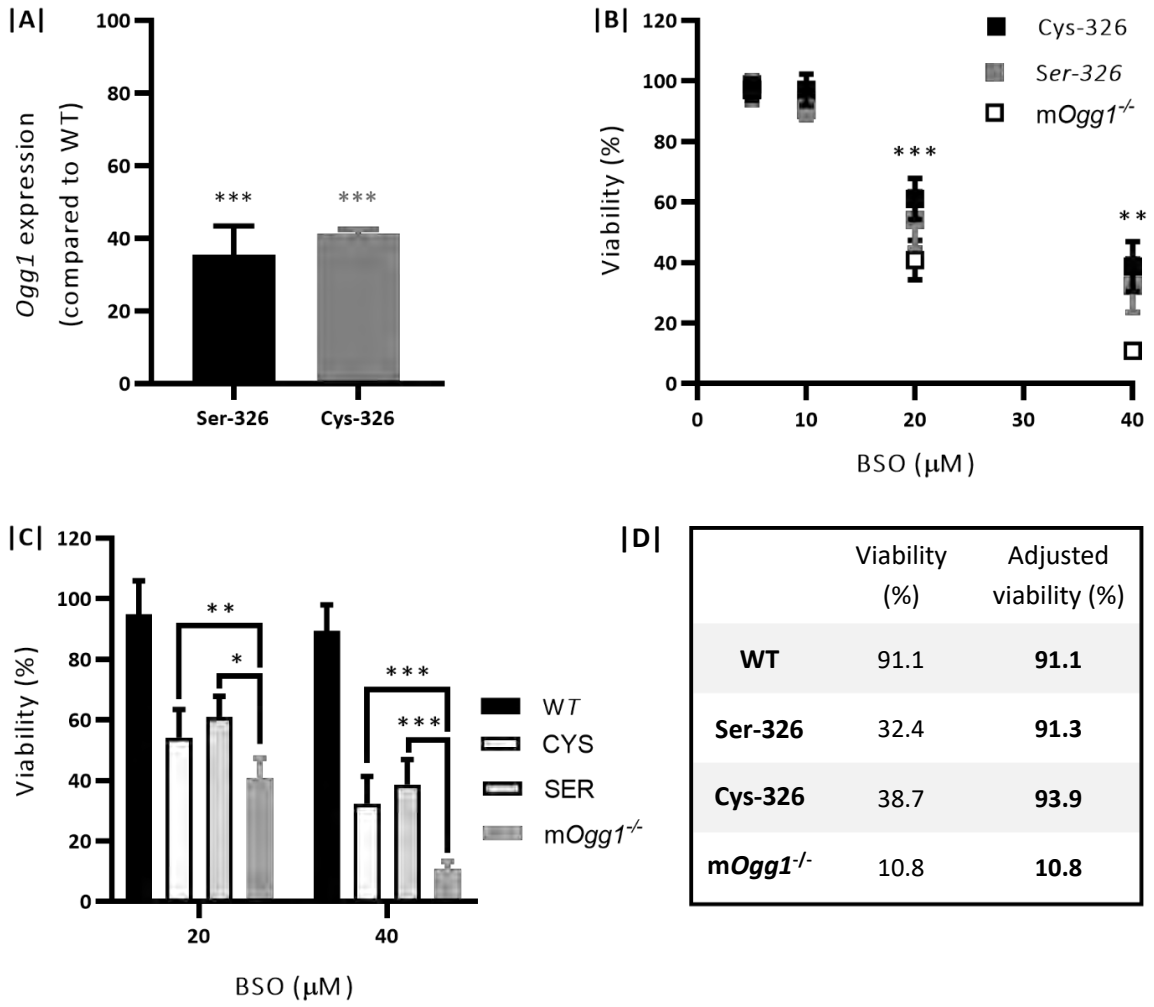


Figure 2.11. The levels of 8-oxoG were measured using a hOGG1-modified comet assay. Mean values are presented ± SD (N=4), and significance determined with a two-way ANOVA and subsequent Bonferroni testing (unless otherwise stated). **|A|** There is no significant difference between the tail intensity (% TI) of untreated WT (0.52 ± 1.2%) and m*Ogg1*$^{-/-}$ MEFs (1.1 ± 1.04%) ($p > 0.05$). **|B|** BSO treatment (15 μM; 24 h) resulted in an increase in the 8-oxoG level in m*Ogg1*$^{-/-}$ MEFs (7.1 ± 0.8%) ($p < 0.001$), however no such increase was induced in WT MEFs (0.61 ± 0.63%) ($p > 0.05$). **|C|** There were significantly more 8-oxoG sites in H_2O_2-treated MEFs (50 μM; 1 h) when compared to BSO-treated MEFs in both cell-types ($p < 0.001$). **|D|** MTT assay following treatment with H_2O_2 (12.5-100 μM, 24 h), with no significant decrease in viability measured in WT or m*Ogg1*$^{-/-}$ MEFs at any of the concentrations tested ($p > 0.05$) as determined with a two-way ANOVA and Dunnett's post-hoc analysis.

2.3.11. Re-expression of *Ogg1* results in a partial rescue in viability following GSH depletion

To further understand the role of OGG1 in the cellular response following GSH depletion, m*Ogg1*$^{-/-}$ MEFs that were stably-transfected to express two different variants of OGG1 were utilised (Figure **2.12.**). These cells were either transfected with a fully-repair competent OGG1 variant (Ser-326) or a repair-impaired OGG1 variant (Cys-326). *Ogg1* was expressed at a significantly lower level in the transfected MEFs when compared to WT MEFs (normalised to 100%) ($p < 0.001$), however, there was no significant difference in the level of *Ogg1* expression between Ser-326 (35.5 ± 1.4%) and Cys-326 (41.2 ± 7.9%) MEFs ($p > 0.05$). Both variants resulted in a partial rescue in viability in response to GSH depletion, however there was no significant difference between the viability of the two variants at any of the BSO doses tested ($p > 0.05$). Following 20 μM BSO treatment, a significantly higher viability was measured in Ser-326 (54.1 ± 9.4%) and Cys-326 MEFs (61 ± 6.8%), when compared to m*Ogg1*$^{-/-}$ MEFs (40.7 ± 5.6%) ($p < 0.05$). The viability (%) of cells following 40 μM BSO treatment was normalised to levels of *Ogg1* expression. There was no significant difference between the adjusted viabilities of WT (91.1%), Ser-326 (91.3%) and Cys-326 (93.9%) MEFs.



	Viability (%)	Adjusted viability (%)
WT	91.1	**91.1**
Ser-326	32.4	**91.3**
Cys-326	38.7	**93.9**
m*Ogg1*$^{-/-}$	10.8	**10.8**

Figure 2.12. The viability of m*Ogg1*$^{-/-}$ MEFs following GSH depletion is increased through *Ogg1* re-expression. Mean values are presented ± SD (N=3). **|A|** qPCR shows that the expression of *Ogg1* in transfected MEFs is significantly lower ($p < 0.001$) than the OGG1 expression measured in WT MEFs. There is no significant difference ($p > 0.05$) between the expression of *Ogg1* between Ser-326 MEFs (35.5 + 1.4%) and Cys-326 MEFs (41.2 ± 7.9%), with significance determined with a two-tailed unpaired *t*-test. **|B|** MTT assay following BSO treatment (5-40 μM) for Ser-326 (■), Cys-326 (■), and m*Ogg1*$^{-/-}$ MEFs (□). There is a significant increase in the viability of the transfected MEFs compared to m*Ogg1*$^{-/-}$ MEFs following 20- and 40- μM BSO. There is no significant difference in viability between the two variants at any of the BSO concentrations tested ($p > 0.05$), as determined with a two-way ANOVA and a subsequent Tukey's test.

Figure legend continues on next page

|C| The viability data following 20- and 40- μM BSO treatment was plotted alone, allowing differences to be seen clearly. Following 20 μM BSO, a significantly higher viability was measured in Ser-326 (54.1 ± 9.4%) and Cys-326 (61 ± 6.8%) transfected MEFs, when compared to m*Ogg1*$^{-/-}$ MEFs (40.7 ± 5.6%) ($p < 0.05$). This was again the case at 40 μM; with a higher viability measured in Ser-326 (32.4 ± 8.9%) and Cys-326 (38.7 ± 8.2%) transfected MEFs, when compared to m*Ogg1*$^{-/-}$ MEFs (10.8 ± 2.4%) ($p < 0.001$). **|D|** The viability of cells following 40 μM BSO treatment was adjusted based on their *Ogg1* expression level. Following adjustment, there was no significant difference in the viability of WT (91.1%), Ser-326 (91.3%) and Cys-326 MEFs (93.9%), as determined with a two-tailed unpaired *t*-test.

2.4. Discussion

In the current study we have identified an increased sensitivity to GSH depletion in m*Ogg1*$^{-/-}$ MEFs. GSH was depleted by treating cells with BSO, inhibiting Ɣ-GCS, which is the enzyme catalysing the rate-limiting step of GSH synthesis. This causes the depletion of intracellular GSH stores and induces intracellular oxidative stress (Griffith, 1982; Drew and Miners, 1984; Green *et al.*, 2006). Cytotoxicity and induction of apoptosis in m*Ogg1*$^{-/-}$ MEFs was initially hypothesised to be a consequence of oxidative DNA damage, in response to this induction of intracellular oxidative stress. This combined with the loss of OGG1-inititated BER might be expected to sensitise OGG1 deficient cells with regards to GSH depletion. Instead, we show that apoptosis is independent of oxidative DNA damage. We instead propose that apoptosis is induced in response to an elevation of intracellular ROS, independently of an accumulation of oxidative DNA damage, with this model shown in Figure **2.13.**

BSO treatment significantly decreased both total and mitochondrial GSH levels and, consistent with previous studies, we observed that mitochondrial GSH was relatively resistant to depletion compared to cytoplasmic GSH (Edgren and Révész, 1987; Green *et al.*, 2006). The decrease in GSH measured in the current study was found to be consistent with previous reports that have used concentrations of BSO in this range (< 100 μM) (Byrd *et al.*, 2004; Kurdi *et al.*, 2012; Torrao *et al.*, 2013). There was no significant difference in the depletion of GSH between the two cell-types following BSO treatment, demonstrating that the differences between the viability of WT and m*Ogg1*$^{-/-}$ MEFs (in response to BSO treatment) cannot be attributed to differences in GSH levels between the cell-types.

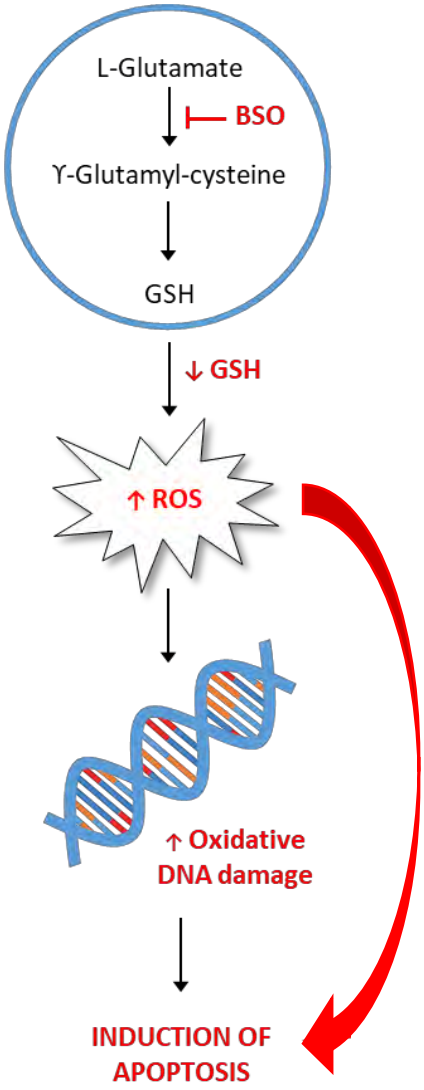


Figure 2.13. Proposed model explaining the induction of apoptosis in m*Ogg1*$^{-/-}$ MEFs. The inhibition of Υ-GCS (*via* BSO treatment), and the subsequent decrease in GSH levels, was expected to increase intracellular ROS levels. It was expected that the elevated level of ROS within the cell would react with DNA to generate oxidative DNA modifications, including the prevalent modification 8-oxoG. It was hypothesised that this was the mechanism through which apoptosis was induced in m*Ogg1*$^{-/-}$ MEFs following BSO treatment. We instead propose that the increase in intracellular ROS induces apoptosis independently of the generation of 8-oxoG lesions.

In agreement with previous studies, GSH depletion increased ROS levels in both cell types in a concentration-dependent manner (Kane *et al.*, 1993; Langie *et al.*, 2007; Kershaw and Hodges, 2012; Kurdi *et al.*, 2012; Torrao *et al.*, 2013; Kaur *et al.*, 2014). Surprisingly however, we observed elevated basal levels of intracellular ROS in m*Ogg1*$^{-/-}$ MEFs compared to WT MEFs in the absence of BSO treatment. Furthermore, this correlated with an elevation of mitochondrial superoxide in m*Ogg1*$^{-/-}$ MEFs, with mitochondrial superoxide detected with MitoSOX™ Red.

Subsets of m*Ogg1*$^{-/-}$ MEFs that possess significantly increased levels of intracellular ROS have been identified previously (Bacsi *et al.*, 2007). Bacsi *et al.* (2007) suggested that a surveillance mechanism may be present in *Ogg1*$^{-/-}$ tissues, which induces apoptosis in high ROS/high 8-oxoG containing cells and therefore prevents the accumulation of 8-oxoG in *Ogg1*$^{-/-}$ cultures. The origin of this excess ROS is however yet to be elucidated. We propose that a likely source of the excess mitochondrial superoxide in m*Ogg1*$^{-/-}$ MEFs is the mitochondrial ETC itself, which is known to produce superoxide during ATP production (Bertram *et al.*, 2006; Indo *et al.*, 2007; Murphy, 2009; Phaniendra, Jestadi and Periyasamy, 2015). Another primary endogenous source of ROS, including superoxide, is the NOX/DUOX family of NADPH oxidases (Lambeth, 2004; Bedard and Krause, 2007). However, we excluded this as a source of the excess ROS in m*Ogg1*$^{-/-}$ MEFs by using the NOX/DUOX inhibitor DPI (Sigma-Aldrich, Merck: catalogue no. D2926) (Massart *et al.*, 2014; Altenhöfer *et al.*, 2015), showing that DPI had no significant effect on the intracellular ROS levels of m*Ogg1*$^{-/-}$ MEFs.

Due to the increased level of mitochondrial superoxide and the subsequent induction of apoptosis, aspects of metabolic and mitochondrial function were investigated. We first measured the ATP content of WT and m*Ogg1*$^{-/-}$ MEFs, and found that there was no significant difference between the cell-types. It is known that in aerobic conditions *in vivo* the majority of cellular ATP is produced by oxidative phosphorylation in the mitochondria (Bertram *et al.*, 2006; Aguer *et al.*, 2011). It has been discovered that in cultured cells however, despite aerobic conditions, the majority of ATP is often produced *via*

glycolysis in the cytoplasm. This phenomenon is known as the Crabtree effect and results in a significant decrease in levels of oxidative phosphorylation occurring within cells. As galactose produces no net ATP from glycolysis, the Crabtree effect can be reversed by culturing cells in the presence of galactose rather than glucose. This switches carbohydrate metabolism to favour oxidative phosphorylation to maintain cellular levels of ATP, and subsequently increases the burden on the mitochondrial ETC (Dykens and Will, 2007; Marroquin *et al.*, 2007; Aguer *et al.*, 2011; Brand and Nicholls, 2011; Swiss and Will, 2011; Kamalian *et al.*, 2015). Therefore, culture of cells in galactose is used as a method to sensitise cells to mitochondrial toxins such as inhibitors of the ETC, rotenone (a complex I inhibitor) and antimycin A (a complex III inhibitor) (Marroquin *et al.*, 2007; Aguer *et al.*, 2011; Brand and Nicholls, 2011; Swiss and Will, 2011; Kamalian *et al.*, 2015). We utilised this same approach to further probe the functional status of the mitochondria in WT and m*Ogg1*$^{-/-}$ MEFs. As expected, culture of MEFs in galactose did sensitise cells to the ETC inhibitors antimycin A and rotenone. In contrast, there was no significant change in the IC50 value of BSO in m*Ogg1*$^{-/-}$ or WT MEFs in response to the switch to galactose-containing media. This observation suggests that the mechanism of BSO-toxicity is not directly dependent on the depletion of mitochondrial GSH, changes in ETC activity and subsequent mitochondrial dysfunction. Furthermore, there was no statistically significant differences in the IC50 values of antimycin A or rotenone between the two cell lines when cultured in galactose. These results suggest that m*Ogg1*$^{-/-}$ MEFs do not possess an enhanced sensitivity towards ETC inhibition and suggest that there are no major differences in mitochondrial function or activity between the two cell lines, and therefore it seems unlikely that dysfunctional m*Ogg1*$^{-/-}$ mitochondrial metabolism explains the difference in sensitivity to BSO (Wallace, 2001; Aguer *et al.*, 2011; Kamalian *et al.*, 2015).

Consistent with elevated levels of mitochondrial superoxide in m*Ogg1*$^{-/-}$ MEFs we also observed an increase in the expression of *Sod2*, a mitochondrial specific isoform of the antioxidant SOD family (Zelko, Mariani and Folz, 2002). The SOD2 enzyme catalyses the dismutation of mitochondrial superoxide into

H_2O_2 (Abreu and Cabelli, 2010), which can then be further detoxified by CAT and GPX (Michiels *et al.*, 1994). Therefore, it might be expected that *Sod2* would be upregulated in response to an increase in mitochondrial levels of superoxide. We do not however observe a subsequent upregulation of either *Cat* or *Gpx*, which catalyse the decomposition of H_2O_2, and we propose that this results in a loss of mitochondrial redox homeostasis and an accumulation of H_2O_2 levels within the mitochondria. H_2O_2 is electrically neutral and therefore permeable to cell membranes, although recent studies have proposed that it is less permeable to certain cellular membranes and therefore H_2O_2 transport may be more regulated than first thought. However, it still remains understood that H_2O_2 is able to diffuse freely throughout the cell, travelling to other compartments of the cell, and subsequently increasing oxidative stress outside of the mitochondria (Antunes and Cadenas, 2000; Makino *et al.*, 2004; Bienert, Schjoerring and Jahn, 2006; Fisher, 2009). An upregulation of *Sod2*, and therefore a subsequent increase in the dismutation of superoxide, has been shown to result in an increase in H_2O_2 previously; having been linked to both tumorigenesis and metastasis (Dasgupta *et al.*, 2006; Hempel, Carrico and Melendez, 2011; Wang *et al.*, 2017). We propose that an increase in superoxide production by the mitochondria of m*Ogg1*$^{-/-}$ MEFs is propagated to cause an increase in oxidative stress throughout the entire cell as a result of the failure to detoxify mitochondrial H_2O_2 (Figure **2.14**). However, as discussed above, the mitochondria of m*Ogg1*$^{-/-}$ MEFs appear to be functioning to the same capabilities as the mitochondria of WT MEFs, despite these elevated levels of mitochondrial superoxide and H_2O_2. Intracellular ROS is then further increased following GSH depletion generating a positive feedback loop and further increasing the production of H_2O_2. This further increases oxidative stress across the cell as shown by oxidative stress markers in other cellular compartments (cytoplasmic ROS and DNA oxidation). This further increase in oxidative stress across the cell ultimately leads to the induction of apoptosis in m*Ogg1*$^{-/-}$ MEFs.

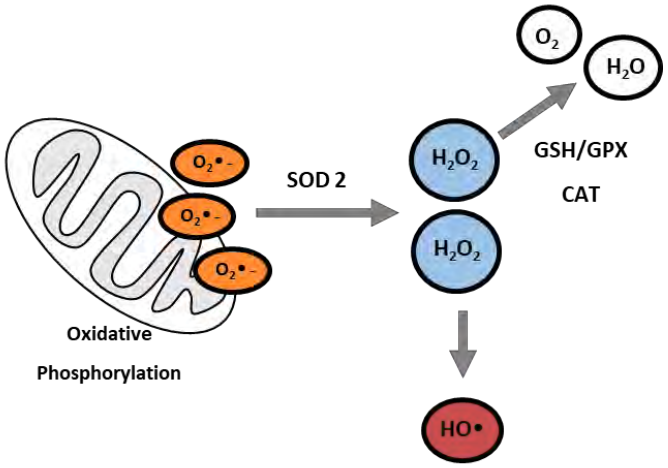


Figure 2.14. The elevation of ROS in m*Ogg1*$^{-/-}$ MEFs could be explained by an increased production of mitochondrial superoxide combined with changes in antioxidant expression. Mitochondrial superoxide ($O_2^{\bullet -}$) is likely generated in the mitochondria during oxidative phosphorylation (Murphy, 2009) , which is then converted into H_2O_2 by SOD2 (Abreu and Cabelli, 2010). H_2O_2 is able to cross cellular membranes and travel to other compartments within the cell (Makino *et al.*, 2004; Bienert, Schjoerring and Jahn, 2006). H_2O_2 can be converted into water and oxygen by both CAT and the GSH/GPX system (Michiels *et al.*, 1994) however, if not detoxified by antioxidants, H_2O_2 can produce hydroxyl radicals ($HO^{\bullet}$) which are highly reactive towards biomolecules (Winterbourn, 1981; Sato *et al.*, 1992). The overexpression of *Sod2* in m*Ogg1*$^{-/-}$ MEFs results in an increase in H_2O_2, however no such upregulation of *Cat* or *Gpx* occurs resulting in an accumulation of H_2O_2. We suggest that these changes in the expression of antioxidants in m*Ogg1*$^{-/-}$ MEFs are sufficient to increase the production of H_2O_2 and $HO^{\bullet}$ across the cell. Intracellular ROS is then further increased across the cell following the depletion of GSH, with this further increase in ROS sufficient to induce apoptosis.

Increased levels of intracellular ROS induce oxidative DNA damage, which if unrepaired could activate apoptotic signalling pathways. However, our experiments appear to exclude this as the mechanism of BSO-induced apoptosis in m*Ogg1*$^{-/-}$ MEFs. Although there is a significant increase in levels of 8-oxoG sites in m*Ogg1*$^{-/-}$ MEFs following BSO treatment, and subsequent GSH depletion, this increase is only moderate when compared to the induction of 8-oxoG by a non-cytotoxic concentration of H_2O_2. Furthermore, by re-expressing *Ogg1* in m*Ogg1*$^{-/-}$ MEFs we showed that the ability of two different OGG1 variants to rescue cells in response to GSH depletion was not dependent on their repair activity. We conclude therefore that an increase in oxidative DNA damage alone is not sufficient to induce apoptosis in m*Ogg1*$^{-/-}$ MEFs and that sensitivity of m*Ogg1*$^{-/-}$ MEFs to BSO is not related to loss of OGG1-initiated repair of genomic DNA.

2.5. Conclusions and future work

The evidence collected suggests that the induction of apoptosis in m*Ogg1*$^{-/-}$ MEFs in response to BSO treatment is independent of DNA damage, and the absence of OGG1-mediated repair. However, a mitochondrial-specific splice variant of *Ogg1* (β-OGG1) exists which is responsible for the repair of oxidative DNA damage in the mitochondria. mtDNA is highly susceptible to oxidation by ROS (Yakes and Van Houten, 1997) and this susceptibility would be even further increased following GSH depletion. Although we have shown that the induction of apoptosis is independent of nuclear oxidative DNA damage, we have not measured mtDNA damage. We therefore cannot completely exclude that oxidative mtDNA damage goes unrepaired in m*Ogg1*$^{-/-}$ MEFs, and ultimately induces apoptosis. Such an increase has already been linked to an increase in mitochondrial ROS production (Indo *et al.*, 2007), and a subsequent decrease in mitochondrial function (Yuzefovych *et al.*, 2013; Leon *et al.*, 2016).

We have not observed such mitochondrial dysfunction in m*Ogg1*$^{-/-}$ MEFs in our experiments, however we do not exclude that possible differences may exist between the mitochondrial activity of WT and m*Ogg1*$^{-/-}$ MEFs that we did not detect. These differences could result in an increased production of mitochondrial superoxide in m*Ogg1*$^{-/-}$ MEFs. In this study, we have simply concluded that the excess mitochondrial superoxide is not being produced as a consequence of highly dysfunctional m*Ogg1*$^{-/-}$ mitochondria. However, further mitochondrial studies (*e.g.* measurement of proton current, seahorse mitochondrial stress testing, oxygen consumption rates) could be performed to fully probe the mitochondrial status of m*Ogg1*$^{-/-}$ MEFs (Aguer *et al.*, 2011; Brand and Nicholls, 2011; Divakaruni, Rogers and Murphy, 2014).

Alternatively the difference in sensitivity could be linked to another distinct biochemical function of OGG1. In further support of a mechanism of toxicity independent of oxidative DNA damage, OGG1 has been implicated into a number of different cellular processes beyond DNA repair, and it could be any number of these roles that protect WT MEFs from apoptosis following GSH depletion (Dantzer *et al.*, 2002; Boldogh *et al.*, 2012; Sampath *et al.*, 2012; Hajas *et al.*, 2013; Allgayer *et al.*, 2016; Ba and Boldogh, 2018) and these are currently the subject of further research in our laboratory. Overall we conclude that it is important to not limit the function of OGG1 to DNA repair, with our experiments showing that the consequence of lacking OGG1 function goes far beyond a decrease in OGG1-mediated BER.

3

Ogg1-null mouse embryonic fibroblasts possess back-up mechanisms to prevent the genomic accumulation of 8-oxoguanine

Adapted from prepared manuscript

Higgs E. B., *Godschalk R., van Schooten F. J., Hodges N. J. mNEIL3 is upregulated in Ogg1-null mouse embryonic fibroblasts as a backup mechanism for 8-oxoG repair*

3.1. Introduction

Mammalian cells possess multiple DNA repair pathways that repair damaged DNA preventing the occurrence of replication errors and the generation of mutations, therefore limiting genomic instability, as discussed in Chapter **1** (*refer to* **1.7.** specifically) (Hansen and Kelley, 2000; Lindahl and Barnes, 2000; Houtgraaf, Versmissen and van der Giessen, 2006; Jackson and Bartek, 2009; Lieber and Wilson, 2010; Freitas and De Magalhães, 2011; Jeggo, Pearl and Carr, 2016).

As previously mentioned, a primary focus of this thesis is the BER pathway, which is responsible for the repair of smaller and non-helix distorting lesions. BER is considered the primary repair pathway in which oxidative DNA damage is repaired, with the prevalent oxidative DNA modification 8-oxoG repaired by OGG1-mediated BER (Klungland, Rosewell, *et al.*, 1999; David, O'Shea and Kundu, 2007; Klungland and Bjelland, 2007; Robertson *et al.*, 2009; Faucher, Doublié and Jia, 2012). The occurrence of oxidative DNA damage and its subsequent repair remains a popular topic of interest, with oxidative DNA damage having been linked to ageing and disease (Boiteux and Radicella, 2000; Bjelland and Seeberg, 2003; Cooke *et al.*, 2003; Evans, Dizdaroglu and Cooke, 2004; Benz and Yau, 2008; Kryston *et al.*, 2011; Helleday, Eshtad and Nik-Zainal, 2014; Jeggo, Pearl and Carr, 2016).

Homozygous *Ogg1*$^{-/-}$ mice were generated by Klungland *et al.* (Klungland, Rosewell, *et al.*, 1999), with these mice models and tissues having subsequently been utilised in numerous studies (Minowa *et al.*, 2000; Osterod *et al.*, 2001; Arai *et al.*, 2002, Arai *et al.,* 2006; Sakumi *et al.*, 2003). Many of these studies have noted an increased level of 8-oxoG being present in the genome of these *Ogg1*$^{-/-}$ mice, however this is tissue-dependent (Klungland, Rosewell, *et al.*, 1999; Minowa *et al.*, 2000; Osterod *et al.*, 2001). Furthermore, we did not identify such an 8-oxoG elevation in the nuclear DNA of m*Ogg1*$^{-/-}$ MEFs (explored in Chapter **2**). Additionally, although one previous study did publish findings describing an increased incidence of lung carcinoma in *Ogg1*$^{-/-}$ mice (Sakumi *et al.*, 2003), such an increase in malignancies was not observed in all studies (Klungland, Rosewell, *et al.*, 1999; Osterod *et al.*, 2001; Arai *et al.*, 2006).

Currently the literature does suggest that a secondary mechanism could exist in mammalian cells which could potentially mediate the removal of 8-oxoG in the absence of OGG1. We therefore hypothesise that the presence of this backup repair mechanism would be capable of preventing an accumulation of 8-oxoG in the genome of *Ogg1*$^{-/-}$ models, as previously observed.

The possibility of an OGG1 back-up has already been the focus of a handful of studies and reviews, with the NER pathway having been suggested as a candidate backup mechanism that can aid in the repair of 8-oxoG (Reardon *et al.*, 1997; Klungland, Höss, *et al.*, 1999; Miao *et al.*, 2000; Shimizu *et al.*, 2003; Slupphaug, Kavli and Krokan, 2003; Hollander *et al.*, 2005; D'errico *et al.*, 2006; Dušinská *et al.*, 2006). The NER pathway has a broad set of substrates that are generally referred to as larger and helix-distorting lesions, with some oxidative DNA lesions included in this broad substrate range (Brooks *et al.*, 2000; Kuraoka *et al.*, 2000). Despite this focus on NER and oxidative DNA damage, there has never been a full mechanism described and it remains unclear whether NER is able to compensate for OGG1, repairing 8-oxoG independently of OGG1. Such an overlap between DNA repair pathways is not unheard of and examples of such crosstalk are becoming increasingly discovered. It is hypothesised that these overlaps between DNA pathways help maintain genomic stability in organisms (Slupphaug, Kavli and Krokan, 2003).

In this chapter, we use gene expression studies to identify possible candidate backup mechanisms in the OGG1-null cell model, m*Ogg1*$^{-/-}$ MEFs. This data, combined with functional comet assay data, suggests that two repair mechanisms are upregulated in m*Ogg1*$^{-/-}$ MEFs; and we suggest that these mechanisms are upregulated in order to remove 8-oxoG from DNA in the absence of OGG1. In line with previous studies (Langie *et al.*, 2007, Langie *et al.,* 2010; Gopalakrishnan *et al.*, 2010), we found that the NER pathway was upregulated in response to oxidative stress, however, we were unable to link this upregulation to 8-oxoG repair specifically. Furthermore, as the NER pathway has never been shown to successfully excise 8-oxoG in the absence of OGG1, we suggest that NER is not able to fully compensate

for OGG1. Upregulation of NER in response to oxidative stress could instead support previous findings suggesting that NER enzymes act as cofactors in OGG1-mediated BER, able to increase the rate of 8-oxoG excision (Klungland, Höss, *et al.*, 1999; Shimizu *et al.*, 2003; D'errico *et al.*, 2006; Dušinská *et al.*, 2006).

Alternatively, we hypothesis that the upregulation of the endonuclease Nei-like DNA glycosylase 3 (NEIL3) is in fact the primary compensatory mechanism, capable of preventing the accumulation of 8-oxoG in the absence of OGG1. NEIL3 is an endonuclease that is endogenously expressed at low levels and the primary substrates of the endonuclease have been identified as two larger DNA lesions, Sp and Gh, which are produced following the oxidation of 8-oxoG (Figure **3.1.**). As described previously, guanine possesses a low redox potential and this explains why guanine is the DNA base that is oxidised the most frequently (Margolin *et al.*, 2006; Paleček and Bartošík, 2012; Fleming and Burrows, 2017). Interestingly, 8-oxoG possesses an even lower redox potential than guanine and is therefore also highly vulnerable to oxidation (Kornyushyna and Burrows, 2003; Niles, Wishnok and Tannenbaum, 2004; Cui *et al.*, 2013; Krokeide *et al.*, 2013).

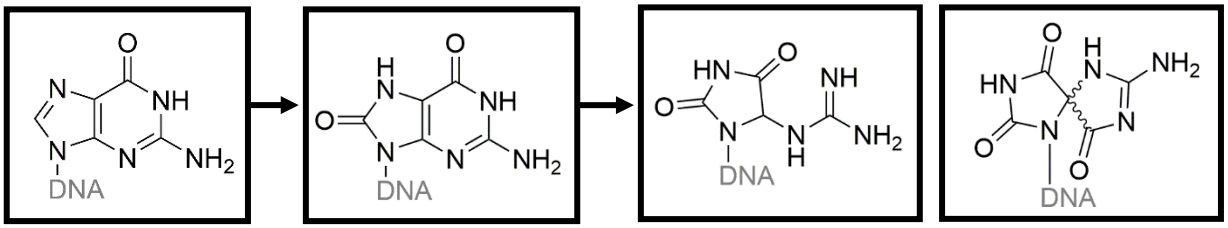


Figure 3.1. Guanine (G), 8-oxoguanine (8-oxoG), 5-guanidinohydantoin (Gh) and spiroiminodihydantoin (Sp). Guanine possesses a low redox potential and is therefore vulnerable to oxidation by ROS, producing 8-oxoG. This addition of oxygen deems 8-oxoG even more vulnerable to oxidation than guanine, decreasing the redox potential further. Oxidation of 8-oxoG results in two primary products, Sp and Gh.

We have shown that there is an increased expression of NEIL3 in m*Ogg1*$^{-/-}$ MEFs compared to WT MEFs, with this upregulation measured at both mRNA (qPCR) and protein level (western blotting). We also utilised a novel adaptation of the comet assay to show that m*Ogg1*$^{-/-}$ MEFs possess an increased genomic level of NEIL3 substrate sites, which we hypothesise are Sp and Gh lesions. Through the results displayed in this chapter, we propose that 8-oxoG within the DNA of m*Ogg1*$^{-/-}$ MEFs is further oxidised to Sp and Gh, which are then subsequently excised following the upregulation of NEIL3. Therefore, we hypothesise a novel mechanism in which the accumulation of genomic 8-oxoG is prevented in OGG1-null cells.

3.2. Materials & methods

3.2.1. Cell culture

WT and m*Ogg1*$^{-/-}$ MEFs were a generous gift from T. Lindahl (Klungland, Rosewell, *et al.*, 1999) (Cancer Research UK, Clare Hall Laboratories). In addition to MEFs, the commonly used human adenocarcinoma alveolar epithelial A549 cells were utilised as substrate cells during NER-comet assays (ECACC number: 86012804). All cells were maintained in DMEM (Gibco: catalogue no. 41965047, with phenol-red, L-glutamine and 4.5 g/L D-Glucose) supplemented with FBS (10% v/v), L-Glutamine (2 mM), penicillin (100 units/mL) and streptomycin (100 μg/mL). All media and supplements were purchased from either Gibco (ThermoFisher Scientific) or Sigma-Aldrich (Merck). Once prepared, complete media was stored at 4°C for a maximum of one month. All cell culture work was carried out under suitable sterile conditions in a Class 1 tissue culture hood (Aura B4, Bio Air, Italy) and cells were incubated at 37°C and 5% CO_2 (Sanyo MCO-19AIC Incubator). Cells were frequently assessed to monitor growth and check for contamination and cells were routinely passaged on reaching 80 - 90% confluence. Full details of cell culture methodology, including mycoplasma testing, is described in the appendix (**7.1.1.**).

3.2.2. Treatment of cells

BSO Treatment

BSO (Sigma-Aldrich, Merck: catalogue no. B2640) was prepared as a stock solution (50 mM) in supplemented DMEM. Diluted aliquots (5 mM) were prepared and stored at -20°C. Aliquots were thawed a maximum of two times before disposal. Immediately prior to use, BSO was further diluted with supplemented DMEM to the required concentration.

H_2O_2 Treatment

H_2O_2 (30% v/v) (VWR International) was freshly prepared immediately prior to an experiment. A stock solution (0.5 M) was prepared in supplemented DMEM on the day of the experiment, and this was further diluted with supplemented DMEM to the required concentration.

3.2.3. DNA repair qPCR array

Total RNA extraction

Total RNA extraction was carried out using the RNeasy Mini Kit (Qiagen), as per the manufacturer's instructions. Full details of this methodology are described in Chapter **2.2.3.**

cDNA synthesis

Extracted RNA was used to synthesise cDNA using the RT^2 first-strand kit as per the manufacturer's instructions (Qiagen: catalogue no. 330401). cDNA (1 μg) was added to the supplied buffer to create a genomic elimination mix, which was incubated at 42°C (5 min). This genomic elimination mix was then added to the supplied reverse transcription mix (1:1 ratio) and incubated at 42°C (15 min). The reaction was terminated by incubating at 95°C (5 min) and cDNA was stored at - 20°C until the experiment for qPCR was set-up.

qPCR

RT^2 profiler PCR arrays were obtained (Qiagen: Product no. 330231, catalogue no. PAMM-042Z), which contained primers against 84 DNA-repair-related genes. Each individual well contained primers against a different gene (*refer to* Table **3.1** for full details) alongside necessary control wells. Control wells included endogenous-control genes, reverse transcription controls, genomic DNA contamination controls and positive PCR controls. A single reaction mastermix was prepared for an entire 96-well array, with both the mastermix and the PCR plate maintained on ice throughout the experimental set-up. The mastermix was prepared so each well would contain the supplied SYBR-Green mastermix (12.5 μl/well), cDNA (0.9 μl/well) and RNase free H_2O (11.6 μl/well). The reaction mastermix was added to each well (total volume = 25 μl/well) and the wells sealed using optical thin-wall cap seals. The plate was centrifuged (600 g, 60 sec) prior to PCR (AriaMx real-time PCR system, Agilent) (*refer to* Table **3.2** for PCR conditions).

Table 3.1. The DNA repair genes included in the qPCR profiler array

Repair pathway	Genes		
Base excision repair (BER)	▪ Apex1 ▪ Apex 2 ▪ Ccno ▪ Lig3 ▪ Mpg ▪ Mutyh ▪ Neil1	▪ Neil2 ▪ Neil3 ▪ Nthl1 ▪ Ogg1 ▪ Parp1 ▪ Parp2 ▪ Parp3	▪ Polb ▪ Smug1 ▪ Tdg ▪ Ung ▪ Xrcc1
Nucleotide excision repair (NER)	▪ Atxn3 ▪ Brip1 ▪ Ccnh ▪ Cdk7 ▪ Ddb1 ▪ Ddb2 (Xpe) ▪ Ercc1 ▪ Ercc2 (Xpd) ▪ Ercc3 (Xpb)	▪ Ercc4 (Xpf) ▪ Ercc5 (Xpg) ▪ Ercc6 ▪ Ercc8 ▪ Lig1 ▪ Mms19 ▪ Pnkp ▪ Poll ▪ Rad23a	▪ Rad23b ▪ Rpa1 ▪ Rpa3 ▪ Slk ▪ Xab2 ▪ Xpa ▪ Xpc
Mismatch repair (MMR)	▪ Mlh1 ▪ Mlh3 ▪ Msh2 ▪ Msh3	▪ Msh4 ▪ Msh5 ▪ Msh6 ▪ Pms1	▪ Pms2 ▪ Pold3 ▪ Trex1
Double-strand break (DSB) repair	▪ Brca1 ▪ Brca2 ▪ Dmc1 ▪ Fen1 ▪ Lig4 ▪ Mre11 ▪ Prkdc	▪ Rad21 ▪ Rad50 ▪ Rad51 ▪ Rad51b ▪ Rad51c ▪ Rad51d ▪ Rad52	▪ Rad54L ▪ Xrcc2 ▪ Xrcc3 ▪ Xrcc4 ▪ Xrcc5 ▪ Xrcc6
Other pathways	▪ Atm ▪ Atp23 ▪ Atr	▪ Exo1 ▪ Mgmt ▪ Rad18	▪ Rfc1 ▪ Top3a ▪ Top3b
Endogenous control genes	▪ Actb ▪ B2m	▪ Gapdh ▪ Gusb	▪ Hsp90ab

Table 3.2. qPCR conditions for RT^2 profiler array

Number of cycles	Temperature (°C)	Duration
1	95	10 min
40	95	15 sec
	60	1 min

Analysis

Three PCR array plates were used for each tested condition (N=3) and the mean Ct value across these replicates were calculated for every gene. Two endogenous control genes (*Gapdh* and *Hsp90ab1*) were then used to calculate the delta Ct (ΔCt) for every gene per condition. For each comparison made (*e.g.* control versus treatment), delta-delta Ct (ΔΔCt) values were calculated, and these were then used to calculate the relative fold-change (as described previously in Equation **2**, and shown again here). Multiple *t*-tests were performed for the analysis to generate *p*-values. These were corrected for multiple comparison testing using a false discovery rate (FDR) approach, using the two-stage linear step-up method of Benjamini, Krieger and Yekutieli (Benjamani and Hochberg, 1995; Benjamani, Krieger and Yekutieli, 2006).

Equation 2 | I. $\boldsymbol{\Delta Ct} = Ct_{Gene} - Ct_{Endogenous\ Control\ Gene}$

II $\boldsymbol{\Delta\Delta Ct} = \Delta Ct_{Treated} - \Delta Ct_{Control}$

III. $\boldsymbol{Fold\ Change} = 2^{-\Delta\Delta Ct}$

3.2.4. Western Blotting

The protein of interest was NEIL3, which is a DNA repair protein that is primarily located in the nucleus. Therefore nuclear-enriched protein extractions were prepared using NE-PER™ Nuclear and Cytoplasmic Extraction Reagents as per the manufacturer's instructions (Thermo Scientific: catalogue no. 78833). The protein concentration of the extracts were determined with the Bradford assay (Bradford, 1976) (appendix **7.1.2.**) and diluted to a constant concentration before being separated using SDS-PAGE. The separated proteins were transferred to a PVDF membrane (GE healthcare Amersham™) and non-specific sites blocked (5% w/v non-fat milk powder in TBST) prior to incubation with a primary antibody overnight at 4°C (*refer to* Table **3.3.** for antibody details). The membrane was washed and incubated with a secondary antibody at RT (1 h) before the blot was visualised using chemiluminescence reagents (SuperSignal™ West Femto, Thermo Scientific: catalogue no. 34094) and x-ray film (HyperFilm™ ECL, GE healthcare Amersham: catalogue no. 28-9068-37). Full details of this methodology are described in Chapter **2.2.4.**

Table 3.3. Antibodies used

Antibody target	Dilution used	Supplier	Catalogue number	Secondary antibody
NEIL3	1:500	Abcam	ab1100049	Goat anti-rabbit IgG (H+L), HRP (Invitrogen, ThermoFisher Scientific) 1:500
β-ACTIN	1: 10,000	Sigma-Aldrich, Merck	A2228	Goat anti-mouse IgG (H+L) HRP (Abcam) 1:10000

3.2.5. Enzyme modified comet assays

As described in Chapter **2**, a standard alkaline comet assay measures single strand breaks in DNA (Singh *et al.*, 1988). However, the comet assay can be modified to recognise different types of DNA damage by incorporating an additional step where DNA is incubated with a DNA repair enzyme (*e.g.* OGG1 or NEIL3). This step allows for the measurement of specific types of DNA damage via the formation of additional single-strand breaks (Cadet *et al.*, 2000; Smith, O'Donovan and Martin, 2006; Collins, 2014). These additional single strand breaks represent sites of substrate recognition by the repair enzyme, resulting in abasic sites and single strand breaks; both of which are subsequently measured as an increase in tail intensity (% TI).

During these hOGG1- and hNEIL3- modified comet assays, each sample was used to produce two paired slides (as depicted previously in Chapter **2:** *refer to* Figure **2.1.)**. One slide was incubated with enzyme buffer (vehicle control slide) and one slide was incubated with hOGG1 (Trevigen: catalogue no. 4130-100-FK) or hNEIL3 (a generous gift from J. Parsons, Institute of Translational Medicine, University of Liverpool, UK). The difference in tail intensity between the two slides is therefore representative of OGG1 or NEIL3 substrate sites (measured in terms of % TI).

Buffers & solutions

NMA: Agarose (1% w/v) in PBS.

LMA: Agarose (0.7% w/v) in PBS.

Lysis solution: NaCl (2.5 M), Na_2EDTA (0.1 M), tris-HCl (8 mM), NaOH (200 mM), DMSO (10% v/v), and triton-X (1% v/v). Adjusted to pH 10.

Enzyme buffer: HEPES (40 mM), KCl (0.1 M), EDTA (0.5 mM), BSA (0.2 mg/mL). Adjusted to pH 8.

Electrophoretic buffer: NaOH (300 mM) and Na_2EDTA (1 mM).

Neutralisation solution: Tris-HCl (0.4 M) adjusted to pH 7.5.

Slide preparation and lysis

Cells were seeded in 12-well plates (4 x 10^4 cells/well) prior to treatment. Following the appropriate treatment, cells were incubated in trypsin-EDTA and the cell suspension was diluted (1 - 5 x 10^4 cells/ml). Cells were briefly centrifuged (3500 rpm, 1 min), the pellet resuspended in PBS, and the sample centrifuged again (3500 rpm, 1 min). The supernatant was removed and the pellet resuspended in LMA (180 μL) and transferred onto two paired slides (90 μL/slide), which had previously been coated with NMA. The slides were incubated at 4°C (20 min) before another 90 μL LMA was added to each slide. The slides were again incubated at 4°C (20 min) and then placed in lysis solution for 1 h.

Enzyme incubation, electrophoresis and fixation

Following lysis, the cells were either incubated with hOGG1 (50 μL, 1 unit/slide), hNEIL3 (50 μL, 1 μg/slide) or enzyme buffer (50 μL) at 37°C (30 min). The slides were transferred to ice immediately following the incubation, preventing any further enzymatic activity. The slides were placed in an electrophoretic chamber containing electrophoretic buffer at 4°C to allow the unwinding of DNA (30 min). Electrophoresis was then carried out (300 mA and 0.78 V/cm) for 30 min. Slides were carefully removed and maintained horizontally to minimise the risk of the gel separating from the surface of the slide. Neutralisation solution was immediately added to each slide (2 mL, 5 min), and slides then fixed with ice-cold EtOH (2 mL).

Comet scoring

Once dry, the slides were stained with SYBR gold staining solution (90 μL, 1: 1000 dilution in dH_2O) (Invitrogen, ThermoFisher Scientific: catalogue no. S11494), and stained overnight in a humid environment (4°C). The cells were evaluated under a fluorescent microscope (Zeiss Axiovert 10 (*20x* objective); $\lambda_{excitation}$ 515-560 nm; 540 nm barrier filter). Cells (50 cells/slide) were scored using Comet Assay IV software, with DNA damage being measured in terms of tail intensity (%) (Duez *et al.*, 2003).

3.2.6. NER-modified comet assay

As described above, a standard alkaline comet assay measures single strand breaks in DNA and further assay modifications can be used to instead measure different types of DNA damage (*e.g.* oxidative DNA damage). However, the comet assay can be alternatively modified to instead measure the repair activity of a cell extract. These modifications rely on the use of a DNA damaging agent to induce damage in substrate cells, followed by the addition of protein extracts which subsequently repair this damage. An increase in repair activity results in the production of abasic sites and single strand breaks (intermediate products of repair) resulting in an increase in tail intensity (% TI).

This principle was used to perform NER-modified comet assays, utilising A549 cells as substrate cells (Langie *et al.*, 2006; Langie *et al.*, 2007; Langie *et al.*, 2010; Speit *et al.*, 2013). Briefly described, A549 cells were lysed and subsequently exposed to the DNA-damaging agent, benzo(a)pyrene diol epoxide (BPDE). This BPDE exposure produces DNA adducts that are recognised and repaired by the NER pathway. Protein extracts of both WT and m*Ogg1*$^{-/-}$ MEFs were added to the A549 cells following this BPDE exposure; allowing for the recognition and subsequent repair of the DNA adducts by NER (summarised in Figure **3.2.**). Paired slides were produced for each tested protein extract, allowing one slide to be exposed to BPDE and one slide to be exposed to DMSO only (vehicle control). Control slides (BPDE-negative/extract-negative and BPDE-positive/extract-negative) were also included per experiment.

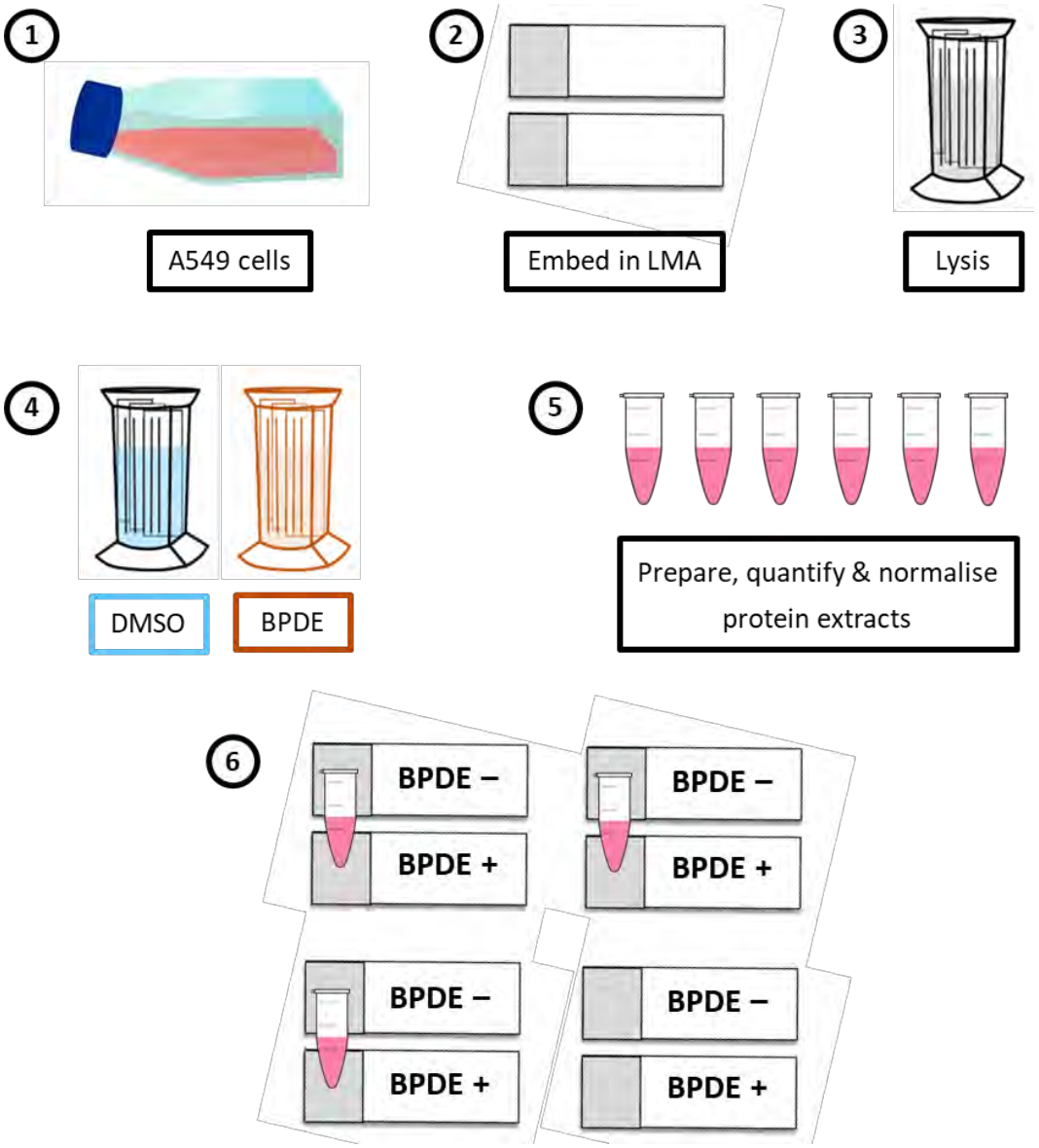


Figure 3.2. The methodology for the NER-modified comet assay is displayed ① A549 cells were grown to be used as substrate cells ② Once confluent, the A549 cells were counted and diluted, prior to be embedded in LMA onto NMA-pre-coated slides ③ The embedded A549 cells were lysed at 4°C (1 h) ④ The slides were washed in PBS and then incubated in either DMSO (vehicle control) or BPDE (1 μM) for 1 h ⑤ Protein extracts of MEFs were prepared, quantified and normalised to ensure all extracts were the same concentration ⑥ Two slides were prepared for each protein extract as shown, BPDE (–) and BPDE (+); and per experiment two extract-negative slides were prepared, BPDE (–) and BPDE (+).

Buffers & solutions

NMA: Agarose (1% w/v) in PBS.

LMA: Agarose (0.7% w/v) in PBS.

Lysis solution: NaCl (2.5 M), Na_2EDTA (0.1 M), tris-HCl (8 mM), NaOH (200 mM), DMSO (10% v/v), and triton-X (1% v/v). Adjusted to pH 10.

Buffer A: HEPES (45 mM), KCl (0.4 mM), EDTA (1 mM), dithiothreitol (0.1 mM), Glycerol (10% v/v). Adjusted to pH 7.8. ***

Buffer A2: Buffer A and Triton-X (1% v/v).

Buffer B: HEPES (40 mM), KCl (0.1 M), EDTA (0.5 mM), BSA (0.2 mg/ml). Adjusted to pH 8.

Electrophoretic buffer: NaOH (300 mM) and Na_2EDTA (1 mM).

Neutralisation solution: Tris-HCl (0.4 M) adjusted to pH 7.5.

*** Buffer A was prepared immediately prior to experiment.*

Preparation of protein extracts

MEFs were grown to confluence in T_{75} flasks and treated with BSO (15 μM, 24 h). Following treatment, cells were trypsinised and the cell suspension diluted to give a density of 2 x 10^6 cells/ml. The cells were centrifuged (4000 rpm, 5 min) and the supernatant subsequently discarded, with it possible to store the pellet (-80°C) at this stage when required. The pellet was subsequently resuspended in buffer A (50 μL) and snap-frozen in liquid nitrogen. The samples were immediately thawed and buffer A2 added to each sample (15 μL), followed by a brief vortex. Samples were then incubated on ice (10 min) and centrifuged at 4°C (11000 rpm, 5 min). The concentration of protein extracts were measured using the DC™ Protein Assay (Bio-Rad: catalogue no. 500-0116) (Lowry *et al.*, 1951) (appendix **7.1.2.**) and extracts were diluted (0.8 mg/mL) in buffer A1. The extract (50 μL) was then added to buffer B (200 μL) and ATP (10 μL).

DNA damage and repair

A549 cells MEFs were grown to confluence in T_{75} flasks. Cells were trypsinised, counted, and the cell suspension diluted in PBS to give a density of 2 x 10^6 cells/ml. To prepare each slide, cell suspension (25 μL) was added to LMA (75 μL), and pipetted onto a slide that had been pre-coated with NMA. The slides were incubated at 4°C (40 min) and then placed in lysis solution at 4°C overnight. Just prior to the lysis finishing, two Coplin jars were prepared for the BPDE exposure, as detailed below:

BPDE-positive: BPDE (3.3 μL of 20 mM stock) added to PBS (66.6 mL), resulting in a final BPDE concentration of 1 μM.

BPDE-negative: DMSO (3.3 μL) added to PBS (66.6 mL).

Following lysis, cells were washed in PBS at 4°C (15 min). The slides were then incubated in the Coplin jar containing the correct treatment on ice (30 min). Following exposure, cells were moved to Coplin jars containing buffer B and incubated at RT (15 min). The prepared protein extracts were then added to appropriately labelled slides and incubated at 37°C (20 min). One the incubation period was complete, slides were immediately transferred to ice to prevent any further enzymatic activity.

Electrophoresis, fixation and scoring

A similar method was followed as before (*refer to* **3.2.5.**), however there were subtle differences as these experiments were performed in a different laboratory (Department of Pharmacology and Toxicology, Maastricht University). Slides were placed in an electrophoretic chamber containing electrophoretic buffer at 4°C (20 min), allowing DNA to unwind. This was followed by electrophoresis (300 mA and 0.78 V/cm) for a further 20 min. As before, slides were carefully removed and maintained horizontally, and neutralisation solution was added to each slide (2 mL, 5 min). Slides were then fixed with ice-cold EtOH (2 mL). Once dry, each slide was stained with EtBr overnight (90 μL, 10 mg/ml in dH_2O). The cells were evaluated under a fluorescent microscope and scored using Comet Assay III software. DNA damage was measured in terms of tail intensity (%) and the results presented as percentage increase in NER activity.

3.2.7. Thiobarbituric acid reactive substances assay

Buffers & solutions

Radioimmunoprecipitation assay (RIPA) lysis buffer: NaCl (150 mM), NP40 (1% v/v), sodium deoxycholate (0.5% w/v), sodium dodecyl sulfate (0.1% w/v), Tris (50 mM). Adjusted to pH 8.

Butylated hydroxyltoluene (BHT): BHT (0.22% w/v) in EtOH.

Thiobarbituric acid (TBA): TBA (0.25% w/v) in NaOH (0.2 M).

TCA: TCA (100% w/v) in dH_2O, prepared at 4°C.

TBARS reagent 1: 5 volumes TCA added to 1 volume HCl (12 N).

TBARS reagent 2: 1 volume TBA added to 1 volume TBARS reagent 1.

Thiobarbituric acid reactive substances (TBARS) assay protocol

TBA can be used as a measure of lipid peroxidation, and is therefore often used as a measure of oxidative stress. The principle of the assay is the reaction of TBA with malondialdehyde (MDA) in conditions of low pH and high temperature, resulting in the formation of a fluorescent and colorimetric product. MDA is an end-product of the decompositions of lipid peroxidation products, therefore the measurement of MDA in a sample is representative of lipid peroxidation (Ohkawa, Ohishi and Yagi, 1979; Chipman *et al.*, 1998; Gaweł *et al.*, 2004).

Cells were seeded in 6-well plates (2 x 10^5 cells/well) and treated appropriately the following day. Following treatment, cells were washed with PBS and ice-cold RIPA lysis buffer (150 μL) added to each well. From this point onwards, the assay was carried out on ice. The cells were thoroughly scraped into the RIPA lysis buffer, ensuring that all cells had detached from the surface. Cell lysates were transferred to sterile Eppendorf tubes, with three replicate wells combined to form one sample to ensure that there was adequate material for detection. Samples were centrifuged at 4°C (13 000 g, 10 min). At this stage, an aliquot of each sample (10 μL) was stored (-80°C) until needed for protein quantification using the DC™ protein assay (Bio-Rad: catalogue no. 500-0116) (Lowry *et al.*, 1951) (appendix **7.1.2.**). The

remaining cell lysate (250 μl) was added to TBARS reagent 2 (50 μL) and BHT (2.5 μL). Samples were heated at 95°C (45 min) and subsequently cooled at RT (10 min). An aliquot of each sample (75 μL) was transferred to duplicate wells of a 96-well black microplate, and fluorescence measured ($\lambda_{excitation}$ 485 nm and $\lambda_{emission}$ 535 nm) (Infinite® 200 Pro, Tecan). Background fluorescence was subtracted using control samples that did not contain lysate. Fluorescence was normalised to total protein (mg/ml) using the DC™ protein assay (Lowry *et al.*, 1951) (appendix **7.1.2.**) and converted to MDA (%).

3.2.8. Statistics

All results are presented as the mean values ± SD (N = number of biological experiments), unless otherwise stated. When two different samples were being compared, a two-tailed unpaired *t*-test was used. Larger datasets were analysed by two-way ANOVA and then corrected for multi-comparison testing using appropriate post-hoc testing. For parametric data, a Dunnett's test (comparison of each group with a control group) or Tukey's test (multi-comparison testing between all groups) was performed; and for non-parametric data, the Bonferroni correction was performed. A detailed report of the statistics performed for each experiment is detailed in the appendix (**7.2.**). Graphs were prepared and statistical analysis performed using GraphPad Prism (version 8.0.1); and $p < 0.05$ was considered statistically significant (*); $p < 0.01$ (**); $p < 0.001$ (***).

3.3. Results

3.3.1. 8-oxoG does not accumulate in m*Ogg1*$^{-/-}$ MEFs

A hOGG1-modified comet assay was used to measure 8-oxoG sites in DNA, with the difference in tail intensity (% TI) between hOGG1 negative and hOGG1 positive slides used as a representative measure of 8-oxoG sites. There was no statistical difference in the basal level of 8-oxoG sites, as represented by tail intensity (% TI), in WT (0.52 ± 1.04%) and m*Ogg1*$^{-/-}$ MEFs (1.10 ± 1.46%) ($p > 0.05$) (Figure **3.3.**)**.** This suggests that there is no accumulation of 8-oxoG in the DNA of m*Ogg1*$^{-/-}$ MEFs, despite the absence of OGG1 activity. The *Ogg1*-null status of m*Ogg1*$^{-/-}$ MEFs was previously confirmed in Chapter **2** (*refer to* Figure **2.2.**).

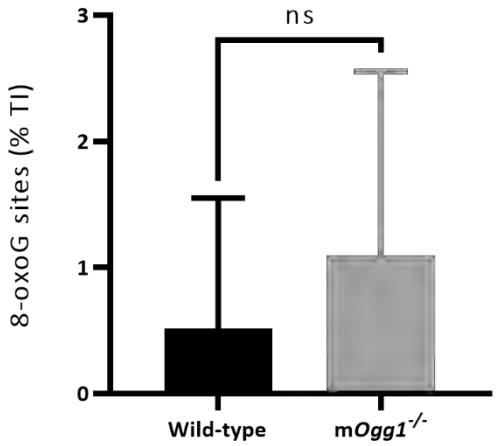


Figure 3.3. There is no difference in the basal level of 8-oxoG in WT (0.52 ± 1.04%) and m*Ogg1*$^{-/-}$ MEFs (1.10 ± 1.46%) ($p > 0.05$). 8-oxoG sites are represented by tail intensity (% TI), which is calculated by subtracting the median tail intensity of hOGG1 negative cells from the median tail intensity of hOGG1 positive cells. Mean ± SD is displayed (N=3), and significance was determined using Bonferroni testing.

3.3.2. The qPCR array passed all quality control requirements

RT^2 profiler qPCR arrays (Qiagen: Product no. 330231, catalogue no. PAMM-042Z) was utilised to probe for possible back-up repair mechanism in m*Ogg1*$^{-/-}$ MEFs, which could prevent the accumulation of 8-oxoG in the absence of OGG1. However, prior to performing the RT^2 profiler qPCR, a quality control (QC) plate was performed (Qiagen: catalogue no. 330291). This experiment was undertaken to ensure that:

1) *The experimental set-up was optimal.*
2) *cDNA samples were of high quality.*
3) *No contamination was present.*

There was minimal variation between the replicate reactions and each QC condition passed the requirements (as determined by the manufacturer). The results of the QC array are displayed (Figure **3.4.**) with the optimal values indicated where appropriate. Two endogenous controls (*Actb* and *Hrpt1*) were included and only a small standard deviation was measured for each control across samples, suggesting that all samples contained RNA with similar integrity. Two control reactions included in the experiment are designed with the purpose to detect DNA contamination; the genomic DNA control (GDC) and the no template control (NTC). Both of these controls confirmed that no such contamination was present. Finally, the Ct values produced by the reverse transcription control (RTC) and PCR positive control (PPC) were used to calculate whether there was any inhibition of the reverse transcription reaction or PCR. The RTC reaction was designed to detect an external RNA control template that was built into the kit, whereas the PPC reaction contained an artificial DNA sequence to been amplified. Neither of these control reactions detected inhibition, and these calculations are displayed in Equation **3**.

Equation 3 | I. $$\boldsymbol{Reverse\ transcription\ inhibiton} = Ct_{\ RTC} - Ct_{\ PPC + H2O}$$

II. $$\boldsymbol{PCR\ inhibition} = Ct_{\ PPC + cDNA} - Ct_{\ PPC + H2O}$$

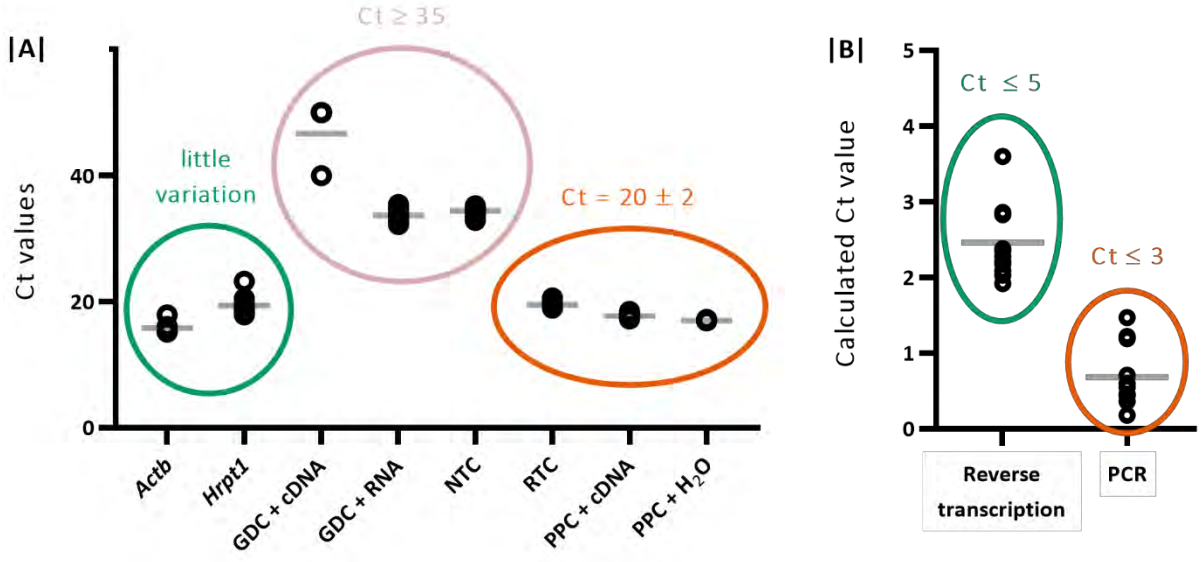


Figure 3.4. Quality control (QC) qPCR. These QC experiments were carried out to ensure that the reagents and samples passed quality control requirements. **|A|** Individual Ct values of each control are displayed (N=12) alongside the mean Ct value. Optimal values are described, where such values were supplied by the manufacturer (Qiagen). The two endogenous control genes (*Actb* and *Hrpt1*) showed little deviation between samples regardless of the cDNA sample used (O). The two genomic DNA control (GDC) experiments (GDC + cDNA) (GDC + RNA) resulted in high Ct values or no detection at all (plotted as Ct > 40). The no template controls (NTC) also resulted in high Ct values confirming that no signal was produced in the absence of template. The high Ct values (≥ 35) produced from these three control experiments (GDC+cDNA) (GDC+RNA) (NTC) are indicative of no template, and therefore confirm that no genomic contamination was present (O). The reverse transcription control (RTC) was included to test the efficiency of the reverse transcription reaction, and two different PCR positive control (PPC) experiments were included (PPC + cDNA) (PPC – cDNA) to test for PCR inhibition. These experiments consistently resulted in the suggested Ct values (Ct = 20 ± 2) (O), and these values were subsequently used to detect reverse transcription or PCR inhibition. **|B|** Inhibition of both the reverse transcription reaction (O) and PCR (O) was investigated. These calculations resulted in Ct values in line with the manufacturer (≤ 5 and ≤ 3 respectively), confirming that no inhibition was present for either reaction.

3.3.3. Candidate back-up mechanisms to OGG1 were identified in *mOgg1*$^{-/-}$ MEFs

Once the quality control parameters had been confirmed, the qPCR experimental set-up was deemed optimal, and the RT^2 profiler arrays were performed. These were performed for both WT and m*Ogg1*$^{-/-}$ MEFs, following no treatment or BSO treatment (15 μM, 24 h). A number of genes were found to be upregulated in m*Ogg1*$^{-/-}$ MEFs when compared to WT MEFs (Table **3.4.**) representing a number of possible back-up repair mechanisms, which may contribute to the repair of oxidative DNA damage in the absence of OGG1 activity. No equivalent down-regulation of genes were identified, except for *Ogg1*. It was calculated that *Ogg1* was down-regulated by 1000 -fold in m*Ogg1*$^{-/-}$ MEFs when compared to WT MEFs. In reality, the large Ct values produced (> 35) are consistent with little template DNA being present within the sample (as was expected). This confirms the m*Ogg1*$^{-/-}$ phenotype shown previously in Chapter **2** (*refer to* Figure **2.2.**).

Furthermore the expression of genes following GSH depletion, and therefore an increase in oxidative stress, were analysed. A number of genes were upregulated in WT MEFs following GSH depletion (*refer to* Table **3.5.**) but these changes were not identified in m*Ogg1*$^{-/-}$ MEFs. All fold-changes of 1.5 or above are displayed in this results section, however see appendix (**7.3.**) for full analysis of all 84 repair-related genes. No significant down-regulation of genes was identified in either cell-type following GSH depletion.

Multiple *t*-tests were carried out in conjunction with FDR testing; using the two-stage linear step-up method of Benjamini, Krieger and Yekutieli (Benjamani and Hochberg, 1995; Benjamani, Krieger and Yekutieli, 2006). The resulting *p*-values and *q*-values are included, with all significant changes displayed in bold; with corresponding volcano plots having been included in the appendix (**7.4.**).

Table 3.4. Gene expression fold-changes in m*Ogg1*$^{-/-}$ MEFs compared to WT MEFs. The qPCR analysis of a set of DNA repair genes resulted in the following significant differences between WT and *mOgg1*$^{-/-}$ MEFs. Genes of interest are grouped by DNA repair pathway and expression changes are presented as a fold-increase in *mOgg1*$^{-/-}$ MEFs compared to WT MEFs. Gene expression changes ≥ 1.5, which passed the FDR testing parameters, are highlighted.

Repair Pathway	Gene symbol	Fold-increase	Standard deviation	*p* value	*q* value		Discovery?
BER	*Apex 1*	1.69	0.31	0.018	0.030	*	No
	Lig1	**1.8**	**0.18**	**0.001**	**0.004**	**	**Yes**
	Tdg	**2.77**	**0.23**	**< 0.001**	**< 0.001**	***	**Yes**
	Nthl1	**1.67**	**0.03**	**< 0.001**	**< 0.001**	***	**Yes**
	Neil3	**37.86**	**1.59**	**< 0.001**	**< 0.001**	***	**Yes**
	Mpg	**4.57**	**0.46**	**< 0.001**	**< 0.001**	***	**Yes**
	Mgmt	**26.54**	**2.63**	**< 0.001**	**< 0.001**	***	**Yes**
NER	***Ercc1***	**2.51**	**0.24**	**< 0.001**	**0.001**	***	**Yes**
	Ercc4	**1.54**	**0.06**	**< 0.001**	**< 0.001**	***	**Yes**
	Ercc5	**1.68**	**0.20**	**0.004**	**0.008**	**	**Yes**
MMR	***Mlh1***	**1.53**	**0.07**	**< 0.001**	**< 0.001**	***	**Yes**
	Msh2	**1.58**	**0.13**	**0.002**	**0.004**	**	**Yes**
	Msh5	1.64	0.23	0.009	0.015	*	No
	Msh6	**1.54**	**0.10**	**< 0.001**	**0.002**	**	**Yes**
	Pms1	1.61	0.02	0.012	0.020	*	No
DSB	***Brip1***	**1.54**	**0.09**	**< 0.001**	**0.001**	***	**Yes**
	Prkdc	**1.67**	**0.03**	**< 0.001**	**< 0.001**	***	**Yes**
	Rad51d	**2.00**	**0.13**	**< 0.001**	**< 0.001**	***	**Yes**
	Xrcc5	1.53	0.39	0.080	0.100	ns	No
Other	***Slk***	**2.20**	**0.17**	**< 0.001**	**< 0.001**	***	**Yes**
	Top3b	1.81	0.52	0.055	0.075	ns	No

Table 3.5 Gene expression fold-changes in WT MEFs following BSO treatment. The qPCR analysis of a set of DNA repair genes resulted in the following significant increases in WT MEFs following GSH depletion. Genes of interest are grouped by DNA repair pathway and expression changes are presented as a fold-increase. These changes were not measured in *mOgg1*$^{-/-}$ MEFs. Gene expression changes ≥ 1.5, which passed the FDR testing parameters, are highlighted.

Repair Pathway	Gene symbol	Fold-increase	Standard deviation	*p* value	*q* value		Discovery?
BER	***Ogg1***	**3.41**	**0.27**	**< 0.001**	**0.001**	***	**Yes**
	Tdg	1.51	0.55	0.181	0.979	ns	No
	Nthl1	**1.96**	**0.04**	**< 0.001**	**< 0.001**	***	**Yes**
	Neil3	**3.01**	**0.17**	**< 0.001**	**< 0.001**	***	**Yes**
	Mgmt	**2.74**	**0.07**	**< 0.001**	**< 0.001**	***	**Yes**
	Mutyh	**1.62**	**0.10**	**< 0.001**	**0.006**	**	**Yes**
NER	***Ercc5***	**1.80**	**0.06**	**< 0.001**	**< 0.001**	***	**Yes**
MMR	*Mlh1*	1.63	0.62	0.153	0.919	ns	No
	Pms1	1.66	0.87	0.257	0.919	ns	No

3.3.4. NER activity is elevated in m*Ogg1*$^{-/-}$ MEFs

Three NER proteins were found to be upregulated in m*Ogg1*$^{-/-}$ MEFs, when compared to WT MEFs (*refer to* Table **3.4.**). Despite this fairly modest up-regulation of *Ercc1* (2.5 ± 0.2 -fold), *Ercc4* (1.5 ± 0.1 -fold) and *Ercc5* (1.7 ± 0.2 -fold), there was a significant difference with respect to NER activity in the two cell-lines, as measured using a NER-modified comet assay (Figure **3.5.**). This methodology was fully described previously (*refer to* **3.2.6**.) with an increase in tail intensity (% TI) measured following incubation with protein extracts representing the NER activity of that extract. Using this repair assay, the NER activity of WT control extracts was adjusted to 100% to allow comparison. A significantly higher level of NER activity was measured in m*Ogg1*$^{-/-}$ MEFs (42.0 ± 7.9% higher) when compared to WT MEFs ($p < 0.01$). Following GSH depletion, NER activity significantly increased in both WT (23.2 ± 2.3%) ($p < 0.05$) and m*Ogg1*$^{-/-}$ MEFs (25.9 ± 10.5%) ($p < 0.01$). This increase did not significantly differ between cell-types ($p > 0.05$) and therefore, following BSO treatment, NER activity remains elevated in m*Ogg1*$^{-/-}$ MEFs compared to WT MEFs.

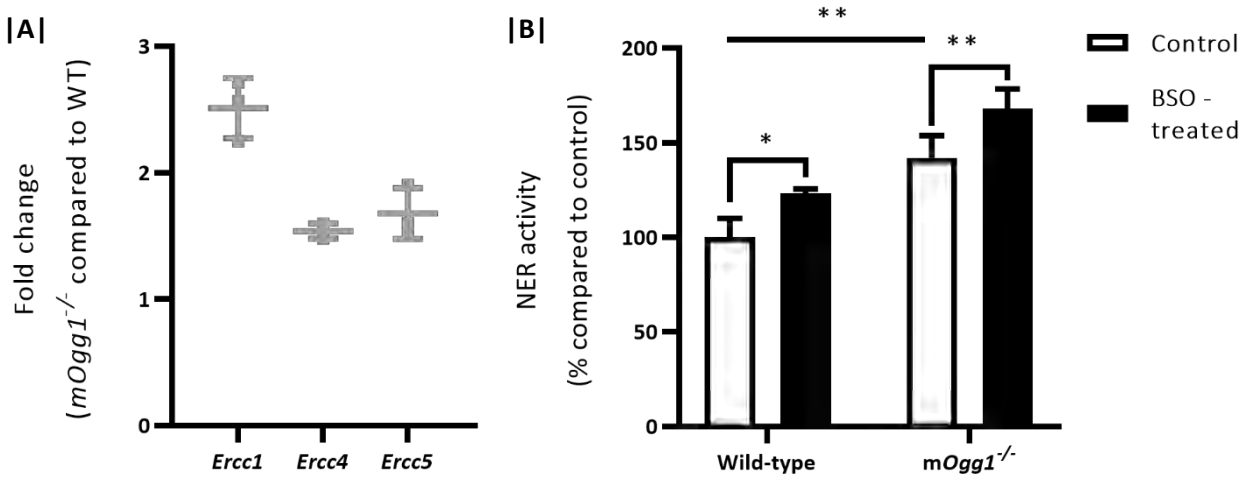


Figure 3.5. NER is upregulated in m*Ogg1*$^{-/-}$ MEFs. **|A|** *Ercc1, Ercc4* and *Ercc5* were all expressed at a significantly higher level in m*Ogg1*$^{-/-}$ MEFs compared to WT MEFs, as measured by qPCR analysis. The Ct values were normalised using endogenous control genes (*Gapdh* and *Hspab1*) and converted to fold-change compared to WT control samples. Individual biological replicates (■) are displayed alongside mean values ± SD (N=3). **|B|** NER-modified comet assay. The NER activity of protein extracts is calculated by subtracting the median tail intensity of BPDE-exposed: extract-negative cells from the median tail intensity of BPDE-exposed: extract-positive cells. This results in a difference in tail intensity (% TI) that is representative of NER activity of the extract. NER activity is significantly increased in m*Ogg1*$^{-/-}$ protein extracts (42.0 ± 7.9%) compared to WT extracts ($p < 0.01$). Following GSH depletion, there was a significant increase in NER activity in WT MEFs (23.2 ± 2.3%) ($p < 0.05$) and m*Ogg1*$^{-/-}$ MEFs (25.9 ± 10.5%) ($p < 0.01$). Mean ± SD (N=4), and significance was determined using a two-way ANOVA and a subsequent Tukey's test.

3.3.5. NEIL3 as a candidate backup mechanism to OGG1

The endonuclease *Neil3* was expressed at a significantly higher level in m*Ogg1*$^{-/-}$ MEFs (37.9 ± 1.6 -fold) compared to WT MEFs (Table **3.4.**). This increase in expression confirmed at protein level, following the testing of the antibody specificity using purified hNEIL3 (see appendix **7.5.**). NEIL3 was confirmed to be expressed at a higher level in m*Ogg1*$^{-/-}$ MEFs compared to WT MEFs (Figure **3.6.**). Two distinct bands can be recognised in the western blot and these correlate with the bands produced by purified hNEIL3. The larger band (~68 kDa) represents the proposed size of NEIL3. However, the smaller band (~40 kDa) has before been observed using this antibody, appearing on the antibody datasheet (abcam: catalogue no. ab10049). Furthermore, this band (~40 kDa) was present in the positive control (purified hNEIL3). The signal intensity of the two bands were analysed using ImageJ, with the intensity under each peak normalised using the β-actin control peaks. Analysis of the images identified two peaks in the m*Ogg1*$^{-/-}$ MEFs, which were not detected in WT MEFs (see appendix **7.6.** for full analysis). Furthermore, a significantly higher level of NEIL3 substrate sites were identified in m*Ogg1*$^{-/-}$ MEFs following BSO treatment (15 μM; 24 h) (3.4 ± 0.4 -fold higher) ($p < 0.001$). No such increase in NEIL3 substrate sites were identified in WT MEFs ($p > 0.05$). These substate sites were measured using a modified-comet assay, using NEIL3 in a similar principle that OGG1 was previosuly used in Chapter **2** (*refer to* schematic in Figure **2.1.**).

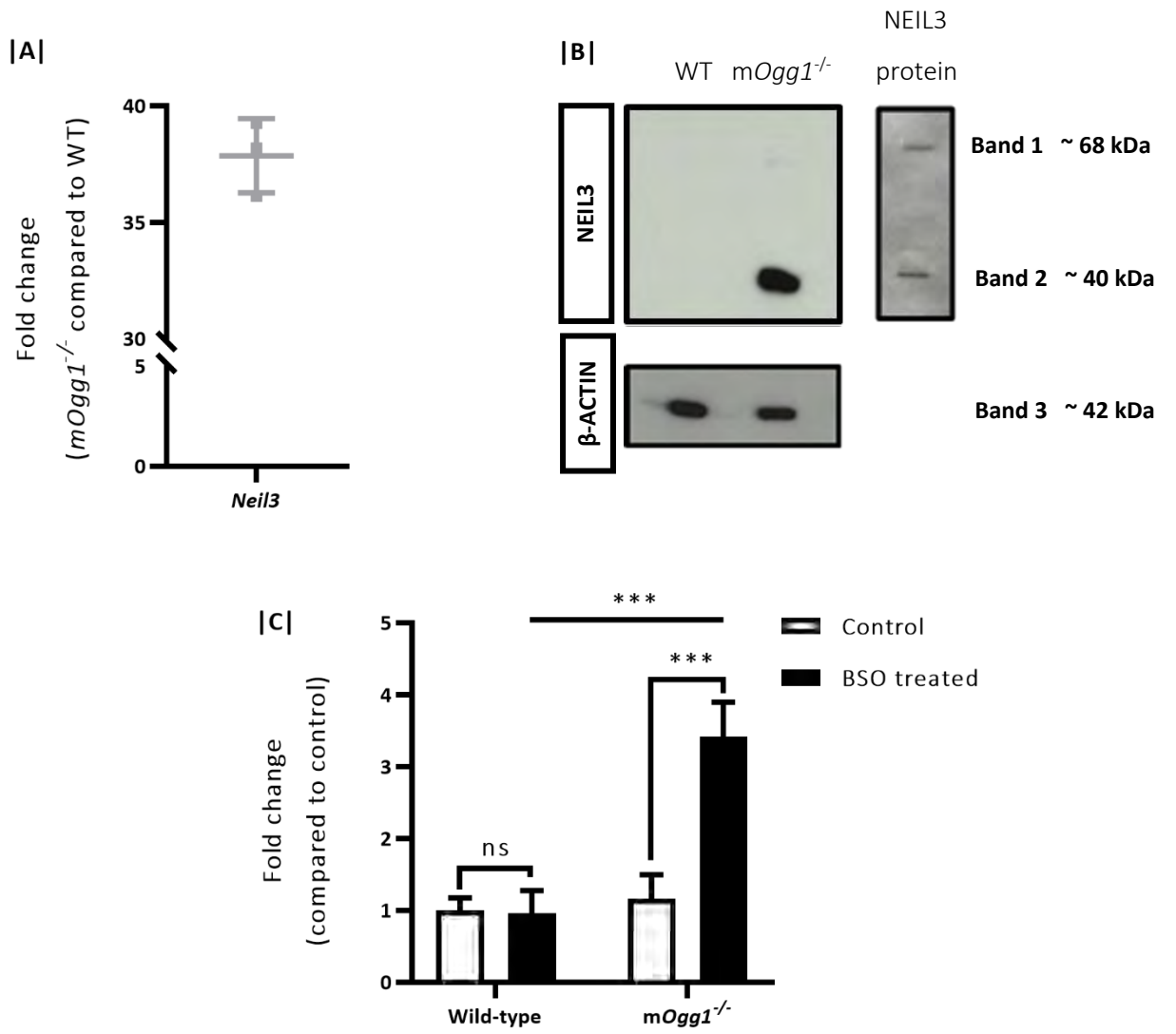


Figure 3.6. NEIL3 is upregulated in m*Ogg1*$^{-/-}$ MEFs. **|A|** *Neil3* is expressed at a higher level in m*Ogg1* $^{-/-}$ compared to WT MEFs (37.86 ± 1.59 -fold), as measured with qPCR. Ct values were normalised using endogenous control genes and converted to fold-change compared to WT control samples. Individual biological replicates (■) are displayed alongside mean values ± SD (N=3). **|B|** NEIL3 protein is expressed at a higher level in m*Ogg1*$^{-/-}$ MEFs compared to WT MEFs as shown with western blotting. The two resulting bands (~40 kDa and 68KDa) are consistent with those produced from purified hNEIL3 protein. ImageJ analysis of the bands confirmed that although these two bands were detectable in m*Ogg1*$^{-/-}$ MEFs, they were not measured in WT MEFs (see appendix **7.6.**). *Figure legend continues on next page*

|C| An increase in NEIL3 substrate sites were identified in m*Ogg1*$^{-/-}$ MEFs, following BSO treatment (15 μM; 24 h) compared to WT MEFs (3.4 ± 0.4 -fold) ($p \leq 0.001$). These NEIL3 sites were measured using a novel hNEIL3-modified comet assay. Mean values displayed ± SD (N=3), and significance was determined with a two-way ANOVA and a subsequent Dunnett's test.

3.3.6. Lipid peroxidation is increased in m*Ogg1*$^{-/-}$ MEFs

Two other dramatic differences observed between WT and m*Ogg1*$^{-/-}$ MEFs, with respect to gene expression, was the significantly higher expression of *Mpg* (4.6 ± 0.5 -fold) and *Mgmt* (26.5 ± 2.6 -fold) in m*Ogg1*$^{-/-}$ MEFs (Table **3.4.**). MPG and MGMT are both involved in the repair of lipid peroxidation-induced DNA damage (Tudek *et al.*, 2017). Using the TBARS method, a significantly higher level of MDA (a prevalent product of lipid peroxidation) was identified in m*Ogg1*$^{-/-}$ MEFs compared to WT MEFs (1.3 ± 0.1 -fold) ($p < 0.05$) (Figure **3.7.**). We hypothesise that this increased level of lipid peroxidation, in response to the elevated ROS levels of m*Ogg1*$^{-/-}$ MEFs, results in an increase in the expression of *Mpg* and *Mgmt*.

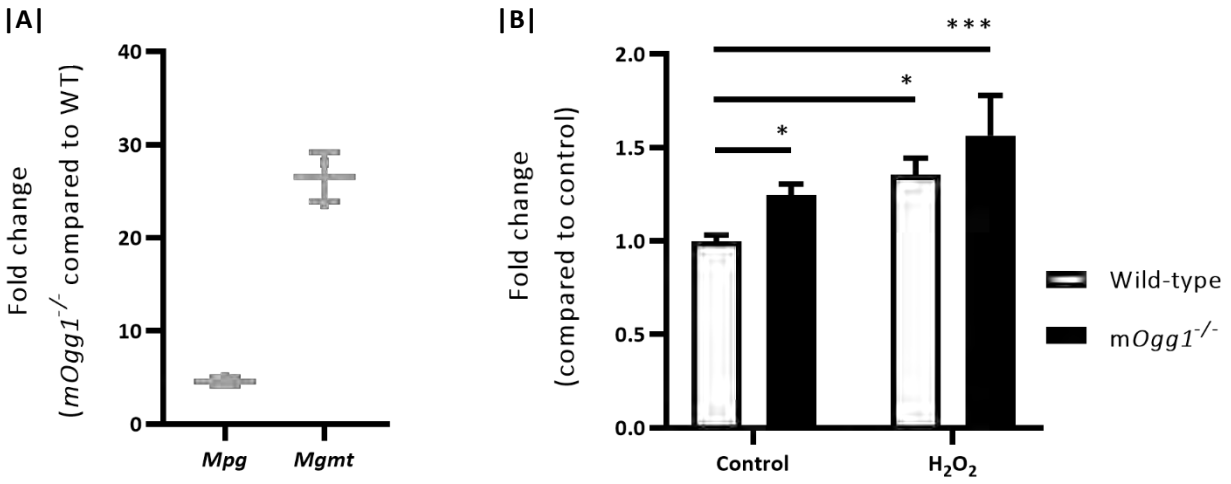


Figure 3.7. Lipid peroxidation is increased in m*Ogg1*$^{-/-}$ MEFs**. |A|** *Mpg* and *Mgmt* are expressed at a higher level in m*Ogg1*$^{-/-}$ MEFs (4.6 ± 0.5- and 26.5 ± 2.6 -fold respectively) when compared to WT MEFs, as measured with qPCR. Individual biological replicates (■) are displayed alongside mean values ± SD (N=3). **|B|** The level of MDA (which is considered a hallmark of lipid peroxidation) was increased in m*Ogg1*$^{-/-}$ MEFs (1.3 ± 0.1 -fold) compared to WT MEFs ($p < 0.05$). H_2O_2 treatment resulted in a further significant increase in lipid peroxidation in both cell-types ($p < 0.01$), when compared to the basal level of WT control MEFs. Mean values ± SD are displayed (N=4), and significance was determined with a two-way ANOVA and a subsequent Tukey's test.

3.3.7. A number of the genes that are upregulated in m*Ogg1*$^{-/-}$ MEFs were upregulated in WT MEFs following BSO treatment

A number of the genes of interest that were found to be expressed at a higher level in m*Ogg1*$^{-/-}$ MEFs, were also found to be upregulated in WT MEFs following BSO treatment (*refer to* Table **3.5.**). BSO treatment decreases intracellular GSH levels and subsequently increases oxidative stress within cells, as described in Chapter **2**. Therefore, the induction of these genes in WT MEFs following BSO treatment suggests that these genes are involved in the oxidative stress response in WT and healthy cells. The genes that were significantly upregulated in WT MEFs following BSO treatment (*Ogg1, Nthl1, Neil3, Mgmt, Mutyh* and *Ercc5*) are displayed alongside the corresponding changes in expression that were measured in m*Ogg1*$^{-/-}$ MEFs compared to WT MEFs (Figure **3.8.**). We suggest that this correlation between the genes upregulated in m*Ogg1*$^{-/-}$ MEFs and in BSO-treated WT MEFs further suggests that these genes do play a role in the repair of oxidative DNA damage in the absence of OGG1.

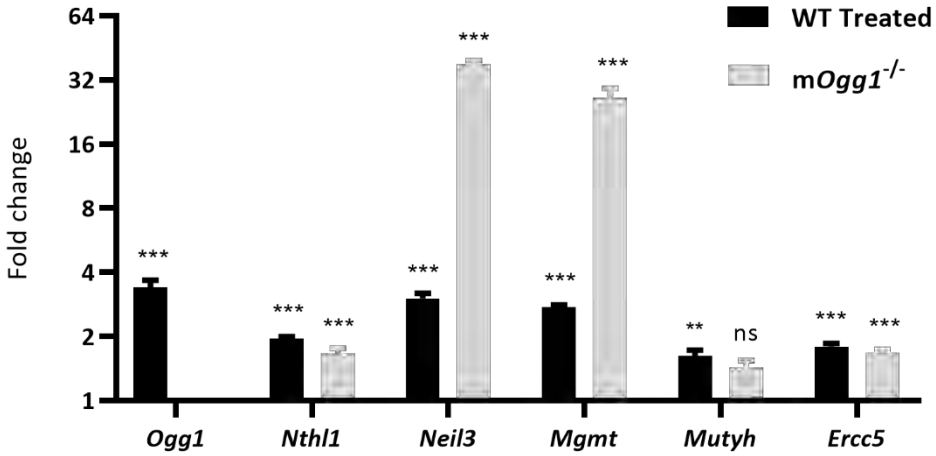


Figure 3.8. The genes upregulated in WT MEFs following BSO treatment (15 μM; 24h) (■) are displayed, alongside the corresponding changes measured in untreated m*Ogg1*$^{-/-}$ MEFs (■). Mean ± SD displayed (N=3). Note that the upregulation of *Muyth* in m*Ogg1*$^{-/-}$ MEFs was not sufficient enough to be included in Table **3.4.** (1.4 ± 0.1 -fold) but has been included here for comparison; additionally no detectable changes were measured for *Ogg1* in m*Ogg1*$^{-/-}$ MEFs due to their *Ogg1*-null status.

3.4. Discussion

DNA damage and DNA repair have long been of interest to researchers; with the first DNA repair mechanism being discovered in America in the 1940s when two independent research groups identified enzymatic photoreactivation (Dulbecco, 1949; Kelner, 1949; Friedberg, 2008). From this, a multitude of studies have discovered new DNA repair mechanisms, providing us with our current understanding of the human DNA damage response (summarised in Chapter **1**). One emergent aspect in DNA-repair is the potential for crosstalk between different pathways. However, this crosstalk and the added complexity that this brings is poorly understood. Particularly, BER glycosylases have been reported to interact with transcription regulation, MMR and NER (Slupphaug, Kavli and Krokan, 2003; Kovtun and McMurray, 2007). Furthermore, the crosstalk between BER and NER has been reported to occur in both directions. For example, NER proteins have been shown to increase the excision activity of BER glycosylases (Klungland, Höss, *et al.*, 1999; D'errico *et al.*, 2006), whilst the BER endonuclease APE1 regulates the NER-initiated repair of platinum adducts (Kim *et al.*, 2015).

Our finding that m*Ogg1*$^{-/-}$ MEFs do not possess a significant increase in genomic 8-oxoG, combined with these examples of crosstalk across DNA repair pathways, is suggestive of another 8-oxoG repair mechanism existing. This led to the hypothesis for this research chapter, which is that a backup repair mechanism exists in mammalian cells that can repair 8-oxoG in the absence of functional OGG1. An obvious potential candidate for this repair mechanism was NER, with examples of BER/NER crosstalk having been established, and this possibility having already been the focus of several studies (Reardon *et al.*, 1997; Klungland, Höss, *et al.*, 1999; Miao *et al.*, 2000; Shimizu *et al.*, 2003; Hollander *et al.*, 2005; D'errico *et al.*, 2006; Dušinská *et al.*, 2006). Some of these studies show that NER proteins interact with OGG1 and increase the efficiency of 8-oxoG removal, however it has not been confirmed that NER can compensate for OGG1. A couple of key papers will be discussed here, however *refer to* Chapter **1.7.4.2.** for a general discussion of this topic.

Reardon *et al.* (1997) created an *in vitro* NER model comprised of six major NER repair factors; XPA, RPA, TFIIH, ERCC5, the XPC-RAD23B heterodimer, and the ERCC1-ERCC4 heterodimer. They showed that this system excised NER substrates, such as thymine dimers, but additionally was capable of excising 8-oxoG, Tg and urea. Their results show that the three different lesions were all removed at a similar rate (within a factor of 2) and hypothesise that it is this role of NER in the removal of oxidative DNA modifications that leads to the neurodegeneration exhibited by many XP patients.

Following this, D'Errico *et al.* (2006) reiterated these findings, showing that XPC-deficient models possess a hypersensitivity to the oxidising effects of potassium bromate ($KBrO_3$). They report that these XPC-deficient cells accumulate genomic 5', 8-purine cyclodeoxynucleosides lesions (which are now accepted to be NER substrates) alongside an observed decrease in 8-oxoG repair. Here, the XPC-RAD23B was shown to act as a co-factor in the OGG1-initiated BER of 8-oxoG, increasing the binding of OGG1 to 8-oxoG. Although an interaction was shown between OGG1 and XPC-RAD23B, it was recognised that this interaction was weak, having only been identified with Far Western analysis. Unlike the neurodegeneration-driven hypothesis of Reardon *et al.* (1997), this study hypothesises that the role of NER in the repair of oxidative DNA damage could explain the internal cancers reported in XP patients.

The upregulation of *Ercc1, Ercc4,* and *Ercc5* in m*Ogg1*$^{-/-}$ MEFs does implicate the NER pathway in the oxidative stress response in our model (Table **3.4.**). The upregulation of these three NER genes in particular is important, with all three essential for the excision of NER substrates (de Laat, Jaspers and Hoeijmakers, 1999; Schärer, 2013). Furthermore, it has previously been identified that an increase in *Ercc1* expression directly correlates with NER capacity (Langie *et al.*, 2007), which was reflected in our NER-modified comet experiments.

The endonuclease ERCC5 is essential for the 3' incision of NER substrates, which is recruited to the substrate site by the 10-subunit complex, TFIIH (Rimel and Taatjes, 2018). Furthermore, ERCC1 and ERCC4 form a heterodimer with one another, which then performs the 5' excision of the substrate (Figure **3.9.**) (O'Donovan *et al.*, 1994; Wood, 1997; de Laat, Jaspers and Hoeijmakers, 1999; Lindahl and Barnes, 2000; Friedberg, 2001; Kim and Wilson, 2012; Schärer, 2013; Manandhar, Boulware and Wood, 2015; Rimel and Taatjes, 2018). Therefore, the upregulation of one (*e.g. Ercc5*) would be expected to be mirrored by the upregulation of the other (*e.g. Ercc1* and *Ercc4*), as observed in this study. Additionally, it has previously been described that the recruitment and subsequent binding of the ERCC1-ERCC4 heterodimer is required in order for ERCC5 to perform the 5' incision. However, although ERCC5 is recruited to the substrate earlier, it does not become catalytically active until the ERCC1-ERRC4 heterodimer is recruited (de Laat, Jaspers and Hoeijmakers, 1999; Friedberg, 2001; Manandhar, Boulware and Wood, 2015). Therefore, we propose that the upregulation of these three particular NER genes together is significant and will result in an increase of substrate excision by NER, as reflected in the increased NER activity measured in m*Ogg1*$^{-/-}$ MEFs.

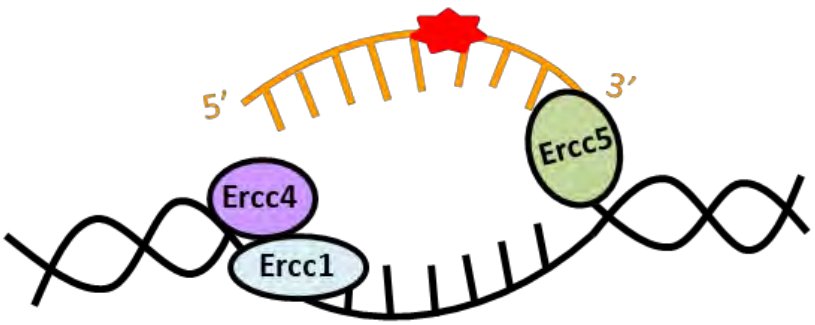


Figure 3.9. Substrate excision in NER is primarily performed by ERCC1, ERCC4, and ERCC5. The ERCC1-ERCC4 heterodimer is recruited to the substrate site by the transcription factor, TFIIH. The complex (in co-operation with other proteins recruited by TFIIH) then performs an incision at the 5' end of the substrate. The endonuclease ERCC5 is then able to perform the 3' incision, with these two events occur almost simultaneously (O'Donovan *et al.*, 1994; Manandhar, Boulware and Wood, 2015).

Our data is consistent with NER possessing a role in the repair of oxidative DNA modifications, with an increase in NER activity following conditions of oxidative stress. Oxidative stress was induced with BSO treatment, which subsequently depletes GSH, with NER activity significantly increasing in both WT and m*Ogg1*$^{-/-}$ MEFs. Furthermore, the basal activity of NER was shown to be significantly higher in m*Ogg1*$^{-/-}$ MEFs than the basal activity of WT MEFs. We propose that this increased level of NER in m*Ogg1*$^{-/-}$ MEFs is again in response to oxidative stress, with our previous study showing that untreated m*Ogg1*$^{-/-}$ MEFs already exist in a state of oxidative stress (*refer to* Chapter **2**). Despite this correlation between NER and oxidative stress, we have not identified a direct link between NER and 8-oxoG repair. It has already been well established that larger oxidative DNA modifications, including 5',8-purine cyclodeoxynucleosides, are substrates of the NER pathway (Klungland, Höss, *et al.*, 1999; Brooks *et al.*, 2000; Kuraoka *et al.*, 2000). Therefore, we suggest that this upregulation of NER is primarily due to an increase in oxidative stress and a subsequent increase in 5',8-purine cyclodeoxynucleosides. Although NER proteins may be capable of increasing OGG1-initiated repair of 8-oxoG, as described previously (Reardon *et al.*, 1997; Klungland, Höss, *et al.*, 1999; Miao *et al.*, 2000; Shimizu *et al.*, 2003; Hollander *et al.*, 2005; D'errico *et al.*, 2006; Dušinská *et al.*, 2006), we suggest that the increase in NER activity measured is not sufficient to compensate for loss of OGG1 activity.

Our data instead suggests that the primary compensatory mechanism for 8-oxoG repair is the endonuclease NEIL3. The first published function of NEIL3 was identified in a study utilising Sf9 insect cells, in which NEIL3 is instead referred to as HFPG2 (Morland *et al.*, 2002). This study found that NEIL3 was capable of removing Fapy lesions, with a significant increase in the removal of these lesions by NEIL3-expressing extracts compared to control extracts. Morland *et al.* (2002) also considered that NEIL3 could represent a possible backup mechanism to OGG1 and therefore investigated the activity of the endonuclease towards 8-oxoG, concluding that NEIL3 was not capable of excising the lesion. Furthermore, a separate study published consistent results and concluded that NEIL3 did not possess

activity towards either Tg or 8-oxoG (Takao *et al.*, 2002). Despite the growing interest in NEIL3, the protein could not be fully investigated until it was purified, a task that proved difficult due to low endogenous expression and the instability of the recombinant protein, however multiple groups have since succeeded in purifying NEIL3 (Krokeide *et al.*, 2009; Takao *et al.*, 2009; Liu *et al.*, 2012). Takao *et al.* (2009) demonstrated that the endonuclease possessed both DNA-binding and AP-site nicking activity, and that this activity was specific for ssDNA. However, the study was unable to identify a NEIL3 substrate despite testing many prevalent DNA modifications (*e.g.* 8-oxoG, Tg). Following their initial purification of NEIL3 (Krokeide *et al.*, 2009), Krokeide *et al.* published a paper (2013) that proposed NEIL3 to be a monofunctional DNA glycosylase that demonstrated a high affinity for the DNA lesions, Sp and Gh (Krokeide *et al.*, 2009; Krokeide *et al.,* 2013). This data was consistent with an earlier paper from Liu *et al.* (2010), which demonstrated the activity of mNEIL3 towards Sp, Gh and Fapy lesions. Again this study demonstrated that NEIL3 did not possess activity towards 8-oxoG, and that NEIL3 had a high activity against lesions in ssDNA and bubble structures. These papers and others clearly demonstrate the endonuclease activity of NEIL3 towards Sp and Gh (Morland *et al.*, 2002; Takao *et al.*, 2002, 2009; Kornyushyna and Burrows, 2003; Niles, Wishnok and Tannenbaum, 2004; Liu *et al.*, 2010; Cui *et al.*, 2013; Krokeide *et al.*, 2013; Liu, Doublié and Wallace, 2013). More recently NEIL3 has been demonstrated to unhook interstand crosslinks (ICL) in Xenopus extracts, implicating NEIL3 in the excision of another bulky DNA substrate (Martin *et* al., 2017; Li *et al*., 2020).

The increased expression of NEIL3 (37.9 -fold) in m*Ogg1*$^{-/-}$ MEFs was significantly higher than the modest upregulation of NER genes (< 5 -fold). Furthermore, western blotting identified an increased expression of NEIL3 protein in m*Ogg1*$^{-/-}$ MEFs when compared to WT MEFs. Despite two bands being produced at ~40 kDa and ~68 kDa, rather than the single expected band at 68 kDa, these two bands correlated with two strong bands produce by the NEIL3-protein control. Furthermore, if the smaller band was non-specific to NEIL3, we would expect to see bands of equal density in both WT and m*Ogg1*$^{-/-}$ MEFs, which

was not the case. We therefore propose that the endonuclease NEIL3 mediates the primary back-up mechanism that prevents an accumulation of genomic 8-oxoG in m*Ogg1*$^{-/-}$ MEFs.

We propose that 8-oxoG is unrepaired in the absence of OGG1 however rather than accumulating, 8-oxoG is further oxidised to produce Sp and Gh. Guanine possesses the lowest redox potential of the four DNA bases, and the oxidation of guanine to produce 8-oxoG lowers this redox potential even further (Henderson *et al.*, 2002; Margolin *et al.*, 2006; Paleček and Bartošík, 2012; Fleming and Burrows, 2017). Therefore, 8-oxoG is vulnerable to oxidation, with this vulnerability likely increased in m*Ogg1*$^{-/-}$ MEFs due to an increased level of intracellular ROS (Chapter **2**). Furthermore, the similarities between the gene expression changes in m*Ogg1*$^{-/-}$ MEFs (compared to WT MEFs), and the expression changes in WT MEFs following BSO treatment, suggest that these two models produce a similar environment of oxidative stress. In response to this oxidation, 8-oxoG is converted to Sp and Gh, with a significantly higher level of NEIL3 substrate sites measured in m*Ogg1*$^{-/-}$ MEFs following BSO treatment, using a novel modified-comet protocol.

We propose that *Neil3* is upregulated in m*Ogg1*$^{-/-}$ MEFs, ensuring that the Sp and Gh lesions are removed before the lesions induce DNA replication stalling and errors (Kornyushyna and Burrows, 2003; Norabuena *et al.*, 2016) (Figure **3.10.**). A further induction of oxidative stress in m*Ogg1*$^{-/-}$ MEFs (*via* BSO treatment) increases the oxidation of DNA further, generating high levels of 8-oxoG within the genome. These 8-oxoG lesions are further oxidised to generate Sp and Gh, however there was no further upregulation of *Neil3* measured in m*Ogg1*$^{-/-}$ MEFs following BSO treatment. This allowed for these NEIL3 substrate sites to accumulate, as measured in our hNEIL3-modified comet assays.

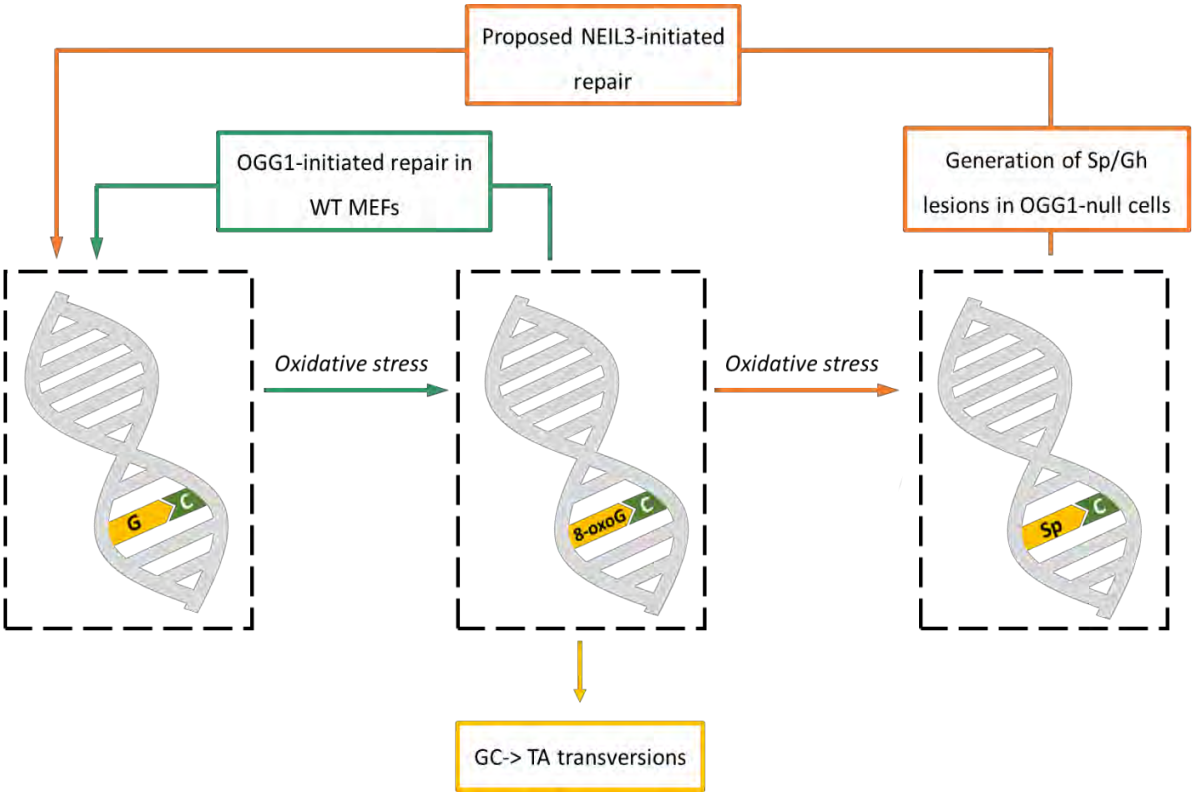


Figure 3.10. Proposed model for the NEIL3-mediated repair of 8-oxoG oxidation products. Guanine (G) forms a Watson-Crick base pair with cytosine (C). Under conditions of oxidative stress, guanine can be oxidised to generate 8-oxogunaine (8-oxoG) lesions, which can be can be repaired by OGG1-initiated BER (Kim and Wilson, 2012). If unrepaired, 8-oxoG lesions are able to form Watson-Crick base pairs with C or a Hoogsteen mispair with adenine (A), with the latter resulting in GC -> TA transversions (Gannett and Sura, 1993). In the absence of OGG1, 8-oxoG can remain in the genome and can once again be vulnerable to oxidation under conditions of oxidative stress. This further oxidation of 8-oxoG generates two primary products; spiroiminodihydantoin (Sp) and 5-guanidinohydantoin (Gh) (Henderson *et al.*, 2002; Kornyushyna and Burrows, 2003; Niles, Wishnok and Tannenbaum, 2004; Martin *et al.*, 2017). We propose that in the absence of OGG1, 8-oxoG in the genome of m*Ogg1*$^{-/-}$ MEFs become further oxidised to produce Sp and Gh. These lesions are recognised by NEIL3, which is upregulated in m*Ogg1*$^{-/-}$ MEFs, therefore preventing an accumulation of genomic 8-oxoG.

3.5. Conclusion and future work

We used a qPCR array to probe the hypothesis that a backup mechanism exists in m*Ogg1*$^{-/-}$ MEFs, which is capable of repairing 8-oxoG, and uncovered two possible mechanisms. We observed increases in NER gene expression and NER activity in conditions of oxidative stress, however these changes were fairly modest and were not directly linked to 8-oxoG repair. Instead we propose that the primary compensatory mechanism for the repair of 8-oxoG in m*Ogg1*$^{-/-}$ MEFs is the upregulation of NEIL3. It has previously been shown that NEIL3 possesses activity towards Sp and Gh, the oxidation products of 8-oxoG. We therefore propose that 8-oxoG goes unrepaired in the absence of OGG1, remaining in the genome until it is further oxidised to produce Sp and Gh, two lesions which can subsequently be excised from DNA by NEIL3. We have summarised our proposed model in Figure **3.10.**

The data presented identifies a strong candidate mechanism to explain the absence of increased genomic 8-oxoG in m*Ogg1*$^{-/-}$ MEFs. This mechanism should be further characterised and ideally NEIL3 would be transiently "knocked-down" in m*Ogg1*$^{-/-}$ MEFs and the levels of 8-oxoG once again measured, identifying whether an accumulation of 8-oxoG occurs in the absence of both OGG1 and NEIL3 activity. Additionally, the use of a novel modified comet assay demonstrated that m*Ogg1*$^{-/-}$ MEFs possessed an increased level of NEIL3 substrate sites, which we hypothesise to be Sp and Gh. In the future, HPLC may be utilised to identify the levels of these lesions in the DNA of WT and m*Ogg1*$^{-/-}$ MEFs, identifying whether the levels of Sp and Gh correlate with the NEIL3-modified comet assay (Henderson *et al.*, 2002; Suzuki and Ohshima, 2002; Niles, Wishnok and Tannenbaum, 2004; Yu *et al.*, 2005; Cui *et al.*, 2013). These levels should be monitored following BSO treatment to measure the occurrence of these lesions following the induction of oxidative stress.

4

Investigating the cellular consequences 8-oxoguanine treatment in WT and m*Ogg1*$^{-/-}$ MEFs

4.1. Introduction

In addition to the important glycosylase role of OGG1, additional cellular functions have also been characterised (as discussed in Chapter **1**). One recently identified function is the downstream signalling activity that occurs following the formation of a complex between OGG1 and 8-oxoG (OGG1: 8-oxoG), with a number of GTPases from the RAS family of proteins having been identified as effector molecules downstream of this OGG1: 8-oxoG complex. The resulting increase in these active (GTP-bound) RAS proteins are linked to multiple cellular consequences including proliferation, cell survival, redox signalling and cytoskeletal rearrangements (Boldogh *et al.*, 2012; German *et al.*, 2013; Hajas *et al.*, 2013; Luo *et al.*, 2014; Ba and Boldogh, 2018).

The RAS superfamily of GTPases includes over 150 proteins that have been identified in humans to date (Colicelli, 2004; Wennerberg, Rossman and Der, 2005). These GTPases are highly conserved with many of these proteins identified in a wide range of species; including drosophila, yeast and plant species (Rojas *et al.*, 2012). The superfamily is divided onto five major branches based on similarities in sequence, structure and function, as shown in Figure **4.1.**).

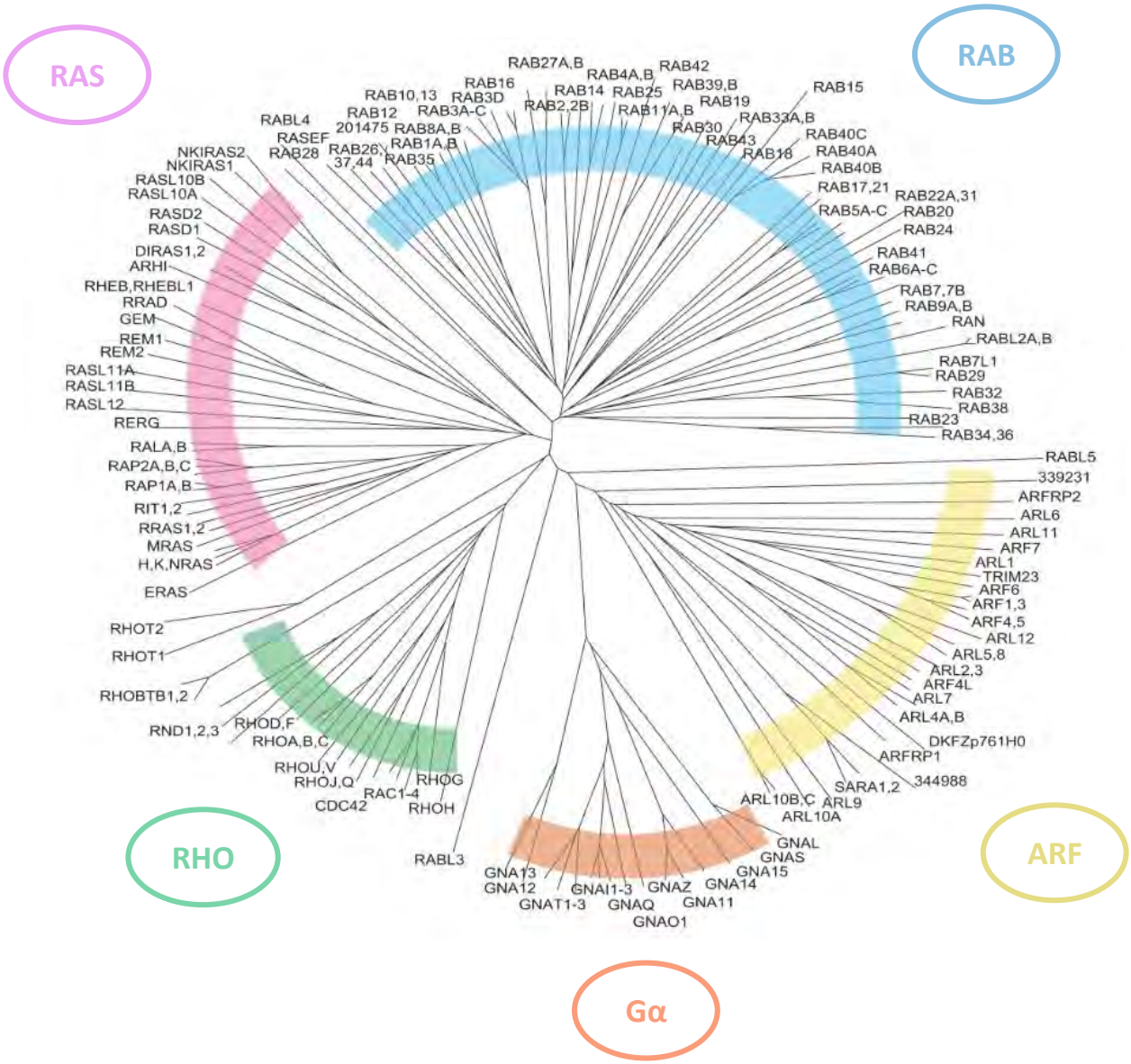


Figure 4.1. The RAS GTPase superfamily is divided into five subfamilies. This is depicted by this unrooted tree diagram of the human RAS protein family, which has been adapted from a review paper by Colicelli (2004).

During the cell culture of WT and m*Ogg1*$^{-/-}$ MEFs, it was clear that there were morphological differences with respect to their appearance. Additionally, we observed a difference in the detachment of cells following trypsin-EDTA incubation (Vogel, 1978; Tokiwa *et al.*, 1979), highlighting potential cytoskeletal differences between the cells (Badley *et al.*, 1980; Sen and Kumar, 2009; Fuhrmann and Engler, 2015).

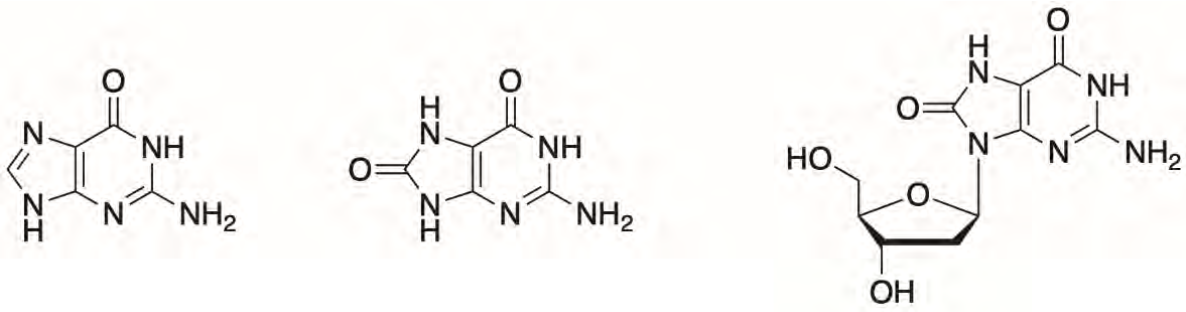
We hypothesised that these differences could be due to the lack of the OGG1:8-oxoG signalling pathway, and in particular, a decrease in active GTP-bound RHO levels. This hypothesis was largely based on a publication by Luo *et al.* (2014) that showed that the addition of 8-oxoG to OGG1-efficient cells resulted in an increase in active (GTP-bound) RHO. This increase in active RHO in turn increased the polymerisation of α-SMA and the subsequent formation of stress fibres (Luo *et al.*, 2014). Stress fibres are contractile bundles of actin (~10-30 actomyosin fibres) and also contain cross-linking proteins (Cramer, Siebert and Mitchison, 1997; Tojkander, Gateva and Lappalainen, 2012). Stress fibres are present in non-muscle cells, with these known to be especially abundant in fibroblasts and epithelial cells. Stress fibres are usually found to be anchored to focal adhesions and can affect multiple properties of a cell, including contraction, motility and attachment (Cramer, Siebert and Mitchison, 1997; Gourlay and Ayscough, 2005 (a); Naumanen, Lappalainen and Hotulainen, 2008; Tojkander, Gateva and Lappalainen, 2012).

In response to DNA damage, reorganisation of the cytoskeleton does occur. This reorganisation includes changes in the structure and formation of actin filaments (*e.g.* the formation of stress fibres) and the formation of cytoplasmic projections (*e.g.* filopodia and lamellipodia) (Luo et al., 2014; Soza et al., 2009; Gourlay and Ayscough, 2005 (a); Gourlay and Ayscough, 2005 (b)). As observed in Luo *et al.* (2014) it is understood that some RAS GTPases play a role in the regulation of the cytoskeleton when activated. Specifically members of the RHO subfamily (*refer to* Figure **4.1.**) are cytoskeletal regulators *via* different mechanisms. The RHO GTPases have been linked to the cytoskeleton, with RHO-A playing a role in the regulation of actomyosin contraction, regulation of tight junctions, and the formation of stress fibres (Wheeler and Ridley, 2004). The RAC1 GTPase has been implicated in both membrane ruffling and

lamellipodia formation, whereas the CDC42 GTPase plays a role in the formation of filopodia (Giry *et al.*, 1995; Nusrat *et al.*, 1995; Naumanen, Lappalainen and Hotulainen, 2008; Tojkander, Gateva and Lappalainen, 2012). These types of changes to the cytoskeleton of cells has been observed in multiple disease models, often having been linked to oxidative stress within the cell (Gourlay and Ayscough, 2005 (a); Gourlay and Ayscough, 2005 (b); Soza et al., 2009). We therefore hypothesise that the OGG1: 8-oxoG signalling molecule may represent the link between oxidative stress and cytoskeletal remodelling, and furthermore hypothesise that the lack of this OGG1:8-oxoG complex contributes to the differences we observed between WT and m*Ogg1*$^{-/-}$ MEFs.

In addition to having been implicated in the formation of membrane ruffling and lamellipodia, the GTPase RAC1 is involved in redox regulation. Hajas *et al.* (2013) showed that the OGG1: 8-oxoG signalling molecule increased the level of active (GTP-bound) RAC1. This occurred *via* a similar mechanism as found with RAS and RHO GTPases (Boldogh *et al.*, 2012; German *et al.*, 2013; Luo *et al.*, 2014). The study showed that 8-oxoG addition resulted in a transient increase in intracellular ROS (Hajas *et al.*, 2013), reflecting the oxidative burst observed in cells treated with 8-oxoG in a previous study (Hajas *et al.*, 2012). Interestingly, this response not observed in OGG1-null cells (Hajas *et al.*, 2013). The authors propose that this increase in intracellular ROS was mediated by RAC1 *via* NADPH oxidase-4 (NOX4), following the induction of RAC1-GTP by the OGG1:8-oxoG signalling complex. They suggest that this transient increase in ROS modulates OGG1 activity and/or localisation to promote the repair of 8-oxoG in conditions of oxidative stress (Hajas *et al.*, 2013). Theoretically, this would be a beneficial feedback loop for the cell, with conditions of oxidative stress resulting in high levels of 8-oxoG, which would need to be repaired *via* OGG1-initiaed BER. This could also explain the resistance to oxidative stress seen in other OGG1-null cells, which are a stark contrast to the constituent oxidative stress measured in our m*Ogg1*$^{-/-}$ model (*refer to* Chapter **1**).

In this study we investigated the cellular consequences of treating cells with 8-oxoG or 8-oxodG. Despite their similar structures (Figure **4.2.**), the consequences greatly differed between treatments with the two molecules. This difference, in combination with differences identified between the responses of WT and m*Ogg1*$^{-/-}$ MEFs, implicate the OGG1:8-oxoG signalling complex in these processes. Furthermore, these differences highlight the likelihood that OGG1 may be required for these effects to occur downstream of 8-oxoG, once again highlighting the cellular importance of OGG1 through roles that are independent of its glycosylase activity.



Guanine (G) 8-oxoguanine (8-oxoG) 8-oxo-2'-deoxyguanosine (8-oxoG)

Figure 4.2. The structure of 8-oxoguanine (8-oxoG) and 8-oxo-2'-deoxyguanosine (8-oxodG). The two structures are similar and are shown alongside the base from which they are generated from; guanine (G).

4.2. Materials and methods

4.2.1. Cell culture

WT and m*Ogg1*$^{-/-}$ MEFs were a generous gift from T. Lindahl (Klungland, Rosewell, *et al.*, 1999) (Cancer Research UK, Clare Hall Laboratories). Also cultured for experiments, were the adenocarcinomic human alveolar A549 cells (ECACC catalogue no. 86012804), and the human cervical carcinoma HeLa cells (ECACC catalogue no. 93021013). All cells were maintained in DMEM (Gibco: catalogue no. 41965047, with phenol-red, L-glutamine and 4.5 g/L D-Glucose) supplemented with FBS (10% v/v), L-Glutamine (2 mM), penicillin (100 units/mL) and streptomycin (100 μg/mL). All media and supplements were purchased from either Gibco (ThermoFisher Scientific) or Sigma-Aldrich (Merck). Once prepared, complete media was stored at 4°C for a maximum of one month. All cell culture work was carried out under suitable sterile conditions in a Class 1 tissue culture hood (Aura B4, Bio Air, Italy) and cells were incubated at 37°C and 5% CO_2 (Sanyo MCO-19AIC Incubator). Cells were frequently assessed to monitor growth and check for contamination and cells were routinely passaged on reaching 80 - 90% confluence. Full details of cell culture methodology, including mycoplasma testing, is described in the appendix (**7.1.1.**).

4.2.2. Treatment of cells

Treatment with oxidised DNA base

8-oxodG (Cayman Chemicals: catalogue no. 89320) and 8-oxoG (Cayman Chemicals: catalogue no. 89290) were prepared as 10 mM stock solution, and stored in aliquots at -80 °C. This stock was further diluted in supplemented DMEM to the required concentration immediately prior to use.

H_2O_2 treatment

H_2O_2 (30% v/v) (VWR International) was freshly prepared immediately prior to an experiment. An initial solution (0.5 M) was prepared in supplemented DMEM, which was then immediately further diluted with supplemented DMEM to the required concentration.

Ascorbic acid treatment

L-Ascorbic acid (Sigma Aldrich, Merck: catalogue no. A4403) was freshly prepared immediately prior to an experiment. A stock solution (0.1 mM) was prepared in dH_2O and then further diluted with supplemented DMEM to the required concentration.

Epidermal growth factor

Epidermal growth factor (EGF) (Gibco: Catalogue no. PHG0314) was prepared as a 1 mg/mL stock solution in PBS, and stored in aliquots at -20 °C. This stock was further diluted in supplemented DMEM to the required concentration, immediately prior to use.

4.2.3. MTT assay

Viability assay

Viability of cells was measured using the MTT assay as described in detail in **2.2.5**. The same method was used in this study to investigate if 8-oxoG (0.1-100 μM) or 8-oxodG (0.1-100 μM) affected the viability of WT and m*Ogg1*$^{-/-}$ MEFs, either in the absence or presence of H_2O_2 (12.5 μM). Briefly described; the media of cells was removed following treatment, and replaced with media (100 μL) containing MTT solution (0.5 mg/mL). The cells were incubated for 3 h (37°C and 5% CO_2), prior to the MTT-containing media being removed and replaced with DMSO (VWR International) (200 μL). Absorbance was measured at 570 nm (Infinite® 200 Pro, Tecan), and converted to percentage using the absorbance values of DMSO blank wells and untreated cells.

Growth rate

The MTT assay was also performed to investigate if there were differences in the growth rate of WT and m*Ogg1*$^{-/-}$ MEFs. MEFs were seeded in 96-well plates (2.5 x 10^3 cells/well) and incubated at 37°C and 5% CO_2. At pre-determined intervals (over a 72 h period) the cells were briefly removed from incubation. During this time, the media was removed from a subset of cells and replaced with media (100 μL) containing MTT solution (0.5 mg/mL). Cells were returned to incubation (37°C, 5%) for 3h, allowing formazan crystals to form. Following this incubation, the media was carefully removed from the wells containing MTT solution, and replaced with DMSO (VWR International) (200 μL). The absorbance of each well was measured at 570 nm (Infinite® 200 Pro, Tecan) and the plate immediately returned to continue incubation. At each time-point, the absorbance of DMSO blank wells (2 replicates) was also measured. The mean absorbance value of the DMSO-blanks was subtracted from the absorbance of the other wells.

Population doubling time

Population doubling time (PDT) is a constant numerical value, which represents the time required for a population of cells to double in number during their exponential growth period. This value will significantly differ between different cell lines, and has been estimated to be ~24 h for MEFs in multiple studies (Yusuf *et al.*, 2013; Amand, Hanover and Shiloach, 2016). There are multiple different methods used to calculate the doubling time of cells (Terry *et al.*, 1991; Zwicker, Proffitt and Reynolds, 1995; Yusuf *et al.*, 2013), and we utilised the simple MTT method to estimate cell number and to calculate the PDT of WT and m*Ogg1*$^{-/-}$ MEFs.

The MTT absorbance values were converted to cell number using a separate calibration plate (1000-20,000 cells/well), and an estimated PDT value was calculated using Equation **4** (Roth, 2006), which is based on the exponential growth of cells. PDT was calculated at each time-point tested and then the mean value calculated (± SD).

Equation 4 | $$\boldsymbol{PDT\ (h)} = \frac{Time\ (h) * log(2)}{log(final\ conc.) - log(initial\ conc.)}$$

4.2.4. RAS activation assay

A commercial enzyme-linked immunosorbent assay (ELISA) was utilised in order to quantify active Ras within cells (Ras G-LISA activation assay kit, Cytoskeleton Incorporated: catalogue no. BK131). The assay is based on the same principle as a conventional ELISA, with each assay well containing an attached RAS-GTP binding protein. Therefore, the addition of cells allows active GTP-bound RAS within the cells to bind. Alternatively, GDP-bound RAS will not bind, and will therefore be removed in subsequent washing steps. The components supplied within the kit (Cytoskeleton Incorporated) are detailed below, alongside appropriate preparation instructions (Table **4.1.**).

Table 4.1. Preparation of RAS-GTP ELISA reagents

Component	**Reconstitution instructions**
96-well RAS-GTP plate	The plate remained in a dehydrated state using the supplied desiccant, not reconstituting until just prior to use.
Anti-Ras antibody	Centrifuged briefly and PBS (200 μL) added
Secondary antibody (HRP conjugated)	Centrifuged briefly and PBS (80 μL) added
Ras control protein	Prepared in lysis buffer (500 μL) immediately prior to use (< 15 min)
Cell lysis buffer	Prepared in dH_2O (100 mL)
Binding buffer	Prepared in dH_2O (5 mL)
Wash buffer	Prepared in dH_2O (1 L), allowing the tablet to resuspend (45-60 min)
Antigen presenting buffer	N/A
Antibody dilution buffer	Prepared in dH_2O (15 mL)
HRP detection reagents (A & B)	Prepared in dH_2O (10 mL) and aliquots stored at -80°C
HRP stop solution	Concentrated (18 M) sulphuric acid (1 mL) added
Protease inhibitor cocktail	DMSO (1 mL) added to produce a stock solution (100x)

Cells were seeded in 6-well plates (6 x 10^4 cells/well) and incubated for 48 h prior to 8-oxoG or 8-oxodG treatment (1 μM; 15 min). Negative control cells were also incubated for 48 h but rather than treatment, cells were instead serum-starved for 24 h in order to inactivate Ras. To serum-starve cells, media was removed and replaced with FBS-negative DMEM (supplemented with L-Glutamine (2 mM), penicillin (100 units/mL) and streptomycin (100 μg/mL)). The positive control cells were instead incubated for 72 h prior to treatment with the RAS-activator, EGF (100 ng/mL, five min).

Following the appropriate treatment, cells were placed on ice and all media removed. Cells were then washed with cold PBS (3 mL), and the PBS then thoroughly removed from the cells. It was important to ensure that PBS was completely removed, as residual PBS has been reported to interfere with results (as reported by manufacturer Cytoskeleton Incorporated). Cold lysis buffer (150 μL) (supplemented with 10 μL/mL protease inhibitor) was added to each well. Cells were thoroughly scraped using a cell scraper, transferred into Eppendorf tubes and centrifuged at 4°C (10 000 g, 60 sec). At this stage, an aliquot (20 μL) of the supernatant was removed for protein quantification using Precision Red™ (Cytoskeleton Incorporated). The remaining supernatant was transferred to new Eppendorf tubes. The supernatant samples were then snap-frozen in liquid nitrogen and stored at -80°C.

Protein quantitation

Reactions were prepared in 96-well plates and duplicate wells were prepared for each sample, with each reaction containing sample (10 μL) sample and Precision Red™ Advanced Protein Assay Reagent (290 μL) (Cytoskeleton Incorporated: catalogue no. ADV02). The plate was incubated at RT (60 sec) and the absorbance then measured at 600 nm (Infinite® 200 Pro, Tecan). The absorbance value of a blank sample (10 μL lysis buffer and 290 μL Precision Red™) was subtracted from each sample, and the resulting absorbance values were multiplied by 3.5 to obtain the protein concentration of each sample (mg/mL). This followed the instructed of the manufacturer, and is described in Equation **5**.

Equation 5 | $$\boldsymbol{Protein\ concentration}\ (\boldsymbol{mg/mL}) = (absorbance - blank)\ x\ 3.5$$

Sample preparation

Prior to the experiment, test samples were removed from -80°C storage and allowed to thaw in a RT water bath. Once thawed, the test samples were prepared as stated below, alongside blank samples and positive controls. Once prepared, all samples remained on ice until use.

Blank sample: Prepared by adding lysis buffer (600 μL) and binding buffer (600 μL)

Positive control: Prepared by adding RAS control protein (6 μL; reconstituted in lysis buffer (500 μL) immediately prior to use), lysis buffer (54 μL) and binding buffer (60 μL).

Test samples: The experimental samples were first diluted with lysis buffer to normalise their concentration (0.75 mg/mL). Then each sample (90 μL) was added to binding buffer (90 μL).

RAS-GTP ELISA

The RAS-GTP ELISA contained 96 individual wells. For each experiment cold dH_2O (100 μL) was added to the number of wells required, which were then placed on ice whilst samples were prepared (see above). The water was then thoroughly removed from the wells, and each sample added to triplicate wells (50 μL/well). The plate was then mixed (400 rpm) (ThermoMixer, Eppendorf) whilst incubated (4°C; 30 min). The samples were then removed, and wells were washed twice with PBS (200 μL). After each PBS wash (throughout the entire experiment), it was important to ensure that all PBS was removed *via* a hard tapping action (5 - 7 times).

Following the PBS washes, antigen-presenting buffer was added to each well (200 μL) and then subsequently removed following a brief incubation at RT (two min). Each well was then washed three times with PBS (200 μL). Next, the anti-Ras primary antibody (50 μL, prepared as described in Table **4.1**.) was added to each well. The plate was then mixed at RT (400 rpm, 45 min) (ThermoMixer, Eppendorf). The antibody was thoroughly removed from wells, and wells were washed three times with PBS (200 μL), which was again thoroughly removed. The secondary antibody (50 μL; prepared as described in Table **4.1**.) was then added to each well, and the plate was mixed again at RT (400 rpm, 45 min) (ThermoMixer, Eppendorf). The secondary antibody was thoroughly removed from wells and wells were once again washed three times with PBS (200 μL), which was again thoroughly removed.

An equal volume of the two HRP reagents (A and B) were combined immediately prior to use and then the combined reagent was subsequently added to each well (50 μL). The plate was incubated at RT (15 min) before the reaction was stopped *via* the addition of HRP stop buffer (50 μL; prepared as described in Table **4.1**.). The absorbance was immediately read at 490 nm (CLARIOstar microplate reader, BMG Labtech). Absorbance was converted to fold-change, with each cell type compared to its respective negative control sample. An overview of the methodology is depicted in Figure **4.3.**

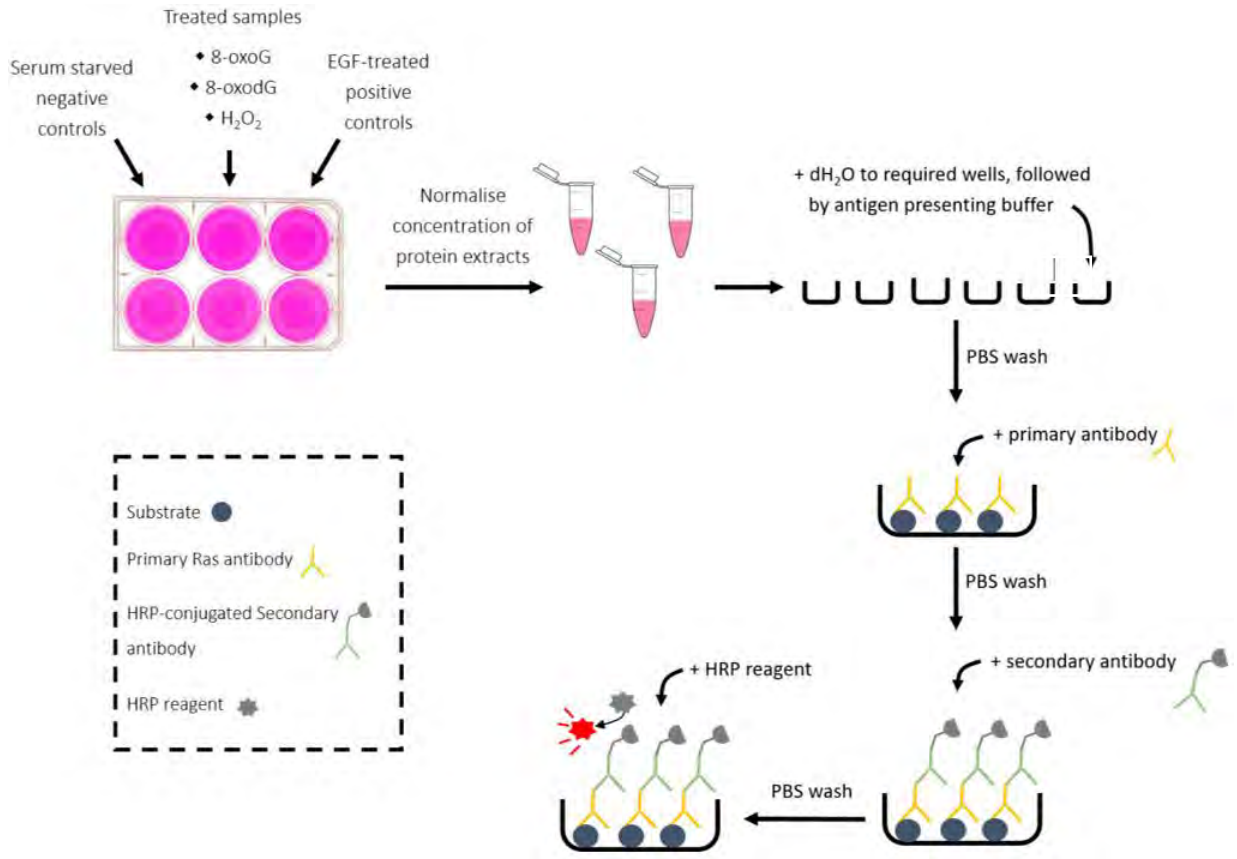


Figure 4.3. The principle of the RAS-GTP ELISA is displayed. Cells were cultured and treated as appropriate, prior to the normalisation of extracts to an equal concentration. dH_2O was added to the ELISA wells that were to be used in the experiment, this was then replaced with antibody presenting buffer (two min). The primary antibody was added, which was specific to RAS-GTP only (and therefore not specific to RAS-GDP). The samples were incubated with the primary antibody (45 min) followed by a PBS wash, and the addition of the HRP-conjugated secondary antibody for another incubation (45 min). The HRP reagent was prepared immediately prior to use, and added to samples (15 min). The reaction was then stopped and the absorbance was immediately measured.

4.2.5. Crystal violet assay

The principle of the crystal violet assay is described in **2.2.6.** The method was adjusted for use in this study, and instead the measurement of adherent cells (*via* crystal violet staining) was used to investigate the rate of attachment and detachment of cells.

Detachment assay

Cells were seeded in a 6-well plate (6 x 10^4 cells/well) and incubated (37 °C, 5% CO_2) for 72 h, allowing the cells to fully attach and enter the exponential growth phase. Cells were treated during this 72 h period if appropriate to the experiment.

Following this, cells were washed with PBS (2 mL) prior to the addition of trypsin-EDTA (750 μL, 0.25% w/v). The cells were then incubated at RT for varying lengths of time (30 - 240 sec). At the end of the appropriate incubation duration, complete DMEM (750 μL) was added to cells, thereby inactivating the trypsin-EDTA. The media was then immediately removed, removing any cells that had detached from the surface of the plate during the trypsin-EDTA incubation. The remaining cells were washed with PBS (2 mL) three times and PFA (1 mL, 4% w/v) was then added to each well, and incubated at RT (15 min). The PFA was removed from cells and crystal violet (1 mL, 0.5% w/v) added to each well. Following incubation at RT (20 min), the crystal violet was removed, and cells were thoroughly washed with dH_2O. The plates were allowed to air-dry for a minimum of 30 min, before the crystal violet was solubilised in acetic acid (1 mL, 10% v/v). The plate was gently rocked at RT (20 min) and then 200 μl of each well was transferred into a corresponding well in a 96-well plate. The absorbance was measured at 595 nm (M2 multimode microplate reader, SpectraMax) alongside duplicate blank samples. The resulting absorbance data was presented as adherent cells (%) compared to control samples, which had not been incubated with trypsin-EDTA.

Attachment assay

Cells were seeded in a 6-well plate (1.5 x 10^6 cells/well) and the media was subsequently removed from cells at different time-points (0.5 - 8 h), which therefore removed cells that had not yet attached to the vessel. Cells were gently washed with PBS (2 mL) three times to ensure that any unattached cells were removed from the well. Following the removal of the last PBS wash, PFA (1 mL, 4% w/v) was added to each well and cells incubated at RT (15 min). The PFA was subsequently removed from cells and replaced with crystal violet (1 mL, 0.5% v/v) and again incubated at RT (20 min). The crystal violet was then removed and the cells were thoroughly washed with dH_2O. The plates were allowed to air-dry for a minimum of 30 min prior to the collection of data *via* two different methods.

During initial range finding experiments, which were carried out in conjunction with MSc student C. Derench (The University of Birmingham), the number of cells in four random quadrants of each well was counted. The total number of cells counted was then converted to percentage cells (%) compared to a negative control. The negative control was prepared by adding cell suspension and then immediately removing the suspension, and washing with PBS. The experiments were then repeated; however acetic acid (1 mL, 10% v/v) was instead added to cells once air-dried. The plate was then gently rocked (RT, 20 min) and absorbance was measured at 595 nm (Infinite® 200 Pro, Tecan), alongside duplicate blank samples (acetic acid only). Absorbance was converted to cell number using a standard curve that was constructed using a calibration plate beforehand (500 - 200,000 cells/well).

4.2.6. Measurement of intracellular ROS

The principle of the H_2DCF-DA assay is described in **2.2.10.**, however the method was adjusted for use in this study as these experiments were carried out in a different laboratory (Department of Pharmacology and Toxicology, Maastricht University). MEFs were seeded in black-walled and clear-bottom 96-well plates (Costar®, Corning) and treated appropriately the following day with 8-oxoG (0.1-10 μM, 1 h), 8-oxodG (0.1-10 μM, 1 h), ascorbic acid (8-128 μM, 24 h) or H_2O_2 (50 μM; 1 h). Following treatment, cells were incubated with H_2DCF-DA (10 μM, 1 h) (Invitrogen, ThermoFisher Scientific). The media was removed and cells were briefly washed with PBS. PBS (100 μl) was then added to each well and fluorescence measured ($\lambda_{excitation}$ 495 nm and $\lambda_{emission}$ 525 nm) (M2 multimode microplate reader, SpectraMax). The fluorescence of H_2DCF-DA-blank cells was subtracted, and the resulting fluorescence values converted to fold-change using the fluorescence of untreated cells.

4.2.7. Acellular deoxyribose assay

All acellular experiments were carried out by BSc student M. Kirova (Maastricht University) under supervision. The principle of the deoxyribose assay is that hydroxyl radicals will be generated from the Fenton reaction, which will then react with deoxyribose, subsequently producing malondialdehyde (MDA). This production of MDA will result in a colorimetric change when thiobarbituric acid (TBA) is added at a high temperature. The ability of 8-oxoG and 8-oxodG to reduce this colorimetric change was measured, with such a decrease representing the reaction of 8-oxoG/8-oxodG with hydroxyl radicals, preventing their reaction with deoxyribose.

Buffers & solutions

Reaction mixture: Deoxyribose (0.42 mM), L-ascorbic acid (0.1mM), H_2O_2 (1mM), EDTA (0.1 mM), $FeCl_3$ (0.1 mM), prepared in phosphate buffer (1mM or 10 mM).

TCA:TBA: TCA (20 % w/v), TBA (0.4 % w/v), prepared in HCl (1 M).

Note: Both the L-ascorbic acid and $FeCl_3$ were prepared immediately before use in dH_2O that had been deaerated using Nitrogen.

Deoxyribose assay protocol

An equal volume of reaction mixture was added to an equal volume of 8-oxoG or 8-oxodG (0.1-10 μM in phosphate buffer). The samples were incubated at 37 °C (1 h) and the reaction subsequently stopped *via* the addition of the TBA:TCA. The samples were then incubated at 100 °C (1 h) to allow the reaction between TBA and MDA to occur. The samples were then subsequently cooled (RT; 10 min) and the absorbance measured at 532 nm (Cary 50 scan UV visible spectrophotometer, Varian). Absorbance was converted to fold-change compared to negative control samples.

4.2.8. Statistics

All results are presented as the mean values ± SD (N = number of biological experiments), unless otherwise stated. When two different samples were being compared, a two-tailed unpaired *t*-test was used. Larger datasets were analysed by two-way ANOVA and then corrected for multi-comparison testing using appropriate post-hoc testing. For parametric data, a Dunnett's test (comparison of each group with a control group) or Tukey's test (multi-comparison testing between all groups) was performed; and for non-parametric data, the Bonferroni correction was performed. A detailed report of the statistics performed for each experiment is detailed in the appendix (**7.2.**). Graphs were prepared and statistical analysis performed using GraphPad Prism (version 8.0.1); and $p < 0.05$ was considered statistically significant (*); $p < 0.01$ (**); $p < 0.001$ (***)

4.3. Results

4.3.1. Neither 8-oxoG or 8-oxodG affects the viability of MEFs

Viability of MEFs was not affected following treatment with 8-oxoG (0.01 -100 μM; 1h) or 8-oxodG (0.01-100 μM; 1h) (Figure **4.4.**). None of the tested concentrations had a significant effect on the viability of WT or m*Ogg1*$^{-/-}$ MEFs, regardless of co-treatment with H_2O_2 (12.5 μM; 1 h). These experiments were repeated following a longer treatment period (24 h), with the only significant differences in viability observed at a concentration of 100 μM (8-oxoG or 8-oxodG) alongside H_2O_2 treatment (12.5 μM) *(p* < 0.01). Therefore, it can be concluded that the treatment conditions chosen for further experiments with the oxidised purines (8-oxoG and 8-oxodG) (0.1 -10 μM) will not have an effect on the viability of WT or m*Ogg1*$^{-/-}$ MEFs, even when co-treated with H_2O_2 (12.5 μM). The viability of WT or m*Ogg1*$^{-/-}$ MEFs following H_2O_2 treatment alone was already investigated (*refer to* Figure **2.11.**), with no significant decrease measured in viability following H_2O_2 treatment (12.5-100 μM; 24 h).

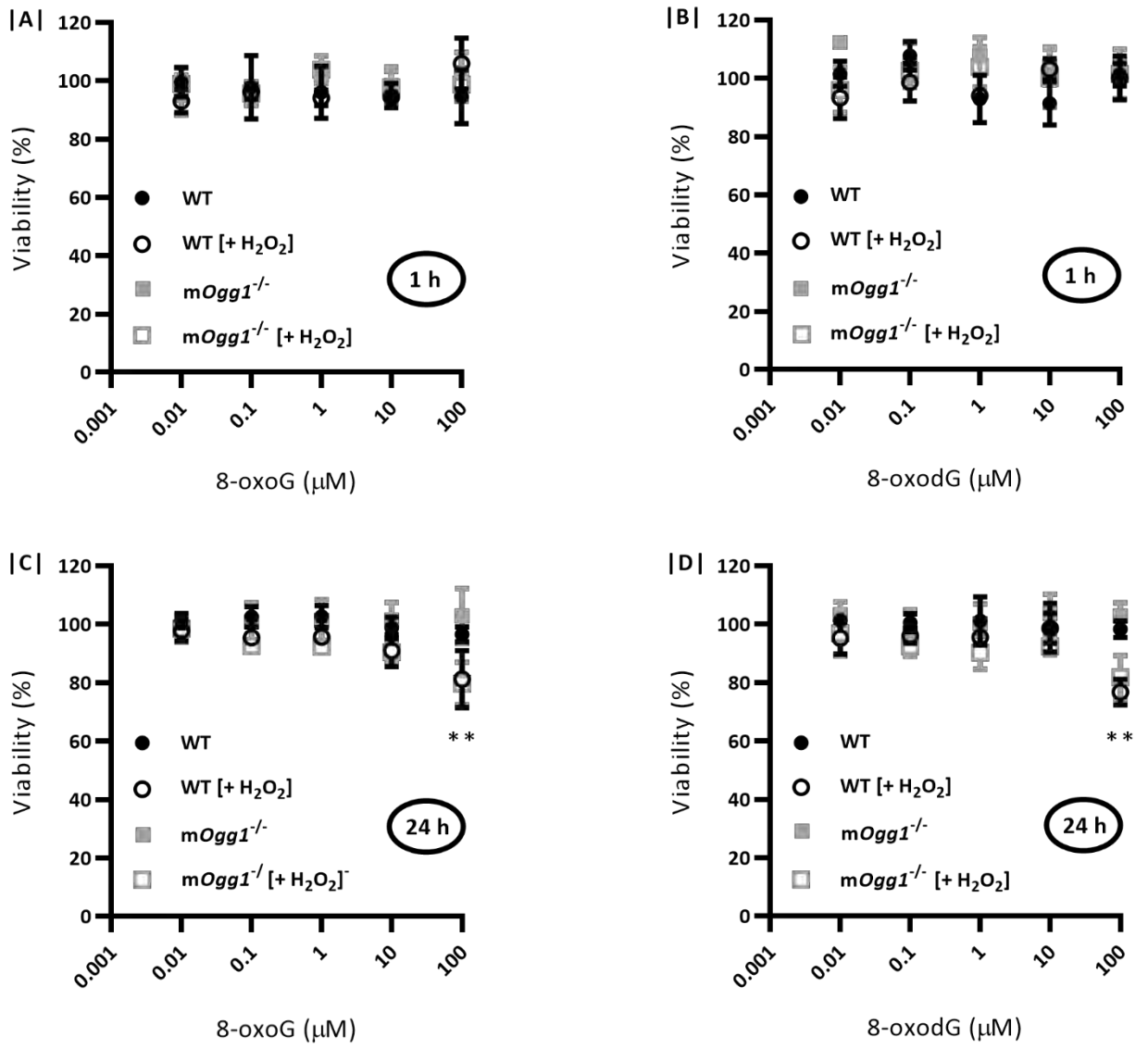


Figure 4.4. 8-oxoG and 8-oxodG treatment does not affect the viability of MEFs (≤ 100 μM), as measured with MTT assays, even following co-treatment with H_2O_2 (12.5 μM). Mean values are presented ± SD (N=4), and significance was determined using a two-way ANOVA and a subsequent Dunnett's test. **|A|** There was no significant changes in the viability of WT or *mOgg1*$^{-/-}$ MEFs following 8-oxoG treatment (0.1-100 μM; 1h) *(p* ≥ 0.05). *Figure legend continues on next page*

|B| There was no significant changes in the viability of WT or *mOgg1*$^{-/-}$ MEFs following 8-oxodG treatment (0.1-100 μM; 1h) *(p* > 0.05). **|C|** There was no significant changes in the viability of WT or *mOgg1*$^{-/-}$ MEFs following 8-oxoG treatment (0.1-10 μM; 24h) *(p* ≥ 0.05). However, the co-treatment of cells with 8-oxoG (100 μM; 24 h) and H_2O_2 (12.5 μM; 24h) did result in a significant decrease in viability in WT (81.2 ± 9.8 %) and m*Ogg1*$^{-/-}$ MEFs (79.7 ± 7.4 %) *(p* < 0.01). **|D|** There was no significant changes in the viability of WT or *mOgg1*$^{-/-}$ MEFs following 8-oxodG treatment (0.1-10 μM; 24h) *(p* ≥ 0.05). The co-treatment of cells with 8-oxodG (100 μM; 24 h) and H_2O_2 (12.5 μM; 24h) did result in a significant decrease in viability in WT (76.8 ± 4.4 %) and m*Ogg1*$^{-/-}$ MEFs (81.8 ± 7.4 %), *(p* < 0.01).

4.3.2. Activation of RAS following 8-oxoG treatment is dependent on OGG1

Active (GTP-bound) RAS was quantified using a commercial ELISA. The optimal protein concentration was determined as 0.75 mg/mL, generating optimal absorbance values as recommended by the manufacturer (Cytoskeleton Incorporated) (see appendix **7.7.**). A significant increase in RAS-GTP levels was observed in WT MEFs (1.97 ± 0.03 -fold) *(p* < 0.001) and HeLa cells (1.80 ± 0.03 -fold) *(p* < 0.001) following 8-oxoG treatment (1 μM, 15 min) (Figure **4.5.**). However, there was no significant increase in m*Ogg1*$^{-/-}$ MEFs (1.02 ± 0.08 -fold) following 8-oxoG treatment (1 μM, 15 min) *(p* > 0.05). Furthermore, there was no significant increase in RAS-GTP levels following 8-oxodG treatment (1 μM, 15 min) in any of three cell-types tested *(p* > 0.05). Positive control HeLa cells (EGF treated: 100 ng/mL, five min) are displayed (2.66 ± 0.07 -fold), with EGF a known RAS activator (Margolis and Skolnik, 1994; Ji *et al.*, 2016). Treatment with H_2O_2 (12.5 μM; 15 min) had no significant effect on the Ras-GTP levels of WT and m*Ogg1*$^{-/-}$ MEFs *(p* > 0.05). However, co-treatment with 8-oxoG and H_2O_2 reduced the effect of 8-oxoG that was previously observed in WT MEFs *(p* < 0.001).

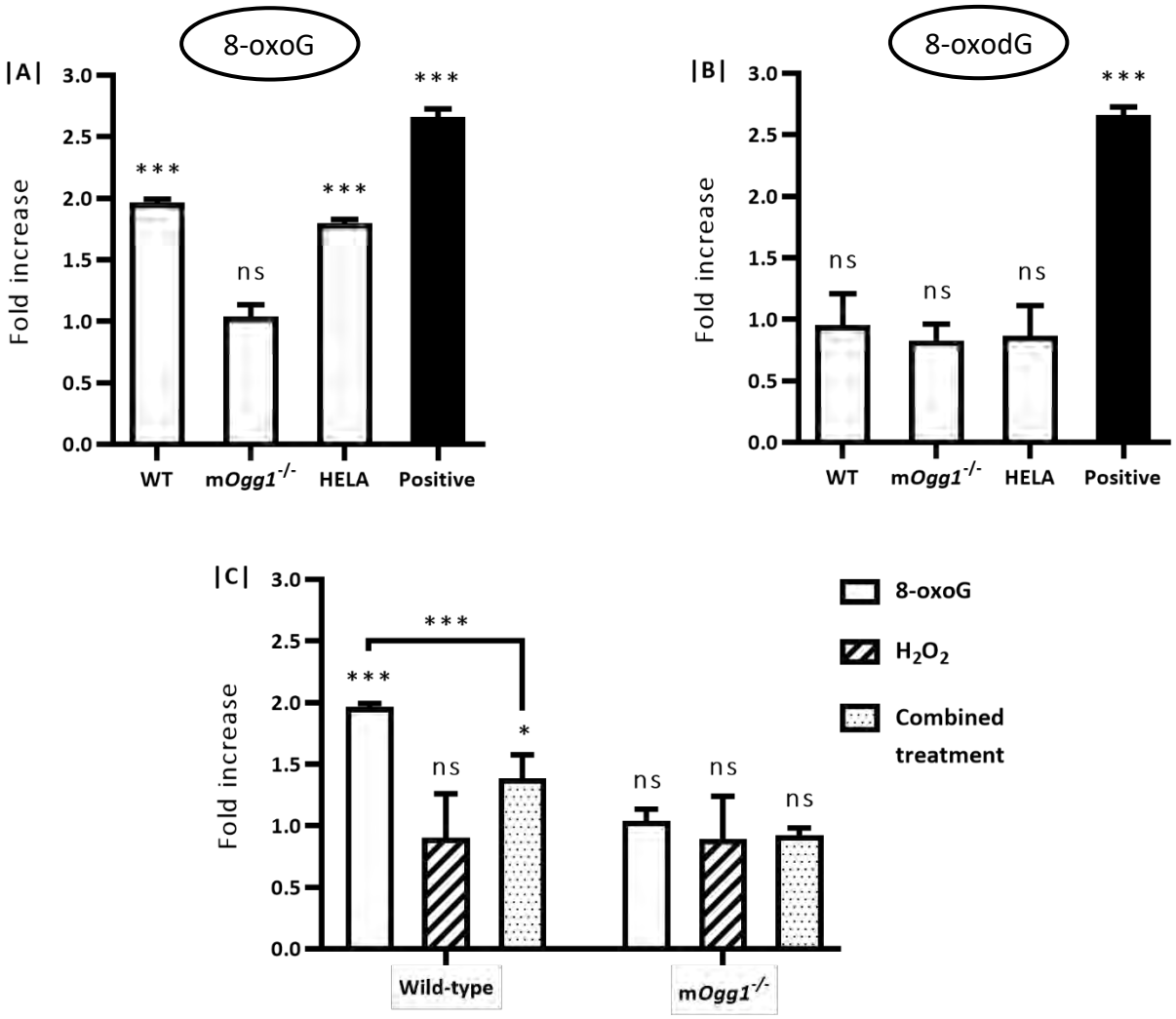


Figure 4.5. Active RAS was measured using a RAS-GTP specific ELISA. **|A|** 8-oxoG (1 μM, 15 min) significantly increased RAS-GTP in WT MEFs (1.97 ± 0.03 -fold) and HeLa cells (1.80 ± 0.03 -fold) *(p* < 0.001). However, 8-oxoG treatment (1 μM, 15 min) did not generate an increase in RAS-GTP levels in m*Ogg1*$^{-/-}$ MEFs (1.02 ± 0.08 -fold). Treatment of HeLa cells with EGF (100 ng/mL, five min), which is a well- characterised RAS-GTP activator, was included as a positive control, increasing active-RAS levels in HeLa cells (2.66 ± 0.07 -fold). Mean values are presented ± SD (N=5), and significance was determined using a two-tailed *t*-test for each cell type. *Figure legend continues on next page*

|B| 8-oxodG (1 μM, 15 min) had no significant effect on RAS-GTP in WT MEFs, m*Ogg1*$^{-/-}$ MEFs, or HeLa cells *(p* > 0.05). Again, the results observed in EGF-treated (100 ng/mL, five min) HeLa cells have been included as a positive control. Mean values are presented ± SD (N=5), and significance was determined using a two-tailed *t*-test for each cell type. **|C|** H_2O_2 (12.5 μM, 15 min) did not have a significant effect on RAS-GTP levels in WT or m*Ogg1*$^{-/-}$ MEFs ($p > 0.05$). Combined treatment of 8-oxoG and H_2O_2 resulted in an increase in RAS-GTP in WT MEFs (1.39 ± 0.19) ($p < 0.05$). However, this response was significantly decreased when compared to 8-oxoG treatment alone (1.97 ± 0.03 -fold) ($p < 0.001$). None of the tested treatment regimens had a significant effect on the levels of RAS-GTP in m*Ogg1*$^{-/-}$ MEFs ($p > 0.05$). Mean values are presented ± SD (N=5), and significance was determined with a two-way ANOVA and a subsequent Tukey's test.

4.3.3. Phenotype of WT and m*Ogg1*$^{-/-}$ MEFs in cell culture

Multiple differences were observed between WT and m*Ogg1*$^{-/-}$ MEFs during the handling of the cells in culture. These morphological differences included m*Ogg1*$^{-/-}$ MEFs appearing to possess a larger size and more cytoplasmic projections (Figure **4.6.**). Due to these size differences, it initially appeared visually that m*Ogg1*$^{-/-}$ MEFs were growing at a faster rate than WT MEFs. However, both cells types were shown to grow at a very similar rate, as quantified using MTT experiments. There is no significant difference *(p* > 0.05) between the MTT absorbance values produced by the two cell lines, with the first measurement being recorded 8 h after seeding. The absorbance values were then converted to cell number using a calibration MTT experiment, with these values plotted on a logarithmic scale, and the PDT for each cell type calculated. There was no significant difference between the doubling time calculated for WT (16.0 ± 1.5 h) and m*Ogg1*$^{-/-}$ MEFs (16.9 ± 1.4 h) ($p > 0.05$).

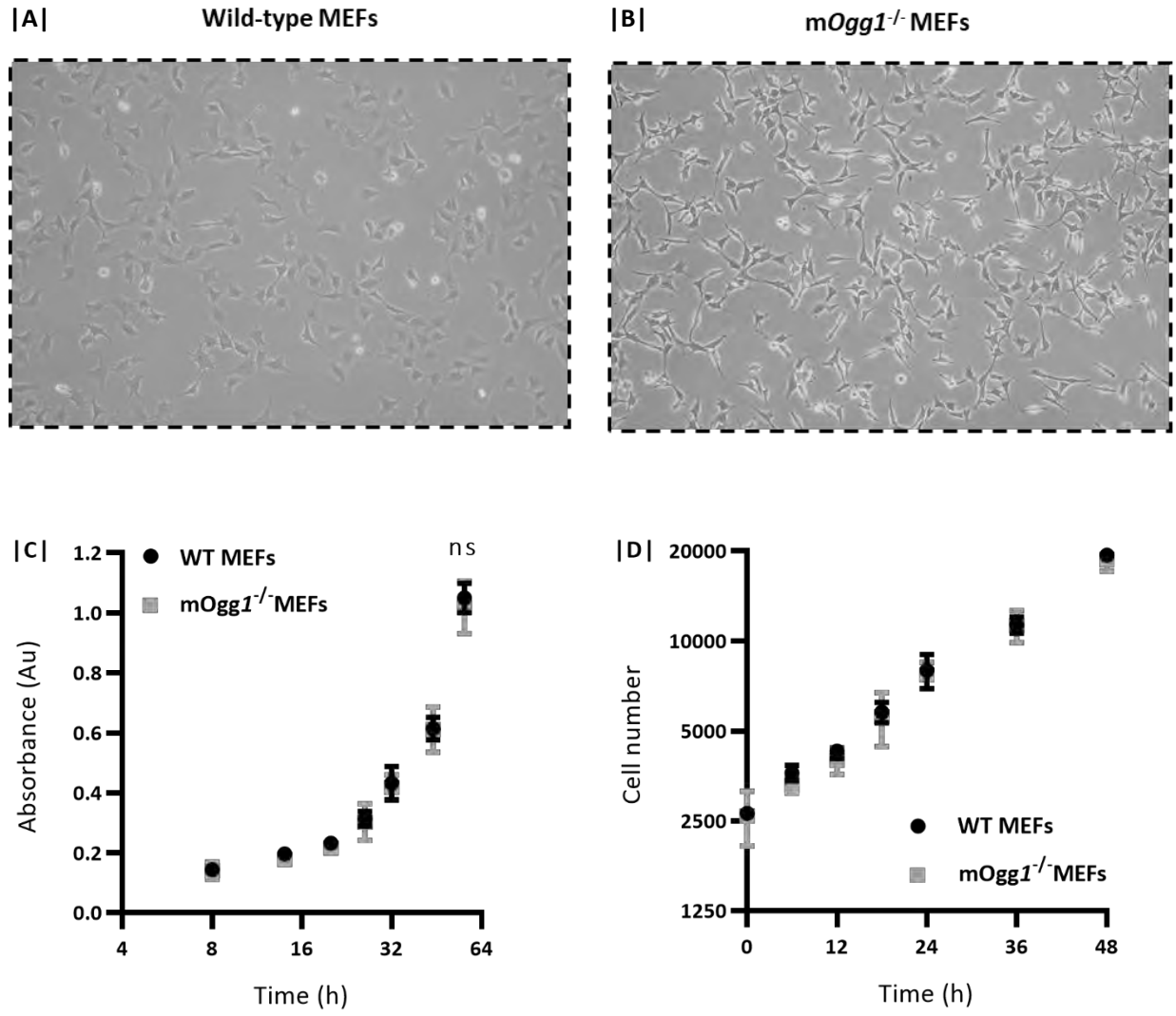


Figure 4.6. Cell morphology and growth kinetics of WT and m*Ogg1*$^{-/-}$ MEFs. **|A|** Image of WT MEFs (*passage number = 5*) and **|B|** image of m*Ogg1*$^{-/-}$ MEFs (*passage number = 5*). **|C|** Cells were seeded and allowed to proliferate over a 56-h period (37°C and 5% CO_2). A series of MTT experiments were then performed on cells during this time and absorbance measured. There was no significant difference between the absorbance generated by WT and m*Ogg1*$^{-/-}$ MEFs over the time course of the experiment ($p > 0.05$). Mean values are presented ± SD (N=3), and significance was determined using a two-way ANOVA and a subsequent Bonferroni test. *Figure legend continues on next page*

|D| The absorbance values measured during the MTT assays were converted to cell number/well using a calibration MTT experiment (1000 - 20,000 cells/well). The first measurement (8 h) is shown as time=0 h and cell number is displayed on a logarithmic scale. The doubling time of cells was calculated, with no significance difference between the PDT of WT (16.0 ± 1.5 h) and m*Ogg1*$^{-/-}$ MEFs (16.9 ± 1.4 h) ($p > 0.05$), with significance determined with an unpaired two-tailed *t*-test.

4.3.4. m*Ogg1*$^{-/-}$ MEFs detach at a faster rate than WT MEFs following incubation with trypsin-EDTA

In addition to the subtle morphological differences, another difference that was identified between WT and m*Ogg1*$^{-/-}$ MEFs was the rate that cells detached following trypsin-EDTA incubation. Initially, this was observed during the routine cell culture of the MEFs, with m*Ogg1*$^{-/-}$ MEFs detaching from the culture flask noticeably faster than WT MEFs. This difference was subsequently quantified using crystal violet to stain cells that remained attached following incubation with trypsin-EDTA. This confirmed that m*Ogg1*$^{-/-}$ MEFs detach at a significantly faster rate than WT MEFs following incubation with tryspin-EDTA (1 - 3 min) *($p < 0.01$)* (Figure **4.7.**). Non-linear regression was performed and used to calculate the incubation time required for the detachment of 50% of cells to occur, see appendix (**7.2.**) for full details of regression model used. This time was calculated to be 1.9 min (1 min and 54 sec) for WT MEFs and 0.96 min (58 sec) for m*Ogg1*$^{-/-}$ MEFs, confirming that there is a significant difference in the rate of detachment of the two cell-types *($p < 0.001$)*.

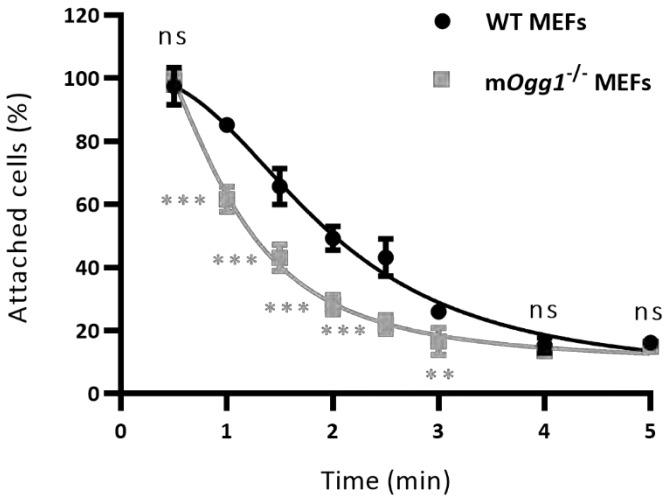


Figure 4.7. m*Ogg1*$^{-/-}$ MEFs detach at a faster rate than WT MEFs. Cells were incubated with trypsin-EDTA (0.25% w/v) for varying lengths of time (0.5 - 5 min) and the number of attached cells measured *via* crystal violet staining (0.5% v/v). It was observed that m*Ogg1*$^{-/-}$ MEFs detached significantly faster than WT MEFs at certain time-points (1 - 3 min) *(*$p < 0.01$). Non-linear regression analysis ([inhibitor] vs. response – variable slope model, GraphPad Prism 8) was performed. Regression was used to calculate the time required to detach 50% of cells *via* determination of the IC50. Analysis showed that significantly less time is required for m*Ogg1*$^{-/-}$ MEFs (0.96 min) (95% CI [0.72 – 1.10 min]) compared to WT MEFs (1.9 min) (95% CI [1.72 – 2.15 min]) ($p < 0.001$).

4.3.5. There are no differences in the rate of attachment between WT and m*Ogg1*$^{-/-}$ MEFs

It was hypothesised that these adhesion differences identified in **4.3.4.** may also be reflected in the rate of attachment of WT and m*Ogg1*$^{-/-}$ MEFs. To investigate this, cells were seeded and subsequently incubated for differing lengths of time (0.5 - 8 h), allowing the cells to adhere to the surface of the culture vessel. Following this incubation period, cells that had failed to properly adhere to the culture vessel were removed, and the remaining attached cells were subsequently stained with crystal violet. The stained cells were the counted; or alternatively the crystal violet stain was solubilised with acetic acid and absorbance measured (Figure **4.8.**). No significant difference was measured between WT and m*Ogg1*$^{-/-}$ MEFs, using either method, at any of the time-points measured *($p > 0.05$)*. In addition to this, non-linear regression was performed on both datasheets (see appendix **7.2.** for full details of the regression method used), with this analysis proving that one model curve could be fitted for both WT and m*Ogg1*$^{-/-}$ MEFs.

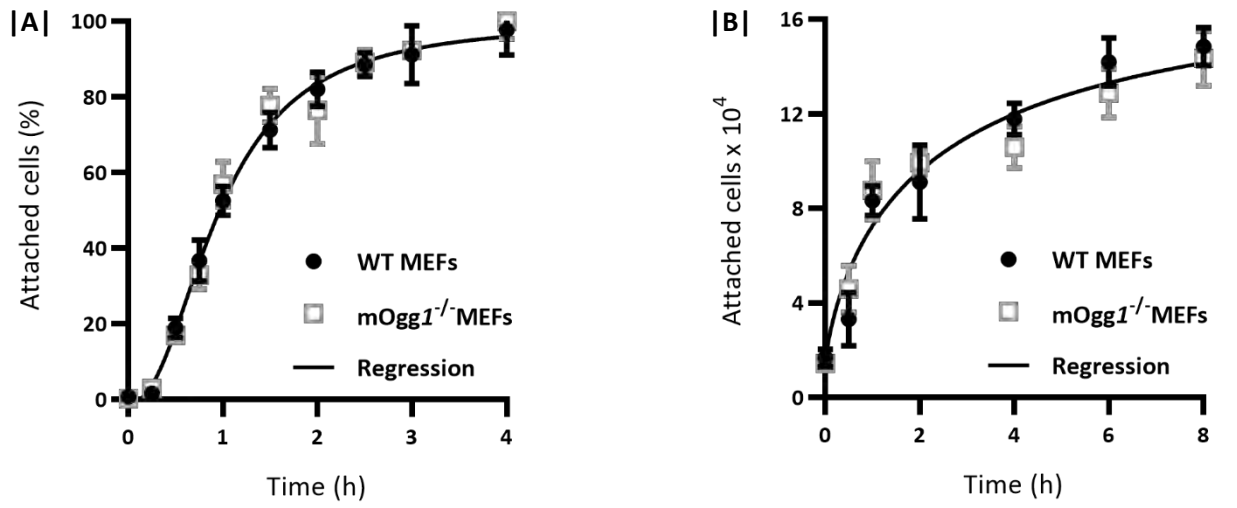


Figure 4.8. The attachment of WT and m*Ogg1*$^{-/-}$ MEFs occurs at the same rate. This was measured using crystal violet and mean values ± SD are presented for both experiments (N=3). A significance difference at each time-point was investigated with a two-way ANOVA and a subsequent Tukey's test, and non-linear regression also performed. **|A|** Following incubation with crystal violet, stained cells within quadrants (four quadrants per well) were counted. The number of cells was then converted to cells (%) using negative controls. Negative controls consisted of samples in which cell suspension was added and then immediately removed. There was no significant difference between the number of WT and m*Ogg1*$^{-/-}$ MEFs that had successfully attached at any of the time-points measured (0 - 4 h) *(p* > 0.05). Non-linear regression analysis was performed using an [agonist] vs response model, which confirmed that the same model curve could be fitted for both WT and m*Ogg1*$^{-/-}$ MEFs. **|B|** An alternative method was then used, and following incubation with crystal violet, the stain was solubilised with acetic acid. The resulting absorbance was measured (595 nm) and converted to cell number using a standard curve generated from a calibration plate (500 - 200,000 cells/well). There was no significant difference between the number of WT and m*Ogg1*$^{-/-}$ MEFs that had successfully attached at any of the time-points measured (0 - 8 h) *(p* > 0.05). Again, non-linear regression analysis ([agonist] vs response) was performed, which again confirmed that the same model curve could be fitted for both WT and m*Ogg1*$^{-/-}$ MEFs.

4.3.6. There are morphological differences between WT and m*Ogg1*$^{-/-}$ MEFs during attachment

Despite no differences in the rate of attachment being quantified (*refer to* **4.3.5.**), differences in the morphology of the two cell types were observed during the 4 h following seeding (Figure **4.9.**).

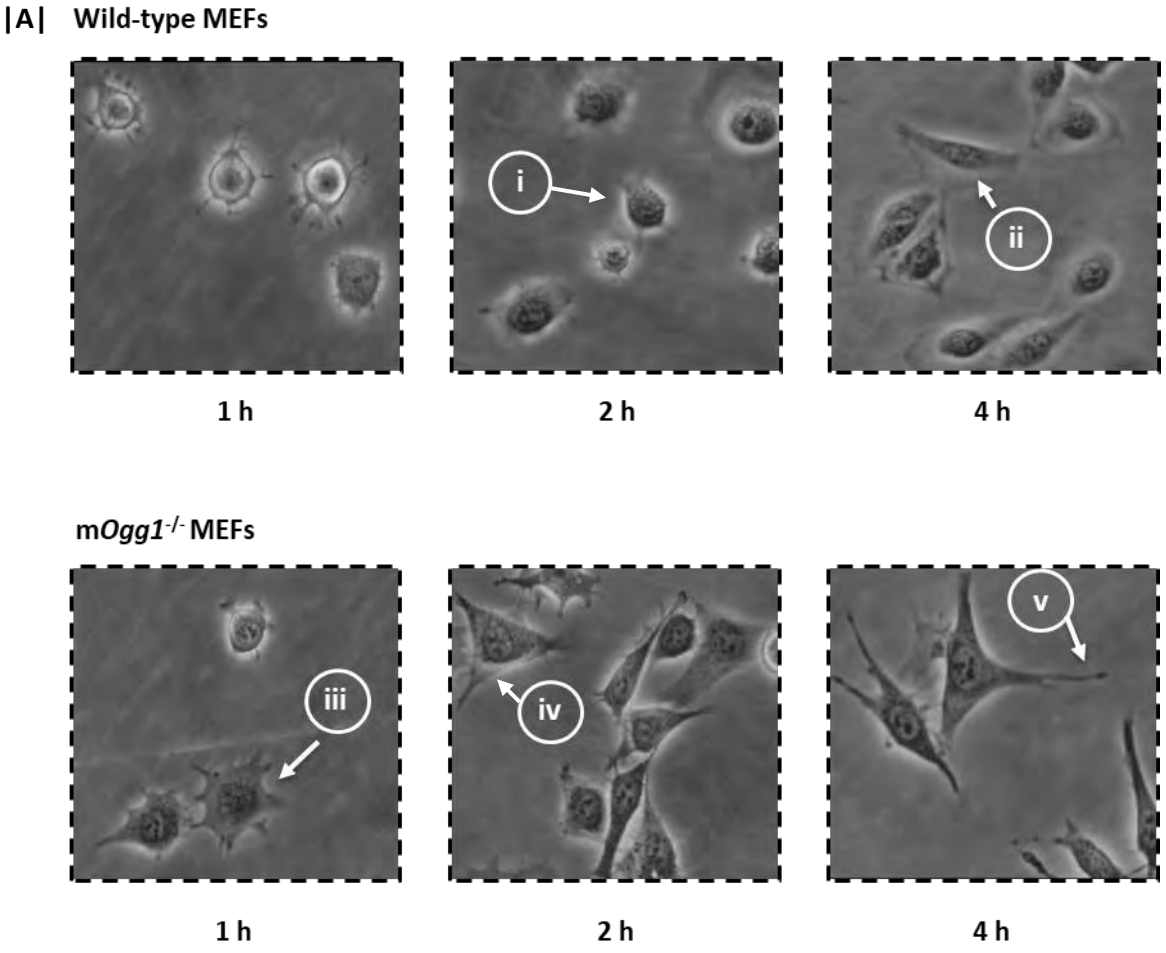


Figure continues on next page

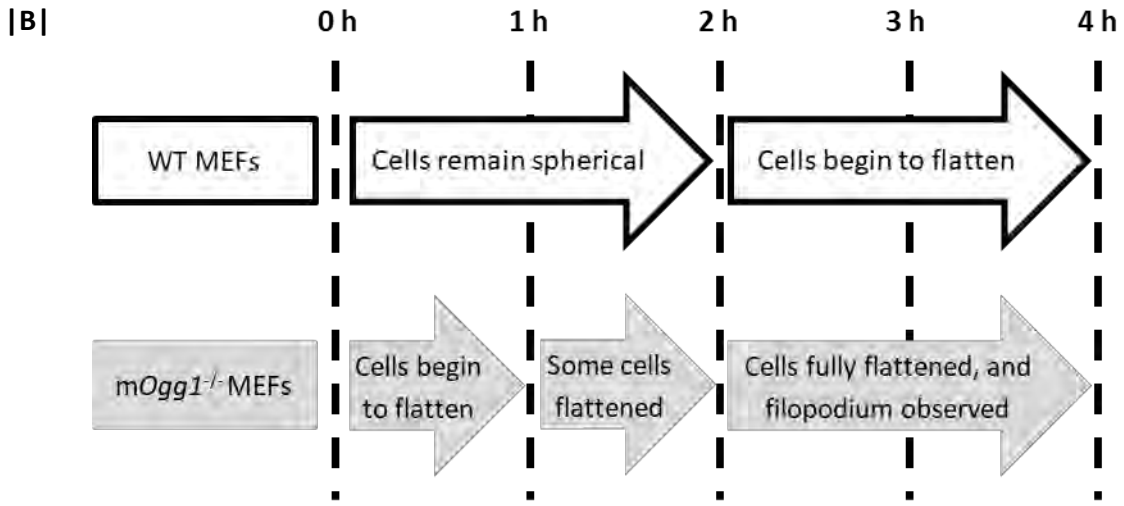


Figure 4.9. Morphological differences exist between WT and m*Ogg1*$^{-/-}$ MEFs in the initial period (1 - 4 h) following the seeding of cells. **|A|** Images of WT and m*Ogg1*$^{-/-}$ MEFs (*x 40* magnification) are shown and important observations have been highlighted; ***(i)*** WT MEFs appear spherical after 2 h, ***(ii)*** WT MEFs become flattened after 4 h, ***(iii)*** m*Ogg1*$^{-/-}$ MEFs begin to flatten after only 2 h, ***(iv)*** m*Ogg1*$^{-/-}$ MEFs continue to flatten, and ***(v)*** m*Ogg1*$^{-/-}$ MEFs become fully flattened after 4 h and substantial cytoplasmic projections have formed. **|B|** These morphological differences between WT and m*Ogg1*$^{-/-}$ MEFs during an the initial period (1 - 4 h) following the seeding of cells have been summarised.

4.3.7. Neither 8-oxoG or 8-oxodG had an effect on the rate of detachment of MEFs

A previous experiment (*refer to* **4.3.4.**) investigated the detachment of cells following the addition of trypsin-EDTA (0.25% w/v), and this experiment was then repeated in combination with different treatment conditions. There was no significant difference measured in the rate at which WT or m*Ogg1*$^{-/-}$ MEFs detached following treatment with 8-oxoG (1-10 μM, 24 h) or 8-oxodG (1-10 μM, 24 h), when compared to control cells (Figure **4.10.**). However, treatment with a non-cytotoxic concentration of H_2O_2 (12.5 μM, 24 h) (previously shown to be non-cytotoxic; *refer to* Figure **2.11.**) did significantly decrease the number of cells that had remained attached following trypsin incubation (1 min) in both WT and m*Ogg1*$^{-/-}$ MEFs ($p < 0.05$). We hypothesised that the treatment of cells with H_2O_2 caused cytoskeletal changes that resulted in a weaker attachment between the cells and culture surface. We investigated whether the combination treatment of H_2O_2 (12.5 μM) with either of the oxidised purines (8-oxoG or 8-oxodG) (1-10 μM; 24 h) could *rescue* cells from the H_2O_2 induced response. However, neither the addition of 8-oxodG or 8-oxoG resulted in a rescue response in WT or m*Ogg1*$^{-/-}$ MEFs ($p > 0.05$). These experiments were also repeated following a longer treatment duration (48 h) with similar results measured, see appendix (**7.8.**)

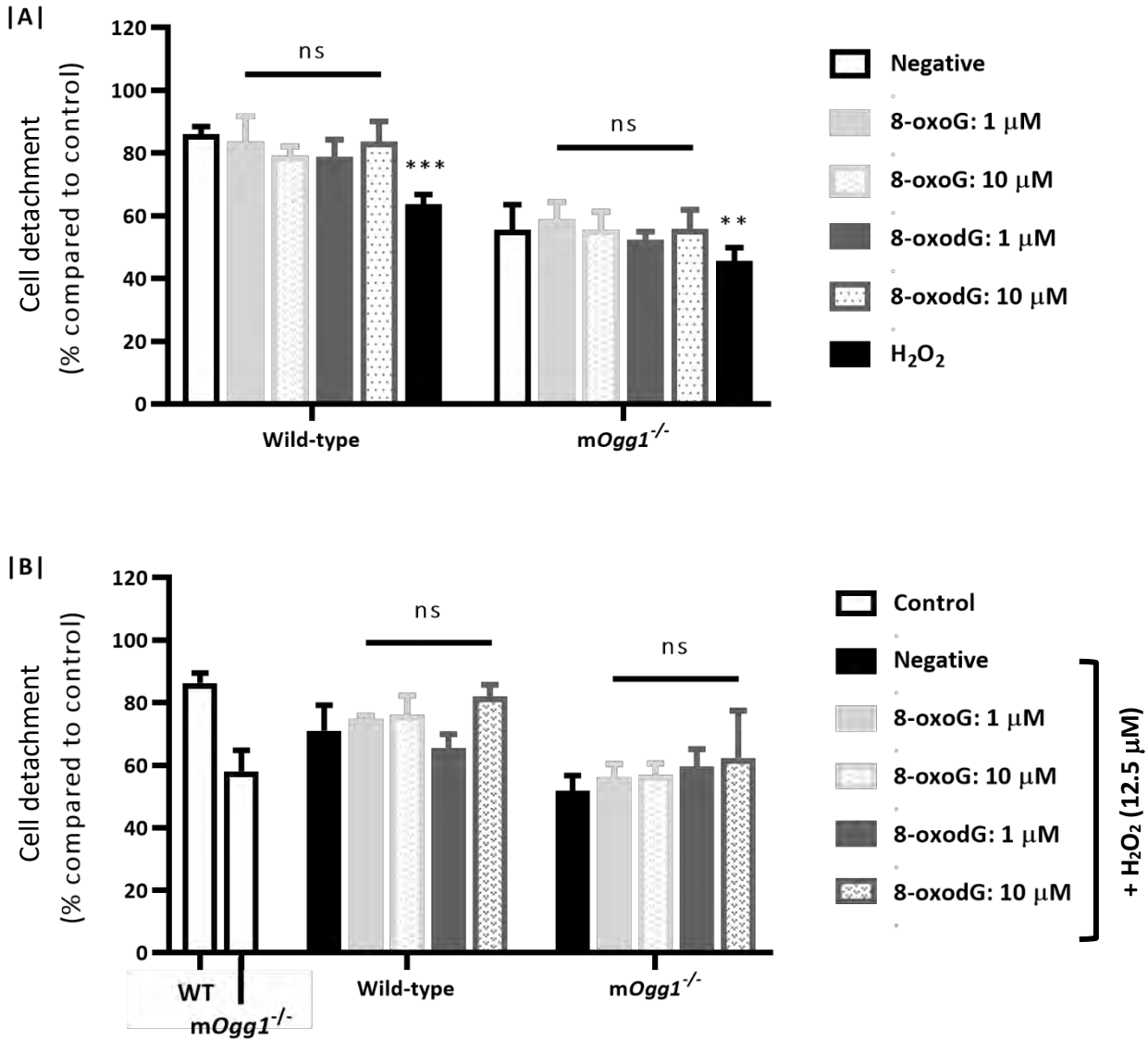


Figure 4.10. Neither 8-oxoG or 8-oxodG treatment had an effect on the rate of detachment of cells following incubation with trypsin-EDTA (0.25% w/v) for 1 min. Mean values are presented ± SD (N=3). **|A|** Treatment with 8-oxoG (□) or 8-oxodG (■) (1-10 μM; 24 h) did not have an effect on the number of WT or m*Ogg1*$^{-/-}$ MEFs that had detached *(p* > 0.05); however treatment with H_2O_2 (■) (12.5 μM; 24 h) significantly increased the rate of detachment of both WT and m*Ogg1*$^{-/-}$ MEFs *(p* < 0.01). Significance was determined with a two-way ANOVA and a subsequent Dunnett's test, with comparisons made against untreated controls (□).

Figure legend continues on next page

|B| The experiment was repeated following the co-treatment of cells with H_2O_2 (12.5 μM; 24 h) and either 8-oxoG (▒) or 8-oxodG (■) (1-10 μM; 24 h). Neither the addition of 8-oxoG or 8-oxodG had an effect on the rate of detachment of cells, when compared to only H_2O_2 treatment (■) ($p > 0.05$). Untreated control (□) cells are also shown for comparison. Significance was determined with a two-way ANOVA and a subsequent Dunnett's test, with comparisons made against H_2O_2 treated controls (■).

4.3.8. 8-oxoG decreases intracellular ROS levels in WT MEFs

Cells were treated with 8-oxoG or 8-oxodG (0.1-100 μM, 1 h) and intracellular ROS levels measured using the redox sensitive probe, H_2DCF-DA assay. 8-oxoG was shown to be capable of significantly reducing basal intracellular ROS in WT MEFs at a concentration of both 10 μM (79.1 ± 2.9 %) and 100 μM (81.7 ± 4.9 %) *(p* < 0.01) (Figure **4.11.**). This result was comparable to the decrease in ROS induced by the antioxidant, ascorbic acid (8 - 32 μM; 1h), with ascorbic acid decreasing intracellular ROS in both WT and m*Ogg1*$^{-/-}$ MEFs in a concentration-dependent manner. Treatment with ascorbic acid (128 μM; 1 h) and treatment with H_2O_2 (50 μM; 1 h) were included in all experiments as positive and negative controls, resulting in a decrease and an increase in intracellular ROS respectively. Unlike the effect of 8-oxoG on WT MEFs, no such effect was observed in m*Ogg1*$^{-/-}$ MEFs *(p* > 0.05). Furthermore, 8-oxodG addition did not have an effect of the intracellular ROS levels of WT or m*Ogg1*$^{-/-}$ MEFs *(p* > 0.05).

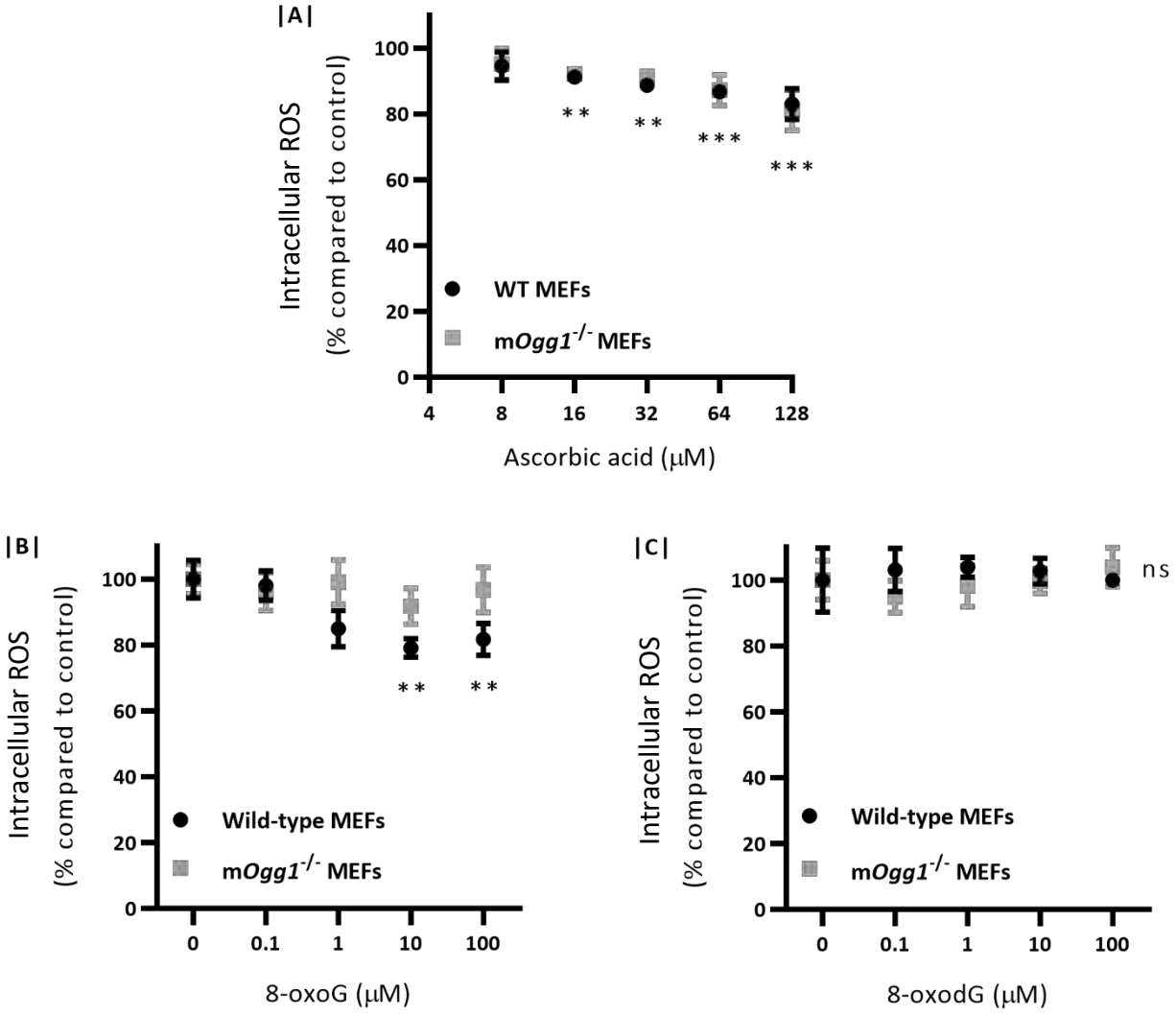


Figure 4.11. Intracellular ROS was measured using the redox-sensitive probe H_2DCF-DA (10 μM; 1 h). Mean values are presented ± SD (N=4), and significance was determined with a two-way ANOVA and a subsequent Dunnett's test. **|A|** Treatment with the antioxidant ascorbic acid (1 h) significantly reduced intracellular ROS levels (≥ 16 μM) in both WT and m*Ogg1*$^{-/-}$ MEFs *(p* < 0.01). **|B|** Treatment with 8-oxoG (0.1 - 100 μM; 1 h) had no significant effect on m*Ogg1*$^{-/-}$ MEFs *(p* > 0.05). However, 8-oxoG treatment (10 - 100 μM) did significantly reduce intracellular ROS levels in WT MEFs *(p* < 0.01). **|C|** Treatment with 8-oxodG (0.1 - 100 μM; 1 h) had no significant effect on WT or m*Ogg1*$^{-/-}$ MEFs *(p* > 0.05).

4.3.9. 8-oxoG possesses antioxidant activity in an acellular model

The H_2DCF-DA assay results (*refer to* **4.3.8.**) were reflected in an acellular model (Figure **4.12.**). 8-oxoG (10 μM) appeared to possess antioxidant capabilities, significantly reducing the reaction of hydroxyl radicals and deoxyribose at both 1 mM PO_4 (50 ± 5 % decrease) and 10 mM PO_4 (42 ± 8 % decrease) *(p* < 0.001). This was not however observed for 8-oxodG (0.1-10 μM) *(p* < 0.05).

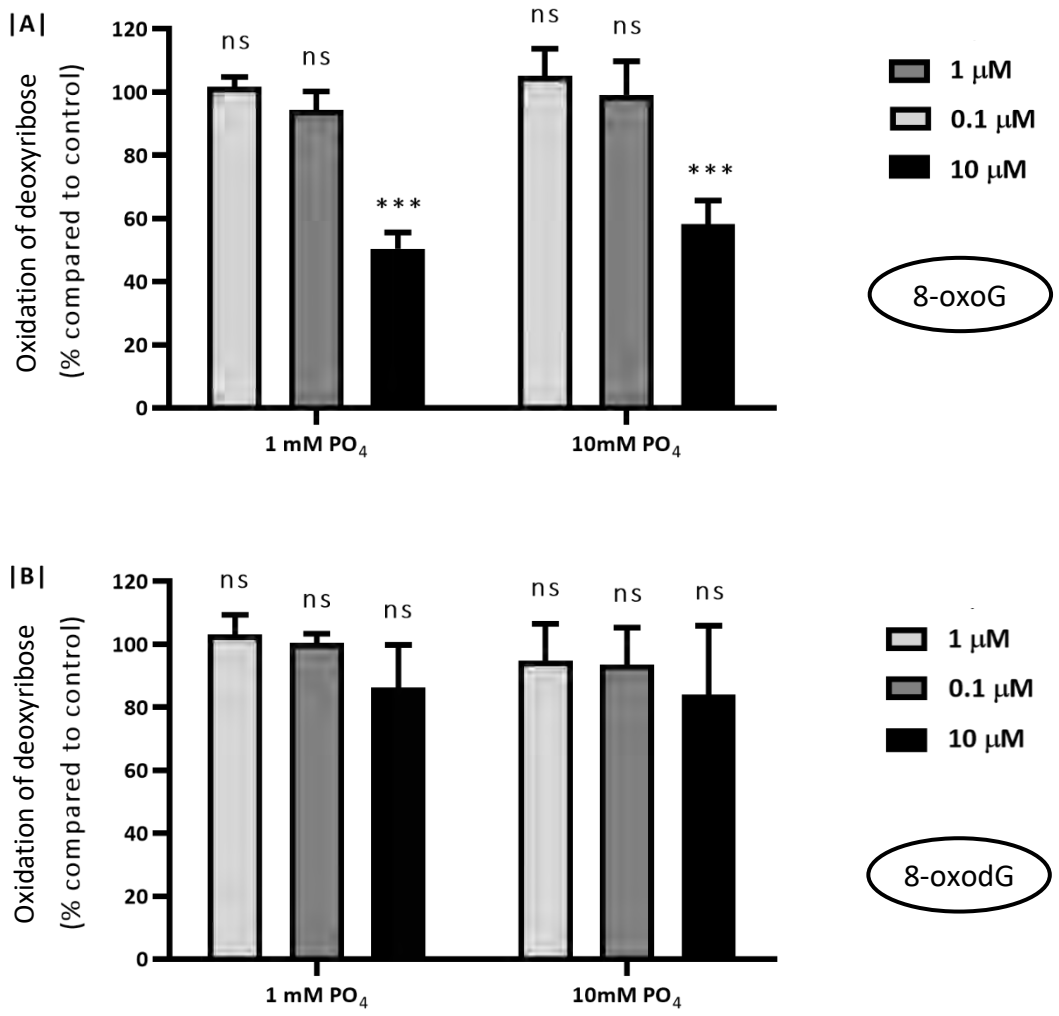


Figure 4.12. Acellular deoxyribose experiments indicate that 8-oxoG possesses antioxidative capabilities but that 8-oxodG does not. Mean values are displayed ± SD (N=3), and significance was determined with a two-way ANOVA and a subsequent Dunnett's test. **|A|** 8-oxoG (10 μM) significantly decreased the oxidation of deoxyribose by hydroxyl radicals at both 1 mM PO_4 (50 ± 5 % decrease) and 10 mM PO_4 (42 ± 8 % decrease) *(p* < 0.001). **|B|** 8-oxoG did not possess antioxidant activity at any of the concentrations tested (0.1 - 10 μM), and did not significantly decrease the oxidation of deoxyribose by hydroxyl radicals *(p* > 0.05).

4.4. Discussion

8-oxoG in genomic DNA is the most extensively studied cellular target of OGG1. In addition to this repair mechanism; it is now known that following the OGG1-initiated excision of 8-oxoG, the two molecules interact with one another to form a signalling complex (OGG1:8-oxoG) (David, O'Shea and Kundu, 2007; Ba and Boldogh, 2018). We hypothesise that 8-oxoG treatment mimics the release of 8-oxoG from DNA that occurs during OGG1-initiated excision (Figure **4.13.**). Therefore, linking any downstream effects following 8-oxoG treatment to this OGG1:8-oxoG signalling complex.

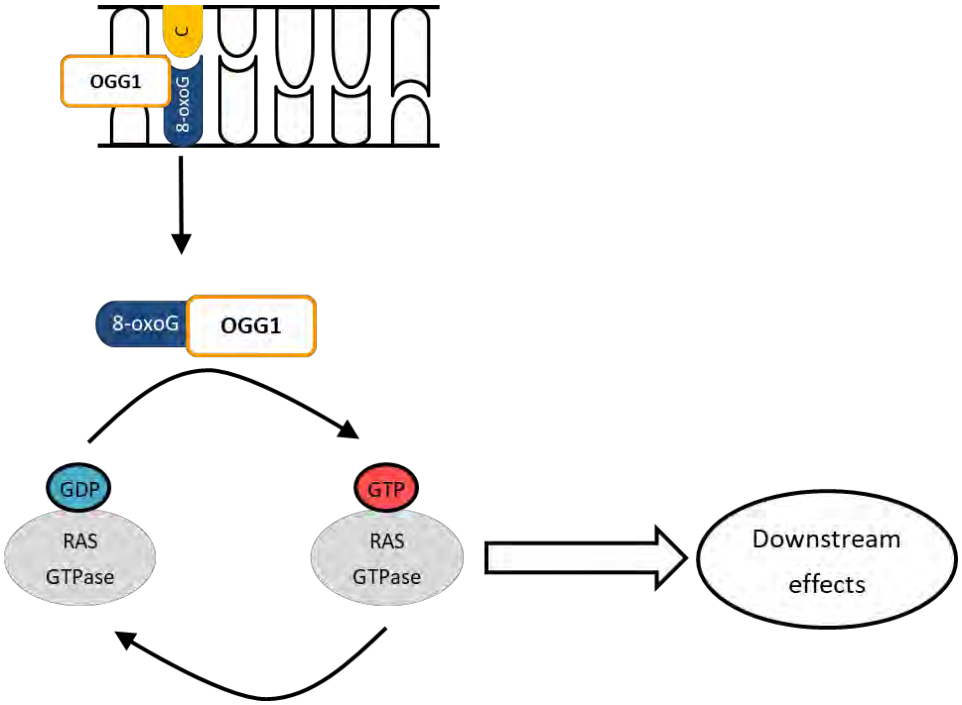


Figure 4.13. The OGG1:8-oxoG signalling molecule. During OGG1-initiated BER of 8-oxoG, the 8-oxoG base is released from the genome. OGG1 and 8-oxoG can then interact with one another to form a signalling complex, which has been reported to activate downstream GTPases through its mechanism as a guanine exchange factor (GEF), thereby inducing the substitution of GDP to GTP. Active (GTP-bound) RAS GTPases are then able to initiate downstream signalling pathways, including those involved in proliferation, cytoskeletal regulation, and redox signalling (Boldogh *et al.*, 2012; Ba and Boldogh, 2018).

The OGG1:8-oxoG complex has been implicated in the activation of RAS GTPases downstream of the signalling complex (Boldogh *et al.*, 2012; German *et al.*, 2013; Hajas *et al.*, 2013; Luo *et al.*, 2014; Pandita, 2014; Ba and Boldogh, 2018). Therefore, the complex has been implicated in the activation of effectors downstream of these RAS GTPases, with these signalling pathways known to facilitate a number of cellular processes (Colicelli, 2004; Wennerberg, Rossman and Der, 2005; Rojas *et al.*, 2012). Once it was confirmed that the treatment of cells with the oxidised purines (8-oxoG and 8-oxodG) (0.1 - 10 μM; 1 - 24 h) did not have an effect on cell viability, the effect of the oxidised purines on intracellular levels of active RAS were investigated. We confirmed that the addition of 8-oxoG (1 μM; 15 min) to WT MEFs caused a subsequent increase in active RAS, reflecting data previously published (Boldogh *et al.*, 2012; German *et al.*, 2013). RAS activation was also observed in HeLa cells with the level of activation induced by 8-oxoG comparable to the activation induced by EGF, which is a physiological activator of RAS. In contrast, there was no such activation observed in m*Ogg1*$^{-/-}$ MEFs, confirming that RAS activation by 8-oxoG is dependent on OGG1. This confirms that the induction of RAS-GTP lies downstream of the OGG1:8-oxoG complex, and furthermore confirms that this response is not mediated by 8-oxoG alone.

We did not observe any such increase in RAS-GTP levels in any of the tested cell-types (WT MEFs, m*Ogg1*$^{-/-}$ MEFs, or HeLa cells) following treatment with 8-oxodG. Although the two molecules share similar structures (*refer to* Figure **4.2.**), 8-oxoG is the molecule released from the genome during OGG1-initiated BER (David, O'Shea and Kundu, 2007; Robertson *et al.*, 2009; Kim and Wilson, 2012). We suggest that this difference in response confirms that 8-oxoG treatment does mimic the release of 8-oxoG that occurs following OGG1-initiated excision. Furthermore, this indicates that induction of RAS-GTP is reliant on the release of 8-oxoG, and therefore lies downstream of the OGG1:8-oxoG signalling complex. Interestingly, we found that co-treatment of cells with 8-oxoG and H_2O_2 decreased the effect that 8-oxoG had on the RAS-GTP levels in WT MEFs. We propose that this is potentially due to the inactivation of OGG1 *via* the oxidation of cysteine residues, which can occur in conditions of high intracellular ROS

(Bravard *et al.*, 2006, 2010; Smart, Chipman and Hodges, 2006; Morreall *et al.*, 2015). This oxidation of cysteine residues would subsequently inhibit OGG1-initiated BER, and decrease the release of 8-oxoG from DNA. This would therefore inhibiting pathways downstream of the OGG1:8-oxoG complex (*e.g.* RAS GTPase signalling). However, this is not the only possibility, with the effects of H_2O_2 within the cell being numerous and broad.

The OGG1:8-oxoG signalling complex may also explain the differences between the morphology of WT and m*Ogg1*$^{-/-}$ MEFs that were observed. In particular, m*Ogg1*$^{-/-}$ MEFs appeared to possess more pronounced cytoplasmic projections than WT MEFs. Currently, the biochemical nature of these is not clear and further research is required. Secondly, we showed that m*Ogg1*$^{-/-}$ MEFs detached significantly faster than WT MEFs following trypsin-EDTA incubation, indicating that there are also differences in substrate attachment of these cell-types that could also be related to differences in the cytoskeleton.

The RHO family of GTPases (*refer to* Figure **4.2.**) play an important role in the actin dynamics of the cell, mediating the morphological response of a cell in response to external stimuli. We hypothesise that differences in the activation of these GTPases (*via* OGG1:8-oxoG) could be the mechanism through which WT MEFs are capable of remaining attached to a surface for a longer duration than m*Ogg1*$^{-/-}$ MEFs when challenged with the protease trypsin (Vogel, 1978; Tokiwa *et al.*, 1979). This OGG1:8-oxoG mediated activation of RHO-A and RAC1 has already been shown by Luo *et al.* (2014) and Hajas *et al.* (2013) respectively. We hypothesise that a loss of OGG1:8-oxoG in m*Ogg1*$^{-/-}$ MEFs would result in a decrease in RHOA activation in response to DNA damage, preventing the assembly of α-SMA into stress fibres. We propose that it is through these mechanisms that the loss of OGG1:8-oxoG could result in some of these morphological and cytoskeletal differences observed in m*Ogg1*$^{-/-}$ MEFs. Furthermore, we hypothesised that 8-oxoG treatment could induce cytoskeletal changes in WT MEFs *via* this RHO signalling. However, we found that 8-oxoG treatment (24 - 48 h) had no effect on the rate of detachment of cells following

trypsin-EDTA incubation. Furthermore, no clear morphological changes were observed following 8-oxoG addition (*data not shown).*

Another RHO GTPase that has been implicated in membrane ruffling is RAC1. Membrane ruffling describes the polymerisation of actin filaments, which aids in the motility of the cell. Furthermore, RAC1 has been implicated in the formation of lamellipodia, which are specific cytoplasmic projections composed of actin that are located at the leading edge of a motile cell (Naumanen, Lappalainen and Hotulainen, 2008; Tojkander, Gateva and Lappalainen, 2012). In addition to these cytoskeletal regulatory roles, RAC1 has also been shown to play a role in redox regulation and has been linked to a transient increase in intracellular ROS (Hajas *et al.*, 2012; Hajas *et al.,* 2013). We therefore hypothesised that differing responses may be observed for WT and m*Ogg1*$^{-/-}$ MEFs following 8-oxoG treatment, with respect to intracellular ROS levels. We hypothesise that this would occur due to the loss of RAC1 activation downstream of OGG1: 8-oxoG in WT MEFs. We measured intracellular ROS levels using the fluorescent probe H_2DCF-DA, and somewhat surprisingly measured a significant decrease in the ROS levels of WT MEFs in response to 8-oxoG. Such a response was not observed in m*Ogg1*$^{-/-}$ MEFs, nor following 8-oxodG treatment in WT or m*Ogg1*$^{-/-}$ MEFs. This result seems to contradict what has previously been observed in other publications (Hajas *et al.*, 2012; Hajas *et al.,* 2013).

In conjunction with the H_2DCF-DA experiments, we carried out a similar experiment in an acellular model, and once again we observed an antioxidant response following 8-oxoG addition. The chosen model utilised the Fenton reaction, in which H_2O_2 is converted to hydroxyl radicals, followed by a well-characterised reaction between deoxyribose and these hydroxyl radicals (Zepp, Faust and Jürg, 1992). Briefly described, hydroxyl radicals are produced from the Fenton reaction, which will then react with deoxyribose to produce MDA. This production of MDA is then linked to a colorimetric change *via* the addition of TBA. The introduction of 8-oxoG into this model resulted in a colorimetric decrease, suggesting that the oxidised base was instead reacting with deoxyribose. This suggests that the

antioxidant response that we measured previously in WT MEFs may have been independent of OGG1: 8-oxoG signalling, with this effect not dependent on OGG1. However, we are unclear of the mechanism behind this, and we hypothesise that it could instead be a result independent of 8-oxoG. For example, this effect could have been a secondary outcome caused by impurities introduced to the compound during preparation. However, 8-oxodG did not produce the same response in the acellular model, despite their similarities in structure. It is clear that this apparent ability of 8-oxoG to act as an antioxidant would need further investigation.

4.5. Conclusions and future work

In conclusion, we have reported differences that exist in the morphology of WT and m*Ogg1*$^{-/-}$ MEFs, which are potentially related to changes to the cytoskeleton. We suggest that these differences are due to the absence of the OGG1:8-oxoG signalling complex in m*Ogg1*$^{-/-}$ MEFs, with no induction of RAS activation measured in these cells following 8-oxoG addition. Alternatively, a significant increase in RAS activation was measured in both WT and HeLa cells following 8-oxoG addition. We propose that these differences are partly due to the lack of actin polymerisation and the failure to assemble stress fibres *via* RHOA signalling, as suggested by Luo *et al* (2014). This is an initial study into these differences and this should be further studied using endpoints for RAS, RHOA and RAC1 signalling *via* gene expression studies, western blotting, and functional assays. An ideal next step would be the investigation into the prevalence of stress fibres in WT and m*Ogg1*$^{-/-}$ MEFs. This could be performed using FITC-conjugated phalloidin and fluorescence microscopy, which will result in the staining and visualisation of F-actin, which is the major actin component of stress fibres. Cells should be challenged with 8-oxoG to investigate if changes in stress fibres can be observed in WT MEFs.

5

General discussion and concluding remarks

5.1 General discussion

5.1.1. m*Ogg1*$^{-/-}$ MEFs and oxidative stress

Throughout this thesis, WT and m*Ogg1*$^{-/-}$ MEFs were used as a model system to investigate the different roles of OGG1 within a mammalian cell. These cell lines were developed and initially described in Klungland, Rosewell *et al.* (1999) (Todaro and Green, 1963; Barnes *et al.*, 1998; Klungland, Rosewell, *et al.*, 1999). They have since been characterised within our research group, and utilised in multiple published studies (Smart, Chipman and Hodges, 2006; Green *et al.*, 2008; Mirbahai *et al.*, 2010; Priestley *et al.*, 2010; Zielinska *et al.*, 2011; Kershaw and Hodges, 2012; Higgs *et al.*, 2020). Furthermore, the WT and m*Ogg1*$^{-/-}$ MEFs used within this thesis were characterised for OGG1 status using PCR and western blot techniques (*refer to* Chapter **2** for details).

Ogg1-null mouse models have been utilised by multiple research groups, with some conflicting results having been published for such models (Sakumi *et al.*, 1993; Klungland *et al.*, 1999; Minowa *et al.*, 2000; Osterod *et al.*, 2001; Arai *et al.*, 2002; Arai *et al.,* 2006). The data presented in this thesis shows that there is no significant accumulation of 8-oxoG lesions within the genome of m*Ogg1*$^{-/-}$ MEFs, however in conditions of oxidative stress (induced using BSO treatment) 8-oxoG levels significantly increase in m*Ogg1*$^{-/-}$ MEFs. These findings are in agreement with other studies that measured an accumulation of genomic 8-oxoG in m*Ogg1*$^{-/-}$ MEFs in conditions of oxidative stress (Arai *et al.*, 2002; Arai *et al.,* 2006), however other studies also measured an accumulation of 8-oxoG in the genome of untreated/unchallenged *Ogg1*-null models (Klungland, Rosewell, *et al.*, 1999; Minowa *et al.*, 2000). Osterod *et al.* (2001) investigated the occurrence of 8-oxoG lesions in different tissues derived from a m*Ogg1*$^{-/-}$ mouse model and hypothesised that this accumulation of genomic 8-oxoG is tissue-dependent. They propose that the consequences of an *Ogg1*-null status differ between cell types, with an accumulation of 8-oxoG restricted to slowly proliferating tissues with a high rate of oxidative metabolism.

Within our studies, oxidative stress was primarily induced *via* BSO treatment. BSO is an inhibitor of an enzyme within the GSH synthetic pathway (Ɣ-GCS) and therefore inhibits the synthesis of GSH, a key cellular antioxidant. We have shown that our treatment regimen with BSO (15 μM; 24 h) depletes GSH and increases intracellular ROS, without reducing cell viability of WT or m*Ogg1*$^{-/-}$ MEFs. Furthermore, the gene expression studies presented in Chapter **3** confirmed that BSO treatment resulted in an upregulation of DNA repair genes in WT MEFs, including *Ogg1*.

Following GSH depletion we identified an increase in 8-oxoG sites in m*Ogg1*$^{-/-}$ MEFs. This increase in 8-oxoG sites was significant ($p < 0.001$), however it was a fairly modest increase (7.1 ± 0.8%). Furthermore, it was significantly lower than the increase in 8-oxoG sites seen following treatment with a non-cytotoxic dose of H_2O_2 (50 μM; 1 h). It is important to recognise that H_2O_2 is a species of ROS itself and therefore will generate a fairly broad range of oxidative DNA damage, including but not limited to 8-oxoG. This H_2O_2-induced damage also includes the generation of strand breaks and alkali labile sites (Andreoli *et al.*, 1999; Driessens *et al.*, 2009; Valverde *et al.*, 2018). Both single-strand DNA breaks and alkali labile sites are intermediate products of DNA repair (including the BER pathway) and both are substrates that will be recognised and measured *via* the comet assay (Singh *et al.*, 1988; Andreoli *et al.*, 1999). In this thesis, oxidative DNA damage was quantified using the hOGG1-modified comet assay (Cadet *et al.*, 2000; Smith, O'Donovan and Martin, 2006) which is largely but not completely specific to 8-oxoG sites because OGG1 is also know to recognise 8-oxoA and FapyG lesions (*refer to* **1.5.**) (Boiteux and Radicella, 2000; Bjørås *et al.*, 2002; Jensen *et al.*, 2003; Hu, de Souza-Pinto, *et al.*, 2005; Klungland and Bjelland, 2007).

This relative specificity of OGG1 was the reason why hOGG1-modified comet assays were utilised rather than the more frequently utilised FPG-modified comet assay (Cadet *et al.*, 2000; Smith, O'Donovan and Martin, 2006; Collins, 2014). FPG is a DNA glycosylase, which was identified in *E. coli* and found to be responsible for the recognition and excision of 8-oxoG (Boiteux *et al.*, 1990; Michaels *et al.*, 1991;

Castaing *et al.*, 1993). The discovery of FPG ultimately paved the way for the identification of an FPG-functional analogue (aka OGG1), which was originally identified in *S. cerevisiae*, before subsequently being purified and characterised in mammalian cells (described in **1.5.1.**) (Nash *et al.*, 1996; van der Kemp *et al.*, 1996; Arai *et al.*, 1997; Kuo and Sklar, 1997; Ishida *et al.*, 1999). Therefore, it was hypothesised in the 1990's that FPG could be effectively used within the context of a comet assay, specifically recognising oxidative DNA damage (Dušinská and Collins, 1996; Gedik and Collins, 2005; Collins, 2014).

Following the development of the FPG-modified comet assay (Dušinská and Collins, 1996), it was later trialled by the European Standards Committee on Oxidative DNA damage (Gedik and Collins, 2005). This trial published promising results showing the FPG-modified comet assay to be less vulnerable to spurious oxidation when compared to other techniques in use (*e.g.* HPLC-ECD, GC-MS). However, they noted that it is not only oxidised purines that are recognised, with FPG also recognising forms of alkylation-induced DNA damage (Speit *et al.*, 2004; Gedik and Collins, 2005; Smith, O'Donovan and Martin, 2006). This broader substrate range of FPG had previously been established (Michaels *et al.*, 1991; Boiteux and Radicella, 2000) and would be expected as bacteria possess a significantly smaller genome than mammalian cells (Shabalina and Spiridonov, 2004; Kreuzer, 2013). A study was performed in response to this non-specificity of FPG (Smith, O'Donovan and Martin, 2006), which investigated the use of two other endonucleases (OGG1 and ENDOIII) in a comet assay. The ability of these endonucleases to measure an increase in damage was investigated, following treatment with compounds that caused either oxidative or alkylating damage. Using both $KBrO_3$ treatment and gamma irradiation, the study showed hOGG1 to be much more specific to oxidative damage in context of the comet assay experiment (Smith, O'Donovan and Martin, 2006). The aim of this thesis was to study OGG1-initiated repair, and therefore the OGG1-modified comet assay represents a more specific approach to measure 8-oxoG using the comet assay compared to other methodologies (Cadet *et al.*, 2000; Smith, O'Donovan and Martin, 2006).

5.1.2. Induction of apoptosis in m*Ogg1*$^{-/-}$ MEFs following GSH depletion

Following GSH depletion, the accumulation of 8-oxoG in m*Ogg1*$^{-/-}$ MEFs does not match the accumulation of 8-oxoG observed following the non-cytotoxic dose of H_2O_2. We therefore propose that an accumulation of genomic 8-oxoG is not the reason why apoptosis is induced.

This result led us to two main hypotheses:

1. *The induction of apoptosis in mOgg1*$^{-/-}$ *MEFs is not a direct consequence of genomic 8-oxoG*
2. *There is a mechanism present in mOgg1*$^{-/-}$ *MEFs that can prevent the accumulation of 8-oxoG in the absence of OGG1 activity*

To further study oxidative stress induced apoptosis in m*Ogg1*$^{-/-}$ MEFs, the mitochondrial status of the cells was investigated. We showed that there was no statistical difference between WT and m*Ogg1*$^{-/-}$ MEFs in levels of whole-cell ATP and observed no difference between the responses of the cells towards mitochondrial inhibitors, suggesting no difference between mitochondrial function and oxidative phosphorylation between the two cell lines. However, we cannot fully exclude subtle differences in the mitochondrial status of WT and m*Ogg1*$^{-/-}$ MEFs due to a potential accumulation of 8-oxoG in the mtDNA, which could result in a degree of mitochondrial dysfunction (Wallace, 2001; Liu and Demple, 2010; Yuzefovych *et al.*, 2013; Cividini *et al.*, 2016; Leon *et al.*, 2016). Mitochondrial dysfunction is understood to primarily occur by one of three mechanisms: deregulation of transmembrane potential; alterations to the complexes ($\mathrm{I} - \mathrm{IV}$) of the ETC; and lastly a reduction in the transport of critical metabolites (NADH, $FADH_2$) into the mitochondria (Yuzefovych *et al.*, 2013; Nicolson, 2014). This highlights a potential avenue for future work, with it possible that subtle mitochondrial changes are responsible for some of the differences observed between WT m*Ogg1*$^{-/-}$ MEFs, including the induction of apoptosis (Esteve *et al.*, 1999; Ruchko *et al.*, 2005; Ricci *et al.*, 2008; Lee, Giordano and Zhang, 2012).

5.1.3. OGG1 backup mechanisms

NER pathway

The NER pathway was significantly upregulated in both WT and m*Ogg1*$^{-/-}$ MEFs following BSO treatment. This indicates that components of the NER pathway are associated with the cellular response against oxidative stress, and this result is in agreement with a previous study that showed H_2O_2 treatment induced the upregulation of the NER pathway in A549 cells (Langie *et al.*, 2007). Furthermore, the NER pathway appeared upregulated in m*Ogg1*$^{-/-}$ MEFs when compared to WT MEFs. Our previous results suggest that m*Ogg1*$^{-/-}$ MEFs already exist in a state of oxidative stress and possess an elevated level of intracellular ROS (*refer to* Chapter **1**), and therefore the upregulation of the NER pathway in m*Ogg1*$^{-/-}$ MEFs is again representing an upregulation of the NER pathway in conditions of oxidative stress.

Upregulation of NER activity in m*Ogg1*$^{-/-}$ MEFs was measured using two methods. Gene expression was quantified by qPCR, and pathway activity was investigated using a NER-modified comet assay (Langie *et al.*, 2006). Three NER genes were upregulated in m*Ogg1*$^{-/-}$ MEFs when compared to WT MEFs. All three of these genes (*Ercc1, Ercc4* and *Ercc5*) encode NER proteins that are crucial for substrate excision steps that occur early on in the NER pathway, with this damage recognition and substrate incision the rate-limiting steps of the NER pathway (Hansen and Kelley, 2000; Politi *et al.*, 2005; Langie *et al.*, 2006).

To perform the NER-modified comet assay, a methodology previously established by Langie *et al.* (2006) was used. The principle of the assay is the generation of DNA damage (*via* BPDE exposure) in substrate (A549) cells, with this damage subsequently repaired by protein extracts *via* their NER capabilities (Hess *et al.*, 1997; Langie *et al.*, 2006). This comet assay methodology is designed to measure the repair capability of extracts, rather than measure the occurrence of specific DNA damage (*e.g.* as the hOGG1-modified comet assay discussed above). This type of comet assay is now referred to as *in vitro* comet assay, and the principle has been shown to be effective in numerous studies, with this methodology having been used to measure the capability of extracts to repair different types of DNA repair, thereby

measuring different mechanisms of DNA repair (Gaivão *et al.*, 2009; van Dyk *et al.*, 2010; Hašplová *et al.*, 2012). Specifically, the NER-modified comet assay (Langie *et al.*, 2006) is able to determine the ability of the cell extracts to perform the initial step of the NER process, which is the recognition and removal of the BPDE-induced DNA lesions. If these lesions are successfully excised, the resulting abasic sites will be converted to single-strand DNA breaks and measured *via* the comet assay procedure. Langie *et al.* (2006) validated the methodology by comparing the results to the data collected in a BPDE-DNA adduct removal study, with a significant linear correlation observed between the two methods. Further validation was performed using NER-deficient cell-lines ($XPA^{-/-}$ and $XPC^{-/-}$), which showed minimal NER capabilities. However a combination of the two deficient cell-lines, which would in contrast possess XPA and XPC activity, restored NER capabilities to the WT level (Langie *et al.*, 2006). Furthermore, in a subsequent study, Langie *et al.* (2007) showed that *Ercc1* expression strongly correlated with NER capacity (as measured with the NER-modified comet assay).

Therefore, the increase in NER activity measured in m*Ogg1*$^{-/-}$ MEFs *via* the NER-modified comet assay represents an increase in substrate recognition and excision, a process mediated by the genes upregulated in m*Ogg1*$^{-/-}$ MEFs (*Ercc1, Ercc4* and *Ercc5*) (Wood, 1997; de Laat, Jaspers and Hoeijmakers, 1999; Lindahl and Barnes, 2000; Schärer, 2013; Rimel and Taatjes, 2018). We are confident that the combined gene expression studies and NER-modified comet assay prove that m*Ogg1*$^{-/-}$ MEFs, which exist in a state of oxidative stress, possess an upregulation of the NER pathway.

We propose that this once again shows a relationship between the NER pathway and the cellular response towards oxidative stress, and therefore oxidative DNA damage. This was further confirmed by the significant increase in NER capacity observed in both WT (*via* comet assay and gene expression studies) and m*Ogg1*$^{-/-}$ MEFs (*via* comet assay only) following BSO treatment. Although we have not directly attributed this increase in NER activity to 8-oxoG, Langie *et al.* (2007) has linked these NER gene genes (*Ercc1, Ercc4* and *Ercc5)* with oxidative stress. Following H_2O_2 treatment in A549 cells, there was a

significant increase in the *Xpa, Xpc, Ercc1, Ercc4* and *Ercc5* genes. The most dramatic increase was in the expression of *Ercc1,* as reflected in our gene expression studies (Langie *et al.*, 2007). These genes were further linked to oxidative stress in a subsequent animal model (Langie *et al.*, 2010), showing changes in NER activity were mediated by oxidative stress.

We propose that utilising cell models that are deficient in both OGG1 activity and specific NER proteins (*Ercc1* and *Ercc5*) could be a potential avenue for a future study. However, as always the case with gene knockout models there is a risk that cells may not be viable, especially with two repair pathways compromised (Yuan *et al.*, 2012; Wu *et al.*, 2019).

NEIL3 pathway

The second backup mechanism identified in these studies was NEIL3, an endonuclease that repairs the further oxidation products of 8-oxoG (Sp and Gh) (Kornyushyna and Burrows, 2003; Niles, Wishnok and Tannenbaum, 2004; Krokeide *et al.*, 2009, 2013; Takao *et al.*, 2009; Liu *et al.*, 2010; Cui *et al.*, 2013; Liu, Doublié and Wallace, 2013).

A significant increase was seen in the expression of *Neil3* in m*Ogg1*$^{-/-}$ MEFs and in BSO-treated WT MEFs, which represent two different models of oxidative stress. This upregulation of *Neil3* was a much more dramatic increase when compared to the NER proteins discussed, and we therefore hypothesise that upregulation of *Neil3* is the primary mechanism through which m*Ogg1*$^{-/-}$ MEFs avoid an accumulation of genomic 8-oxoG. Using a novel NEIL3 modified comet method, we quantified a significant fold increase in NEIL3 substrate sites in m*Ogg1*$^{-/-}$ MEFs following BSO treatment. We did not see an accumulation of NEIL3 substrate sites in untreated m*Ogg1*$^{-/-}$ MEFs, but we hypothesise that this is due to the already substantial increase in the expression of *Neil3* observed in these cells, which allows for the efficient repair of these NEIL3 substrate sites. However, following GSH depletion (and the subsequent increase in ROS), no further increase in *Neil3* expression was measured in m*Ogg1*$^{-/-}$ MEFs. We propose that this further induction of oxidative stress would result in an increase in oxidative damage, resulting in an increase in Sp and Gh lesions. With no further upregulation of *Neil3,* these Sp and Gh lesions remain in the genome for longer and are therefore detected *via* this novel NEIL3-modified comet assay.

As mentioned, this is a novel use of the comet assay. For further development of this method, full validation would need to be performed and published, such as was done by Langie *et al.* (2006) for the NER-modified *in vitro* methodology. To do this, the experiment would need to performed in parallel to a suitable detection process of Sp and Gh (Kornyushyna and Burrows, 2003; Niles, Wishnok and Tannenbaum, 2004; Yu *et al.*, 2005; Liu *et al.*, 2012; Cui *et al.*, 2013; Krokeide *et al.*, 2013; Norabuena *et al.*, 2016).

5.1.4. RAS-GTPase signalling and OGG1:8-oxoG

One aim of this thesis was to investigate the cellular role of OGG1 outside of its traditional glycosylase role. Multiple other potential functions of OGG1 have been identified; including chromatin remodelling, DNA-methylation, transcriptional activation, and cellular signalling (Dantzer *et al.*, 2002; Mabley *et al.*, 2004; Boldogh *et al.*, 2012; German *et al.*, 2013; Hajas *et al.*, 2013; Ba, Aguilera-Aguirre, *et al.*, 2014; Ba, Bacsi, *et al.*, 2014; Luo *et al.*, 2014; Allgayer *et al.*, 2016; Pan *et al.*, 2016; Seifermann and Epe, 2017; Ba and Boldogh, 2018; Sampath and Lloyd, 2019). A number of these roles have since been linked to the OGG1: 8-oxoG signalling complex, which forms following the OGG1-mediated excision of OGG1. We confirmed that this process is active within the WT MEFs but was lacking in m*Ogg1*$^{-/-}$ MEFs. This was confirmed using a commercial RAS-GTP ELISA, which has already been used in multiple published papers (de Lucca Camargo *et al.*, 2013; Gil-Henn *et al.*, 2013; Lee *et al.*, 2013).

We propose that it is *via* these GTPase signalling pathways, that cytoskeletal differences between WT and m*Ogg1*$^{-/-}$ MEFs are mediated. However, these are early stages and this should be further investigated. Ideally, phalloidin should be utilised to demonstrate that there are differences between the actin composition (*e.g.* stress fibres) of WT and m*Ogg1*$^{-/-}$ MEFs. Luo *et al.* (2014) performed a similar experiment and showed that there was an increase in the formation of stress fibres in WT MEFs and MRC5 cells following 8-oxoG addition. However, such an increase was not observed in *Ogg1*-null MEFs (Luo *et al.*, 2014). This experiment should be repeated with our WT and m*Ogg1*$^{-/-}$ MEFs, and differences in the actin composition between the cells in the absence of treatment.

5.2. Future work

The work presented in this thesis has opened up three main avenues for potential future work, as described below.

1. An investigation fully probing the mitochondrial status of m*Ogg1*$^{-/-}$ MEFs

Our experiments showed that the mitochondria of m*Ogg1*$^{-/-}$ MEFs were functioning, with m*Ogg1*$^{-/-}$ MEFs possessing the same level of whole-cell ATP (primarily produced by the mitochondria) as WT MEFs, and not showing an increased sensitivity to two mitochondrial inhibitors (antimycin-A and rotenone). However, a full investigation of the mitochondrial status of m*Ogg1*$^{-/-}$ MEFs should be performed, including assessment of the electron transport chain (*e.g.* measurement of proton current), assessment of mitochondrial respiration, oxygen consumption and glycolysis rate (*e.g.* mitochondrial stress testing) (Aguer *et al.*, 2011; Brand and Nicholls, 2011; Divakaruni, Rogers and Murphy, 2014).

2. Full validation of the NEIL3-modified comet assay methodology described within Chapter 2.

In addition to the upregulation of the *Neil3* gene in m*Ogg1*$^{-/-}$ MEFs, we also utilised a novel modified comet assay. Using a similar methodology to hOGG1-modified comet assays, we showed an increase in NEIL3 substrate sites in m*Ogg1*$^{-/-}$ MEFs following BSO treatment. We hypothesise that this increase in NEIL3 substrate sites, which was represented by an increase in tail intensity (%), represents genomic Sp and Gh lesions. However, these lesions should also be detected with a second technique, such as HPLC (Niles, Wishnok and Tannenbaum, 2004; Yu *et al.*, 2005; Cui *et al.*, 2013)

3. Continuing the investigation of RAS-GTPase signalling and the OGG1:8-oxoG signalling complex.

We showed that 8-oxoG treatment resulted in an increase in RAS-GTP in WT MEFs, in agreement with previous studies (Boldogh *et al.*, 2012; German *et al.*, 2013; Hajas *et al.*, 2013; Luo *et al.*, 2014). We were intrigued at the possible consequences of losing this OGG1:8-oxoG induced RAS-GTP signalling, with our initials studies implicating this pathway in cytoskeletal changes. We therefore hypothesise that subtle

differences observed between WT and m*Ogg1*$^{-/-}$ MEFs (*e.g.* morphological differences) could be caused by the lack of this signalling pathway, with these differences never having been linked to the glycosylase activity of OGG1. The downstream effects of these signalling pathways should be further investigated (*e.g.* western blotting) and we are especially interested in actin reorganisation and the formation of stress fibres (Luo *et al.*, 2014).

4. Complementation studies using alternative models

WT and *Ogg1*-null MEFs were used as the primary cellular model throughout this thesis. It would however be beneficial to repeat aspects of this work with alternative cellular models. The simplest method to do this would be to re-express *Ogg1* into the *Ogg1*$^{-/-}$ null MEFS, with similar experiments already performed in the laboratory to result in the Ser-326 and Cys-326 MEFs used within this thesis (*refer to* **2.3.11.**). Alternatively, OGG1 could be knocked down in WT MEFs. One methodology that could be used to achieve this knockdown would be the use of using small interfering RNA (siRNA), which would result in short-term silencing of *Ogg1*. Key end-points measured within this work could then be measured in these cells. This would include intracellular ROS levels, 8-oxoG levels, viability measurements, detection of apoptosis, and the gene of important genes.

5.3. Concluding remarks

Within this thesis, we show the importance of OGG1 in roles that are independent to its glycosylase role in BER. We show that the lack of OGG1 activity results in an induction of apoptosis in m*Ogg1*$^{-/-}$ MEFs in conditions of oxidative stress, although this does not correlate in an accumulation of 8-oxoG within their genome. We also show that this lack of OGG1 activity prevents the activation of RAS GTPases, inhibiting pathways downstream of these pathways, and we implicate this to cytoskeletal changes in m*Ogg1*$^{-/-}$ MEFs. As others before us have suggested, we show that the role of OGG1 within the cell is expansive, and that these non-canonical roles of OGG1 deserve further investigation.

Lastly we propose that two mechanisms are upregulated in m*Ogg1*$^{-/-}$ MEFs, proposing that these mechanisms (NER pathway and NEIL3 glycosylase) prevent the accumulation of genomic 8-oxoG in m*Ogg1*$^{-/-}$ MEFs. Due to the more significant increase in *Neil3* expression when compared to the increase in expression of NER genes (*Ercc1, Ercc4* and *Ercc5*), we propose that this is the major mechanism that prevents this accumulation of 8-oxoG. We hypothesise that due to the low redox potential of 8-oxoG, these lesions in m*Ogg1*$^{-/-}$ MEFs are oxidised to form Sp and Gh lesions, which in turn are repaired *via* NEIL3.

6

References

6. References

Abreu, I. A. and Cabelli, D. E. (2010) Superoxide dismutases: A review of the metal-associated mechanistic variations, *Biochimica et Biophysica Acta - Proteins and Proteomics*, 1804, 263–274.

Aburatani, H. *et al.* (1997) Cloning and characterization of mammalian 8-hydroxyguanine-specific DNA glycosylase/apurinic, apyrimidinic lyase, a functional mutM homologue, *Cancer Research*, 57 (11), 2151–2156.

Aguer, C. *et al.* (2011) Galactose enhances oxidative metabolism and reveals mitochondrial dysfunction in human primary muscle cells, *PLoS ONE*, 6 (12), e28536.

Aguilera-Aguirre, L. *et al.* (2014) Innate inflammation induced by the 8-oxoguanine DNA glycosylase-1-KRAS-NFκB pathway, *The Journal of Immunology*, 193, 4643–4653.

Alexeyev, M. *et al.* (2013) The maintenance of mitochondrial DNA integrity - Critical analysis and update, *Cold Spring Harbor Perspectives in Biology*, 5, 1–17.

Allgayer, J. *et al.* (2016) Widespread transcriptional gene inactivation initiated by a repair intermediate of 8-oxoguanine, *Nucleic Acids Research*, 44 (15), 7267–7280.

Altenhöfer, S. *et al.* (2015) Evolution of NADPH oxidase inhibitors: Selectivity and mechanisms for target engagement, *Antioxidants & Redox Signaling*, 23 (5), 406–427.

Amand, M. M., Hanover, J. A. and Shiloach, J. (2016) A comparison of strategies for immortalizing mouse embryonic fibroblasts, *Journal of Biological Methods*, 3 (2), e41.

Andreoli, C. *et al.* (1999) Processing of DNA damage induced by hydrogen peroxide and methyl methanesulfonate in human lymphocytes: Analysis by alkaline single cell gel electrophoresis and cytogenetic methods, *Mutagenesis*, 14 (5), 497–503.

Antunes, F. and Cadenas, E. (2000) Estimation of H2O2 gradients across biomembranes, *FEBS Letters*, 475 (2), 121–126.

Arai, K. *et al.* (1997) Cloning of a human homolog of the yeast OGG1 gene that is involved in the repair of oxidative DNA damage, *Oncogene*, 14 (23), 2857–2861.

Arai, T. *et al.* (2002) High accumulation of oxidative DNA damage, 8-hydroxyguanine, in Mmh/Ogg1 deficient mice by chronic oxidative stress, *Carcinogenesis*, 23 (12), 2005–2010.

Arai, T. *et al.* (2006) The study using wild-type and Ogg1 knockout mice exposed to potassium bromate shows no tumor induction despite an extensive accumulation of 8-hydroxyguanine in kidney DNA, *Toxicology*, 221, 179–186.

Aubry, J. P. *et al.* (1999) Annexin V used for measuring apoptosis in the early events of cellular cytotoxicity, *Cytometry*, 37 (3), 197–204.

Audebert, M. *et al.* (2000) Alterations of the DNA repair gene OGG1 in human clear cell carcinomas of the kidney, *Cancer Research*, 60 (17), 4740–4744.

Ba, X., Bacsi, A., *et al.* (2014) 8-oxoguanine DNA glycosylase-1 augments proinflammatory gene expression by facilitating the recruitment of site-specific transcription factors, *The Journal of Immunology*, 192, 2384–2394.

Ba, X., Aguilera-Aguirre, L., *et al.* (2014) The role of 8-oxoguanine DNA glycosylase-1 in inflammation, *International Journal of Molecular Sciences*, 15 (9), 16975–16997.

Ba, X. *et al.* (2015) 8-oxoguanine DNA glycosylase-1-driven DNA base excision repair: role in asthma pathogenesis, *Current Opinion in Allergy and Clinical Immunology*, 15 (1), 89–97.

Ba, X. and Boldogh, I. (2018) 8-oxoguanine DNA glycosylase 1: Beyond repair of the oxidatively modified base lesions, *Redox Biology*, 14, 669–678.

Bacsi, A. *et al.* (2007) Increased ROS generation in subsets of OGG1 knockout fibroblast cells, *Mechanisms of Ageing and Development*, 128 (11), 637–649.

Bacsi, A. *et al.* (2013) Down-regulation of 8-oxoguanine DNA glycosylase 1 expression in the airway epithelium ameliorates allergic lung inflammation, *DNA Repair*, 12, 18–26.

Badley, R. A. *et al.* (1980) Cytoskeleton changes in fibroblast adhesion and detachment, *Journal of Cell Science*, 43, 379–390.

Banda, D. M. *et al.* (2017) Repair of 8-oxoG: A mismatches by the MUTYH glycosylase: Mechanism, metals and medicine, *Free Radical Biology and Medicine*, 107, 202–215.

Barnes, D. E. *et al.* (1998) Targeted disruption of the gene encoding DNA ligase IV leads to lethality in embryonic mice, *Current Biology*, 8 (25), 1395–1398.

Barrett, T. E. *et al.* (1998) Crystal structure of a G:T/U mismatch-specific DNA glycosylase: mismatch recognition by complementary-strand interactions, *Cell*, 92, 117–129.

Bartosz, G. (2006) Use of spectroscopic probes for detection of reactive oxygen species, *Clinica Chimica Acta*, 368, 53–76.

Bedard, K. and Krause, K. (2007) The NOX family of ROS-generating NADPH oxidases: Physiology and pathophysiology, *Physiological Reviews*, 87, 245–313.

Benjamani, Y. and Hochberg, Y. (1995) Controlling the false discovery rate : A practical and powerful approach to multiple testing, *Journal of the Royal Statistical Society (Methodological)*, 57 (1), 289–300.

Benjamani, Y., Krieger, A. M. and Yekutieli, D. (2006) Adaptive linear step-up procedures that control the false discovery rate, *Biometrika*, 93 (3), 491–507.

Benz, C. C. and Yau, C. (2008) Ageing, oxidative stress & cancer: Paradigms in parallax, *Nature reviews Cancer*, 8, 875–879.

Bertram, R. *et al.* (2006) A simplified model for mitochondrial ATP production, *Journal of Theoretical Biology*, 243, 575–586.

Bhakat, K. K. *et al.* (2006) Acetylation of human 8-oxoguanine-DNA glycosylase by p300 and its role in 8-oxoguanine repair in vivo, *Molecular and Cellular Biology*, 26 (5), 1654–1665.

Bhattacharya, S. (2015) '*Reactive oxygen species and cellular defense system'*, *Free Radicals in Human Health and Disease*, pp. 17–29. Springer, New Delhi.

Bienert, G. P., Schjoerring, J. K. and Jahn, T. P. (2006) Membrane transport of hydrogen peroxide, *Biochimica et Biophysica Acta*, 1758, 994–1003.

Bjelland, S. and Seeberg, E. (2003) Mutagenicity, toxicity and repair of DNA base damage induced by oxidation, *Mutation Research*, 531, 37–80.

Bjørås, M. *et al.* (1997) Opposite base-dependent reactions of a human base excision repair enzyme on DNA containing 7,8-dihydro-8-oxoguanine and abasic sites, *EMBO Journal*, 16 (20), 6314–6322.

Bjørås, M. *et al.* (2002) Reciprocal "flipping" underlies substrate recognition and catalytic activation by the human 8-oxo-guanine DNA glycosylase, *Journal of Molecular Biology*, 317, 171–177.

Blons, H. *et al.* (1999) Frequent allelic loss at chromosome 3p distinct from genetic alterations of the 8-oxoguanine DNA glycosylase 1 gene in head and neck cancer, *Molecular Carcinogenesis*, 26 (4), 254–260.

Boiteux, S. *et al.* (1990) Homogeneous Escherichia coli FPG protein, *The Journal of Biological Chemistry*, 265 (7), 3916–3922.

Boiteux, S. and Radicella, J. P. (2000) The human OGG1 gene: Structure, functions, and its implication in the process of carcinogenesis, *Archives of Biochemistry and Biophysics*, 377 (1), 1–8.

Boland, C. R. *et al.* (2005) Infection, inflammation, and gastrointestinal cancer, *Gut*, 54, 1321–1331.

Boldogh, I. *et al.* (2012) Activation of Ras signaling pathway by 8-oxoguanine DNA glycosylase bound to its excision product, 8-oxoguanine, *Journal of Biological Chemistry*, 287 (25), 20769–20773.

Bos, J. L., Rehmann, H. and Wittinghofer, A. (2007) GEFs and GAPs: Critical elements in the control of small G proteins, *Cell*, 129, 865–877.

Bowden, N. A. *et al.* (2015) Understanding xeroderma pigmentosum complementation groups using gene expression profiling after UV-light exposure, *International Journal of Molecular Sciences*, 16, 15985–15996.

Bradford, M. M. (1976) A rapid and sensitive method for the quantitation of microgram quantities of protein utilizing the principle of protein-dye binding, *Analytical Biochemistry*, 72, 248–254.

Brand, M. D. and Nicholls, D. G. (2011) Assessing mitochondrial dysfunction in cells, *Biochemical Journal*, 435, 297–312.

Bravard, A. *et al.* (2006) Redox regulation of human OGG1 activity in response to cellular oxidative stress, *Molecular and Cellular Biology*, 26 (20), 7430–7436.

Bravard, A. *et al.* (2009) Oxidation status of human OGG1-S326C polymorphic variant determines cellular DNA repair capacity, *Cancer Research*, 69 (8), 3642–3649.

Bravard, A. *et al.* (2010) Inactivation by oxidation and recruitment into stress granules of hOGG1 but not APE1 in human cells exposed to sub-lethal concentrations of cadmium, *Mutation Research*, 685, 61–69.

Brinkmann, K. *et al.* (2015) Regulation of the DNA damage response by ubiquitin conjugation, *Frontiers in Genetics*, 6, article 98.

Brooks, P. J. *et al.* (2000) The oxidative DNA lesion 8,5'-(S)-cyclo-2'-deoxyadenosine is repaired by the nucleotide excision repair pathway and blocks gene expression in mammalian cells, *Journal of Biological Chemistry*, 275 (29), 22355–22362.

Bruner, S. D., Norman, D. P. G. and Verdine, G. L. (2000) Structural basis for recognition and repair of the endogenous mutagen 8-oxoguanine in DNA, *Nature*, 403 (6772), 859–866.

Byrd, A. S. *et al.* (2004) Effects of glutathione depletion on the viability of human NT2-derived neuronal and astroglial cultures, *Neuron Glia Biology*, 1 (4), 317–326.

Cadet, J. *et al.* (2000) Oxidative base damage to DNA: specificity of base excision repair enzymes, *Mutation Research*, 462, 121–128.

Cadet, J. *et al.* (2012) Biologically relevant oxidants and terminology, classification and nomenclature of oxidatively generated damage to nucleobases and 2-deoxyribose in nucleic acids, *Free Radical Research*, 46 (4), 367–381.

Cadet, J. and Wagner, J. R. (2013) DNA base damage by reactive oxygen species, oxidizing agents, and UV radiation, *Cold Spring Harbor Perspectives in Biology*, 5, a012559.

Campalans, A. *et al.* (2015) Interaction with OGG1 is required for efficient recruitment of XRCC1 to base excision repair and maintenance of genetic stability after exposure to oxidative stress, *Molecular and Cellular Biology*, 35 (9), 1648–1658.

Cardozo-Pelaez, F., Sanchez-Contreras, M. and Nevin, A. B. C. (2012) OGG1 null mice exhibit age-associated loss of the nigrostriatal pathway and increased sensitivity to MPTP, *Neurochemistry International*, 61 (5), 721–730.

Carini, M. *et al.* (2000) Fluorescent probes as markers of oxidative stress in keratinocyte cell lines following UVB exposure, *Il Farmaco*, 55, 526–534.

Castaing, B. *et al.* (1993) Cleavage and binding of a DNA fragment containing a single 8-oxoguanine by wild type and mutant FPG proteins, *Nucleic Acids Research*, 21 (12), 2899–2905.

Chakravarti, B. and Chakravarti, D. N. (2007) Oxidative modification of proteins: Age-related changes, *Gerontology*, 53 (3), 128–39.

Chipman, J. K. *et al.* (1998) DNA oxidation by potassium bromate; a direct mechanism or linked to lipid peroxidation?, *Toxicology*, 126 (2), 93–102.

Cividini, F. *et al.* (2016) O-GlcNAcylation of 8-oxoguanine DNA glycosylase (Ogg1) impairs oxidative mitochondrial DNA lesion repair in diabetic hearts, *Journal of Biological Chemistry*, 291 (51), 26515–26528.

Clayton, D. A., Doda, J. N. and Friedberg, E. C. (1974) The absence of a pyrimidine dimer repair mechanism in mammalian mitochondria, *Proceedings of the National Academy of Sciences of the United States of America*, 71 (7), 2777–2781.

Cleaver, J. E. (1968) Defective repair replication of DNA in xeroderma pigmentosum, *Nature*, 218, 652–656.

Cleaver, J. E. (2005) Cancer in xeroderma pigmentosum and related disorders of DNA repair, *Nature reviews. Cancer*, 5, 564–73.

Cleaver, J. E., Lam, E. T. and Revet, I. (2009) Disorders of nucleotide excision repair: The genetic and molecular basis of heterogeneity, *Nature reviews. Genetics*, 10, 756–768.

Colicelli, J. (2004) Human RAS superfamily proteins and related GTPases, *Science Signalling*, 250, re13.

Collins, A. R. (2014) Measuring oxidative damage to DNA and its repair with the comet assay, *Biochimica et Biophysica Acta*, 1840, 794–800.

Cooke, M. S. *et al.* (2003) Oxidative DNA damage: mechanisms, mutation, and disease, *The FASEB Journal*, 17, 1195–1214.

Cramer, L. P., Siebert, M. and Mitchison, T. J. (1997) Identification of novel graded polarity actin filament bundles in locomoting heart fibroblasts: Implications for the generation of motile force, *Journal of Cell Biology*, 136 (6), 1287–1305.

Crowley, L. C. *et al.* (2016) Quantitation of apoptosis and necrosis by annexin V binding, propidium iodide uptake, and flow cytometry, *Cold Spring Harbor Protocols*, 11, p. 087288.

Cui, L. *et al.* (2013) Comparative analysis of four oxidized guanine lesions from reactions of DNA with peroxynitrite, singlet oxygen, and γ-radiation, *Chemical Research in Toxicology*, 26, 195–202.

D'errico, M. *et al.* (2006) New functions of XPC in the protection of human skin cells from oxidative damage, *The EMBO Journal*, 25, 4305–4315.

Dalhus, B. *et al.* (2011) Separation-of-function mutants unravel the dual-reaction mode of human 8-oxoguanine DNA glycosylase, *Structure*, 19, 117–127.

Dalle-Donne, I. *et al.* (2008) Molecular mechanisms and potential clinical significance of S-glutathionylation, *Antioxidants & Redox Signaling*, 10 (3), 445–474.

Dantzer, F. *et al.* (2002) Human OGG1 undergoes serine phosphorylation and associates with the nuclear matrix and mitotic chromatin in vivo, *Nucleic Acids Research*, 30 (11), 2349–2357.

Dasgupta, J. *et al.* (2006) Manganese superoxide dismutase protects from TNF-alpha induced apoptosis by increasing steady state production of H2O2, *Antioxidants & Redox Signaling*, 8, 7–8.

David, S. S., O'Shea, V. L. and Kundu, S. (2007) Base-excision repair of oxidative DNA damage, *Nature*, 447, 941–950.

Davies, K. J. A. (2001) Degradation of oxidized proteins by the 20S proteasome, *Biochimie*, 83, 301–310.

de Laat, W. L., Jaspers, N. G. J. and Hoeijmakers, J. H. J. (1999) Molecular mechanism of nucleotide excision repair, *Genes & Development*, 13, 768–785.

de Lucca Camargo, L. *et al.* (2013) Endo-PDI is required for TNFα-induced angiogenesis, *Free Radical Biology and Medicine*, 65, 1398–1407.

de Souza-Pinto, N. C. *et al.* (2001) Repair of 8-oxodeoxyguanosine lesions in mitochondrial DNA depends on the oxoguanine DNA glycosylase (OGG1) gene and 8-oxoguanine accumulates in the mitochondrial DNA of OGG1-defective mice, *Cancer Research*, 61, 5378–5381.

Delaney, S. *et al.* (2012) Chemical and biological consequences of oxidatively damaged guanine in DNA, *Free Radical Research*, 46 (4), 420–441.

Devasagayam, T. P. A. *et al.* (2004) Free radicals and antioxidants in human health: current status and future prospects, *Journal of Association of Physicians of India*, 52, 794–804.

Dexheimer, T. S. (2013) DNA repair of cancer stem cells, in Mathews, L. A., Cabarcas, S. M., and Hurt, E. M. (eds) *DNA Repair of Cancer Stem Cells*. Dordrecht: Springer, 19–32.

Dickinson, D. A. and Forman, H. J. (2002) Cellular glutathione and thiols metabolism, *Biochemical Pharmacology*, 64, 1019–1026.

Divakaruni, A. S., Rogers, G. W. and Murphy, A. N. (2014) Measuring mitochondrial function in permeabilized cells using the seahorse XF analyzer or a clark-type oxygen electrode, *Current Protocols in Toxicology*, 60 (1), 25.2.1-25.2.16.

Dodson, M. L., Michaels, M. L. and Lloyd, R. S. (1994) Unified catalytic mechanism for DNA glycosylases, *The Journal of Biological Chemistry*, 269 (52), 32709–32712.

Drew, R. and Miners, J. O. (1984) The effects of buthionine sulphoximine (BSO) on glutathione depletion and xenobiotic biotransformation, *Biochemical Pharmacology*, 33 (19), 2989–2994.

Driessens, N. *et al.* (2009) Hydrogen peroxide induces DNA single- and double-strand breaks in thyroid cells and is therefore a potential mutagen for this organ, *Endocrine-Related Cancer*, 16 (3), 845–856.

Duez, P. *et al.* (2003) Statistics of the comet assay: A key to discriminate between genotoxic effects, *Mutagenesis*, 18 (2), 159–166.

Dulbecco, R. (1949) Reactivation of ultra-violet-inactivated bacteriophage by visible light, *Nature*, 163 (4155), 949–950.

Dušinská, M. *et al.* (2006) Possible involvement of XPA in repair of oxidative DNA damage deduced from analysis of damage, repair and genotype in a human population study, *Mutagenesis*, 21 (3), 205–211.

Dušinská, M. and Collins, A. R. (1996) Detection of oxidised purines and UV-induced photoproducts in DNA of single cells, by inclusion of lesion-specific enzymes in the comet assay, *Alternatives to Laboratory Animals*, 24 (3), 405–411.

Dykens, J. A. and Will, Y. (2007) The significance of mitochondrial toxicity testing in drug development, *Drug Discovery Today*, 12 (17–18), 777–785.

Edgren, M. and Révész, L. (1987) Compartmentalised depletion of glutathione in cells treated with buthionine sulphoximine, *The British Journal of Radiology*, 60 (715), 723–724.

Egert, S. and Rimbach, G. (2011) Which sources of flavonoids: complex diets or dietary supplements?, *Advances in Nutrition*, 2, 8–14.

Eruslanov, E. and Kusmartsev, S. (2010) Identification of ROS using oxidized DCFDA and flow-cytometry, in *Advanced Protocols in Oxidative Stress II. Methods in Molecular Biology*, 57–72.

Esteve, J. M. *et al.* (1999) Oxidative damage to mitochondrial DNA and glutathione oxidation in apoptosis: Studies in vivo and in vitro, *The FASEB Journal*, 13 (9), 1055–1064.

Evans, M. D., Dizdaroglu, M. and Cooke, M. S. (2004) Oxidative DNA damage and disease: Induction, repair and significance, *Mutation Research*, 567, 1–61.

Fadok, V. A. *et al.* (2000) A receptor for phosphatidylserine-specific clearance of apoptotic cells, *Nature*, 405 (6782), 85–90.

Fantini, D. *et al.* (2013) Rapid inactivation and proteasome-mediated degradation of OGG1 contribute to the synergistic effect of hyperthermia on genotoxic treatments, *DNA Repair*, 12 (3), 227–237.

Faucher, F., Doublié, S. and Jia, Z. (2012) 8-oxoguanine DNA glycosylases: One lesion, three subfamilies, *International Journal of Molecular Sciences*, 13, 6711–6729.

Fishel, R. *et al.* (1993) The human mutator gene homolog MSH2 and its association with hereditary nonpolyposis colon cancer, *Cell*, 75, 1027–1038.

Fishel, R. and Wilson, T. (1997) MutS homologs in mammalian cells, *Current Opinion in Genetics and Development*, 7 (1), 105–113.

Fisher, A. B. (2009) Redox signaling across cell membranes, *Antioxidants & Redox Signaling*, 11 (6), 1349–1356.

Fleming, A. M. and Burrows, C. J. (2017) Formation and processing of DNA damage substrates for the hNEIL enzymes, *Free Radical Biology and Medicine*, 107, 35–52.

Fleming, Y. M. *et al.* (2009) TGF-β-mediated activation of RhoA signalling is required for efficient V12HaRas and V600EBRAF transformation, *Oncogene*, 28, 983–993.

Forman, H. J. and Torres, M. (2001) Redox signaling in macrophages, *Molecular Aspects of Medicine*, 22, 189–216.

Forman, H. J., Zhang, H. and Rinna, A. (2009) Glutathione: overview of its protective roles, measurement and biosynthesis, *Molecular Aspects of Medicine*, 30 (1–2)

Fortini, P. *et al.* (1999) The type of DNA glycosylase determines the base excision repair pathway in mammalian cells, *Journal of Biological Chemistry*, 274 (21), 15230–15236.

Foster, S. S. *et al.* (2012) Cell cycle- and DNA repair pathway-specific effects of apoptosis on tumor suppression, *Proceedings of the National Academy of Sciences*, 109 (25), 9953–9958.

Fotouhi, A. *et al.* (2011) Reduction of 8-oxodGTP in the nucleotide pool by hMTH1 leads to reduction in mutations in the human lymphoblastoid cell line TK6 exposed to UVA, *Mutation Research - Fundamental and Molecular Mechanisms of Mutagenesis*, 715, 13–18.

Freitas, A. A. and De Magalhães, J. P. (2011) A review and appraisal of the DNA damage theory of ageing, *Mutation Research - Reviews in Mutation Research*, 728 (1–2), 12–22.

Friedberg, E. C. (2001) How nucleotide excision repair protects against cancer, *Nature reviews. Cancer*, 1, 22–33.

Friedberg, E. C. (2008) A brief history of the DNA repair field, *Cell Research*, 18, 3–7.

Fuhrmann, A. and Engler, A. J. (2015) The cytoskeleton regulates cell attachment strength, *Biophysical Journal*, 109 (1), 57–65.

Fujikawa, K. *et al.* (1999) The oxidized forms of dATP are substrates for the human MutT homologue, the hMTH1 protein, *Journal of Biological Chemistry*, 274 (25), 18201–18205.

Furihata, C. (2015) An active alternative splicing isoform of human mitochondrial 8-oxoguanine DNA glycosylase (OGG1), *Genes and Environment*, 37 (1).

Gaivão, I. *et al.* (2009) Comet assay-based methods for measuring DNA repair *in vitro* ; estimates of inter- and intra-individual variation, *Cell Biology and Toxicology*, 25 (1), 45–52.

Gannett, P. M. and Sura, T. P. (1993) Base Pairing of 8-oxoguanosine and 8-oxo-2'-deoxyguanosine with 2'-deoxyadenosine, 2'-deoxycytosine, 2'-deoxyguanosine, and thymidine, *Chemical Research in Toxicology*, 6 (5), 690–700.

Gaweł, S. *et al.* (2004) Malondialdehyde (MDA) as a lipid peroxidation marker, *Wiadomości Lekarskie*, 57 (9), 453–455.

Gedik, C. M. and Collins, A. (2005) Establishing the background level of base oxidation in human lymphocyte DNA: Results of an interlaboratory validation study, *The FASEB Journal*, 19 (1), 82–84.

German, P. *et al.* (2013) Activation of cellular signaling by 8-oxoguanine DNA glycosylase-1-initiated DNA base excision repair, *DNA Repair*, 12, 856–863.

Gil-Henn, H. *et al.* (2013) Arg/Abl2 promotes invasion and attenuates proliferation of breast cancer in vivo, *Oncogene*, 32, 2622–2630.

Giry, M. *et al.* (1995) Transient expression of RhoA, -B, and -C GTPases in HeLa cells potentiates resistance to Clostridium difficile toxins A and B but not to Clostridium sordellii lethal toxin, *Infection and Immunity*, 63 (10), 4063–4071.

Giustarini, D. *et al.* (2017) Assessment of glutathione/glutathione disulphide ratio and S-glutathionylated proteins in human blood, solid tissues, and cultured cells, *Free Radical Biology and Medicine*, 112, 360–375.

Gomes, A., Fernandes, E. and Lima, J. L. F. C. (2005) Fluorescence probes used for detection of reactive oxygen species, *Journal of Biochemical and Biophysical Methods*, 65, 45–80.

Goode, E. L., Ulrich, C. M. and Potter, J. D. (2002) Polymorphisms in DNA repair genes and associations with cancer risk, *Cancer Epidemiology Biomarkers and Prevention*, 11 (12), 1513–1530.

Gopalakrishnan, K. *et al.* (2010) Hydrogen peroxide induced genomic instability in nucleotide excision repair-deficient lymphoblastoid cells, *Genome Integrity*, 1 (16), 1–14.

Gourlay, C. W. and Ayscough, K. R. (2005a) The actin cytoskeleton: A key regulator of apoptosis and ageing?, *Nature Reviews Molecular Cell Biology*, 6, 583–589.

Gourlay, C. W. and Ayscough, K. R. (2005b) The actin cytoskeleton in ageing and apoptosis, *FEMS Yeast Research*, 5 (12), 1193–1198.

Gredilla, R. (2011) DNA damage and base excision repair in mitochondria and their role in aging, *Journal of Aging Research*, 2011, ID: 257093.

Green, R. M. *et al.* (2006) Subcellular compartmentalization of glutathione: Correlations with parameters of oxidative stress related to genotoxicity, *Mutagenesis*, 21 (6), 383–390.

Green, R. M. *et al.* (2008) Reactive oxygen species from the uncoupling of human cytochrome P450 1B1 may contribute to the carcinogenicity of dioxin-like polychlorinated biphenyls, *Mutagenesis*, 23 (6), 457–463.

Griffith, O. W. (1982) Mechanism of action, metabolism, and toxicity of buthionine sulfoximine and its higher homologs, potent inhibitors of glutathione synthesis, *The Journal of Biological Chemistry*, 257 (22), 13704–13712.

Grollman, A. P. and Moriya, M. (1993) Mutagenesis by 8-oxoguanine: An enemy within, *Trends in Genetics*, 9 (7), 246–249.

Hajas, G. *et al.* (2012) Biochemical identification of a hydroperoxide derivative of the free 8-oxo-7,8-dihydroguanine base, *Free Radical Biology and Medicine*, 52, 749–756.

Hajas, G. *et al.* (2013) 8-oxoguanine DNA glycosylase-1 links DNA repair to cellular signaling via the activation of the small GTPase Rac1, *Free Radical Biology and Medicine*. Elsevier, 61, 384–394.

Hall, D. B., Holmlin, E. and Barton, J. K. (1996) Oxidative DNA damage through long-range electron transfer, *Nature*, 382, 731–735.

Halliwell, B. and Aruoma, O. (1991) DNA damage by oxygen-derived species: Its mechanism and measurement in mammalian systems, *FEBS Letters*, 281 (1–2), 9–19.

Hansen, W. K. and Kelley, M. K. R. (2000) Review of mammalian DNA repair and translational implications, *The Journal of Pharmacology and Experimental Therapeutics*, 295 (1), 1–9.

Hao, W. *et al.* (2020) Enzymatically inactive OGG1 binds to DNA and steers base excision repair toward gene transcription, *FASEB Journal*, 34 (6), 7427–7441.

Hart, G. W. *et al.* (2011) Cross Talk between O-GlcNAcylation and phosphorylation: Roles in signaling, transcription, and chronic disease, *Annual Review of Biochemistry*, 80, 825–858.

Hashiguchi, K. *et al.* (2018) The roles of human MTH1, MTH2 and MTH3 proteins in maintaining genome stability under oxidative stress, *Mutation Research - Fundamental and Molecular Mechanisms of Mutagenesis*, 808, 10–19.

Hašplová, K. *et al.* (2012) DNA alkylation lesions and their repair in human cells: Modification of the comet assay with 3-methyladenine DNA glycosylase (AlkD), *Toxicology Letters*, 208 (1), 76–81.

Hayashi, H. *et al.* (2002) Replication-associated repair of Adenine:8-oxoguanine mispairs by MYH, *Current Biology*, 12 (4), 335–339.

Hegde, V., Wang, M. and Deutsch, W. A. (2004) Human ribosomal protein S3 interacts with DNA base excision repair proteins hAPE/Ref-1 and hOGG1, *Biochemistry*, 43, 14211–14217.

Helleday, T., Eshtad, S. and Nik-Zainal, S. (2014) Mechanisms underlying mutational signatures in human cancers, *Nature reviews. Genetics*, 15 (9), 585–598.

Hempel, N., Carrico, P. M. and Melendez, J. A. (2011) Manganese superoxide dismutase (SOD2) and redox-control of signaling events that drive metastasis, *Anti-cancer Agents in Medicinal Chemistry*, 11 (2), 191–201.

Henderson, P. T. *et al.* (2002) Oxidation of 7,8-dihydro-8-oxoguanine affords lesions that are potent sources of replication errors in vivo, *Biochemistry*, 41, 914–921.

Hess, M. T. *et al.* (1997) Base pair conformation-dependent excision of benzo[a]pyrene diol epoxide-guanine adducts by human nucleotide excision repair enzymes., *Molecular and Cellular Biology*, 17 (12), 7069–7076.

Higgs, E. B. *et al.* (2020) Induction of apoptosis in Ogg1-null mouse embryonic fibroblasts by GSH depletion is independent of DNA damage, *Toxicology Letters*, 332, 27–35.

Hill, J. W. *et al.* (2001) Stimulation of human 8-oxoguanine-DNA glycosylase by AP-endonuclease: Potential coordination of the initial steps in base excision repair, *Nucleic Acids Research*, 29 (2), 430–438.

Hill, J. W. and Evans, M. K. (2006) Dimerization and opposite base-dependent catalytic impairment of polymorphic S326C OGG1 glycosylase, *Nucleic Acids Research*, 34 (5), 1620–1632.

Hislop, K. A. and Bolton, J. R. (1999) The photochemical generation of hydroxyl radicals in the UV-vis/ferrioxalate/H2O2 system, *Environmental Science and Technology*, 33 (18), 3119–3126.

Hissin, P. J. and Hilf, R. (1976) A fluorometric method for determination of oxidized and reduced glutathione in tissues, *Analytical Biochemistry*, 74, 214–226.

Hobbs, G. A. *et al.* (2014) Rho GTPases, oxidation, and cell redox control, *Small GTPases*, 5, p. e28579

Hollander, M. C. *et al.* (2005) Deletion of XPC leads to lung tumors in mice and is associated with early events in human lung carcinogenesis, *Proceedings of the National Academy of Sciences of the United States of America*, 102 (37), 13200–5.

Hooten, N. N. *et al.* (2011) Poly(ADP-ribose) polymerase 1 (PARP-1) binds to 8-oxoguanine-DNA glycosylase (OGG1), *Journal of Biological Chemistry*, 286 (52), 44679–44690.

Houtgraaf, J. H., Versmissen, J. and van der Giessen, W. J. (2006) A concise review of DNA damage checkpoints and repair in mammalian cells, *Cardiovascular Revascularization Medicine*, 7 (3), 165–172.

Hu, J., Imam, S. A., *et al.* (2005) Phosphorylation of human oxoguanine DNA glycosylase (α-OGG1) modulates its function, *Nucleic Acids Research*, 33 (10), 3271–3282.

Hu, J., de Souza-Pinto, N. C., *et al.* (2005) Repair of formamidopyrimidines in DNA involves different glycosylases: role of the OGG1, NTH1, and NEIL1 enzymes, *The Journal of Biological Chemistry*, 280 (49), 40544–40551.

Hu, J. *et al.* (2016) Cisplatin DNA damage and repair maps of the human genome at single-nucleotide resolution, *Proceedings of the National Academy of Sciences of the United States of America*, 113 (41), 11507–11512.

Hughes, J. H. and Parsons, J. L. (2020) The E3 ubiquitin ligase NEDD4L targets OGG1 for ubiquitylation

and modulates the cellular DNA damage response, *Frontiers in Cell and Developmental Biology,* 8, 1341.

Husain, S. R., Cillard, J. and Cillard, P. (1987) Hydroxyl radical scavengin activity of flavinoids, *Phytochemistry*, 26 (9), 2489–2491.

Hussain, R. F., Nouri, A. M. E. and Oliver, R. T. D. (1993) A new approach for measurement of cytotoxicity using colorimetric assay, *Journal of Immunological Methods*, 160, 89–96.

Igarashi, H. *et al.* (1997) Organization and expression of the mouse MTH1 gene for preventing transversion mutation, *Journal of Biological Chemistry*, 272 (6), 3766–3772.

Indo, H. P. *et al.* (2007) Evidence of ROS generation by mitochondria in cells with impaired electron transport chain and mitochondrial DNA damage, *Mitochondrion*, 7, 106–118.

Ishida, T. *et al.* (1999) Structure and chromosome location of human OGG1, *Cytogenetic and Genome Research*, 85 (3–4), 232–236.

Jackson, S. P. and Bartek, J. (2009) The DNA-damage response in human biology and disease, *Nature*. Nature Publishing Group, 461, 1071–1078.

Jeggo, P. A., Pearl, L. H. and Carr, A. M. (2016) DNA repair, genome stability and cancer: A historical perspective., *Nature reviews. Cancer*, 16, 35–42.

Jensen, A. *et al.* (2003) Mammalian 8-oxoguanine DNA glycosylase 1 incises 8-oxoadenine opposite cytosine in nuclei and mitochondria, while a different glycosylase incises 8-oxoadenine opposite guanine in nuclei, *Journal of Biological Chemistry*, 278 (21), 19541–19548.

Ji, H. *et al.* (2016) EGFR phosphorylates FAM129B to promote Ras activation, *Proceedings of the National Academy of Sciences of the United States of America*, 113 (3), 644–649.

Jiricny, J. and Marra, G. (2003) DNA repair defects in colon cancer, *Current Opinion in Genetics and Development*, 13, 61–69.

Kaina, B. (2003) DNA damage-triggered apoptosis: critical role of DNA repair, double-strand breaks, cell proliferation and signaling, *Biochemical Pharmacology*, 66 (8), 1547–1554.

Kalam, M. A. *et al.* (2006) Genetic effects of oxidative DNA damages: Comparative mutagenesis of the imidazole ring-opened formamidopyrimidines (Fapy lesions) and 8-oxo-purines in simian kidney cells, *Nucleic Acids Research*, 34 (8), 2305–2315.

Kamalian, L. *et al.* (2015) The utility of HepG2 cells to identify direct mitochondrial dysfunction in the absence of cell death, *Toxicology in Vitro*, 29 (4), 732–740.

Kane, D. J. *et al.* (1993) Bcl-2 inhibition of neural death: decreased generation of reactive oxygen species, *Science*, 262, 1274–1277.

Kang, D. and Hamasaki, N. (2002) Maintenance of mitochondrial DNA integrity: Repair and degradation, *Current Genetics*, 41 (5), 311–322.

Kang, L. *et al.* (2015) Acetylated 8-oxoguanine DNA glycosylase 1 and its relationship with p300 and SIRT1 in lens epithelium cells from age-related cataract, *Experimental Eye Research*, 135, 102–108.

Kannan, K. and Jain, S. K. (2000) Oxidative stress and apoptosis, *Pathophysiology*, 7 (27), 153–163.

Karpinich, N. O. *et al.* (2002) The course of etoposide-induced apoptosis from damage to DNA and p53 activation to mitochondrial release of cytochrome c, *Journal of Biological Chemistry*, 277 (19), 16547–16552.

Kaur, M. P. *et al.* (2014) Cellular accumulation of Cys326-OGG1 protein complexes under conditions of oxidative stress, *Biochemical and Biophysical Research Communications*, 447, 12–18.

Kelner, A. (1949) Effect of visible light on the recovery of streptomyces griseus conidia from ultra-violet irradiation injury, *Proceedings of the National Academy of Sciences*, 35 (2), 73–79.

Kershaw, R. M. and Hodges, N. J. (2012) Repair of oxidative DNA damage is delayed in the Ser326Cys polymorphic variant of the base excision repair protein OGG1, *Mutagenesis*, 27 (4), 501–510.

Kim, H. S. *et al.* (2015) APE1, the DNA base excision repair protein, regulates the removal of platinum adducts in sensory neuronal cultures by NER, *Mutation Research - Fundamental and Molecular Mechanisms of Mutagenesis*. Elsevier B.V., 779, 96–104.

Kim, Y. and Wilson, D. M. (2012) Overview of base excision repair biochemistry, *Current Molecular Pharmacology*, 5 (1), 3–13.

Klungland, A., Rosewell, I., *et al.* (1999) Accumulation of premutagenic DNA lesions in mice defective in removal of oxidative base damage, *Proceedings of the National Academy of Sciences of the United States of America*, 96 (23), 13300–13305.

Klungland, A., Höss, M., *et al.* (1999) Base excision repair of oxidative DNA damage activated by XPG protein, *Molecular Cell*, 3, 33–42.

Klungland, A. and Bjelland, S. (2007) Oxidative damage to purines in DNA: Role of mammalian Ogg1, *DNA Repair*, 6, 481–488.

Kohen, R. and Nyska, A. (2002) Oxidation of biological systems: Oxidative stress phenomena, antioxidants, redox reactions, and methods for their quantification, *Toxicologic Pathology*, 30 (6), 620–650.

Kohno, T. *et al.* (1998) Genetic polymorphisms and alternative splicing of the hOGG1 gene, that is involved in the repair of 8-hydroxyguanine in damaged DNA, *Oncogene*, 16 (25), 3219–3225.

Kornyushyna, O. and Burrows, C. J. (2003) Effect of the oxidized guanosine lesions spiroiminodihydantoin and guanidinohydantoin on proofreading by Escherichia coli DNA polymerase I (klenow fragment) in different sequence contexts, *Biochemistry*, 42, 13008–13018.

Korolainen, M. A. *et al.* (2006) Oxidative modification of proteins in the frontal cortex of Alzheimer's disease brain, *Neurobiology of Aging*, 27 (1), 42–53.

Kovtun, I. V. and McMurray, C. T. (2007) Crosstalk of DNA glycosylases with pathways other than base excision repair, *DNA Repair*, 6, 517–529.

Kozłowska, A. and Szostak-Wegierek, D. (2014) Flavonoids - food sources and health benefits, *Roczniki Państwowego Zakładu Higieny*, 65 (2), 79–85.

Kreuzer, K. N. (2013) DNA damage responses in prokaryotes: Regulating gene expression, modulating growth patterns, and manipulating replication forks, *Cold Spring Harbor Perspectives in Biology*, 5 (11), a012674.

Krokan, H. E. and Bjørås, M. (2013) Base Excision Repair, *Cold Spring Harb Perspect Biol.*, 5 (4), a012583.

Krokan, H. E., Standal, R. and Slupphaug, G. (1997) DNA glycosylases in the base excision repair of DNA, *Biochemical Journal*, 325, 1–16.

Krokeide, S. Z. *et al.* (2009) Expression and purification of NEIL3, a human DNA glycosylase homolog, *Protein Expression and Purification*, 65 (2), 160–164.

Krokeide, S. Z. *et al.* (2013) Human NEIL3 is mainly a monofunctional DNA glycosylase removing spiroimindiohydantoin and guanidinohydantoin, *DNA Repair*, 12, 1159–1164.

Kryston, T. B. *et al.* (2011) Role of oxidative stress and DNA damage in human carcinogenesis, *Mutation Research - Fundamental and Molecular Mechanisms of Mutagenesis*, 711, 193–201.

Kuiper, J. W. P. *et al.* (2011) Rac regulates PtdInsP 3 signaling and the chemotactic compass through a redox-mediated feedback loop, *Blood*, 118 (23), 6164–6171.

Kuo, F. C. and Sklar, J. (1997) Augmented expression of a human gene for 8-oxoguanine DNA glycosylase (MutM) in B lymphocytes of the dark zone in lymph node germinal centers, *Journal of Experimental Medicine*, 186 (9), 1547–1556.

Kuraoka, I. *et al.* (2000) Removal of oxygen free-radical-induced 5',8-purine cyclodeoxynucleosides from DNA by the nucleotide excision-repair pathway in human cells, *Proceedings of the National Academy of Sciences of the United States of America*, 97 (8), 3832–3837.

Kurdi, M. *et al.* (2012) Depletion of cellular glutathione modulates LIF-induced JAK1-STAT3 signaling in cardiac myocytes, *International Journal of Biochemistry and Cell Biology*. Elsevier Ltd, 44 (12), 2106–2115.

Lambeth, J. D. (2004) NOX enzymes and the biology of reactive oxygen, *Nature Reviews Immunology*, 4 (3), 181–189.

Langie, S. A. S. *et al.* (2006) Development and validation of a modified comet assay to phenotypically assess nucleotide excision repair, *Mutagenesis*, 21 (2), 153–158.

Langie, S. A. S. *et al.* (2007) The role of glutathione in the regulation of nucleotide excision repair during oxidative stress, *Toxicology Letters*, 168, 302–309.

Langie, S. A. S. *et al.* (2010) The effect of oxidative stress on nucleotide-excision repair in colon tissue of newborn piglets, *Mutation Research*, 695, 75–80.

Lee, A. J., Hodges, N. J. and Chipman, J. K. (2005) Interindividual variability in response to sodium dichromate-induced oxidative DNA damage: Role of the Ser326Cys polymorphism in the DNA-repair protein of 8-oxo-7,8-dihydro-2'-deoxyguanosine DNA glycosylase 1, *Cancer Epidemiology Biomarkers and Prevention*, 14 (2), 497–505.

Lee, J., Giordano, S. and Zhang, J. (2012) Autophagy, mitochondria and oxidative stress: Cross-talk and redox signalling, *Biochemical Journal*, 441 (2), 523–540.

Lee, S. J. *et al.* (2013) Regulation of hypoxia-inducible factor 1α (HIF-1α) by lysophosphatidic acid is dependent on interplay between p53 and Krüppel-like factor 5, *Journal of Biological Chemistry*, 288 (35), 25244–25253.

Leon, J. *et al.* (2016) 8-Oxoguanine accumulation in mitochondrial DNA causes mitochondrial dysfunction and impairs neuritogenesis in cultured adult mouse cortical neurons under oxidative conditions, *Scientific Reports*, 6 (22086)

Levine, R. L. and Stadtman, E. R. (2001) Oxidative modification of proteins during aging, *Experimental Gerontology*, 55 (1), 53–69.

Li, G. *et al.* (2012) 8-oxoguanine-DNA glycosylase 1 deficiency modifies allergic airway inflammation by regulating STAT6 and IL-4 in cells and in mice, *Free Radical Biology and Medicine*, 52 (2), 392–401.

Li, G. M. (2008) Mechanisms and functions of DNA mismatch repair, *Cell Research*, 18 (1), 85–98.

Li, N. *et al.* (2020) Cooperation of the NEIL3 and Fanconi anemia/BRCA pathways in interstrand crosslink repair, *Nucleic Acids Research,* 48 (6), 3014–3028

Lieber, M. R. (2010) The mechanism of double-strand DNA break repair by the nonhomologous DNA end joining pathway, *Annual Review of Biochemistry*, 79, 181–211.

Lieber, M. R. and Wilson, T. E. (2010) SnapShot: nonhomologous DNA end joining (NHEJ), *Cell*, 142, 496.

Lindahl, T. and Barnes, D. E. (2000) Repair of endogenous DNA damage, *Cold Spring Harbor Symposia on Quantitative Biology*, 65, 127–133.

Liu, M. *et al.* (2010) The mouse ortholog of NEIL3 is a functional DNA glycosylase in vitro and in vivo, *Proceedings of the National Academy of Sciences of the United States of America*, 107 (11), 4925–4930.

Liu, M. *et al.* (2012) Expression and purification of active mouse and human NEIL3 proteins, *Protein Expression and Purification*, 84 (1), 130–139.

Liu, M., Doublié, S. and Wallace, S. S. (2013) Neil3, the final frontier for the DNA glycosylases that recognize oxidative damage, *Mutation Research - Fundamental and Molecular Mechanisms of Mutagenesis*, 743–744, 4–11.

Liu, P. and Demple, B. (2010) DNA repair in mammalian mitochondria: Much more than we thought?, *Environmental and Molecular Mutagenesis*, 51, 417–426.

Lowry, O. H. *et al.* (1951) Protein measurement with the Folun phenol reagent, *Journal of Biological Chemistry*, 193, 265–275.

Lu, R., Nash, H. M. and Verdine, G. L. (1997) A mammalian DNA repair enzyme that excises oxidatively

damaged guanines maps to a locus frequently lost in lung cancer, *Current biology*, 7 (6), 397–407.

Lu, S. C. (2014) Glutathione Synthesis, *Biochim Biophys Acta*, 1830 (5), 3143–3153.

Luna, L. *et al.* (2005) Dynamic relocalization of hOGG1 during the cell cycle is disrupted in cells harbouring the hOGG1-Cys326 polymorphic variant, *Nucleic Acids Research*, 33 (6), 1813–1824.

Luo, J. *et al.* (2014) 8-oxoguanine DNA glycosylase-1-mediated DNA repair is associated with Rho GTPase activation and α-smooth muscle actin polymerisation, *Free Radical Biology and Medicine*, 73, 430–438.

Mabley, J. G. *et al.* (2004) Potential role for 8-oxoguanine DNA glycosylase in regulating inflammation, *The FASEB Journal*, 19 (2), 290–292.

Maier, C. M. and Chan, P. H. (2002) Role of superoxide dismutases in oxidative damage and neurodegenerative disorders, *The Neuroscientist*, 8 (4), 323–334.

Makino, N. *et al.* (2004) A metabolic model describing the H2O2 elimination by mammalian cells including H2O2 permeation through cytoplasmic and peroxisomal membranes: comparison with experimental data, *Biochimica et Biophysica Acta*, 1673, 149–159.

Manandhar, M., Boulware, K. S. and Wood, R. D. (2015) The ERCC1 and ERCC4 (XPF) genes and gene products, *Gene*, 569 (2), 153–161.

Margolin, Y. *et al.* (2006) Paradoxical hotspots for guanine oxidation by a chemical mediator of inflammation, *Nature Chemical Biology*, 2 (7), 365–366.

Margolis, B. and Skolnik, E. Y. (1994) Activation of Ras by receptor tyrosine kinases, *Journal of the American Society of Nephrology*, 5 (6), 1288–1299.

Marroquin, L. D. *et al.* (2007) Circumventing the crabtree effect: Replacing media glucose with galactose increases susceptibility of HepG2 cells to mitochondrial toxicants, *Toxicological Sciences*, 97 (2), 539–547.

Marsin, S. *et al.* (2003) Role of XRCC1 in the coordination and stimulation of oxidative DNA damage repair initiated by the DNA glycosylase hOGG1, *Journal of Biological Chemistry*, 278 (45), 44068–44074.

Martin, P. R. *et al.* (2017) The Human DNA glycosylases NEIL1 and NEIL3 excise psoralen-induced DNA-DNA cross-links in a four-stranded DNA structure, *Scientific Reports*, 7 (17438), 1–13.

Massart, C. *et al.* (2014) Diphenyleneiodonium, an inhibitor of NOXes and DUOXes, is also an iodide-

specific transporter, *FEBS Open Bio*, 4, 55–59.

McCain, J. (2013) The MAPK (ERK) pathway: Investigational combinations for the treatment of BRAF-mutated metastatic melanoma, *Pharmacy and therapeutics*, 38 (2), 96–108.

Meisenberg, C. *et al.* (2012) Ubiquitin ligase UBR3 regulates cellular levels of the essential DNA repair protein APE1 and is required for genome stability, *Nucleic Acids Research*, 40(2), 701–711.

Miao, F. *et al.* (2000) 3-Methyladenine-DNA glycosylase (MPG protein) interacts with human RAD23 proteins, *The Journal of Biological Chemistry*, 275(37), 28433–28438.

Michaels, M. L. *et al.* (1991) Mutm, a protein that prevents G C→T A transversions, is formamidopyrimidine-DNA glycosylase, *Nucleic Acids Research*, 19 (13), 3629–3632.

Michiels, C. *et al.* (1994) Importance of Se-glutathione peroxidase, catalase, and Cu/Zn-SOD for cell survival against oxidative stress, *Free Radical Biology and Medicine*, 17 (3), 235–248.

Minowa, O. *et al.* (2000) Mmh/Ogg1 gene inactivation results in accumulation of 8-hydroxyguanine in mice, *Proceedings of the National Academy of Sciences*, 97 (8), 4156–4161.

Mirbahai, L. *et al.* (2010) Use of a molecular beacon to track the activity of base excision repair protein OGG1 in live cells, *DNA Repair*, 9 (2), 144–152.

Mol, C. D. *et al.* (1995) Crystal structure and mutational analysis of human uracil-DNA glycosylase: Structural basis for specificity and catalysis, *Cell*, 80, 869–878.

Moosmann, B. and Behl, C. (2002) Antioxidants as treatment for neurodegenerative disorders, *Expert Opinion on Investigational Drugs*, 11 (10), 1407–1435.

Morland, I. *et al.* (2002) Human DNA glycosylases of the bacterial Fpg/MutM superfamily: an alternative pathway for the repair of 8-oxoguanine and other oxidation products in DNA, *Nucleic Acids Research*, 30 (22), 4926–4936.

Morreall, J. *et al.* (2015) Inactivation of a common OGG1 variant by TNF-alpha in mammalian cells, *DNA Repair*, 26, 15–22.

Mosteller, R. D., Han, J. and Broek, D. (1994) Identification of residues of the H-Ras protein critical for functional interaction with guaninine nucleotide exchange factors, *Molecular and Celluar Biology*, 14 (2), 1104–1112.

Mukhopadhyay, P. *et al.* (2007) Simple quantitative detection of mitochondrial superoxide production in live cells, *Biochemical and Biophysical Research Communications*, 358 (1), 203–208.

Murphy, M. P. (2009) How mitochondria produce reactive oxygen species, *Biochemical Journal*, 417 (1), 1–13.

Nagase, M. *et al.* (2012) Oxidative stress causes mineralocorticoid receptor activation in rat cardiomyocytes: Role of small GTPase Rac1, *Hypertension*, 59 (2), 500–506.

Nakabeppu, Y. (2001) Molecular genetics and structural biology of human MutT homolog, MTH1, *Mutation Research - Fundamental and Molecular Mechanisms of Mutagenesis*, 477 (1–2), 59–70.

Nash, H. M. *et al.* (1996) Cloning of a yeast 8-oxoguanine DNA glycosylase reveals the existence of a base-excision DNA-repair protein superfamily, *Current Biology*, 6 (8), 968–980.

Naumanen, P., Lappalainen, P. and Hotulainen, P. (2008) Mechanisms of actin stress fibre assembly, *Journal of Microscopy*, 231 (3), 446–454.

Nicolson, G. L. (2014) Mitochondrial dysfunction and chronic disease: Treatment with natural supplements, *Integrative Medicine*, 13 (4), 35–43.

Niles, J. C., Wishnok, J. S. and Tannenbaum, S. R. (2004) Spiroiminodihydantoin and guanidinohydantoin are the dominant products of 8-oxoguanosine oxidation at low fluxes of peroxynitrite: Mechanistic studies with (18)O, *Chemical Research in Toxicology*, 17, 1510–1519.

Norabuena, E. M. *et al.* (2016) Effect of the spiroiminodihydantoin lesion on nucleosome stability and positioning, *Biochemistry*, 55, 2411–2421.

Norbury, C. J. and Zhivotovsky, B. (2004) DNA-damage-induced apoptosis, *Oncogene*, 23, 2797–2808.

Nusrat, A. *et al.* (1995) Rho protein regulates tight junctions and perijunctional actin organization in polarized epithelia, *Proceedings of the National Academy of Sciences of the United States of America*, 92, 10629–10633.

O'Byrne, D. J. *et al.* (2002) Comparison of the antioxidant effects of Concord grape juice flavonoids and α-tocopherol on markers of oxidative stress in healthy adults, *The American Journal of Clinical Nutrition*, 76, 1367–1374.

O'Donovan, A. *et al.* (1994) XPG endonuclease makes the 3' incision in human DNA nucleotide excision repair, *Nature*, 371(6496), 432–435.

Ohkawa, H., Ohishi, N. and Yagi, K. (1979) Assay for lipid peroxides in animal tissues by thiobarbituric acid reaction, *Analytical Biochemistry*, 95 (2), 351–358.

Osterod, M. *et al.* (2001) Age-related and tissue-specific accumulation of oxidative DNA base damage in 7,8-dihydro-8-oxoguanine-DNA glycosylase (Ogg1) deficient mice, *Carcinogenesis*, 22 (9), 1459–1463.

Pal, R. *et al.* (2015) CUX2 protein functions as an accessory factor in the repair of oxidative DNA damage, *Journal of Biological Chemistry*, 290 (37), 22520–22531.

Paleček, E. and Bartošík, M. (2012) Electrochemistry of nucleic acids, *Chemical Reviews*, 112, 3427–3481.

Pan, L. *et al.* (2016) Oxidized guanine base lesions function in 8-oxoguanine DNA glycosylase-1-mediated epigenetic regulation of nuclear factor κB-driven gene expression, *Journal of Biological Chemistry*, 291 (49), 25553–25566.

Pandita, T. K. (2014) Unraveling the novel function of the DNA repair enzyme 8-oxogunaine-DNA glycosylase in activating key signalling pathways, *Free Radical Biology and Medicine*, 73, 439–440.

Parsons, J. L. *et al.* (2008) CHIP-mediated degradation and DNA damage-dependent stabilization regulate base excision repair proteins, *Molecular Cell*, 29 (4), 477–487.

Parsons, J. L. *et al.* (2009) Ubiquitin ligase ARF-BP1/Mule modulates base excision repair, *EMBO Journal*, 28 (2009), 3207–3215.

Percy, M. E. (1984) Catalase: an old enzyme with a new role?, *Canadian Journal of Biochemistry and Cell Biology*, 62 (10), 1006–1014.

Phaniendra, A., Jestadi, D. B. and Periyasamy, L. (2015) Free radicals: properties, sources, targets, and their implication in various diseases, *Indian Journal of Clinical Biochemistry*, 30 (1), 11–26.

Politi, A. *et al.* (2005) Mathematical modeling of nucleotide excision repair reveals efficiency of sequential assembly strategies, *Molecular Cell*, 19 (5), 679–690.

Pommier, Y. *et al.* (2004) Apoptosis defects and chemotherapy resistance: molecular interaction maps and networks, *Oncogene*, 23, 2934–2949.

Poulsen, H. E. *et al.* (2014) Detection and interpretation of 8-oxodG and 8-oxoGua in urine, plasma and cerebrospinal fluid, *Biochimica et Biophysica Acta*, 1840, 801–808.

Priestley, C. C. *et al.* (2010) Anomalous genotoxic responses induced in mouse lymphoma L5178Y cells by potassium bromate, *Toxicology*. Elsevier Ireland Ltd, 267, 45–53.

Raghavamenon, A. *et al.* (2009) α-Tocopherol is ineffective in preventing the decomposition of preformed lipid peroxides and may promote the accumulation of toxic aldehydes: A potential explanation for the failure of antioxidants to affect human atherosclerosis, *Antioxidants & Redox Signaling*, 11 (6), 1237–1248.

Ramdzan, Z. M. *et al.* (2017) The DNA repair function of CUX1 contributes to radioresistance, *Oncotarget*, 8 (12), 19021–19038.

Ray, P. D., Huang, B. and Tsuji, Y. (2012) Reactive oxygen species (ROS) homeostasis and redox regulation in cellular signaling., *Cellular signalling*, 24 (5), 981–90.

Reardon, J. T. *et al.* (1997) In vitro repair of oxidative DNA damage by human nucleotide excision repair system: Possible explanation for neurodegeneration in Xeroderma pigmentosum patients, *Proceedings of the National Academy of Sciences of the United States of America*, 94, 9463–9468.

Ricci, C. *et al.* (2008) Mitochondrial DNA damage triggers mitochondrial-superoxide generation and apoptosis, *American Journal of Physiology - Cell Physiology*, 294 (2), 413–422.

Rimel, J. K. and Taatjes, D. J. (2018) The essential and multifunctional TFIIH complex, *Protein Science*, 27, 1018–1037.

Rizzo, A. M. *et al.* (2010) Endogenous Antioxidants and Radical Scavengers, in Giardi, M. T., Rea, G., and Berra, Bruno (eds) *Advances in Experimental Medicine and Biology (Vol. 698)*. Boston, MA: Springer US, 52–67.

Robertson, A. B. *et al.* (2009) Base excision repair: The long and short of it, *Cellular and Molecular Life Sciences*, 66 (6), 981–993.

Rojas, A. M. *et al.* (2012) The Ras protein superfamily: Evolutionary tree and role of conserved amino acids, *Journal of Cell Biology*, 196 (2), 189–201.

Romanowska, M. *et al.* (2007) DNA damage, superoxide, and mutant K-ras in human lung adenocarcinoma cells, *Free Radical Biology and Medicine*, 43, 1145–1155.

Roos, W. P. and Kaina, B. (2006) DNA damage-induced cell death by apoptosis, *Trends in molecular*

medicine, 12 (9), 440–50.

Roos, W. P. and Kaina, B. (2013) DNA damage-induced cell death: From specific DNA lesions to the DNA damage response and apoptosis, *Cancer Letters*. Elsevier Ireland Ltd, 332 (2), 237–248.

Rossi, R. *et al.* (2006) Oxidized forms of glutathione in peripheral blood as biomarkers of oxidative stress, *Clinical Chemistry*, 52 (7), 1406–1414.

Roth, V. (2006) *Doubling time computing*. *Available at:* www.doubling-time.com/compute.php.

Roychoudhury, S. *et al.* (2017) Human apurinic/apyrimidinic endonuclease (APE1) is acetylated at DNA damage sites in chromatin, and acetylation modulates its DNA repair activity, *Molecular and Celluar Biology*, 37 (6), e00401–e00416.

Ruchko, M. *et al.* (2005) Mitochondrial DNA damage triggers mitochondrial dysfunction and apoptosis in oxidant-challenged lung endothelial cells, *American Journal of Physiology - Lung Cellular and Molecular Physiology*, 288 (3), L530–L535.

Russo, M, T. *et al.* (2004) Accumulation of the oxidative base lesion 8-hydroxyguanine in DNA of tumor-prone mice defective in both the Myh and Ogg1 DNA glycosylases, *Cancer Research*, 64 (13), 4411–4414.

Sahai, E. and Marshall, C. J. (2002) Rho-GTPases and cancer, *Nature Reviews Cancer*, 2, 133–142.

Saitoh, T. *et al.* (2001) Enhancement of OGG1 protein AP lyase activity by increase of APEX protein, *Mutation Research*, 486, 31–40.

Sakumi, K. *et al.* (1993) Cloning and expression of cDNA for a human enzyme that hydrolyzes 8-Oxo-dGTP, a mutagenic substrate for DNA synthesis, *Journal of Biological Chemistry*, 268 (31), 23524–23530.

Sakumi, K. *et al.* (2003) Ogg1 knockout-associated lung tumorigenesis and its suppression by Mth1 gene disruption, *Cancer Research*, 63, 902–905.

Sampath, H. *et al.* (2012) 8-Oxoguanine DNA Glycosylase (OGG1) Deficiency Increases Susceptibility to Obesity and Metabolic Dysfunction, *PLoS ONE*, 7 (12), e51697.

Sampath, H. and Lloyd, R. S. (2019) Roles of OGG1 in transcriptional regulation and maintenance of metabolic homeostasis, *DNA Repair*. Elsevier, 81, 102667.

Saotome, K., Morita, H. and Umeda, M. (1989) Cytotoxicity test with simplified crystal violet staining method using microtitre plates and its application to injection drugs, *Toxicology in Vitro*, 3 (4), 317–321.

Sato, K. *et al.* (1992) Hydroxyl radical production by H2O2 plus Cu,Zn-superoxide dismutase reflects the activity of free copper released from the oxidatively damaged enzyme, *Journal of Biological Chemistry*, 267 (35), 25371–25377.

Sattler, U. *et al.* (2003) Long-patch DNA repair synthesis during base excision repair in mammalian cells., *EMBO reports*, 4 (4), 363–367.

Schärer, O. D. (2013) Nucleotide excision repair in Eukaryotes, *Cold Spring Harbor Perspectives in Biology*, 5 (10), 1–19.

Seifermann, M. and Epe, B. (2017) Oxidatively generated base modifications in DNA: not only carcinogenic risk factor but also regulatory mark?, *Free Radical Biology and Medicine*. Elsevier B.V., 107, 258–265.

Sekiguchi, T. *et al.* (2013) Elimination and utilization of oxidized guanine nucleotides in the synthesis of RNA and its precursors, *Journal of Biological Chemistry*, 288 (12), 8128–8135.

Sen, S. and Kumar, S. (2009) Cell-matrix de-adhesion dynamics reflect contractile mechanics, *Cellular and Molecular Bioengineering*, 2 (2), 218–230.

Shabalina, S. A. and Spiridonov, N. A. (2004) The mammalian transcriptome and the function of non-coding DNA sequences, *Genome Biology*, 5 (4), p. 105.

Shigenaga, M. K., Gimeno, C. J. and Ames, B. N. (1989) Urinary 8-hydroxy-2'-deoxyguanosine as a biological marker of in vivo oxidative DNA damage, *Proceedings of the National Academy of Sciences of the United States of America*, 86, 9697–9701.

Shimizu, Y. *et al.* (2003) Xeroderma pigmentosum group C protein interacts physically and functionally with thymine DNA glycosylase, *The EMBO journal*, 22 (1), 164–173.

Shringarpure, R. *et al.* (2003) Ubiquitin conjugation is not required for the degradation of oxidized proteins by proteasome, *Journal of Biological Chemistry*, 278 (1), 311–318.

Shringarpure, R. and Davies, K. J. A. (2002) Protein turnover by the proteasome in aging and disease, *Free Radical Biology and Medicine*, 32 (11), 1084–1089.

Sidorenko, V. S. *et al.* (2009) Substrate specificity and excision kinetics of natural polymorphic variants and phosphomimetic mutants of human 8-oxoguanine-DNA glycosylase, *FEBS Journal*, 276 (18), 5149–5162.

Sies, H. (1991) Oxidative stress: From basic research to clinical application, *The American Journal of Medicine*, 91, 31–38.

Sies, H. (2015) Oxidative stress: A concept in redox biology and medicine, *Redox Biology*, 4, 180–183.

Singh, N. P. *et al.* (1988) A simple technique for quantitation of low levels of DNA damage in individual cells, *Experimental Cell Research*, 175, 184–191.

Singh, R. P., Sharad, S. and Kapur, S. (2004) Free Radicals and Oxidative Stress in Neurodegenerative Diseases: Relevance of dietary antioxidants, *Journal Indian Acedemy of Clinical Medicine*, 5 (3), 218–225.

Sinha, R. P. and Häder, D. (2002) UV-induced DNA damage and repair: A review, *Photochemical & Photobiological Sciences*, 1 (4), 225–236.

Slupphaug, G., Kavli, B. and Krokan, H. E. (2003) The interacting pathways for prevention and repair of oxidative DNA damage, *Mutation Research*, 531, 231–251.

Smart, D. J., Chipman, J. K. and Hodges, N. J. (2006) Activity of OGG1 variants in the repair of pro-oxidant-induced 8-oxo-2'-deoxyguanosine, *DNA Repair*, 5, 1337–1345.

Smith, C. C., O'Donovan, M. R. and Martin, E. A. (2006) hOGG1 recognizes oxidative damage using the comet assay with greater specificity than FPG or ENDOIII, *Mutagenesis*, 21 (3), 185–190.

Soza, S. *et al.* (2009) DNA ligase I deficiency leads to replication-dependent DNA damage and impacts cell morphology without blocking cell cycle progression, *Molecular and Cellular Biology*, 29 (8), 2032–2041.

Speit, G. *et al.* (2004) Sensitivity of the FPG protein towards alkylation damage in the comet assay, *Toxicology Letters*, 146 (2), 151–158.

Speit, G. *et al.* (2013) Further investigations on the modified comet assay for measuring aphidicolin-block nucleotide excision repair, *Mutagenesis*, 28 (2), 145–151.

Spencer, D. H., Zhang, B. and Pfeifer, J. (2015) *Single nucleotide variant detection using next generation sequencing*. 1st edn, *Clinical Genomics*. 1st edn. Edited by S. Kulkarni and J. Pfeifer. Elsevier Inc.

Sugimura, H. *et al.* (1999) hOGG1 Ser326Cys polymorphism and lung cancer susceptibility, *Cancer Epidemiology Biomarkers and Prevention*, 8 (8), 669–674.

Suzuki, T. and Ohshima, H. (2002) Nicotine-modulated formation of spiroiminodihydantoin nucleoside

via 8-oxo-7,8-dihydro-2'-deoxyguanosine in 2'-deoxyguanosine-hypochlorous acid reaction, *FEBS Letters*, 516, 67–70.

Swiss, R. and Will, Y. (2011) Assessment of mitochondrial toxicity in HepG2 cells cultured in high-glucose or galactose-containing media, *Current Protocols in Toxicology*, (Supplement 49), 1–14.

Takao, M. *et al.* (2002) Novel nuclear and mitochondrial glycosylases revealed by disruption of the mouse Nth1 gene encoding an endonuclease III homolog for repair of thymine glycols, *EMBO Journal*, 21 (13), 3486–3493.

Takao, M. *et al.* (2009) Human Nei-like protein NEIL3 has AP lyase activity specific for single-stranded DNA and confers oxidative stress resistance in Escherichia coli mutant, *Genes to Cells*, 14, 261–270.

Terry, N. H. A. *et al.* (1991) Evaluation of flow cytometric methods for determining population potential doubling times using cultured cells, *Cytometry*, 12 (3), 234–241.

Thannickal, V. J. and Fanburg, B. L. (2000) Reactive oxygen species in cell signaling, *American Journal of Physiology*, 279, L1005–L1028.

Thompson, L. H. (2012) Recognition, signaling, and repair of DNA double-strand breaks produced by ionizing radiation in mammalian cells: The molecular choreography, *Mutation Research*. Elsevier B.V., 751 (2), 158–246.

Todaro, G. J. and Green, H. (1963) Quantitative studies of the growth of mouse embryo cells in culture and their development into established lines., *The Journal of cell biology*, 17 (6), 299–313.

Tojkander, S., Gateva, G. and Lappalainen, P. (2012) Actin stress fibers - assembly, dynamics and biological roles, *Journal of Cell Science*, 125 (8), 1855–1864.

Tokiwa, T. *et al.* (1979) Mechanism of cell dissociation with trypsin and EDTA, *Acta Med Okayama*, 33 (1), 1–4.

Torrao, R. B. D. C. *et al.* (2013) Healthy ageing and depletion of intracellular glutathione influences T cell membrane thioredoxin-1 levels and cytokine secretion, *Chemistry Central Journal*, 7 (150), 1–10.

Tsuzuki, T. *et al.* (2001) Spontaneous tumorigenesis in mice defective in the MTH1 gene encoding 8-oxo-dGTPase., *Proceedings of the National Academy of Sciences of the United States of America*, 98 (20), 11456–61.

Tubbs, A. and Nussenzweig, A. (2017) Endogenous DNA Damage as a source of genomic instability in

cancer, *Cell*, 168 (4), 644–656.

Tudek, B. *et al.* (2017) Lipid peroxidation in face of DNA damage, DNA repair and other cellular processes, *Free Radical Biology and Medicine*, 107, 77–89.

Valverde, M. *et al.* (2018) Hydrogen peroxide-induced DNA damage and repair through the differentiation of human adipose-derived mesenchymal stem cells, *Stem Cells International*.

van Buul, J. D., Geerts, D. and Huveneers, S. (2014) Rho GAPs and GEFs: Controling switches in endothelial cell adhesion, *Cell Adhesion and Migration*, 8 (2), 108–124.

van Dyk, E. *et al.* (2010) Hereditary tyrosinemia type 1 metabolites impair DNA excision repair pathways, *Biochemical and Biophysical Research Communications*, 401 (1), 32–36.

van der Kemp, P. A. *et al.* (1996) Cloning and expression in Escherichia coli of the OGG1 gene of Saccharomyces cerevisiae, which codes for a DNA glycosylase, *Proceedings of the National Academy of Sciences*, 93, 5197–5202.

van der Klift, H. *et al.* (2005) Molecular characterization of the spectrum of genomic deletions in the mismatch repair genes MSH2, MLH1, MSH6, and PMS2 responsible for hereditary nonpolyposis colorectal cancer (HNPCC), *Genes Chromosomes and Cancer*, 44 (2), 123–138.

Vermes, I. *et al.* (1995) A novel assay for apoptosis flow cytometric detection of phosphatidylserine expression on early apoptotic cells using fluorescein labelled Annexin V, *Journal of Immunological Methods*, 184 (1), 39–51.

Vivekananthan, D. P. *et al.* (2003) Use of antioxidant vitamins for the prevention of cardiovascular disease: Meta-analysis of randomised trials, *Lancet*, 361, 2017–2023.

Vogel, K. G. (1978) Effects of hyaluronidase, trypsin, and EDTA on surface composition and topography during detachment of cells in culture, *Experimental Cell Research*, 113 (2), 345–357.

Wallace, D. C. (2001) A mitochondrial paradigm for degenerative diseases and ageing, *Novartis Foundation Symposia*, 235, 248–267.

Wang, D., Kreutzer, D. A. and Essigmann, J. M. (1998) Mutagenicity and repair of oxidative DNA damage: Insights from studies using defined lesions, *Mutation Research - Fundamental and Molecular Mechanisms of Mutagenesis*, 400 (1–2), 99–115.

Wang, W. *et al.* (2017) Hexokinase 2 enhances the metastatic potential of tongue squamous cell

carcinoma via the SOD2-H2O2 pathway, *Oncotarget*, 8 (2), 3344–3354.

Wang, Z., Gucek, M. and Hart, G. W. (2008) Cross-talk between GlcNAcylation and phosphorylation: Site-specific phosphorylation dynamics in response to globally elevated O-GlcNAc, *Proceedings of the National Academy of Sciences of the United States of America*, 105 (37), 13793–13798.

Weiss, J. M. *et al.* (2005) Polymorphic variation in hOGG1 and risk of cancer: A review of the functional and epidemiologic literature, *Molecular Carcinogenesis*, 42 (3), 127–141.

Wennerberg, K., Rossman, K. . and Der, C. . (2005) The RAS superfamily at a glance, *Journal of Cell Science*, 118 (5), 843–846.

Wheeler, A. P. and Ridley, A. J. (2004) Why three Rho proteins? RhoA, RhoB, RhoC, and cell motility, *Experimental Cell Research*, 301, 43–49.

Wiederholt, C. J. and Greenberg, M. M. (2002) FapydG instructs klenow exo- to misincorporate deoxyadenosine, *Journal of the American Chemical Society*, 124 (25), 7278–7279.

Winterbourn, C. C. (1981) Production of hydroxyl radicals from paraquat radicals and H2O2, *FEBS Letters*, 128 (2), 339–342.

Wood, R. *et al.* (2001) Human DNA repair genes, *Science*, 291, 1284–1289.

Wood, R. D. (1997) Nucleotide excision repair in mammalian cells, *Journal of Biological Chemistry*, 272 (38), 23465–8.

Woods, D. and Turchi, J. J. (2013) Chemotherapy induced DNA damage response: Convergence of drugs and pathways, *Cancer Biology and Therapy*, 14 (5), 379–389.

Wu, L. L. *et al.* (2004) Urinary 8-OHdG: A marker of oxidative stress to DNA and a risk factor for cancer, atherosclerosis and diabetics, *Clinica Chimica Acta*, 339, 1–9.

Wu, Y. *et al.* (2019) Generating viable mice with heritable embryonically lethal mutations using the CRISPR-Cas9 system in two-cell embryos, *Nature Communications*, 10 (2883), 1–13.

Xing, D. *et al.* (2001) Ser326Cys polymorphism in hOGG1 gene and risk of esophageal cancer in a chinese population, *International Journal of Cancer*, 95 (3), 140–143.

Yakes, F. M. and Van Houten, B. (1997) Mitochondrial DNA damage is more extensive and persists longer

than nuclear DNA damage in human cells following oxidative stress, *Proceedings of the National Academy of Sciences of the United States of America*, 94, 514–9.

Yamagata, Y. *et al.* (1996) Three-dimensional structure of a DNA repair enzyme, 3-methyladenine DNA glycosylase II, from Escherichia coli, *Cell*, 86, 311–319.

Yamane, A. *et al.* (2004) Differential ability of polymorphic OGG1 proteins to suppress mutagenesis induced by 8-hydroxyguanine in human cell in vivo, *Carcinogenesis*, 25 (9), 1689–1694.

Yoshihara, M. *et al.* (2014) Genome-wide profiling of 8-oxoguanine reveals its association with spatial positioning in nucleus, *DNA Research*, 21 (6), 603–612.

Yu, H. *et al.* (2005) Quantitation of four guanine oxidation products from reaction of DNA with varying doses of peroxynitrite, *Chemical Research in Toxicology*, 18, 1849–1857.

Yuan, Y. *et al.* (2012) Predicting the lethal phenotype of the knockout mouse by integrating comprehensive genomic data, *Bioinformatics*, 28 (9), 1246–1252.

Yusuf, B. *et al.* (2013) Embryonic fibroblasts represent a connecting link between mesenchymal and embryonic stem cells, *Development Growth and Differentiation*, 55 (3), 330–340.

Yuzefovych, L. V. *et al.* (2013) Mitochondrial DNA damage and dysfunction, and oxidative stress are associated with endoplasmic reticulum stress, protein degradation and apoptosis in high fat diet-induced insulin resistance mice, *PLoS ONE*, 8 (e54509), 1–8.

Zelko, I. N., Mariani, T. J. and Folz, R. J. (2002) Superoxide disumutase multigene family: A comparison of the CuZn-SOD (SOD1), Mn-SOD (SOD2), and EC-SOD (SOD3) gene structures, evolution and expression, *Free Radical Biology and Medicine*, 33 (3), 337–349.

Zepp, R. G., Faust, B. C. and Jürg, H. (1992) Hydroxyl radical formation in aqueous reactions (pH 3-8) of Iron(II) with hydrogen peroxide: The photo-Fenton reaction, *Environmental Science and Technology*, 26 (2), 313–319.

Zielinska, A. *et al.* (2011) Direct visualization of repair of oxidative damage by OGG1 in the nuclei of live cells, *Journal of Biochemical and Molecular Toxicology*, 25 (1), 1–7.

Zitka, O. *et al.* (2012) Redox status expressed as GSH:GSSG ratio as a marker for oxidative stress in paediatric tumour patients, *Oncology Letters*, 4, 1247–1253.

Zwicker, J. I., Proffitt, R. T. and Reynolds, C. P. (1995) A microcomputer program for calculating cell population doubling time in vitro and in vivo, *Cancer Chemotherapy and Pharmacology*, 37 (3), 203–210.

7

Appendix

7.1. Supplementary methods and materials

7.1.1. Cell culture

Passaging of cells

When cells reached confluence, they were passaged and cells were seeded at a suitable density which would maintain exponential growth. The existing media was removed and cells were briefly washed with PBS or Hank's balanced salt solution (HBSS). Trypsin-EDTA (0.05 %) (Gibco, ThermoFisher Scientific: catalogue no. 25300054) was added to the cells and incubated until all cells had entirely detached from the surface of the flask. Trypsin-EDTA was inactivated via the addition of supplemented DMEM and the cell suspension thoroughly resuspended to ensure a single cell suspension. The suspension was centrifuged (1500 rpm, 10 min) and the resulting supernatant removed from the cells. The pellet was resuspended in supplemented media and a suitable volume transferred into a sterile T_{75} flask (Nunc, ThermoFisher Scientific, or, CELLSTAR®, Greiner Bio-One International). The volume of suspension transferred was dependent on the split desired. The newly passaged MEFs were again incubated and frequently assessed until cells once again reached confluence. Both WT and m*Ogg1*$^{-/-}$ MEFs were passaged 2-3 times a week.

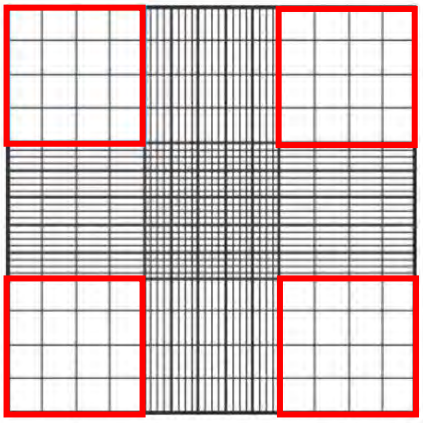
Cryopreservation of cells

Once MEFs had been established in culture, a sample of cell suspension was cryopreserved for future use. Confluent cells were passaged as described above, however the pellet was instead resuspended in media suitable for long-term liquid nitrogen storage. Freezing media consisted of FBS containing 10% (v/v) sterile DMSO, with the addition of DMSO preventing the formation of crystals. The cell suspension was transferred to a 1 mL cryovial (Nalgene™, ThermoFisher Scientific: catalogue no. 5000-1012) and placed in a Mr. Frosty™ freezing container (ThermoFisher Scientific) containing isopropyl alcohol. The

cells were stored in the isopropyl at -80°C for a minimum of 24-hours before being transferred to liquid nitrogen for long-term storage.

Seeding cells

Cells were regularly seeded at suitable densities in suitable tissue-culture vessels. All plasticware was purchased from Corning Costar™ or Greiner Bio-one International. Cells were counted using a haemocytometer, which allowed the number of cells per ml to be calculated, see Equation **6.** This allowed a suitable stock solution of cells to be made, and appropriate volumes of this solution were then transferred to appropriate vessels to give the required cell density.



Equation 6 |

$$\boldsymbol{cell\ count} = \frac{no.of\ cells\ counted\ in\ four\ quadrants}{4}$$

$$\boldsymbol{cells/_{ml}} = average\ cell\ no.\ \times 10^4$$

Mycoplasma testing

All cells were regularly tested for the presence of mycoplasma using the commercial EZ-PCR™ mycoplasma detection kit (Biological Industries: catalogue no. 20-700-20). A sample of supernatant was removed from cells and briefly centrifuged (250 g) to pellet any cellular debris in the sample. The supernatant was transferred to a sterile Eppendorf and centrifuged (20,000 g, 10 min) resulting in the sedimentation of mycoplasma bacteria if present. The supernatant was carefully discarded and the pellet, which was not necessarily visible, resuspended in the supplied buffer. All samples were subsequently heated (95°C, three min). The PCR reaction mixes were prepared: 17.5 μL H_2O, 5 μL reaction mix

(Biological Industries), and 2.5 μL test sample. These reactions were prepared alongside a negative (H_2O) and positive PCR control (Biological Industries). The PCR conditions described by the manufacturer were followed (*refer to* Table **7.1.**) and the resulting PCR products separated on a 2% agarose gel containing EtBr (0.5 μg/mL). The gel was imaged under UV light (Geneflash, Syngene Bio imaging) with a band present at 270 bp indicative of a positive mycoplasma result.

Table 7.1. Mycoplasma PCR conditions

Number of cycles	Temperature (°C)	Duration (sec)
1	94	30
35	94	30
	60	120
	72	60
1	94	30
	60	60
	72	300

7.1.2. Protein determination assays

Bradford assay

The Bradford assay (Bradford, 1976) is a simple colorimetric assay that is used to measure the concentration of total protein in a sample. The principle of the assay is the colorimetric change from brown to blue in acidic conditions in response to the binding of proteins to the coomassie dye.

The Bradford assay was carried out in 96-well plates, with each sample of interest (2-5 μL; dependent on concentration) added to a well containing 250 μL Bradford reagent (0.05 % (w/v) Coomassie brilliant blue G-250). Varying volumes of a bovine serum albumin (BSA) stock solution (0.5 mg/mL) were also added to wells to produce a standard curve (Figure **7.1.**). The absorbance of each well was measured at 595 nm (Infinite® 200 Pro, Tecan) and the standard curve was used to calculate the amount of protein present in each sample (μg/μL).

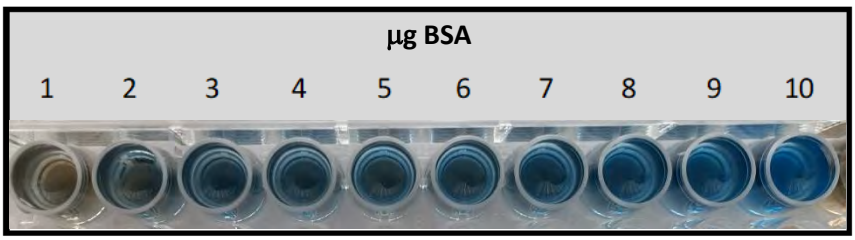


Figure 7.1. Example BSA standard curve of a Bradford assay. 250 μL Bradford reagent was added to wells, followed by the addition of BSA (0.5 mg/ml stock) to give the concentrations needed for a suitable standard curve (1-10 μg). The colour change from brown to blue is measured via absorbance at 595 nm.

DC™ protein assay

The DC™ Protein Assay (Bio-Rad: catalogue no. 500-0116) is a simple colorimetric assay and is based on the Lowry method, which has a similar principle to the Bradford assay (Lowry *et al.*, 1951). Proteins within a sample will react with the alkaline copper tartrate solution present in the supplied reagent (*reagent A*), the product of this reaction is then subsequently able to reduce the Folin regent (*reagent B*). This reduction results in a colorimetric change, from brown to blue, and this is used to measure the concentration of total protein in a sample.

The DC protein assay was set-up in 96-well plate, with each sample of interest added to duplicate wells (5 μL/well). Alongside samples, a BSA standard curve was also set-up by adding varying volumes of a BSA stock solution (0.5 mg/mL) to duplicate wells. Reagent A (25 μL) and reagent B (200 μL) were then added to all wells. The plate was gently rocked at RT (60 sec) and then incubated in the dark at RT (15 min). Absorbance was measured at 750 nm and the standard curve was used to calculate the amount of protein present in each sample (μg/μL).

7.2. Statistical analysis

Table 7.2. Details of statistical analysis

Experiment description	Statistical analysis	Figure
Measuring *Ogg1* expression: Determining difference between Ct values produced from qPCR	Two-tailed unpaired *t*-test	2.2.
Viability following BSO treatment: MTT, crystal violet and CellTox™ Green assays	Two-way ANOVA & Dunnett's test	2.3.
Measurement of apoptosis: BSO treatment	Two-way ANOVA & Dunnett's test	2.4.
GSH determination assay: Basal GSH measurements	Two-tailed unpaired *t*-test	2.5.
GSH determination assay: Whole-cell GSH measurements	Two-way ANOVA and Dunnett's test	2.5.
GSH determination assay: Mitochondrial GSH measurements	Two-way ANOVA and Tukey's test	2.5.
Intracellular ROS measurements: Determining if data is normally distributed	Shapiro-Wilks	2.6.
Intracellular ROS measurements: Basal ROS levels	Two-tailed unpaired *t*-test	2.6.
Intracellular ROS measurements: H_2DCF-DA and MitoSOX Red™ experiments	Two-way ANOVA and Tukey's test	2.7.
Antioxidant gene expression studies: qPCR analysis	Two-way ANOVA and Tukey's test	2.8.
Whole-cell ATP measurements	Two-way ANOVA and Bonferroni correction	2.9.
Galactose MTT assay: Comparison of viability in cells cultured in glucose versus galactose	Two-way ANOVA and Dunnett's test	2.10.

Galactose MTT assay: Comparison of IC50 values of antimycin-A and rotenone	Two-tailed unpaired *t*-test	2.10.
hOGG1-modified comet assay	Two-way ANOVA and Bonferroni correction	2.11.
Viability following H_2O_2 treatment: MTT assay	Two-way ANOVA and Dunnett's test	2.11.
Re-expression of *Ogg1*: Efficiency of *Ogg1* re-expression	Two-tailed unpaired *t*-test	2.12.
Re-expression of *Ogg1*: Viability following BSO treatment measured with MTT assays	Two-way ANOVA and Tukey's test	2.12.
Re-expression of *Ogg1*: Re-adjusted viability	Two-tailed unpaired *t*-test	2.12.
Comet assay: Comparison of basal 8-oxoG levels	Two-way ANOVA and Bonferroni correction	3.3.
NER-modified comet assay	Two-way ANOVA and Tukey's test	3.5.
NEIL3-modified comet assay	Two-way ANOVA and Tukey's test	3.6.
TBARS: Measurement of lipid peroxidation	Two-way ANOVA and Tukey's test	3.7.
Viability following treatment with oxidised purines: MTT assay	Two-way ANOVA and Dunnett's test	4.4.
Measurement of active-RAS: Oxidised purines	Two-tailed *t*-test	4.5.
Measurement of active-RAS: Oxidised purines and H_2O_2	Two-way ANOVA and Tukey's test	4.5.
Growth kinetics: MTT assay	Two-way ANOVA and Bonferroni correction	4.6.
Growth kinetics: Calculation of PDT	Two-tailed unpaired *t*-test	4.6.

Detachment assay: Non-linear regression	[Inhibitor] vs response (variable slope) model	4.7.
Attachment assay	Two-way ANOVA and Tukey's test	4.8.
Attachment assay: Non-linear regression	[Agonist] vs response model	4.8.
Intracellular ROS measurements: H_2DCF-DA experiments following addition of oxidised purines	Two-way ANOVA and Dunnett's test	4.10.
Acellular deoxyribose assay	Two-way ANOVA and Dunnett's test	4.10.

7.3. qPCR analysis

Table 7.3. ΔCt values of WT control samples (N=3)

Gene	Ct			ΔCt		
Apex1	23.82	22.86	23.6	6.52	5.56	6.30
Apex2	25.84	24.96	25.37	8.54	7.66	8.07
Atm	25.80	25.25	25.9	8.50	7.95	8.60
Atr	25.12	24.33	25.48	7.82	7.03	8.18
Atxn3	24.97	24.26	24.72	7.67	6.96	7.42
Brca1	23.14	22.70	22.88	5.84	5.40	5.58
Brca2	23.95	23.71	23.66	6.65	6.41	6.36
Brip1	24.71	23.94	24.42	7.41	6.64	7.12
Ccnh	23.03	22.35	22.86	5.73	5.05	5.56
Ccno	29.38	28.58	30.45	12.08	11.28	13.15
Cdk7	25.85	25.09	25.71	8.55	7.79	8.41
Ddb1	19.99	19.16	20.48	2.69	1.86	3.18
Ddb2	24.81	24.02	24.98	7.51	6.72	7.68
Dmc1	34.19	34.10	34.29	16.89	16.80	16.99
Ercc1	23.20	22.74	22.53	5.90	5.44	5.23
Ercc2	25.61	24.83	24.99	8.31	7.53	7.69
Ercc3	23.82	22.91	23.1	6.52	5.61	5.80
Ercc4	25.68	24.89	25.95	8.38	7.59	8.65
Ercc5	25.40	24.72	25.01	8.10	7.42	7.71
Ercc6	25.64	24.83	25.43	8.34	7.53	8.13
Ercc8	25.55	24.76	25.9	8.25	7.46	8.60
Exo1	23.91	23.16	23.49	6.61	5.86	6.19
Fen1	22.71	21.77	23.16	5.41	4.47	5.86
Lig1	22.71	21.98	22.37	5.41	4.68	5.07
Lig3	23.63	22.77	24.02	6.33	5.47	6.72
Lig4	24.23	23.80	24.19	6.93	6.50	6.89
Mgmt	28.65	27.72	27.26	11.35	10.42	9.96
Mlh1	24.20	23.92	23.69	6.90	6.62	6.39
Mlh3	25.55	24.87	25.68	8.25	7.57	8.38
Mms19	25.79	24.85	26.24	8.49	7.55	8.94
Mpg	25.66	24.80	25.58	8.36	7.50	8.28
Mre11a	22.80	22.12	22.55	5.50	4.82	5.25

Msh2	22.67	22.08	22.33	5.37	4.78	5.03
Msh3	24.03	23.65	23.85	6.73	6.35	6.55
Msh4	No Ct	No Ct	No Ct	n/a	n/a	n/a
Msh5	30.40	29.43	30.45	13.10	12.13	13.15
Msh6	22.48	21.83	22.27	5.18	4.53	4.97
Mutyh	26.04	25.67	26.01	8.74	8.37	8.71
Neil1	26.51	25.61	27.06	9.21	8.31	9.76
Neil2	33.20	32.19	31.97	15.90	14.89	14.67
Neil3	29.04	27.79	27.08	11.74	10.49	9.78
Nthl1	24.94	24.38	24.53	7.64	7.08	7.23
Ogg1	23.63	22.90	No Ct	6.33	5.60	n/a
Parp1	22.88	22.08	23.31	5.58	4.78	6.01
Parp2	24.83	24.33	24.54	7.53	7.03	7.24
Parp3	24.62	23.83	25	7.32	6.53	7.70
Pms1	26.35	25.76	25.97	9.05	8.46	8.67
Pms2	24.40	23.94	24.39	7.10	6.64	7.09
Pnkp	26.33	25.49	26.88	9.03	8.19	9.58
Polb	23.68	23.01	23.35	6.38	5.71	6.05
Pold3	23.96	23.58	24.3	6.66	6.28	7.00
Poll	24.50	23.70	25.09	7.20	6.40	7.79
Prkdc	25.59	24.92	26.03	8.29	7.62	8.73
Rad18	22.71	21.96	22.64	5.41	4.66	5.34
Rad21	20.81	20.00	20.72	3.51	2.70	3.42
Rad23a	22.20	21.74	22.47	4.90	4.44	5.17
Rad23b	20.17	19.77	20.44	2.87	2.47	3.14
Rad50	22.82	22.28	22.76	5.52	4.98	5.46
Rad51	22.06	21.42	21.67	4.76	4.12	4.37
Rad51c	25.69	24.81	25.2	8.39	7.51	7.90
Rad51b	24.59	24.09	24.64	7.29	6.79	7.34
Rad51d	29.45	29.04	28.95	12.15	11.74	11.65
Rad52	24.88	24.50	24.56	7.58	7.20	7.26
Rad54l	23.73	22.98	23.5	6.43	5.68	6.20
Rfc1	21.66	20.94	21.55	4.36	3.64	4.25
Rpa1	22.93	22.22	23.4	5.63	4.92	6.10
Rpa3	21.92	21.12	21.52	4.62	3.82	4.22
Slk	21.85	21.17	21.5	4.55	3.87	4.20

Smug1	25.57	24.73	25.99	8.27	7.43	8.69
Tdg	27.92	27.67	27.49	10.62	10.37	10.19
Top3a	25.84	25.03	25.51	8.54	7.73	8.21
Top3b	24.10	23.70	24.09	6.80	6.40	6.79
Trex1	25.36	24.62	25.9	8.06	7.32	8.60
Ung	23.99	23.46	24.2	6.69	6.16	6.90
Xab2	23.47	22.64	23.94	6.17	5.34	6.64
Xpa	24.16	23.77	24.14	6.86	6.47	6.84
Xpc	26.83	25.97	26.5	9.53	8.67	9.20
Xrcc1	23.74	22.92	23.44	6.44	5.62	6.14
Xrcc2	24.61	23.92	24.99	7.31	6.62	7.69
Xrcc3	25.44	24.75	25.09	8.14	7.45	7.79
Xrcc4	24.53	23.83	24.23	7.23	6.53	6.93
Xrcc5	23.78	23.21	23.53	6.48	5.91	6.23
Xrcc6	22.84	22.05	22.35	5.54	4.75	5.05
Xrcc6bp1	26.72	26.25	26.57	9.42	8.95	9.27

Table 7.4. Fold-change values of m*Ogg1*$^{-/-}$ MEFs compared to WT MEFs (N=3)

Gene	Ct			ΔCt			ΔΔCt			Fold-Change			Mean	SD	*p* value	*q* value
Apex1	23.26	22.93	22.72	5.59	5.26	5.05	-0.45	-0.78	-0.99	1.366	1.717	1.986	**1.690**	0.311	0.018425	0.029776
Apex2	25.86	25.32	24.97	8.19	7.65	7.30	0.09	-0.45	-0.80	0.940	1.366	1.741	**1.349**	0.401	0.205968	0.204378
Atm	26.62	26.43	26.44	8.95	8.76	8.77	0.73	0.54	0.55	0.605	0.690	0.685	**0.660**	0.048	0.000247	0.000823
Atr	25.32	25.01	25.15	7.65	7.34	7.48	0.22	-0.09	0.05	0.856	1.061	0.963	**0.960**	0.103	0.536278	0.409891
Atxn3	25.22	24.9	24.76	7.55	7.23	7.09	0.23	-0.09	-0.22	0.850	1.061	1.169	**1.026**	0.162	0.790023	0.551650
Brca1	23.74	23.2	23.16	6.07	5.53	5.49	0.45	-0.09	-0.13	0.732	1.064	1.094	**0.964**	0.201	0.767721	0.549650
Brca2	24.73	24.75	24.66	7.06	7.08	6.99	0.53	0.55	0.46	0.693	0.683	0.727	**0.701**	0.023	0.000023	0.000165
Brip1	24.16	24	24.05	6.49	6.33	6.38	-0.54	-0.70	-0.65	1.449	1.619	1.564	**1.544**	0.087	0.000408	0.001153
Ccnh	22.94	22.88	22.84	5.27	5.21	5.17	-0.12	-0.18	-0.22	1.087	1.133	1.165	**1.128**	0.039	0.004775	0.008712
Ccno	29.58	28.46	28.52	11.91	10.79	10.85	0.23	-0.89	-0.83	0.853	1.853	1.778	**1.494**	0.557	0.198796	0.200784
Cdk7	26.11	25.82	25.73	8.44	8.15	8.06	0.27	-0.02	-0.11	0.829	1.014	1.079	**0.974**	0.130	0.745952	0.540911
Ddb1	21.05	20.77	20.13	3.38	3.10	2.46	1.11	0.82	0.18	0.465	0.564	0.880	**0.636**	0.217	0.043850	0.065159
Ddb2	25.74	25.71	25.6	8.07	8.04	7.93	0.95	0.92	0.81	0.516	0.527	0.568	**0.537**	0.028	0.000008	0.000066
Dmc1 ***	No Ct	No Ct	No Ct	16.95	n/a	n/a	n/a	n/a	n/a	0.930	n/a	n/a	**n/a**	n/a	n/a	n/a
Ercc1	22.17	21.98	21.9	4.50	4.31	4.23	-1.17	-1.36	-1.44	2.250	2.567	2.713	**2.510**	0.237	0.000381	0.001136
Ercc2	25.87	25.64	25.5	8.20	7.97	7.83	0.28	0.05	-0.09	0.824	0.966	1.064	**0.951**	0.121	0.523321	0.405466
Ercc3	24.44	23.87	23.75	6.77	6.20	6.08	0.71	0.14	0.02	0.613	0.911	0.990	**0.838**	0.198	0.230995	0.217752
Ercc4	25.09	25.03	24.98	7.42	7.36	7.31	-0.57	-0.63	-0.68	1.479	1.542	1.597	**1.539**	0.059	0.000093	0.000528
Ercc5	24.82	24.75	24.5	7.15	7.08	6.83	-0.61	-0.68	-0.93	1.526	1.602	1.905	**1.678**	0.201	0.004249	0.008287
Ercc6	25.99	25.78	25.53	8.32	8.11	7.86	0.38	0.18	-0.07	0.766	0.886	1.053	**0.902**	0.144	0.302808	0.267607
Ercc8	25.55	25.55	25.36	7.88	7.88	7.69	0.02	0.02	-0.17	0.983	0.983	1.121	**1.029**	0.080	0.562633	0.418718

Exo1	23.7	23.15	23.57	6.03	5.48	5.90	-0.21	-0.76	-0.34	1.153	1.688	1.261	**1.367**	0.283	0.087748	0.105597
Fen1	22.98	22.6	21.95	5.31	4.93	4.28	0.37	-0.01	-0.66	0.774	1.007	1.580	**1.120**	0.415	0.641725	0.471376
Lig1	22.04	21.77	21.81	4.37	4.10	4.14	-0.68	-0.95	-0.91	1.597	1.925	1.873	**1.798**	0.176	0.001427	0.003669
Lig3	24.11	24.01	23.83	6.44	6.34	6.16	0.54	0.44	0.26	0.688	0.737	0.835	**0.753**	0.075	0.004658	0.008712
Lig4	25.67	25.67	25.82	8.00	8.00	8.15	1.29	1.29	1.44	0.410	0.410	0.370	**0.397**	0.023	0.000001	0.000034
Mgmt	24	23.75	23.74	6.33	6.08	6.07	-4.56	-4.81	-4.82	23.507	27.954	28.149	**26.537**	2.626	0.000073	0.000457
Mlh1	23.88	23.76	23.8	6.21	6.09	6.13	-0.55	-0.67	-0.63	1.464	1.591	1.548	**1.534**	0.065	0.000138	0.000709
Mlh3	28.39	28.23	27.7	10.72	10.56	10.03	2.81	2.65	2.12	0.143	0.159	0.230	**0.177**	0.046	0.000007	0.000063
Mms19	26.27	25.68	25.6	8.60	8.01	7.93	0.58	-0.01	-0.09	0.669	1.007	1.064	**0.913**	0.214	0.520780	0.405466
Mpg	23.5	23.49	23.25	5.83	5.82	5.58	-2.10	-2.11	-2.35	4.287	4.317	5.098	**4.567**	0.460	0.000177	0.000772
Mre11a	23.71	23.49	22.99	6.04	5.82	5.32	0.88	0.66	0.16	0.543	0.633	0.895	**0.690**	0.183	0.042686	0.065159
Msh2	22.23	22	22.04	4.56	4.33	4.37	-0.52	-0.75	-0.71	1.429	1.676	1.630	**1.578**	0.131	0.001588	0.003904
Msh3	24.9	24.64	24.6	7.23	6.97	6.93	0.69	0.43	0.39	0.620	0.742	0.763	**0.708**	0.077	0.002821	0.006137
Msh4 ***	No Ct	No Ct	No Ct	n/a	n/a	n/a	n/a	n/a	n/a	n/a	n/a	n/a	**n/a**	n/a	n/a	n/a
Msh5	29.8	29.39	29.55	12.13	11.72	11.88	-0.49	-0.90	-0.74	1.400	1.860	1.664	**1.641**	0.231	0.008572	0.014691
Msh6	22	21.88	21.82	4.33	4.21	4.15	-0.53	-0.65	-0.71	1.439	1.564	1.630	**1.544**	0.097	0.000627	0.001690
Mutyh	25.85	25.65	25.65	8.18	7.98	7.98	-0.38	-0.58	-0.58	1.297	1.490	1.490	**1.425**	0.111	0.002705	0.006120
Neil1	27.36	26.72	26.64	9.69	9.05	8.97	0.93	0.29	0.21	0.525	0.818	0.865	**0.736**	0.184	0.068070	0.089536
Neil2 **	33.15	32.84	37.53	15.48	15.17	19.86	0.08	-0.22	4.47	0.943	1.169	0.045	**0.719**	0.594	0.458964	0.370843
Neil3	23.61	23.49	23.53	5.94	5.82	5.86	-5.18	-5.30	-5.26	36.127	39.260	38.187	**37.858**	1.592	0.000002	0.000034
Nthl1	24.3	24.37	24.21	6.63	6.70	6.54	-0.73	-0.66	-0.82	1.659	1.580	1.765	**1.668**	0.093	0.000238	0.000823
Ogg1 *	32.98	33.51	39.86	15.38	15.91	22.26	9.42	9.95	16.30	0.001	0.001	0.000	**0.001**	0.001	<0.000001	<0.000001
Parp1	23.67	23.08	22.88	6.00	5.41	5.21	0.82	0.23	0.03	0.566	0.853	0.979	**0.799**	0.212	0.175925	0.180915

Parp2	24.92	24.64	24.42	7.25	6.97	6.75	-0.03	-0.31	-0.53	1.021	1.240	1.444	**1.235**	0.211	0.126673	0.140482
Parp3	25.67	25.42	24.89	8.00	7.75	7.22	1.08	0.82	0.29	0.475	0.564	0.815	**0.618**	0.176	0.019902	0.031268
Pms1	25.94	25.78	25.52	8.27	8.11	7.85	-0.48	-0.64	-0.90	1.400	1.564	1.873	**1.612**	0.240	0.011548	0.019210
Pms2	24.81	24.2	24.13	7.14	6.53	6.46	0.27	-0.34	-0.41	0.829	1.266	1.329	**1.141**	0.272	0.419507	0.343874
Pnkp	26.76	26.32	25.67	9.09	8.65	8.00	0.48	0.04	-0.61	0.717	0.973	1.526	**1.072**	0.414	0.777986	0.550036
Polb	23.72	23.65	23.62	6.05	5.98	5.95	0.00	-0.07	-0.09	0.997	1.046	1.068	**1.037**	0.037	0.152639	0.159875
Pold3	24.62	24.48	23.97	6.95	6.81	6.30	0.48	0.34	-0.17	0.717	0.790	1.125	**0.877**	0.218	0.384092	0.324242
Poll	25.1	24.81	24.53	7.43	7.14	6.86	0.63	0.34	0.06	0.646	0.790	0.959	**0.798**	0.157	0.089655	0.105643
Prkdc	24.89	24.91	24.86	7.22	7.24	7.19	-0.74	-0.72	-0.77	1.664	1.641	1.699	**1.668**	0.029	0.000002	0.000034
Rad18	22.78	22.63	22.09	5.11	4.96	4.42	0.08	-0.07	-0.61	0.949	1.053	1.532	**1.178**	0.311	0.377571	0.323567
Rad21	20.64	20.21	19.99	2.97	2.54	2.32	-0.14	-0.57	-0.79	1.098	1.479	1.723	**1.434**	0.315	0.075761	0.097387
Rad23a	22.9	22.73	22.16	5.23	5.06	4.49	0.56	0.39	-0.18	0.678	0.763	1.133	**0.858**	0.242	0.366805	0.319177
Rad23b	20.98	20.84	20.65	3.31	3.17	2.98	0.64	0.50	0.31	0.642	0.707	0.807	**0.718**	0.083	0.004226	0.008287
Rad50	23.48	23	22.96	5.81	5.33	5.29	0.56	0.08	0.04	0.678	0.946	0.973	**0.866**	0.163	0.226825	0.217445
Rad51	21.99	21.9	21.93	4.32	4.23	4.26	-0.12	-0.21	-0.18	1.087	1.157	1.133	**1.125**	0.036	0.003613	0.007568
Rad51c	26.45	25.91	25.53	8.78	8.24	7.86	0.83	0.29	-0.09	0.563	0.818	1.064	**0.815**	0.251	0.270028	0.246335
Rad51b	25.93	25.78	25.97	8.26	8.11	8.30	1.22	1.07	1.26	0.429	0.476	0.418	**0.441**	0.031	0.000006	0.000063
Rad51d	28.58	28.73	28.55	10.91	11.06	10.88	-1.04	-0.88	-1.06	2.049	1.847	2.092	**1.996**	0.131	0.000191	0.000772
Rad52	24.79	24.73	24.71	7.12	7.06	7.04	-0.27	-0.33	-0.35	1.206	1.257	1.275	**1.246**	0.036	0.000285	0.000896
Rad54l	24.65	24.04	23.97	6.98	6.37	6.30	0.92	0.31	0.24	0.527	0.804	0.844	**0.725**	0.173	0.050898	0.071248
Rfc1	22.69	22.51	21.84	5.02	4.84	4.17	1.02	0.84	0.17	0.493	0.559	0.889	**0.647**	0.212	0.044929	0.065159
Rpa1	23.28	22.89	22.18	5.61	5.22	4.51	0.34	-0.05	-0.77	0.793	1.039	1.699	**1.177**	0.469	0.548588	0.413709
Rpa3	21.88	21.76	21.74	4.21	4.09	4.07	-0.01	-0.13	-0.15	1.007	1.094	1.110	**1.070**	0.055	0.092880	0.107211

Slk	20.85	20.75	20.63	3.18	3.08	2.96	-1.03	-1.13	-1.25	2.042	2.189	2.378	**2.203**	0.169	0.000245	0.000823
Smug1	25.92	25.77	25.47	8.25	8.10	7.80	0.40	0.25	-0.05	0.758	0.841	1.035	**0.878**	0.142	0.211359	0.206112
Tdg	26.83	26.67	26.59	9.16	9.00	8.92	-1.34	-1.50	-1.58	2.523	2.819	2.979	**2.774**	0.232	0.000186	0.000772
Top3a	25.92	25.71	25.11	8.25	8.04	7.44	0.11	-0.10	-0.70	0.923	1.068	1.619	**1.203**	0.367	0.391826	0.325907
Top3b	23.79	23.56	23.01	6.12	5.89	5.34	-0.48	-0.71	-1.26	1.395	1.636	2.395	**1.809**	0.522	0.055008	0.074078
Trex1	26.28	25.65	25.49	8.61	7.98	7.82	0.92	0.29	0.13	0.529	0.818	0.914	**0.753**	0.201	0.100315	0.113477
Ung	24.42	23.78	23.69	6.75	6.11	6.02	0.32	-0.32	-0.41	0.798	1.244	1.324	**1.122**	0.283	0.497366	0.396212
Xab2	23.84	23.6	23.44	6.17	5.93	5.77	0.42	0.18	0.02	0.750	0.886	0.990	**0.875**	0.120	0.147246	0.157136
Xpa	24.86	24.7	24.56	7.19	7.03	6.89	0.52	0.36	0.22	0.695	0.776	0.856	**0.776**	0.080	0.008481	0.014691
Xpc	27.85	26.99	26.24	10.18	9.32	8.57	1.08	0.22	-0.53	0.473	0.859	1.444	**0.925**	0.489	0.804441	0.554868
Xrcc1	23.74	23.54	22.94	6.07	5.87	5.27	0.04	-0.16	-0.76	0.973	1.117	1.693	**1.261**	0.381	0.301059	0.267607
Xrcc2	25.24	24.7	24.67	7.57	7.03	7.00	0.60	0.06	0.04	0.657	0.956	0.976	**0.863**	0.178	0.254885	0.236332
Xrcc3	25.32	25.2	24.73	7.65	7.53	7.06	-0.15	-0.27	-0.73	1.106	1.202	1.664	**1.324**	0.299	0.133119	0.144793
Xrcc4	24.46	23.86	23.85	6.79	6.19	6.18	-0.09	-0.69	-0.70	1.064	1.613	1.625	**1.434**	0.320	0.078899	0.098806
Xrcc5	23.62	23.34	22.9	5.95	5.67	5.23	-0.25	-0.53	-0.97	1.185	1.439	1.952	**1.525**	0.391	0.080359	0.098806
Xrcc6	22.76	22.57	22.55	5.09	4.90	4.88	-0.06	-0.25	-0.27	1.039	1.185	1.202	**1.142**	0.090	0.051647	0.071248
Xrcc6bp1	28.29	27.56	28.17	10.62	9.89	10.50	0.83	0.10	0.72	0.561	0.930	0.609	**0.700**	0.201	0.002121	0.004998

Important notes:

* This average threshold cycle (Ct) is high (> 30) in one sample, and reasonably low in the other (< 30). Therefore, the gene expression is relatively low in one sample and reasonably detected in the other sample; suggesting that the actual fold-change value is at least as large as this reported fold-change result.

** This gene's average threshold cycle is high (> 30), meaning that its relative expression level is low in both samples. Therefore, the p-value for the fold-change is either unavailable or erroneous.

*** This gene's average threshold cycle is not determined in both samples meaning that the target was undetected. Therefore, no fold-change result or p-value are reported.

Table 7.5. Fold-change values of WT MEFs following BSO treatment (15 μM; 24 h) (N=3)

Gene	Ct			ΔCt			ΔΔCt			Fold-Change			Mean	SD	*p* value	*q* value
Apex1	23.74	22.89	24.02	6.14	5.29	6.42	0.10	-0.75	0.38	0.933	1.682	0.768	1.128	0.487	0.673016	0.918570
Apex2	25.74	24.99	26.81	8.14	7.39	9.21	0.04	-0.71	1.11	0.973	1.636	0.463	1.024	0.588	0.947208	0.918570
Atm	25.79	25.17	26.62	8.19	7.57	9.02	-0.03	-0.65	0.80	1.025	1.575	0.576	1.059	0.500	0.849286	0.918570
Atr	24.91	24.52	25.92	7.31	6.92	8.32	-0.12	-0.51	0.89	1.083	1.419	0.538	1.013	0.445	0.961232	0.918570
Atxn3	24.98	24.42	25.21	7.38	6.82	7.61	0.07	-0.49	0.30	0.956	1.409	0.815	1.060	0.311	0.754242	0.918570
Brca1	23.02	22.33	23.37	5.42	4.73	5.77	-0.20	-0.89	0.15	1.149	1.853	0.901	1.301	0.494	0.350649	0.918570
Brca2	23.81	23.3	24.11	6.21	5.70	6.51	-0.32	-0.83	-0.02	1.248	1.778	1.014	1.347	0.391	0.199653	0.918570
Brip1	24.02	23.72	24.84	6.42	6.12	7.24	-0.61	-0.91	0.21	1.521	1.873	0.862	1.418	0.513	0.230855	0.918570
Ccnh	23.02	22.21	23.36	5.42	4.61	5.76	0.03	-0.78	0.37	0.979	1.717	0.774	1.157	0.496	0.613203	0.918570
Ccno	29.6	28.7	30.88	12.00	11.10	13.28	0.32	-0.58	1.60	0.801	1.495	0.330	0.875	0.586	0.731059	0.918570
Cdk7	25.84	25.05	26.26	8.24	7.45	8.66	0.07	-0.72	0.49	0.953	1.647	0.712	1.104	0.486	0.729609	0.918570
Ddb1	20.11	19.34	20.86	2.51	1.74	3.26	0.23	-0.54	0.98	0.850	1.449	0.505	0.935	0.478	0.824202	0.918570
Ddb2	24.58	24.03	25.44	6.98	6.43	7.84	-0.14	-0.69	0.72	1.098	1.608	0.605	1.104	0.501	0.738514	0.918570
Dmc1 **	37.58	37.91	No Ct	19.98	20.31	n/a	3.14	3.47	n/a	0.114	0.091	n/a	0.102	0.016	0.000002	0.000051
Ercc1	23.3	22.84	23.91	5.70	5.24	6.31	0.03	-0.43	0.64	0.979	1.347	0.642	0.989	0.353	0.961204	0.918570
Ercc2	25.77	24.81	26.43	8.17	7.21	8.83	0.25	-0.71	0.91	0.841	1.636	0.532	1.003	0.569	0.993243	0.918570
Ercc3	23.63	22.93	24.54	6.03	5.33	6.94	-0.04	-0.73	0.88	1.025	1.664	0.545	1.078	0.561	0.821531	0.918570
Ercc4	25.79	24.83	26.33	8.19	7.23	8.73	0.20	-0.76	0.74	0.868	1.688	0.597	1.051	0.568	0.884829	0.918570
Ercc5	24.58	24.47	24.51	6.98	6.87	6.91	-0.78	-0.89	-0.85	1.717	1.853	1.803	1.791	0.069	0.000028	0.000533
Ercc6	25.5	24.73	25.84	7.90	7.13	8.24	-0.04	-0.81	0.31	1.025	1.747	0.809	1.194	0.491	0.532079	0.918570
Ercc8	25.7	24.77	26.22	8.10	7.17	8.62	0.24	-0.69	0.76	0.844	1.608	0.588	1.013	0.530	0.967378	0.918570

Exo1	23.24	22.89	23.88	5.64	5.29	6.28	-0.60	-0.95	0.04	1.510	1.925	0.969	1.468	0.479	0.165862	0.918570
Fen1	22.93	21.92	23.6	5.33	4.32	6.00	0.39	-0.62	1.06	0.763	1.537	0.480	0.927	0.547	0.827569	0.918570
Lig1	22.6	21.83	22.76	5.00	4.23	5.16	-0.04	-0.82	0.12	1.032	1.759	0.923	1.238	0.455	0.415576	0.918570
Lig3	23.57	22.84	24.45	5.97	5.24	6.85	0.07	-0.66	0.95	0.953	1.580	0.518	1.017	0.534	0.959204	0.918570
Lig4	23.99	23.73	24.63	6.39	6.13	7.03	-0.33	-0.59	0.31	1.253	1.500	0.804	1.186	0.353	0.414070	0.918570
Mgmt	26.99	27.07	27.04	9.39	9.47	9.44	-1.50	-1.42	-1.45	2.819	2.676	2.732	2.742	0.072	0.000002	0.000051
Mlh1	23.85	23.14	24.17	6.25	5.54	6.57	-0.51	-1.22	-0.19	1.424	2.329	1.141	1.631	0.621	0.152960	0.918570
Mlh3	25.85	24.95	26.14	8.25	7.35	8.54	0.34	-0.56	0.63	0.790	1.474	0.646	0.970	0.442	0.912645	0.918570
Mms19	25.89	25.33	26.7	8.29	7.73	9.10	0.27	-0.29	1.08	0.829	1.223	0.473	0.842	0.375	0.505071	0.918570
Mpg	24.98	24.66	25.96	7.38	7.06	8.36	-0.55	-0.87	0.43	1.464	1.828	0.742	1.345	0.552	0.340682	0.918570
Mre11a	22.81	21.96	22.93	5.21	4.36	5.33	0.05	-0.80	0.17	0.966	1.741	0.889	1.199	0.471	0.505928	0.918570
Msh2	21.99	21.82	22.75	4.39	4.22	5.15	-0.69	-0.86	0.07	1.608	1.809	0.949	1.455	0.450	0.154265	0.918570
Msh3	24.16	23.64	24.84	6.56	6.04	7.24	0.02	-0.50	0.70	0.986	1.414	0.616	1.005	0.400	0.982647	0.918570
Msh4 ***	No Ct	No Ct	No Ct	n/a	n/a	n/a	n/a	n/a	n/a	n/a	n/a	n/a	n/a	n/a	n/a	n/a
Msh5 *	31.13	30.23	30.9	13.53	12.63	13.30	0.91	0.01	0.68	0.530	0.990	0.622	0.714	0.243	0.111218	0.918570
Msh6	21.99	21.68	22.66	4.39	4.08	5.06	-0.47	-0.78	0.20	1.380	1.711	0.868	1.320	0.425	0.262649	0.918570
Mutyh	25.43	25.568	25.385	7.83	7.97	7.79	-0.73	-0.59	-0.77	1.653	1.502	1.705	1.620	0.105	0.000499	0.005475
Neil1	26.85	25.97	27.51	9.25	8.37	9.91	0.49	-0.39	1.15	0.712	1.310	0.451	0.824	0.441	0.527987	0.918570
Neil2 **	33.18	33.64	33.39	15.58	16.04	15.79	0.18	0.65	0.40	0.880	0.639	0.760	0.760	0.120	0.025733	0.246913
Neil3	27.769	27.74	27.55	10.17	10.14	9.95	-0.95	-0.98	-1.17	1.927	1.966	2.242	2.045	0.172	0.000036	0.000546
Nthl1	24.26	23.965	23.985	6.66	6.37	6.39	-0.70	-1.00	-0.98	1.625	1.993	1.966	1.861	0.205	0.000001	0.000051
Ogg1	21.67	21.87	21.855	4.07	4.27	4.26	-1.90	-1.70	-1.71	3.719	3.238	3.272	3.410	0.269	0.000099	0.001273
Parp1	22.85	22.05	23.72	5.25	4.45	6.12	0.07	-0.73	0.94	0.953	1.659	0.521	1.044	0.574	0.900440	0.918570

Parp2	24.95	24.06	24.99	7.35	6.46	7.39	0.07	-0.82	0.11	0.953	1.765	0.927	1.215	0.477	0.478792	0.918570
Parp3	24.54	23.73	25.4	6.94	6.13	7.80	0.01	-0.80	0.87	0.990	1.735	0.545	1.090	0.601	0.808226	0.918570
Pms1	25.89	24.96	26.4	8.29	7.36	8.80	-0.46	-1.40	0.05	1.380	2.630	0.969	1.660	0.865	0.256872	0.918570
Pms2	24.36	23.79	24.87	6.76	6.19	7.27	-0.11	-0.68	0.40	1.079	1.602	0.758	1.146	0.426	0.583813	0.918570
Pnkp	26.46	25.68	27.22	8.86	8.08	9.62	0.25	-0.53	1.01	0.841	1.444	0.497	0.927	0.480	0.805383	0.918570
Polb	23.55	22.83	23.78	5.95	5.23	6.18	-0.09	-0.82	0.14	1.068	1.759	0.911	1.246	0.451	0.398670	0.918570
Pold3	23.91	23.57	24.7	6.31	5.97	7.10	-0.16	-0.50	0.63	1.117	1.414	0.646	1.059	0.387	0.804201	0.918570
Poll	24.5	23.68	25.53	6.90	6.08	7.93	0.10	-0.72	1.13	0.933	1.647	0.457	1.012	0.599	0.973170	0.918570
Prkdc	25.63	24.83	26.5	8.03	7.23	8.90	0.07	-0.73	0.94	0.949	1.653	0.519	1.041	0.572	0.908215	0.918570
Rad18	22.63	21.81	23	5.03	4.21	5.40	0.00	-0.82	0.37	1.003	1.772	0.776	1.184	0.521	0.574475	0.918570
Rad21	20.65	19.93	21.11	3.05	2.33	3.51	-0.06	-0.78	0.40	1.039	1.711	0.755	1.168	0.491	0.584366	0.918570
Rad23a	22.59	21.69	22.88	4.99	4.09	5.28	0.32	-0.58	0.61	0.801	1.495	0.655	0.984	0.449	0.952857	0.918570
Rad23b	20.2	19.79	20.82	2.60	2.19	3.22	-0.07	-0.48	0.55	1.050	1.395	0.683	1.042	0.356	0.846272	0.918570
Rad50	22.84	21.98	23.19	5.24	4.38	5.59	-0.01	-0.87	0.34	1.007	1.828	0.790	1.208	0.547	0.545931	0.918570
Rad51	21.57	21.19	22.09	3.97	3.59	4.49	-0.47	-0.85	0.05	1.385	1.803	0.966	1.385	0.418	0.186550	0.918570
Rad51c	25.14	24.7	25.64	7.54	7.10	8.04	-0.41	-0.85	0.09	1.329	1.803	0.940	1.357	0.432	0.225846	0.918570
Rad51b	24.83	24.12	25.07	7.23	6.52	7.47	0.19	-0.52	0.43	0.877	1.434	0.742	1.018	0.367	0.937727	0.918570
Rad51d	29.3	28.44	29.45	11.70	10.84	11.85	-0.24	-1.10	-0.09	1.185	2.151	1.068	1.468	0.594	0.244268	0.918570
Rad52	24.57	23.93	24.98	6.97	6.33	7.38	-0.42	-1.06	-0.01	1.338	2.085	1.007	1.477	0.552	0.209252	0.918570
Rad54l	23.62	22.93	23.91	6.02	5.33	6.31	-0.04	-0.73	0.25	1.025	1.653	0.838	1.172	0.427	0.524175	0.918570
Rfc1	21.58	20.81	21.94	3.98	3.21	4.34	-0.02	-0.79	0.34	1.014	1.729	0.790	1.178	0.490	0.564364	0.918570
Rpa1	22.95	22.3	23.81	5.35	4.70	6.21	0.07	-0.57	0.93	0.949	1.490	0.523	0.987	0.484	0.966104	0.918570
Rpa3	21.53	20.92	21.91	3.93	3.32	4.31	-0.29	-0.90	0.09	1.223	1.866	0.940	1.343	0.475	0.279341	0.918570

Slk	21.83	21	21.89	4.23	3.40	4.29	0.02	-0.81	0.08	0.986	1.753	0.946	1.229	0.455	0.433342	0.918570
Smug1	26.45	24.94	26.46	8.85	7.34	8.86	1.00	-0.51	1.01	0.500	1.424	0.497	0.807	0.535	0.565349	0.918570
Tdg	27.71	27	27.96	10.11	9.40	10.36	-0.39	-1.10	-0.14	1.306	2.136	1.098	1.513	0.549	0.180785	0.918570
Top3a	25.77	25.04	25.97	8.17	7.44	8.37	0.03	-0.70	0.23	0.976	1.619	0.850	1.148	0.412	0.567465	0.918570
Top3b	23.85	23.09	24.54	6.25	5.49	6.94	-0.35	-1.11	0.34	1.275	2.158	0.790	1.408	0.694	0.366370	0.918570
Trex1	25.34	24.56	26.51	7.74	6.96	8.91	0.05	-0.73	1.22	0.966	1.659	0.429	1.018	0.616	0.962181	0.918570
Ung	24.43	23.55	24.64	6.83	5.95	7.04	0.40	-0.48	0.61	0.755	1.390	0.653	0.933	0.399	0.784818	0.918570
Xab2	23.74	22.64	24.31	6.14	5.04	6.71	0.39	-0.71	0.96	0.766	1.641	0.516	0.974	0.591	0.943735	0.918570
Xpa	24.53	23.74	24.58	6.93	6.14	6.98	0.27	-0.53	0.31	0.832	1.439	0.804	1.025	0.359	0.909771	0.918570
Xpc	26.99	26.05	27.09	9.39	8.45	9.49	0.29	-0.65	0.39	0.818	1.569	0.763	1.050	0.450	0.856699	0.918570
Xrcc1	23.2	22.85	23.9	5.60	5.25	6.30	-0.43	-0.78	0.27	1.347	1.717	0.829	1.298	0.446	0.311664	0.918570
Xrcc2	24.54	23.9	25.44	6.94	6.30	7.84	-0.03	-0.67	0.88	1.017	1.586	0.545	1.049	0.521	0.877407	0.918570
Xrcc3	25.38	24.75	26.58	7.78	7.15	8.98	-0.02	-0.65	1.19	1.010	1.564	0.440	1.005	0.562	0.989202	0.918570
Xrcc4	24.45	23.67	24.65	6.85	6.07	7.05	-0.03	-0.81	0.17	1.021	1.753	0.889	1.221	0.466	0.457146	0.918570
Xrcc5	23.66	22.97	23.95	6.06	5.37	6.35	-0.14	-0.83	0.15	1.098	1.772	0.898	1.256	0.458	0.387552	0.918570
Xrcc6	22.67	21.94	22.79	5.07	4.34	5.19	-0.08	-0.81	0.04	1.053	1.747	0.969	1.257	0.427	0.356620	0.918570
Xrcc6bp1	26.51	26.19	27.07	8.91	8.59	9.47	-0.88	-1.20	-0.32	1.834	2.289	1.244	1.789	0.524	0.417323	0.918570

Important notes:

* This average threshold cycle (Ct) is high (> 30) in one sample, and reasonably low in the other (< 30). Therefore, the gene expression is relatively low in one sample and reasonably detected in the other sample; suggesting that the actual fold-change value is at least as large as this reported fold-change result.

** This gene's average threshold cycle is high (> 30), meaning that its relative expression level is low in both samples. Therefore, the p-value for the fold-change is either unavailable or erroneous.

*** This gene's average threshold cycle is not determined in both samples meaning that the target was undetected. Therefore, no fold-change result or p-value are reported.

Table 7.6. Fold-change values of m*Ogg1*$^{-/-}$ MEFs following BSO treatment (15 μM; 24 h) (N=3)

Gene	Ct			ΔCt			ΔΔCt			Fold-Change			Mean	SD	*p* value	*q* value
Apex1	22.75	22.43	22.19	5.50	5.18	4.94	0.20	-0.12	-0.36	0.871	1.087	1.283	1.080	0.207	0.536580	0.959505
Apex2	24.96	24.85	24.79	7.71	7.60	7.54	0.00	-0.11	-0.17	1.002	1.082	1.128	1.071	0.063	0.127319	0.424291
Atm	26.03	26.09	25.81	8.78	8.84	8.56	-0.05	0.01	-0.27	1.033	0.991	1.203	1.076	0.112	0.307856	0.767619
Atr	25.32	25.58	24.79	8.07	8.33	7.54	0.58	0.84	0.05	0.669	0.559	0.966	0.731	0.211	0.091600	0.424291
Atxn3	24.74	25.16	24.12	7.49	7.91	6.87	0.20	0.62	-0.42	0.871	0.651	1.338	0.953	0.351	0.829086	0.959505
Brca1	22.97	23.23	22.8	5.72	5.98	5.55	0.02	0.28	-0.15	0.984	0.822	1.107	0.971	0.143	0.743022	0.959505
Brca2	24.72	24.34	24.09	7.47	7.09	6.84	0.43	0.05	-0.20	0.744	0.968	1.151	0.955	0.204	0.717761	0.959505
Brip1	23.89	23.93	23.25	6.64	6.68	6.00	0.24	0.28	-0.40	0.847	0.824	1.320	0.997	0.280	0.986081	0.959505
Ccnh	22.52	22.53	22.15	5.27	5.28	4.90	0.05	0.06	-0.32	0.964	0.957	1.245	1.055	0.165	0.590967	0.959505
Ccno	28.61	28.47	27.91	11.36	11.22	10.66	0.18	0.04	-0.52	0.885	0.975	1.437	1.099	0.296	0.593632	0.959505
Cdk7	25.87	25.99	25.22	8.62	8.74	7.97	0.40	0.52	-0.25	0.756	0.696	1.186	0.879	0.268	0.477923	0.959505
Ddb1	20.23	20.18	20.14	2.98	2.93	2.89	0.00	-0.05	-0.09	1.000	1.035	1.064	1.033	0.032	0.149063	0.475751
Ddb2	25.47	25.33	24.78	8.22	8.08	7.53	0.21	0.07	-0.48	0.867	0.955	1.398	1.073	0.285	0.678466	0.959505
Dmc1 ***	No Ct	No Ct	No Ct	n/a	n/a	n/a	n/a	n/a	n/a	n/a	n/a	n/a	n/a	n/a		
Ercc1	21.81	21.75	21.6	4.56	4.50	4.35	0.21	0.15	0.00	0.863	0.899	0.998	0.920	0.070	0.118514	0.424291
Ercc2	25.47	25.09	24.98	8.22	7.84	7.73	0.22	-0.16	-0.27	0.859	1.117	1.206	1.061	0.180	0.591165	0.959505
Ercc3	23.79	23.7	23.46	6.54	6.45	6.21	0.19	0.10	-0.14	0.877	0.933	1.102	0.971	0.117	0.686839	0.959505
Ercc4	24.7	24.86	24.68	7.45	7.61	7.43	0.09	0.25	0.07	0.942	0.843	0.955	0.913	0.061	0.070404	0.401254
Ercc5	24.56	24.47	23.84	7.31	7.22	6.59	0.29	0.20	-0.43	0.818	0.871	1.347	1.012	0.292	0.946548	0.959505
Ercc6	25.7	25.74	25.02	8.45	8.49	7.77	0.35	0.39	-0.33	0.783	0.761	1.254	0.933	0.279	0.696899	0.959505
Ercc8	25.32	25.34	24.69	8.07	8.09	7.44	0.25	0.27	-0.38	0.839	0.827	1.298	0.988	0.269	0.942022	0.959505

Exo1	23.23	23.17	22.81	5.98	5.92	5.56	0.18	0.12	-0.24	0.885	0.922	1.184	0.997	0.163	0.976096	0.959505
Fen1	21.86	22.01	21.96	4.61	4.76	4.71	-0.23	-0.08	-0.13	1.173	1.057	1.094	1.108	0.059	0.034284	0.227960
Lig1	21.79	21.73	21.15	4.54	4.48	3.90	0.34	0.28	-0.30	0.792	0.825	1.234	0.950	0.246	0.744416	0.959505
Lig3	23.71	23.76	23.62	6.46	6.51	6.37	0.15	0.20	0.06	0.903	0.873	0.961	0.912	0.045	0.027424	0.227960
Lig4	25.56	25.66	24.67	8.31	8.41	7.42	0.26	0.36	-0.63	0.835	0.779	1.548	1.054	0.428	0.837985	0.959505
Mgmt	23.68	23.77	23.16	6.43	6.52	5.91	0.27	0.36	-0.25	0.829	0.779	1.189	0.933	0.224	0.627991	0.959505
Mlh1	23.83	23.71	22.92	6.58	6.46	5.67	0.44	0.32	-0.47	0.739	0.803	1.388	0.977	0.358	0.915477	0.959505
Mlh3	27.7	27.89	27.46	10.45	10.64	10.21	0.01	0.20	-0.23	0.991	0.869	1.170	1.010	0.152	0.914430	0.959505
Mms19	25.46	25.56	25.43	8.21	8.31	8.18	0.03	0.13	0.00	0.979	0.914	1.000	0.964	0.045	0.240323	0.651950
Mpg	22.86	22.94	22.81	5.61	5.69	5.56	-0.13	-0.05	-0.18	1.097	1.038	1.136	1.090	0.049	0.033820	0.227960
Mre11a	23.13	23.04	22.79	5.88	5.79	5.54	0.15	0.06	-0.19	0.899	0.957	1.138	0.998	0.125	0.979163	0.959505
Msh2	22.12	22.09	21.71	4.87	4.84	4.46	0.45	0.42	0.04	0.732	0.747	0.973	0.817	0.135	0.079095	0.420732
Msh3	24.19	24.09	23.83	6.94	6.84	6.58	-0.10	-0.20	-0.46	1.074	1.151	1.379	1.201	0.158	0.092794	0.424291
Msh4 ***	No Ct	No Ct	No Ct	n/a	n/a	n/a	n/a	n/a	n/a	n/a	n/a	n/a	n/a	n/a		
Msh5	29.65	29.39	29.93	12.40	12.14	12.68	0.49	0.23	0.77	0.712	0.853	0.586	0.717	0.133	0.021396	0.213395
Msh6	21.8	21.91	21.02	4.55	4.66	3.77	0.32	0.43	-0.46	0.801	0.742	1.376	0.973	0.350	0.900231	0.959505
Mutyh	25.59	25.64	24.95	8.34	8.39	7.70	0.29	0.34	-0.35	0.816	0.788	1.272	0.959	0.271	0.805197	0.959505
Neil1	26.45	26.54	26.4	9.20	9.29	9.15	-0.04	0.05	-0.09	1.026	0.964	1.062	1.017	0.050	0.577441	0.959505
Neil2 **	33.35	No Ct	33.8	16.1	n/a	16.55	9.12	n/a	9.57	0.002	n/a	0.001	0.002	0.000	<0.000001	<0.000001
Neil3	23.42	23.53	22.73	6.17	6.28	5.48	0.30	0.41	-0.39	0.814	0.754	1.313	0.961	0.307	0.833824	0.959505
Nthl1	24.34	24.35	24	7.09	7.10	6.75	0.47	0.48	0.13	0.724	0.719	0.916	0.786	0.113	0.030079	0.227960
Ogg1 **	No Ct	No Ct	38.7	n/a	n/a	21.45	n/a	n/a	3.60	n/a	n/a	0.082	0.082	n/a	0.957866	0.959505
Parp1	22.81	22.88	22.79	5.56	5.63	5.54	0.02	0.09	0.00	0.986	0.940	1.000	0.975	0.032	0.245125	0.651950

Parp2	24.44	24.56	23.82	7.19	7.31	6.57	0.20	0.32	-0.42	0.871	0.801	1.338	1.003	0.292	0.985169	0.959505
Parp3	24.85	24.87	24.68	7.60	7.62	7.43	-0.06	-0.04	-0.23	1.040	1.026	1.170	1.079	0.080	0.161318	0.495061
Pms1	25.62	25.6	24.85	6.86	8.35	7.60	0.29	0.27	-0.48	0.816	0.827	1.392	1.012	0.329	0.954030	0.959505
Pms2	24.11	24.24	23.82		6.99	6.57	0.15	0.28	-0.14	0.901	0.824	1.102	0.942	0.144	0.524825	0.959505
Pnkp	25.74	25.82	25.66	8.49	8.57	8.41	-0.09	-0.01	-0.17	1.064	1.007	1.125	1.065	0.059	0.127622	0.424291
Polb	23.55	23.54	22.86	6.30	6.29	5.61	0.31	0.30	-0.38	0.809	0.814	1.304	0.976	0.285	0.889343	0.959505
Pold3	23.88	23.94	23.77	6.63	6.69	6.52	-0.06	0.00	-0.17	1.040	0.998	1.122	1.053	0.063	0.216849	0.640828
Poll	24.57	24.61	24.55	7.32	7.36	7.30	0.18	0.22	0.16	0.885	0.861	0.897	0.881	0.019	0.000356	0.009477
Prkdc	24.91	24.77	24.57	7.66	7.52	7.32	0.44	0.30	0.10	0.735	0.810	0.931	0.826	0.099	0.037692	0.231339
Rad18	22.1	22.07	21.79	4.85	4.82	4.54	0.02	-0.01	-0.29	0.986	1.007	1.223	1.072	0.131	0.395644	0.928484
Rad21	19.99	20	19.83	2.74	2.75	2.58	0.13	0.14	-0.03	0.914	0.908	1.021	0.947	0.064	0.227099	0.647151
Rad23a	22.02	22.03	21.91	4.77	4.78	4.66	-0.16	-0.15	-0.27	1.115	1.107	1.203	1.142	0.053	0.009982	0.113778
Rad23b	20.22	20.18	20.09	2.97	2.93	2.84	-0.18	-0.22	-0.31	1.136	1.167	1.243	1.182	0.055	0.004605	0.061244
Rad50	22.91	22.89	22.61	5.66	5.64	5.36	0.18	0.16	-0.12	0.881	0.893	1.084	0.953	0.114	0.511456	0.959505
Rad51	21.89	21.91	21.25	4.64	4.66	4.00	0.37	0.39	-0.27	0.774	0.763	1.206	0.914	0.253	0.588560	0.959505
Rad51c	25.75	25.66	25.56	8.50	8.41	8.31	0.21	0.12	0.02	0.867	0.922	0.989	0.926	0.061	0.103911	0.424291
Rad51b	25.8	25.83	25.49	8.55	8.58	8.24	0.33	0.36	0.02	0.797	0.781	0.989	0.856	0.115	0.096908	0.424291
Rad51d	28.38	28.56	27.6	11.13	11.31	10.35	0.18	0.36	-0.60	0.883	0.779	1.516	1.059	0.399	0.809399	0.959505
Rad52	24.47	24.7	24.01	7.22	7.45	6.76	0.15	0.38	-0.31	0.903	0.770	1.243	0.972	0.244	0.852104	0.959505
Rad54l	23.94	23.92	23.68	6.69	6.67	6.43	0.14	0.12	-0.12	0.908	0.920	1.087	0.971	0.100	0.649505	0.959505
Rfc1	22.06	22.09	21.77	4.81	4.84	4.52	0.13	0.16	-0.16	0.912	0.893	1.115	0.973	0.123	0.726458	0.959505
Rpa1	22.21	22.13	22.19	4.96	4.88	4.94	-0.15	-0.23	-0.17	1.112	1.176	1.128	1.138	0.033	0.001961	0.031290
Rpa3	21.7	21.79	21.09	4.45	4.54	3.84	0.33	0.42	-0.28	0.797	0.749	1.217	0.921	0.257	0.623243	0.959505

Slk	20.69	20.71	19.93	3.44	3.46	2.68	0.37	0.39	-0.39	0.776	0.765	1.313	0.951	0.314	0.801175	0.959505
Smug1	24.98	25.07	25.45	7.73	7.82	8.20	-0.32	-0.23	0.15	1.248	1.173	0.901	1.107	0.183	0.366155	0.885318
Tdg	26.58	26.11	25.97	9.33	8.86	8.72	0.30	-0.17	-0.31	0.810	1.122	1.237	1.057	0.221	0.681591	0.959505
Top3a	25.09	25.08	24.88	7.84	7.83	7.63	-0.07	-0.08	-0.28	1.050	1.057	1.214	1.107	0.093	0.116306	0.424291
Top3b	23.01	23.22	22.92	5.76	5.97	5.67	-0.02	0.19	-0.11	1.016	0.879	1.082	0.992	0.104	0.904148	0.959505
Trex1	25.4	25.42	25.72	8.15	8.17	8.47	0.01	0.03	0.33	0.991	0.977	0.794	0.921	0.110	0.279410	0.719166
Ung	23.63	23.63	23.67	6.38	6.38	6.42	0.09	0.09	0.13	0.942	0.942	0.916	0.933	0.015	0.001536	0.030648
Xab2	22.83	22.88	22.86	5.58	5.63	5.61	-0.38	-0.33	-0.35	1.298	1.254	1.272	1.275	0.022	0.000028	0.001103
Xpa	24.6	24.48	23.84	7.35	7.23	6.59	0.31	0.19	-0.45	0.805	0.875	1.363	1.014	0.304	0.938832	0.959505
Xpc	26.48	26.4	26.6	9.23	9.15	9.35	-0.13	-0.21	-0.01	1.092	1.154	1.005	1.083	0.075	0.124936	0.424291
Xrcc1	23.06	23.03	22.82	5.81	5.78	5.57	0.07	0.04	-0.17	0.950	0.970	1.122	1.014	0.094	0.809288	0.959505
Xrcc2	24.49	24.48	24.33	7.24	7.23	7.08	0.04	0.03	-0.12	0.973	0.979	1.087	1.013	0.064	0.743318	0.959505
Xrcc3	24.68	24.78	24.58	7.43	7.53	7.33	0.02	0.12	-0.08	0.989	0.922	1.059	0.990	0.069	0.812858	0.959505
Xrcc4	23.84	23.89	23.04	6.59	6.64	5.79	0.20	0.25	-0.60	0.869	0.839	1.512	1.073	0.380	0.755096	0.959505
Xrcc5	23.02	22.97	22.33	5.77	5.72	5.08	0.15	0.10	-0.54	0.899	0.931	1.451	1.094	0.310	0.628255	0.959505
Xrcc6	22.63	22.12	21.86	5.38	4.87	4.61	0.42	-0.09	-0.35	0.746	1.062	1.272	1.026	0.265	0.869991	0.959505
Xrcc6bp1	27.63	27.56	27.38	10.38	10.31	10.13	0.04	-0.03	-0.21	0.970	1.019	1.154	1.048	0.095	0.435142	0.959505

Important notes:

** This gene's average threshold cycle is high (> 30), meaning that its relative expression level is low in both samples. Therefore, the p-value for the fold-change is either unavailable or erroneous.

*** This gene's average threshold cycle is not determined in both samples meaning that the target was undetected. Therefore, no fold-change result or p-value are reported.

7.4. qPCR volcano plots

The data analysed in **7.3.** was used to generate volcano plots, as shown in Figure **7.2.** A volcano plot was produced for the fold-change in m*Ogg1*$^{-/-}$ MEFs compared to WT MEFs, and for both WT and m*Ogg1*$^{-/-}$ MEFs following BSO treatment (15 μM; 24h).

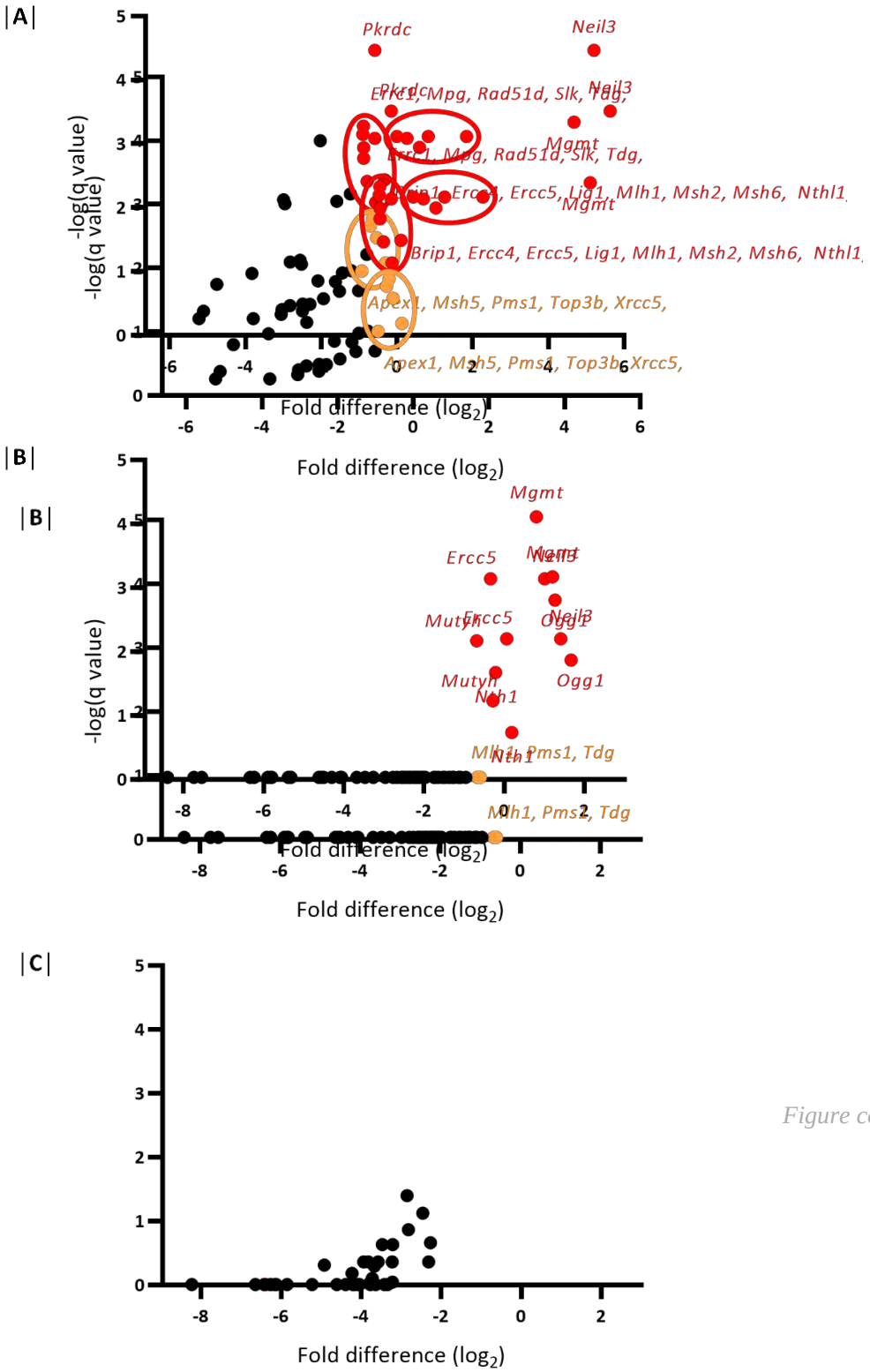


Figure continues on next page

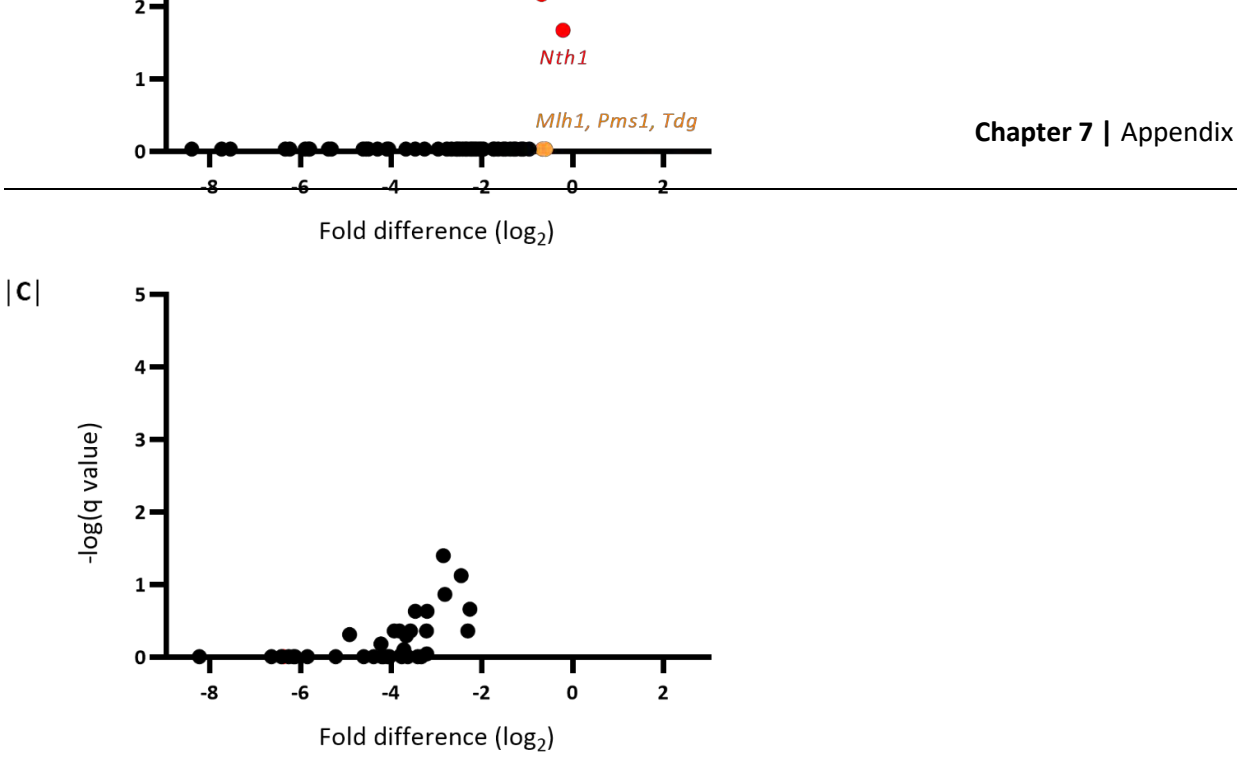


Figure 7.2. Volcano plots were produced for the qPCR gene expression analysis. The mean value is displayed (N=3) and key results are highlighted and labelled. Results highlighted in **red** represent fold-changes of ≥ 1.5 *(log2 (1.5) = 0.585)* and $q \leq 0.01$ *(-log (0.01) = 2)*. Results highlighted in **orange** instead represent fold-changes of ≥ 1.5, which were considered *'false discoveries'* ($q \geq 0.01$). |**A**| Gene fold-changes between WT and m*Ogg1*$^{-/-}$ MEFs. |**B**| Gene fold-changes in WT MEFs following BSO treatment (15 μM; 24h). |**C**| Gene fold-changes in m*Ogg1*$^{-/-}$ MEFs following BSO treatment (15 μM; 24h).

7.5. NEIL3 dot blot

Prior to investigating NEIL3 expression *via* western blotting, the specificity of the NEIL3 antibody (Abcam: catalogue no. ab110049) was tested using purified hNEIL3. The antibody was tested against different dilutions of hNEIL3 (1:1 - 1: 1000) using a simple dot-blot method (Figure **7.3.**), confirming that the antibody was capable of NEIL3 binding. Additionally, this experiment was used to determine the optimum hNEIL3 concentration to use as a positive control in western blot experiments, which was determined to be a dilution of 1:10.

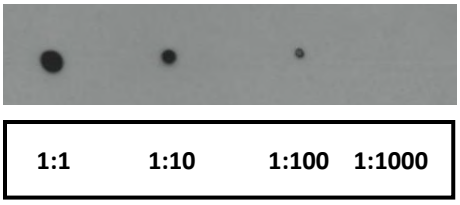


Figure 7.3. NEIL3 dot blot using different dilutions of hNEIL3 (1:1 – 1:1000) followed by incubation with a NEIL3 specific antibody (1:500 dilution). The antibody shows a concentration-dependent response to the hNEIL3 protein, allowing for the optimal concentration (1:10) to be chosen for future experiments.

7.6. NEIL3 western blot analysis

The western blot results described in 3.3.5. were analysed using ImageJ (Figure **7.4.**). In addition to the primary band (~40 kDa) observed in the m*Ogg1*$^{-/-}$ MEFs, a less intense band was also detected (~68 kDa). These corresponding peaks are shown alongside the original western blot image. Furthermore, the detected β-actin bands were found to be more intense in the WT MEFs when compared to the m*Ogg1*$^{-/-}$ MEFs, confirming that differences in protein concentration are not an explanation for the differences detected in NEIL3 expression. For quantification, the area under the curves were calculated (using ImageJ). Values were normalised using the area under the peaks detected for the β-actin controls of WT (76890) and m*Ogg1*$^{-/-}$ MEFs (51477) respectively. Following this it was calculated that the major peak at ~40 kDa was stronger in the m*Ogg1*$^{-/-}$ MEFs (1622 -fold) and that the minor peak at ~62 kDa was also stronger in m*Ogg1*$^{-/-}$ MEFs (7 -fold).

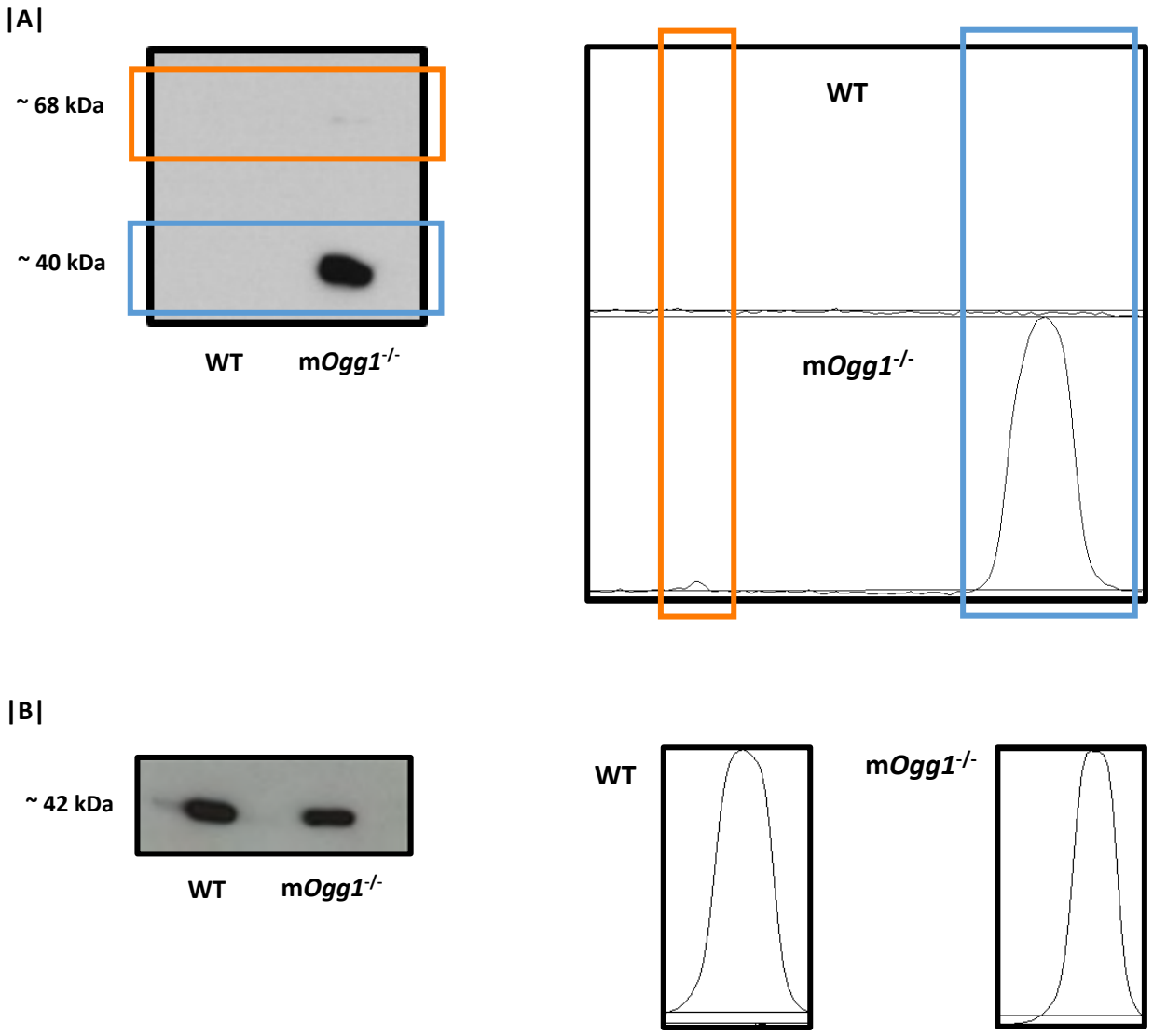


Figure 7.4. The bands generated in the NEIL3 western blot were analysed using ImageJ. The bands were detected and the area under the corresponding peaks collected. **|A|** For the NEIL3 blot, this analysis included the detection of a major band at ~ 40 kDa and a minor band at ~ 62 kDa in m*Ogg1*$^{-/-}$ MEFs. Neither peaks can be seen in the WT MEFs. **|B|** The intensity of the NEIL3 bands were quantified following normalisation with β-actin controls in WT and m*Ogg1*$^{-/-}$ MEFs.

7.7. RAS-GTP ELISA optimisation

The instructions from the manufacturer (Cytoskeleton Incorporated) were followed to determine the protein concentration to use. Firstly, it is recommended that the final concentration of lysates is between 0.25 – 1 mg/mL, so this was the range tested. We showed that as protein concentration increased, absorbance increased in a linear manner (R_2 > 0.98) (Figure **7.5.**). As the absorbance values generated were lower than published by the manufacturer, a relatively high concentration (0.75 mg/mL) was chosen, ensuring that this did not exceed the absorbance generated by the RAS positive control.

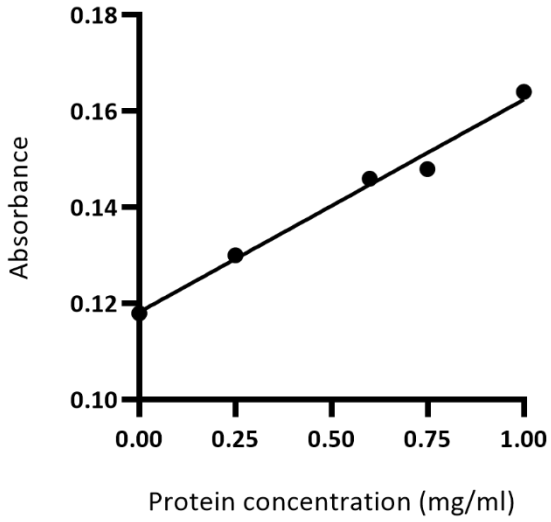


Figure 7.5. Determination of optimal protein concentration for RAS-GTP ELISA experiments. Different concentrations (0.25 – 1 mg/mL) were tested and can be seen to increase absorbance in a linear manner (R = 0.9872).

7.8. Neither 8-oxoG or 8-oxodG had an effect on the rate of detachment of MEFs following a longer treatment duration

The experiments described in **4.3.7.** were also performed following a longer treatment period (48 h). Correlating with the previous results, there was no significant difference measured in the rate at which WT or m*Ogg1*$^{-/-}$ MEFs detached following treatment with 8-oxoG (1-10 μM, 24 h) or 8-oxodG (1-10 μM, 24 h), when compared to control cells (Figure **7.6**). However, again treatment with a non-cytotoxic concentration of H_2O_2 (12.5 μM; 24 h) did significantly decrease the number of cells that remained attached following trypsin incubation (0.25% w/v; 30 sec) *(p* < 0.05). However, neither the addition of 8-oxodG or 8-oxoG resulted in a rescue response in WT or m*Ogg1*$^{-/-}$ MEFs *(p* > 0.05), reflecting what was seen following a 24 h treatment regime.

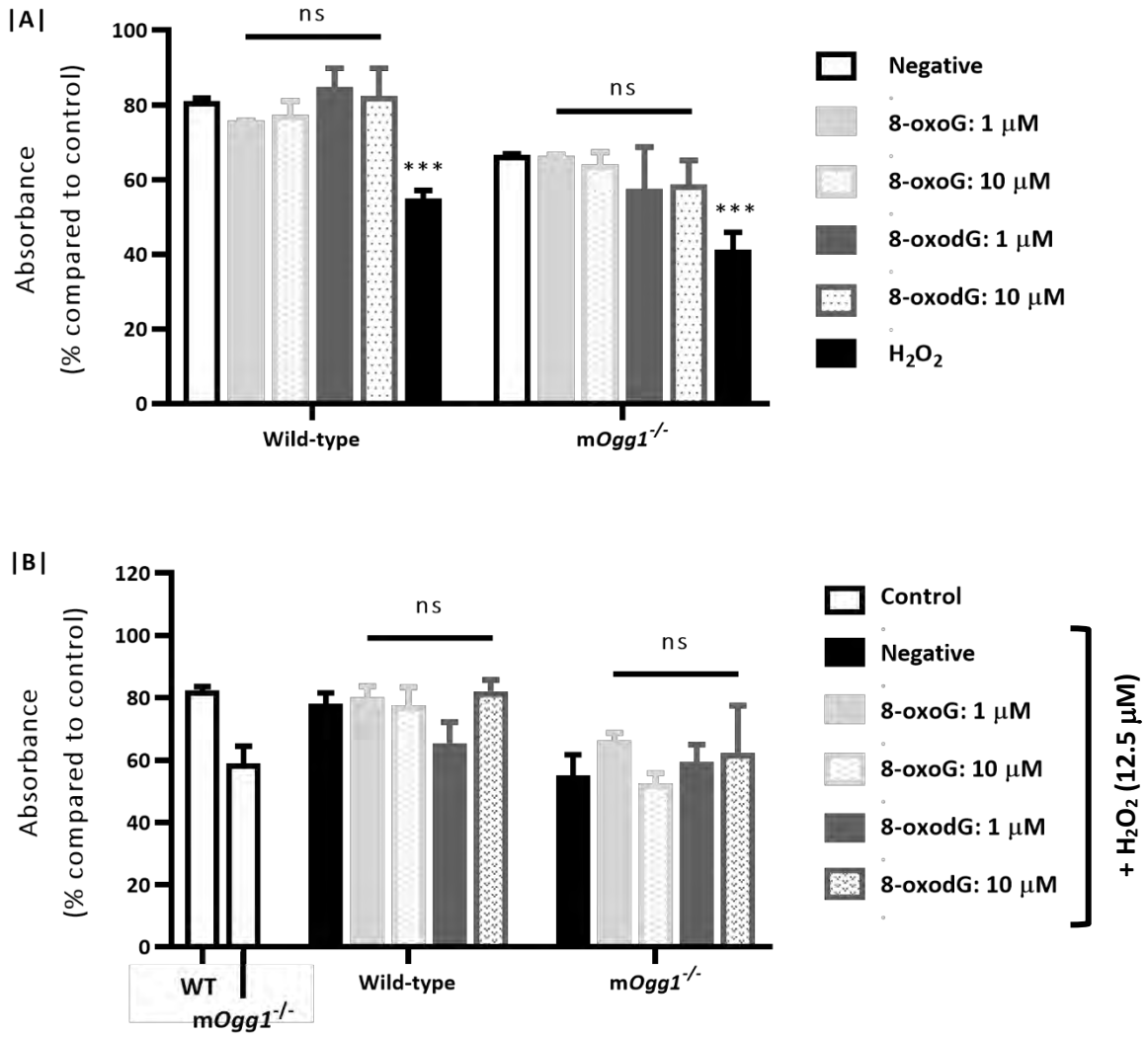


Figure 7.6. Neither treatment with 8-oxoG or 8-oxodG had an effect on the rate of detachment of cells following incubation with trypsin-EDTA (0.25% w/v, 1 min) (extended treatment duration). Mean ± SD (N=3). **|A|** Treatment with 8-oxoG (▫) or 8-oxodG (■) (1-10 μM; 48 h) did not have an effect on the number of WT or m*Ogg1*$^{-/-}$ MEFs that had detached *(p* > 0.05). Treatment with H_2O_2 (■) (12.5 μM; 48 h) did result in significantly less cells remaining attached following trypsin incubation *(p* < 0.001). Significance was determined with a two-way ANOVA and subsequent Dunnett's post-hoc testing (compared to untreated controls (□).

Figure legend continues on next page

|B| This experiment was repeated following the co-treatment of cells with H_2O_2 (12.5 μM; 48 h) and either 8-oxoG (▒) or 8-oxodG (■) (1-10 μM; 48 h). Neither the addition of 8-oxoG or 8-oxodG had an effect on the rate of detachment of cells, when compared to H_2O_2 alone (■) ($p > 0.05$). Untreated control (□) cells are also shown for comparison. Significance was determined with a two-way ANOVA and subsequent Dunnett's post-hoc testing (compared to H_2O_2 treated controls (■).

7.9. Full details of publications

Kamlesh Patel, Thomas B. Smith, Desley A. H. Neil, Alpesh Thakker, Yugo Tsuchiya, **Ellen B. Higgs**, Nikolas J. Hodges, Andrew R. Ready, Jay Nath, and Christian Ludwig. "The effects of oxygenation on ex vivo kidneys undergoing hypothermic machine perfusion." *Transplantation* 103, no. 2 (2019): 314-322.

Ellen B. **Higgs**, Roger Godschalk, Nicholas J. Coltman, Grant S. Stewart, Frederik-Jan van Schooten, and Nikolas J. Hodges. Induction of apoptosis in Ogg1-null mouse embryonic fibroblasts by GSH depletion is independent of DNA damage. *Toxicology Letters* 332 (2020): 27-35.

Ellen B. Higgs, Roger Godschalk, Frederik-Jan van Schooten, and Nikolas J. Hodges. mNEIL3 is upregulated in *Ogg1*-null mouse embryonic fibroblasts as a backup mechanism for 8-oxoG repair. *Manuscript prepared and submitted* (2020)